THE UNIVERSITY OF CHICAGO

VACCINATION WITH ENGINEERED PROTEIN-GLYCO-ADJUVANT CONJUGATES TO INDUCE ROBUST AND DURABLE IMMUNE RESPONSES IN CANCER AND INFECTIOUS DISEASE

A DISSERTATION SUBMITTED TO

THE FACULTY OF THE PRITZKER SCHOOL OF MOLECULAR ENGINEERING

IN CANDIDACY FOR THE DEGREE OF

DOCTOR OF PHILOSOPHY

BY

LAURA TAYLOR GRAY

CHICAGO, ILLINOIS

DECEMBER 2021

To my parents, Tom and Janet Gray, for always believing in me and supporting me in every way possible.

TABLE OF CONTENTS

LIST OF FIGURES

LIST OF TABLES

ACKNOWLEDGEMENTS

I am very lucky to have had the support of a number of people throughout my life and especially over the past 6 years in graduate school. Without this support, this work would not have been possible, so I am incredibly grateful to every person who has helped me and supported me along the way.

First of all, I would like to thank my advisor, Jeff Hubbell. It has truly been a pleasure to work with Jeff, and I am grateful for everything that he has taught me. Jeff has always been incredibly supportive of my ideas, and his constant confidence in my abilities has allowed me to develop a great deal as a scientist. I am also extremely appreciative of the collaborative and friendly lab culture that Jeff has worked to foster. While the past 6 years haven't been easy, I am so thankful to have been able to work with such a positive and supportive mentor in an environment like this.

Next, I would like to thank the members of my thesis committee: Melody Swartz and Marsha Rosner. Melody, I have really enjoyed getting to work with you and your lab over the years. I have benefited greatly from the collaborations between the Hubbell and Swartz labs, and I will greatly miss our lab family. Marsha, I have really appreciated your feedback and insightful questions, which have helped guide my work and assisted in my development as a scientist.

The work I've been able to complete also would not have been possible without the people that closely mentored me throughout graduate school. First, I want to thank Scott Wilson, who developed the technology that I had the pleasure of working with. Scott was always available to answer my many questions (as silly as they sometimes were and no matter what time of day or night it was) and provided endless support whenever I was struggling. His insightful

feedback also really helped to guide me through my projects. Second, I would like to thank Jun Ishihara. Jun patiently helped me when I was first starting *in vivo* work. He has remained constantly available to answer any questions, even after having left the lab. His optimism has also helped get me through some of the more challenging times in my work. Lastly, I would like to thank Annie Gai, who mentored me early on in my PhD. She helped really set me up for success, so I am extremely grateful for the help, friendship, and support that she provided me as I navigated through some of the uncertainties at the beginning of graduate school.

Next, I would like to thank all of the members of both the Hubbell and Swartz labs, past and present. It has been such a pleasure to get to work with each of you, and I feel very lucky to have been a part of such a friendly, collaborative, and supportive lab. First of all, thank you to John-Michael Williford, Sarah MacEwan, Michael White, Elyse Watkins, Andrew Tremain, Jialu Liu, Suzana Gomes, and Marcin Kwissa being so welcoming and incredibly helpful when I joined the lab. That truly made a huge difference for me at the start of graduate school. Next, thank you to Tiffany Marchell and Michal Raczy for being wonderful collaborators within the lab. I am so appreciative of how helpful you both were (and continue to be) to me. Thank you to Ani Solanki who isn't an official part of our lab but has provided me with so much help on my *in vivo* work over the years and has always done so happily (even on nights and weekends). Thank you also to Aaron Alpar and Rachel Wallace, who have both been wonderful friends to me within the lab and who have both been incredibly generous by helping me out with experiments and always being willing to talk through things or answer any of my questions without judgement. I'd like to extend a special thank you to Suzana Gomes who takes care of everyone in the lab, no matter what she has going on in her life. Additionally, thank you to the other people who I have been able to work directly with on various projects over the years: Kirsten Refvik,

Joe Reda, Jenni Antane, Lisa Volpatti, Mindy Ngyuen, Abbey Lauterbach, Nick Mitrousis, Shijie Cao, Claudia Battistella, Anna Slezak, Levi Bennish, Aslan Mansurov, Koichi Sasaki, Ruyi Wang, Ako Ishihara, Erica Budina, Wendan Hou, Priscilla Briquez, Sylvie Hauert, Maria Stella Sasso, Ruolan Zhou, Yue Wang, and Shann Yu. I have learned so much from all of you.

I am also appreciative of the staff in the PME for everything they have done behind the scenes to help make things run smoothly, which could not have been easy in a new department. In particular, I'm thankful that I've been able to work in various capacities with Laura Rico-Beck, Rovana Popoff, and David Taylor.

I would further like to thank my friends outside of the lab for their support throughout this journey. Thank you to the 2015 PME cohort – things have changed a lot since we started, and I'm glad that I was able to meet and work with all of you. Ryan McEvoy, thank you for all of the time you spent helping me in class and for always being supportive. Elizabeth Ashley, I am so grateful for your friendship, even though it started later in grad school. I have really appreciated your support, open-mindedness, and the reminders to take breaks. Kyle McGinty, I am so glad that we have remained friends since our freshman year of undergrad. I am lucky to have such a supportive friend in you.

Additionally, I would like to thank all of my teachers and mentors who have helped me along my educational and scientific journey that led up to graduate school. In particular, I'd like to thank my undergraduate advisor, Professor Douglas Van Citters, for always being incredibly kind and supportive, pushing me to do my best, and showing me what a passion for science truly looks like. I'd also like to thank Hemanta Baruah, who was my supervisor during my time working in industry prior to graduate school. Thank you, Hemanta, for helping me to figure out

the type of research I wanted to pursue in graduate school, for patiently answering all of my questions, and for always trusting and supporting me.

Last, but certainly not least, I would like to thank my family for their unending support and for providing me with the opportunities that have allowed me to pursue my graduate studies. To my sister, Megan, thank you for being there for me through all of the tough times and happy times over the past 6 years. Thank you for always letting me come visit you when I needed a break and for being willing to be my travel buddy on multiple occasions. To my parents, Tom and Janet, thank you for everything you have given me throughout my entire life. You both have taught me the value of hard work and perseverance. Without you, there is no way that I would have been able to get to where I am today. Thank you for also inspiring me to want to make a difference in the world. Seeing you both constantly care for other people has made me want to do the same. I know the past 6 years haven't been the easiest, so thank you from the bottom of my heart for always believing in me and encouraging me to keep going. I couldn't have done this without you.

ABSTRACT

The development of new prophylactic and therapeutic vaccines is challenging due to a lack of strong, clinically approved adjuvants. To address this challenge, we have created a modular vaccine platform, consisting of a mannosylated TLR7-agonizing polymer, p(Man-TLR7), conjugated to a protein, which can have different functionalities depending on the context. Here, we investigate the efficacy of this vaccine platform both as a therapeutic cancer vaccine and as a prophylactic COVID-19 vaccine. In the context of cancer, we observe a therapeutic benefit in multiple cold tumor models when p(Man-TLR7) is targeted to the tumor extracellular matrix via conjugation to various targeting proteins. This therapeutic benefit is accompanied by an increase in the proportion of $CD8^+$ effector cells in the tumor, as well as an increase in the proportion of activated cross-presenting $CD103^+$ DCs in the tumor. In the context of COVID-19, p(Man-TLR7), when conjugated to SARS-CoV-2 antigens, induces high titers of neutralizing antibodies, as well as robust antigen-specific T cell responses. Overall, our results demonstrate the adaptability and broad clinical translational potential of our engineered protein-glyco-adjuvant vaccine platform.

CHAPTER 1

INTRODUCTION

1.1 Overview of Vaccines

The overall goal of vaccines is to induce a specific immune response that will provide protection against a pathogen. Vaccines have been instrumental in reducing the incidence of many different diseases and are estimated to save 2-3 million lives per year [1].

Vaccines have been in existence for hundreds of years [1], and while extensive vaccine development has occurred since then, the same basic design principles still apply. First, because a vaccine aims to induce an immune response against a specific pathogen, it must contain some kind of material from the pathogen. In some cases, the pathogen itself is used as the target antigen, such as in attenuated vaccines. In other cases, the antigen is just a portion of the antigen, such as a protein or a peptide. Recent advances, particularly driven by the COVID-19 pandemic, have also been made in using genetic material encoding a protein from the pathogen of interest as the antigen source as well [2,3].

In some cases, vaccination with this antigen source alone is sufficient to drive a potent immune response. However, in other cases, the addition of an adjuvant is necessary (or beneficial) for driving the desired immune response [1]. An adjuvant usually activates a portion of the innate immune system, such as a pattern-recognition receptor, and thus helps to kickstart a potent immune response. One major challenge in the clinic for vaccines requiring an adjuvant, though, is that there are only a few clinically-approved adjuvants [4]. Alum (an aluminum hydroxide wet gel suspension) is one of these adjuvants, but its mechanism of action is not fully

understood. As a result, there is a large amount of ongoing work to develop novel potent adjuvants [4].

Traditionally, vaccines are thought of as tools for the prevention of infection or disease. Prophylactic vaccines are administered prior to exposure to the pathogen in question, and the goal is to prevent future infection or disease. Prophylactic vaccines are particularly prevalent against various infectious diseases. Vaccines can also be used when an infection or disease is already ongoing. Therapeutic vaccines are administered during an active infection or disease, and the goal is to bolster the immune response in order to clear the injection or cure the disease. Therapeutic vaccines have been investigated as potential treatments for chronic viral infection, as well as cancer.

Despite having slightly different goals, both vaccine approaches have a similar desired immune response: an antibody-generating humoral response (generally considered to be the most important response), as well as a T cell response (the importance of which is less well understood in vaccines, though) [1]. As a result, similar approaches can be taken to develop both prophylactic and therapeutic vaccines, with modifications to both based on the therapeutic context. Along these lines, here we seek to develop two vaccines for two different contexts while using the same platform: a therapeutic cancer vaccine and a prophylactic antiviral vaccine. In the following sections, we will describe the relationship between the immune system and cancer or viruses, which is helpful for learning how to harness this relationship for vaccine development, as well as understanding the results presented here.

1.2 Cancer and the Immune System

1.2.1 Overview

It is estimated that more than 1.9 million new cases of cancer will be diagnosed and over 600,000 people will die from cancer in the United States in 2021 [5]. Unfortunately, though, there are limited effective treatments for cancer. In response, cancer immunotherapy has emerged as a prevalent therapeutic strategy for cancer treatment, and it has shown promising clinical results [6–9]. The goal of cancer immunotherapy is to create an immune response against a tumor, but this is not an easy task. There are multiple steps required to mount an anti-cancer immune response. First, dendritic cells (DCs) must sample tumor-associated antigens (TAAs) from the tumor microenvironment. At the same time, upon TAA encounter, a DC must also receive an activation signal, which allows it to promote immunity rather than tolerance. Next, TAA-loaded DCs must present these antigens to T cells in lymphoid organs in order to generate a protective T cell response. Lastly, the cancer-specific T cells have to enter the tumor microenvironment to perform their function. However, the battle is not over here. Tumors are able to escape immune attack using various mechanisms of immunosuppression, so these immunosuppressive mechanisms must also be overcome. Thus, successful cancer immunotherapy is not easily achieved, as evidenced by the fact that cancer immunotherapy has only worked in a subset of patients [10–13]. Novel immunotherapeutic strategies are needed for the treatment of cancer.

1.2.2 Tumor microenvironment

Cancer cells are not the only component of the tumor microenvironment. The components can be classified into three main groups: cells of hematopoietic origin, cells of mesenchymal origin, and non-cellular components [14].

Cells of hematopoietic origin include cells of the lymphoid lineage, cells of the myeloid lineage, DCs, and platelets. Cells of the lymphoid lineage include T cells, B cells, and natural killer (NK) cells. Cells of the myeloid lineage include macrophages (such as tumor associated macrophages (TAMs)), neutrophils, and myeloid-derived suppressor cells (MDSCs). Depending on the specific subtypes of each of these cells, they can either promote tumor survival or tumor elimination [15–17]. Interactions among the different cell types can also either promote tumor survival or elimination [14,18].

Cells of mesenchymal origin include fibroblasts, myofibroblasts, mesenchymal stem cells (MSCs), adipocytes, and endothelial cells. Myofibroblasts and MSCs have been shown to support cancer stem cells (CSCs) by creating a favorable niche and facilitating tumor progression [19]. Adipocytes secrete factors that aid in tumor progression [20]. Endothelial cells and pericytes constitute the walls of blood vessels and thus play a role in angiogenesis, vascular functionality, and regulation of cancer cell dissemination [14,21].

The main non-cellular component in the tumor microenvironment is the extracellular matrix (ECM), which contains many distinct components that contribute to the its structure and function. These components include proteins, glycoproteins, and proteoglycans [22]. The ECM can be subdivided into the basement membrane and the interstitial matrix. The basement membrane is rich in type IV collagen, laminin, and fibronectin [22]. The interstitial matrix

consists of fibrillar collagens, proteoglycans, and glycoproteins that contribute to the tensile strength of the tissue [22]. The ECM can help maintain tissue architecture and prevent cancer cell invasion. However, an abnormal ECM has been shown to promote tumor progression and angiogenesis [14,22].

1.2.3 Immune response to cancer

The immune system can exhibit antitumor effects. These antitumor effects rely on many different innate and adaptive immune effector mechanisms. When normal cells transform into cancer cells, they undergo epigenetic and genetic modifications. This is often accompanied by the emission of "danger signals" and the expression of ectopic or mutated proteins. This allows the innate and adaptive immune systems to detect cancer cells [23]. NK cells can detect transformed cancer cells when they encounter specific ligands on tumor cells [24]. This can directly lead to the destruction of some cancer cells and to the uptake and processing of the cancer cell fragments by macrophages and DCs. These macrophages and DCs can then secrete inflammatory cytokines and present TAAs to T and B cells. Activation of the T and B cells leads to the production of additional cytokines that can further promote activation of innate immunity and support the expansion and production of tumor-specific T cells and antibodies.

More specifically, tumor-infiltrating lymphocytes (TILs) have been shown to be capable of killing tumors. When TILs are removed from a tumor, expanded *ex vivo*, and then transferred back into a lymphodepleted host, complete eradication of tumors has been observed in the case of human metastatic melanoma [25]. Additionally, in general, T cells infiltrating a tumor have been associated with an improved prognosis in cancer [26,27]. For instance, a major subset of colorectal cancer patients has been found to have a spontaneous infiltration of activated $CD8^+$ T cells in the tumor, and this has been shown to be a superior prognostic factor to conventional

clinical staging [28]. Furthermore, $CD4^+$ type 1 helper T (Th1) cells have been found to be a positive prognostic factor in melanoma patients [29].

Professional antigen-presenting cells (APCs), such as DCs, present exogenous antigens to T cells in the context of major histocompatibility complex (MHC) class II molecules or in the context of MHC class I molecules, a process known as cross-presentation [16]. Thus, APCs can lead to both $CD8^+$ and $CD4^+$ T cells that can contribute to antitumor effects. $CD8^+$ T cells have been established as having a cytotoxic function in antitumor immunity [30]. $CD4^+$ T cells can activate and regulate different aspects of the innate and adaptive immune response to cancer. They are most traditionally thought of as providing regulatory signals required for the priming of $CD8^+$ CTLs, which then can mediate tumor killing. However, they also play other roles in the host response to a tumor. They can activate innate immune cells, such as eosinophils and macrophages, which help to destroy the tumor. They can also engage and 'license' APCs, which then recruit additional T cells and can further activate the innate immune system against the tumor [31,32].

This antitumor immunity naturally exists in the body, but it is in the context of immunosuppression. As a result, this natural antitumor immune response is often not enough to completely eradicate cancer, and therapeutic strategies must be employed. The therapeutic strategies of adoptive T cell transfer and vaccination seek to enhance this existing antitumor immunity.

1.2.4 Immunosuppression and immunotherapy in cancer

Tumors are able to evade the immune system using a variety of mechanisms. This immunosuppression can be achieved by cells infiltrating tumors. Regulatory T (T_{reg}) cells,

natural killer T (NKT) cells, NK cells, γδ T cells, interleukin (IL)-10 producing B cells, and B regulatory cells are all suppressive lymphocytes that have been reported in cancer [13,33–35]. Myeloid lineage cells can also promote immune suppression, including MDSCs and TAMs [36,37]. Additionally, tumor stroma cells can promote the recruitment and function of immunosuppressive cells [13]. Immunosuppression can also be achieved by paracrine mediators [38]. They can suppress DCs, which indirectly inhibits T cell penetration into the tumor. They can also directly suppress effector T cell activation and enhance the function of T_{reg} cells [13]. Furthermore, immunosuppression can be achieved by changes in expression of different proteins. Tumor cells can downregulate MHC class I to avoid detection by APCs or disable other components of the antigen processing machinery in order to escape T cell recognition [39]. They can also upregulate inhibitory surface receptors and ligands to evade the immune system [13,40].

In particular, these inhibitory surface receptors and ligands have been studied extensively and have become of interest in immunotherapy. Normally, these immune checkpoint pathways maintain self-tolerance and limit collateral tissue damage during anti-microbial immune responses. However, cancer can co-opt these pathways. The first checkpoint receptors to be discovered were cytotoxic T-lymphocyte antigen 4 (CTLA4) and programmed cell death protein 1 (PD-1), and they have been extensively studied in the context of cancer. CTLA4 is a transmembrane protein expressed on regulatory T cells and activated $CD8^+$ T cells [41]. It induces immunosuppressive signals by binding CD80 or CD86 on APCs. It inhibits co-stimulation of T cells by CD28, as CD28 also binds CD80 and CD86 [40,42]. PD-1 is expressed on activated T cells, and its ligand, programmed death-ligand 1 (PD-L1), is expressed on some tumor cells [43–45]. The interaction of PD-1 with PD-L1 results in decreased cytokine

production, inhibition of proliferation, and apoptosis of T cells, thus allowing tumors to evade the immune response.

Clinical approaches to overcoming the immunosuppressive environment of the tumor have largely focused on blockade of these immune checkpoint pathways. For instance, CTLA4 blocking antibodies have been developed that inhibit the inactivation of T cells. In particular, ipilimumab is an anti-CTLA4 antibody that has been approved by the US Food and Drug Administration (FDA). In the clinic, ipilimumab treatment has led to improved survival of melanoma patients [9]. Additionally, anti-PD-1 and anti-PD-L1 antibodies have been developed. These antibodies have inhibited tumor growth in mouse models and in clinical trials with nivolumab (anti-PD-1) and atezolizumab (anti-PD-L1), which are now approved by the US FDA [6–8]. Nonetheless, despite promising results of using checkpoint blockade monotherapies, most tumor regressions are not complete, and the majority of patients do not achieve objective responses [7,40,46]. Based on these results, another clinical strategy has been to combine anti-PD-L1 and anti-CTLA4 antibody treatment, since their pathways are non-redundant, and this has been shown to strengthen the anti-tumor effects of these antibodies [47]. In hopes of achieving synergistic effects, it is also possible to combine checkpoint blockade therapy with other cancer therapies, such as chemotherapy, tyrosine kinase inhibitors, focal irradiation, cancer vaccines, adoptive T cell transfer, or immune agonist monoclonal antibodies [40].

1.2.5 Approach for reduced toxicity of immunotherapeutics

In addition to the fact that checkpoint blockade therapy only induces lasting responses in a subset of patients, another major downfall of many cancer immunotherapies is their toxicity. The long-lasting antitumor immune responses that can be induced by these therapies is oftentimes is accompanied by the incidence of immune-related adverse events (irAEs). These

irAEs can be severe enough to cause patients to be taken off of the immunotherapy in question [48,49].

As a result, a future direction in the development of immunotherapies is to create therapies that are not only more effective but also less toxic for the patients. One approach to this is creating targeted immunotherapies, where immunotherapies are somehow preferentially localized to and retained within the tumor. There are numerous potential targets within the tumor, but only one will be discussed in detail due to the relevance to the studies presented here.

As mentioned above, the ECM is composed of many different proteins, glycoproteins, proteoglycans, and polysaccharides that all work together to maintain tissue homeostasis. However, this network can become deregulated in disease states, such as cancer. In the case of cancer, ECM remodeling occurs, where there is abnormal ECM buildup and deregulated expression of ECM remodeling enzymes, such as matrix metalloproteinases. This ECM remodeling affects epithelial, endothelial, and immune cells in the tumor microenvironment, as well as other stromal cells [22]. As such, this remodeling creates a unique ECM within the tumor, which makes the tumor ECM amenable to targeting of cancer therapeutics. Several specific ECM components that are deregulated in cancer and have been used as targets for various cancer therapies are described below.

Fibronectin has been of interest as a target for cancer therapies because two alternatively spliced domains, extra-domain A (EDA) and extra-domain B (EDB), have been shown to be over-expressed in some cancers. In particular, EDA is over-expressed in the neo-vasculature or stroma structures of some aggressive solid tumors, and EDB is a marker of angiogenesis that is strongly expressed in most aggressive solid cancer types [50,51]. Targeting strategies for both EDA and EDB have been developed in the form of antibody fragments [50,52], and both of these

targeting strategies have been used to deliver various small molecules and proteins, such as cytokines and chemokines, to the tumor [53,54]. The anti-EDB antibody L19 has shown particularly promising results when fused to the cytokines IL-2 and TNF, as both of these antibody-cytokine fusions are being tested in the clinic [54]. Meanwhile, fusion of the anti-EDA antibody F8 with those same cytokines, in addition to others, have shown promising anticancer effects in preclinical studies [55,56]. These studies indicate that targeting fibronectin is an effective way to deliver cancer therapeutics to the tumor *in vivo*.

Tenascin-C is highly expressed in the ECM of many solid tumors, lymphomas, and in the bone marrow of acute leukemias but is almost undetectable in normal tissue [57,58], making it a potentially promising candidate for delivering cancer vaccines to the tumor. Brack et al. isolated novel antibodies against tenascin-C and illustrated tumor-targeting with these antibodies [59]. One antibody in particular, F16, has been used further to target different cancer therapeutics to the tumor, such as IL-2 [60] and the anthracycline PNU159682 [58]. F16-IL2 (Teleukin) has gone on to be tested in clinical trials for several different solid tumors [54]. Other approaches for targeting tenascin-C include functionalizing liposomes or nanoparticles with tenascin-C binding peptides[61–63] or using sulfatide, a glyosphingolipid that binds tenascin-C [64,65].

Laminins are part of the basement membrane of the ECM, and one particular isoform, laminin-332 (previously known as laminin 5), is known to promote tumorigenesis. As such, it is expressed in several squamous and epithelial tumors [66], making it a potentially interesting candidate for targeting cancer therapeutics. However, laminin-332 is also important for epithelial-mesenchymal cohesion in normal tissues, which makes targeting laminin-332 specifically in cancer more challenging. One strategy to overcome this challenge is to target a portion of laminin, G45, that is specific to cancer, as it is proteolytically cleaved in healthy

tissues [67]. A polyclonal antibody specific to G45 in laminin-332 [68] has been shown to decrease human squamous cell carcinoma tumorigenesis *in vivo* without any additional therapy [67]. As a result, it is possible that using this strategy to target a cancer vaccine to G45 in laminin-332 could result in further improved anticancer efficacy.

Collagen is another potential ECM component that can be targeted, as it is present at higher levels in many types of tumors compared to normal tissue [69,70]. As such, collagen can be used to target cancer therapies delivered locally to the tumor. For example, Momin et al. intratumorally administered a collagen binding protein, lumican, fused to the cytokines IL-2 and IL-12. They observed prolonged local retention and reduced systemic exposure with their targeted therapies. Additionally, they observed improved antitumor efficacy when they combined local administration of their lumican cytokine-fusions with systemic immunotherapies [71].

Although collagen is expressed in almost all tissues, it is not exposed to the blood stream in healthy tissues. However, due to the highly permeable nature of blood vessels in tumors, collagen in the tumor can be accessible to molecules in the blood stream, making collagen a promising target for cancer therapies that are administered systemically, as well [72]. For instance, Liang et al. showed that a collagen binding peptide fused to an anti-EGFR Fab delivered intraperitoneally exhibited localization to A431 xenografts and enhanced retention time compared to un-targeted anti-EGFR Fab [73]. Furthermore, Ishihara et al. showed tumor targeting and suppression of tumor growth in multiple cancer models when they used a collagen binding protein from von Willibrand factor to target checkpoint blockade antibodies and IL-2 to the tumor [74].

Hyaluronan, a glycosaminoglycan (GAG), is a major component of the ECM in most tissues, but the levels of hyaluronan in malignant tumors are usually higher than in normal

tissues [75]. Hyaluronan has been shown to be involved in cancer progression, and it is associated with both solid tumors and cancers of circulating cells [75,76]. Because of this overexpression, Ikemoto et al. investigate the use of a hyaluronan-binding peptide, IP3, to target peritoneal tumors. They observed targeting of silver nanoparticles functionalized with the IP3 peptide to peritoneal tumors, illustrating that this strategy could be used to deliver other cancer therapeutics to tumors [77]. This approach could potentially be expanded to use other hyaluronan binding molecules, as well.

Another GAG component of the ECM that could be targeted for delivery of cancer vaccines is chondroitin sulfate. Chondroitin sulfate is expressed at higher levels in many types of cancers compared to healthy tissues, and the sulfation pattern of chondroitin sulfate different between cancerous and healthy tissues [78]. These differences in cancerous versus healthy tissues make chondroitin sulfate amenable to targeting. One method to target chondroitin sulfate is to use a protein, VAR2CSA, or a peptide derived from this protein, expressed by the malarial parasite *Plasmodium falciparum* that binds to one specific form of chondroitin sulfate, chondroitin sulfate A (CSA), which is normally expressed in the placenta but has also been shown to be expressed on malignant cells [79,80]. A recombinant version of VAR2CSA has been shown to localize to tumors and inhibit cancer growth when fused to diphtheria toxin or conjugated to hemiasterlin compounds [79]. Additionally, the CSA-binding peptide has been used to target nanoparticles loaded with doxorubicin to human choriocarcinoma in mice, and improved antitumor efficacy was observed compared to an untargeted control nanoparticles [80]. Other approaches to target chondroitin sulfate include using antibody fragments [81] and liposomes containing a cationic lipid TRX-20 [82].

Other proteoglycans and GAGs in the tumor microenvironment, such as aggrecan and heparan sulfate, are also potential targets for site-specific targeting of cancer vaccines [83]. Similar methods to those described above could be used to target these ECM components.

Another approach for targeting the ECM of cancer is to target multiple ECM components at the same time rather than just a single component at a time. One strategy using this approach involves the heparin binding domain (HBD) of placenta growth factor-2 (PlGF-$2_{123-144}$), which has been shown to have a high affinity for multiple ECM proteins [84]. In one study, PlGF-$2_{123-144}$ was used to retain checkpoint blockade antibodies within the tumor environment, resulting in improved antitumor efficacy and decreased side effects [85]. However, this approach is limited to local delivery (intra/peritumoral injection) of the cancer therapeutic. Another strategy using this approach involves the use of a bispecific peptide (PL1) that binds both fibronectin EDB and tenascin-C. Lingasamy et al. used this peptide to target iron oxide nanoworms loaded with proapoptotic peptides and saw decreased tumor growth of glioblastoma and prostate carcinoma xenografts [86]. Other methods involving targeting of multiple ECM components could offer therapeutic benefit, as well, potentially offering enhanced targeting compared to methods involving targeting a single ECM component.

1.3 Viruses and the Immune System

1.3.1 Overview

Viruses are pathogens that infect host cells and rely on this infection in order to reproduce. There are a wide variety of viruses that can infect humans and their effects vary extensively. In the case of most viral infections, the immune system is able to clear the virus. However, in some cases, viral infections become chronic.

1.3.2 Anti-inflammatory immune response

One of our first lines of defense against viral infection is the innate immune system, which has pattern recognition receptors (PRRs) capable of recognizing certain pathogen-associated molecular patterns (PAMPs) found on viruses [87]. One such class of PRRs that recognize viral components are the endosomal Toll-like receptors (TLRs), which recognize viral DNA and RNA. Activation of these or other PRRs results in the production of pro-inflammatory cytokines and chemokines. In particular, type I interferons (IFN) can help prevent viral replication and activate natural killer (NK) cells, which can then kill infected cells [88].

The innate immune response can also help to start the adaptive immune response, as innate responses such as activating the TLRs can result in the activation of APCs and the migration of APCs and lymphocytes to infection-draining lymph nodes or the spleen [88]. Subsequently, B cells become activated and can produce antibodies for the purpose of neutralizing the ability of viruses to infect host cells [88]. Additionally, $CD8^+$ T cells can become activated upon encountering their antigen presented on DCs, at which point they act to kill infected host cells [88]. $CD4^+$ T cells can also play a role in the antiviral response by acting as effector cells, acting as helper cells in the antibody and $CD8^+$ T cell responses, and releasing cytokines [88]. After this adaptive response peaks, a contraction phase follows, with the remaining B cells and effector T cells becoming memory cells that can help to provide protection upon reinfection [88]. However, it should be noted that this immune response can act as a double-edged sword. While this inflammatory immune response can help to clear viral infection, it can also cause host tissue damage and potentially trigger autoimmunity [89]. This is a particular concern with chronic viral infection.

1.3.3 Viral immune evasion

Viruses, similarly to cancer cells, have evolved ways to evade the immune system. These mechanisms allow for viruses that cause chronic infections, such as cytomegalovirus (CMV) and Epstein-Barr virus (EBV), to persist long-term in the host. There are multiple mechanisms by which this immune evasion can occur. For example, viruses can cause DCs to produce high levels of anti-inflammatory cytokines, such as IL-10, in order to dampen the antiviral response [90]. Other evasive mechanisms include infecting APCs, preventing apoptosis induced by cytotoxic $CD8^+$ T cells, inhibiting antigen processing, downregulating MHC molecules on infected cells in order to escape recognition, and rapid evolution of viral antigens [89].

1.3.4 Challenges to therapeutic approaches

There are two approaches for combating viral infection: vaccines that prevent infection and therapeutics that can treat ongoing injections. Vaccines against viruses have been quite effective in slowing the spread of a number of viral diseases. In September 2019, there were a total of 87 clinically approved vaccines against 14 human viruses [91–93]. In the past, vaccination has even lead to the eradication of smallpox, which is causes by variola virus (VARV), highlighting the promise that vaccines hold [94]. Nevertheless, there are still diseases for which vaccines have proven to be elusive, such as with HIV [95]. One of the reasons behind this will be discussed below.

On the other hand, only 10 antiviral drugs that have been clinically approved [91–93]. These drugs are primarily antiretroviral medications or monocolonal antibodies. The treatments that are available are effective, but there is a need for more of these medications, related to the challenges discussed below.

One of these challenges is the fact that, despite the existence of these successful antiviral vaccines and treatments, there are still viruses that remain difficult to treat. The fact that a virus can evade the natural antiviral immune response means that therapeutic and vaccination strategies are also susceptible to this evasion. In particular, rapid evolution of viral antigens, such as that seen with HIV and even SARS-CoV-2, makes it challenging to develop therapeutics that will still remain effective as the virus mutates [95,96].

Additionally, as recently brought to light with the COVID-19 pandemic, emerging infectious diseases pose a big public health threat and require the swift development of both antiviral medications and vaccines to help reduce spread of the virus. In the case of the COVID-19 pandemic, vaccine development and distribution was very fast compared to the normal amount of time to get a vaccine into the clinic [91]. Nevertheless, there still was a wait for this vaccine, as well as for SARS-CoV-2 specific antiviral therapies. In the future, having access to a wider range of readily available antiviral medications would allow more patients to be treated at the outset of such an outbreak, at which time a virus may spread very rapidly within a population without any pre-existing immunity. As a result, there is a continual need for the development of novel antiviral therapeutic and vaccination strategies.

1.4 Polymeric Glyco-Adjuvant Vaccine Platform

1.4.1 Platform development and in vivo efficacy

Based on the ongoing need for new vaccine development and particularly new adjuvant development, we recently developed a polymeric glyco-adjuvant vaccine platform that

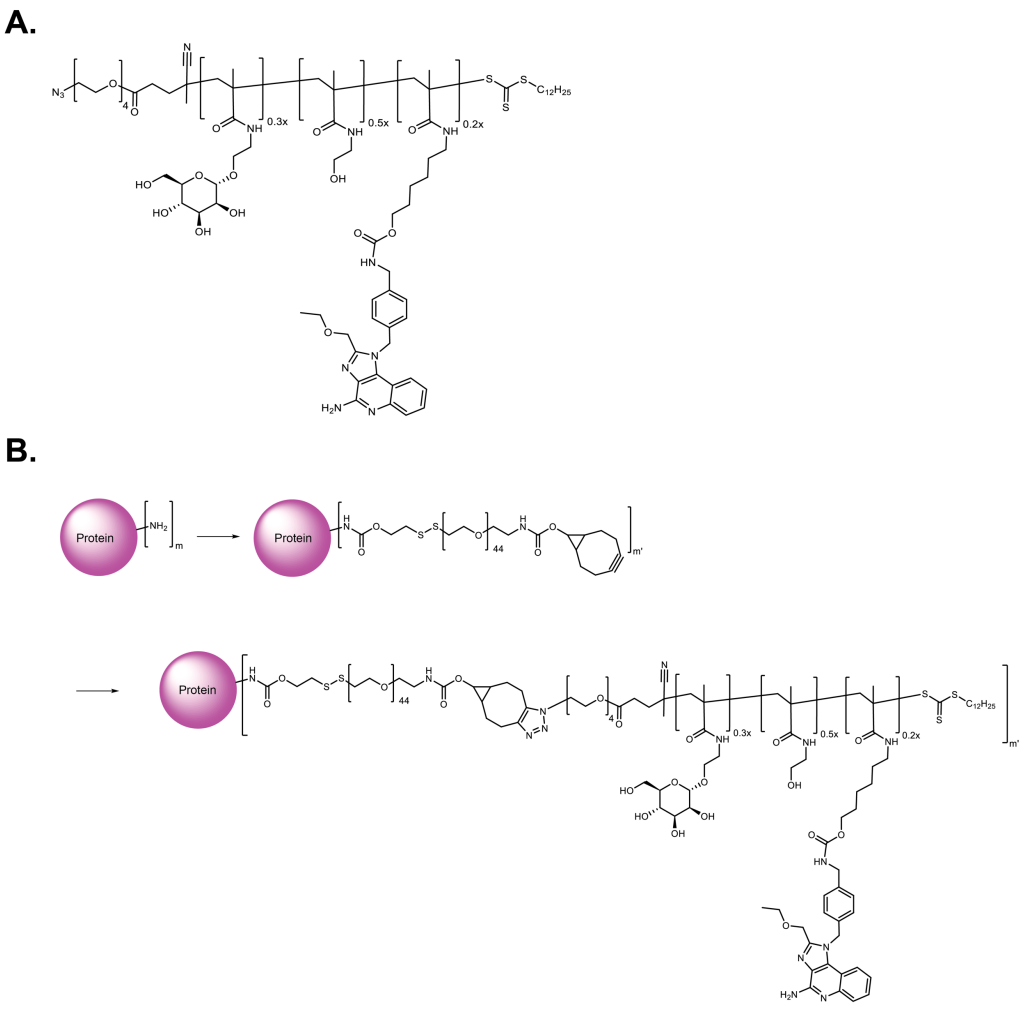

Figure 1.1: Polymeric glyco-adjuvant structure.

(A) The polymeric glycol-adjuvant p(Man-TLR7) is a random copolymer composed of monomers with pendant mannose and TLR7 agonist moieties. (B) The p(Man-TLR7) polymer is conjugated to amine-containing proteins via a two-step conjugation reaction. First, heterobifunctional PEG2000-based linker is attached to the antigen, forming an antigen-linker conjugate. Then, p(Man-TLR7) is reacted with the antigen-linker conjugate via copper-free click-chemistry to form the final antigen-p(Man-TLR7) conjugate.

incorporates multiple copies of a novel toll-like receptor 7 (TLR7) agonist, as well as multiple copies of mannose, on a backbone of poly(hydroxypropylmethacrylamide) (HPMA) (**Fig. 1.1A**) [97]. This polymer, hereby referred to as p(Man-TLR7), is synthesized by copolymerizing the TLR7 agonist monomer with HPMA and mannose via reversible addition-fragmentation chain-

transfer (RAFT) polymerization, which allows for very precise polymerization with narrow molecular weight distributions. This results in a terpolymer of the three components mentioned above (TLR7 agonist, mannose, and HPMA). HPMA is used here because it has been used in many drug nanomaterial drug delivery applications [98]. The other two components are described in further detail below.

TLR7 is a member of the TLR family of pattern-recognition receptors in the innate immune system. It is localized to the endosome within the cell and recognizes single stranded RNA. In mice, TLR7 is expressed in DCs (both conventional and plasmacytoid DCs; cDCs and pDCs, respectively), monocytes, macrophages, NK cells, neutrophils, B cells, and some T cell subsets. In humans, TLR7 expression is a little more restricted, as it is expressed mostly in pDCs as opposed to both DC subsets, and the expression level is reduced in monocytes and neutrophils, as compared to mice [99–102]. Ligand binding results in the activation of nuclear factor (NF)-κB, mitogen-activated protein kinase, and other signaling pathways. This then leads to the secretion of cytokines such as interferon (IFN)-α and tumor necrosis factor (TNF)-α [103–106]. This results in the overall activation and maturation of APCs, such as DCs. Mature DCs can then fully activate $CD8^+$ effector T cells and drive a more potent immune response [106–108].

The downstream signaling that occurs upon TLR7 activation results in an immune response that is favorable in multiple clinical contexts. As a result, synthetic nucleoside analogues that activate TLR7 and or Toll-like receptor 8 (TLR8; a receptor closely related to TLR7), especially those from the imidazoquinoline family, have been developed and extensively studied for use in the clinic, particularly for use as topical therapies for skin conditions, cancer treatments, and antiviral medications for infectious disease. Imiquimod, a TLR7 agonist, is the

only TLR7 and/or TLR8 agonist that is currently approved by the US FDA. It is approved for the treatment of external genital and perianal warts, actinic keratosis, and basal cell carcinoma [99,109]. Nevertheless, there are numerous other TLR7/8 agonists currently in preclinical development or clinical trials. For instance, resiquimod (R848) has been shown to reduce tumor growth in the B16F10 murine melanoma model when bound to the surface of tumor cells in preclinical studies [110] and has shown promising results in treating cutaneous T cell lymphoma in a phase I clinical trial [99]. Thus, TLR7 was chosen for incorporation into our polymeric glyco-adjuvant vaccine platform due to these promising therapeutic results in multiple clinical indications. One important thing to note is that TLR7/8 agonists often have high associated toxicities, which have caused the cessation of multiple clinical trials for different indications [99].

TLR7 is an endosomal receptor, but a polymer, unlike a small molecule drug, cannot passively reach the endosome. As a result, we incorporated mannose in the polymer, as well. Mannose can bind the mannose receptor or other C-type lectin receptors, which are expressed by macrophages, DCs, and some nonvascular endothelial cells [111,112]. These receptors are highly endocytic, meaning that targeting these receptors can allow access to the endosome. Additionally, based on the expression patterns of these receptors, mannose can also be used to target DCs. This targeting has been shown to increase antigen internalization and trafficking into intracellular pathways that promote cross-presentation, as well as presentation to $CD4^+$ T cells, which are both necessary for driving cellular and humoral immune responses [113–118]. All of these characteristics of the receptors for mannose make it a valuable addition to our vaccine polymer.

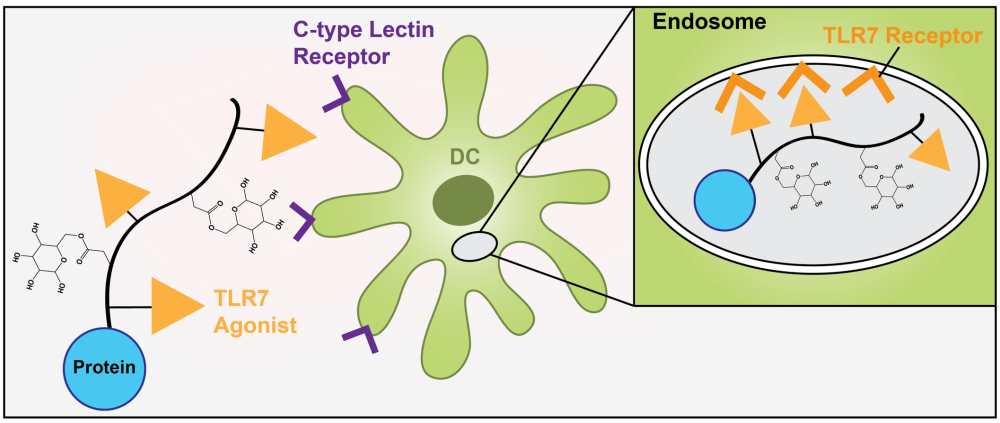

Figure 1.2: Schematic for polymeric glyco-adjuvant.

The polymeric glyco-adjuvant serves as the adjuvant portion of a vaccine. An antigen is needed, though, in order to drive an antigen-specific immune response. As a result, p(Man-TLR7) was designed such that it can be chemically conjugated to any primary-amine containing moiety, such as a protein or a peptide (**Fig. 1.1B**) [97]. Importantly, this conjugation involves the use of a self-immolative linker that can be reduced within the endosome and release unmodified antigen, meaning there is no risk for creating a new immunogenic epitope on an antigen due to conjugation to p(Man-TLR7) [97]. This assures that any immune response that is induced will be against the desired antigen.

All of these components led to the development of an effective vaccine capable of eliciting potent immune responses. We observed robust antigen-specific $CD8^+$ T cell responses when mice were vaccinated with ovalbumin conjugated to p(Man-TLR7) as a model vaccine or with circumsporozoite protein (CSP) conjugated to p(Man-TLR7) as a malaria vaccine [97]. In the case of malaria vaccination, the immune responses observed upon vaccination of mice with CSP-p(Man-TLR7) were demonstrated to be protective, as well [97]. **Figure 1.2** shows a schematic for the mechanism of our vaccine platform.

1.4.2 Present work: use of p(Man-TLR7) as a therapeutic cancer vaccine and a prophylactic COVID-19 vaccine

Based on the promising results observed with p(Man-TLR7) vaccination described above and the need for vaccine development, we wanted to expand the use of our vaccine to new therapeutic contexts in the work described here. The antigen-specific $CD8^+$ T cell responses observed upon vaccination with p(Man-TLR7) make this an attractive approach for generating a cancer vaccine, as well as an antiviral vaccine. As a result, in the following chapters we report on the creation of an extracellular-matrix (ECM) targeted cancer vaccine (Chapter 2) and a COVID-19 vaccine (Chapter 3).

CHAPTER 2

TARGETING A POLYMERIC GLYCO-ADJUVANT TO THE TUMOR EXTRACELLULAR MATRIX FOR THE INDUCTION OF ANTI-TUMOR IMMUNITY

2.1 Abstract

Immunotherapy for cancer treatment has had a tremendous impact in the clinic, but it only works in a subset of patients. Immunotherapy relies on endogenous anti-tumor immune responses, so one potential way to expand the efficacy is to enhance those endogenous anti-tumor immune responses. Therapeutic cancer vaccination is one way that has been used to try to do this, but cancer vaccination is challenging due to a lack of strong, clinically approved adjuvants and difficulty in identifying cancer-specific antigens. Here, in order to address these challenges, we report the creation of a cancer vaccine consisting of a tumor-targeted polymeric glyco-adjuvant. This polymeric glyco-adjuvant vaccine contains two components: (1) a mannosylated, toll-like receptor 7 (TLR7)-agonizing polymer, p(Man-TLR7), and (2) a protein targeted to the tumor extracellular matrix. This targeting protein is one of two different proteins: (1) an antigen-binding fragment (Fab) of an antibody specific to the extra domain A (EDA) of fibronectin or (2) the collagen binding domain of von Willebrand factor fused to serum albumin (CBD-SA). By chemically conjugating p(Man-TLR7) to a matrix-targeted protein, our engineered vaccine aims to retain this strong adjuvant within the tumor microenvironment, promoting the immunogenic processing of endogenous tumor antigens. Upon treatment of both EMT6 and B16F10 tumor-bearing mice with intratumorally delivered targeted-p(Man-TLR7), we observed a slowing of tumor growth and improved survival when our vaccine is combined with checkpoint blockade therapy. In EMT6, vaccination also results in antitumor immunologic memory, as complete responders reject a tumor rechallenge. Upon further analysis of B16F10

tumors, we observe an increase in the proportion of $CD8^+$ effector T cells in the tumor, an increase in the proportion of activated $CD103^+$ DCs in the tumor, and the induction of antigen-specific cellular responses in both the tumor and tumor-draining lymph nodes when mice are vaccinated with CBD-SA-p(Man-TLR7) in combination with checkpoint blockade therapy. At the same time, we do not see increased levels of the toxicity markers ALT, BUN, and T. Bili in either tumor model. Furthermore, we see promising results upon intravenous administration of our vaccines in the B16F10 tumor model, although further optimization of our vaccine is required for this administration route. In conclusion, vaccination with our tumor matrix-targeted polymeric glyco-adjuvant synergizes with checkpoint antibody therapy to provide therapeutic benefit in treatment of two different cold murine tumor models.

2.2 Introduction

Generating a robust adaptive immune response against cancer-specific antigens plays a major role in tumor eradication. The advent of checkpoint blockade antibodies, which help T cells overcome the immunosuppressive tumor environment by reinvigorating the T cells' efficacy, has been a breakthrough cancer treatment for extending survival time for patients with metastatic melanoma. Despite its success, immunotherapy provides durable clinical results in only a minority of patients, for only a subset of cancers [119]. It is well established that the extent of T cell infiltration into the tumor is highly predictive of patient responses to immunotherapy [120]. However, many patients have dominantly immunosuppressive tumors or lack any pre-existing anti-tumor immunity that could be reinvigorated [121]. For these populations, few effective therapies exist for initiating T cell responses, expanding tumor-reactive cells, or making the tumor microenvironment more inflammatory.

Cancer vaccines are one form of immunotherapy by which tumor proteins, or antigens, are used to activate cellular and humoral immune responses against cancer. Typically, these vaccines are comprised of specific antigens along with immunostimulatory adjuvants. The adjuvant activates antigen presenting cells (APCs), licensing them to activate cancer-recognizing T cells.

To overcome the multiple immune evasion mechanisms cancer cells use to avoid attack, cancer vaccines must activate a large enough immune response to multiple tumor antigens. In particular, the initiation of $CD8^+$ T cell responses are critically important to tumor control and rejection [122,123] with the magnitude of functional $CD8^+$ T cell responses being a highly predictive indicator of the overall therapeutic efficacy [124]. However, lack of strong, clinically approved adjuvants, combined with the difficulty of identifying cancer-specific antigens, poses a major barrier to successful cancer vaccination. Despite the success of various therapeutic cancer vaccine approaches in preclinical murine cancer models, few have accomplished the necessary breadth and magnitude of cellular and humoral responses required for tumor control [125]. In translation to the clinical treatment of cancer, many vaccines ultimately fail to activate the sufficient magnitude and functionality of cytotoxic $CD8^+$ T cell responses required for therapeutic efficacy [126–128]. There remains a critical need for additional methods to induce the cellular immune responses against cancer cells required for tumor control.

In previous work, we have shown that vaccination with a polymeric glyco-adjuvant, termed p(Man-TLR7), is capable of priming strong $CD8^+$ T cell responses in traditional model antigen, or malaria vaccination models [97]. The design of this mannosylated, toll-like receptor 7 (TLR7)-agonizing polymer endows the adjuvant with its unique $CD8^+$ T cell priming ability. The mannose and TLR7 agonist composition work synergistically to promote APC targeting, uptake, and cross-presentation of co-delivered antigen. The mannose component enhances uptake by

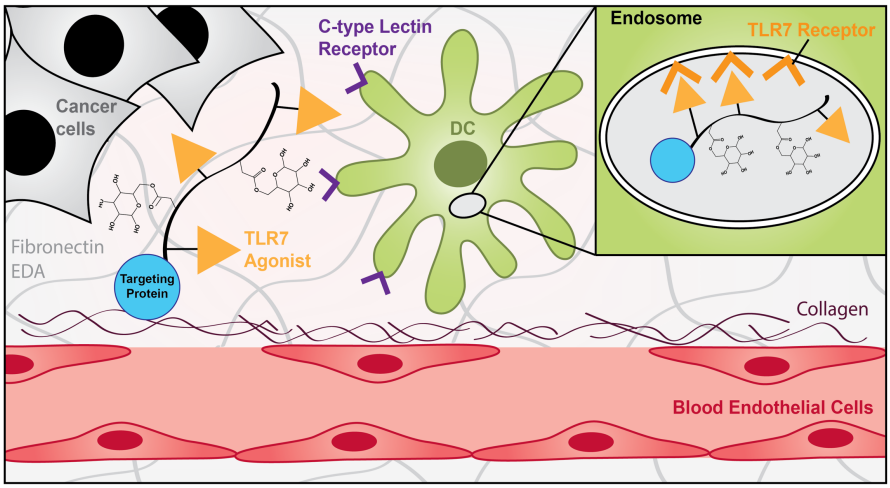

Figure 2.1: Schematic for polymeric glyco-adjuvant for use as a cancer vaccine.

various mannose-recognizing C-type lectin receptors, such as the mannose receptor [129], which have been shown to route antigen for cross-presentation to $CD8^+$ T cells [116]. C-type lectin receptor endocytosis then shuttles the adjuvant polymer to the endosome where it can activate the recipient cell via binding to TLR7. TLR7 signaling is important for the production and release of cytokines and other soluble immune activating molecules that promote cross-presentation to, and priming of $CD8^+$ T cell responses[130]. Studies done with imidizaoquinoline-based TLR7 agonists, similar to that used in p(Man-TLR7), show TLR7 activation stimulates interferon production in plasmacytoid DC subsets, and IL-12 production from the $CD11b^+$ DC subset, both of which have been shown to promote antigen cross presentation in other DC subsets such as $CD8\alpha^+$ DCs, Langerhans cells, and dermal DCs [131]. Together, p(Man-TLR7) provides the appropriate APC activation and cytokine environment for adaptation to use in a cancer vaccine, for which the generation of cellular responses is vital.

Therefore, here we report the creation of a therapeutic cancer vaccine using the p(Man-TLR7) polymeric glyco-adjuvant. Our vaccine material is composed of p(Man-TLR7)

conjugated to one of two matrix-targeting proteins: (1) an antigen-binding fragment (Fab) of an antibody specific to the extra domain A (EDA) of fibronectin or (2) the collagen binding A3 domain of von Willebrand factor fused to serum albumin (CBD-SA) (**Fig. 2.1**). EDA is an alternatively spliced domain of fibronectin that has been shown to be over-expressed in the neo-vasculature or stroma of many aggressive solid tumors but is absent in most normal tissues, making this a promising candidate for targeting our vaccine [51,132,133]. We decided to use previously isolated anti-EDA antibody fragments that have been shown to selectively bind neo-vascular structures in a variety of tumor types and to preferentially localize to tumor tissue after intravenous injection [50]. CBD-SA combines the active tumor targeting mechanisms of CBD binding to collagen I and III within the tumor [74] and the passive targeting mechanisms of SA [134]. Thus, these proteins serve as a means to localize our adjuvant to the tumor and then slow adjuvant drainage through the tumor as the proteins bind their ligand in the tumor microenvironment.

2.3 Results

2.3.1 Design and characterization of ECM-binding polymeric glyco-adjuvant conjugates

We first produced both murine CBD-SA and a murinized version of the anti-EDA Fab (containing murine variable regions and human constant regions) recombinantly and then chemically linked p(Man-TLR7) to free amines on either protein using our previously published conjugation strategy and bifunctional bicyclononyne (BCN) linker (**Fig. 2.2, A-D**) [97]. For each step of conjugation, we observe consistent shifts in protein mobility via sodium dodecyl sulfate-polyacrylamide gel electrophoresis (SDS-PAGE) that correspond with increasing overall molecular weight of our material following the reaction of protein to linker and protein-linker to

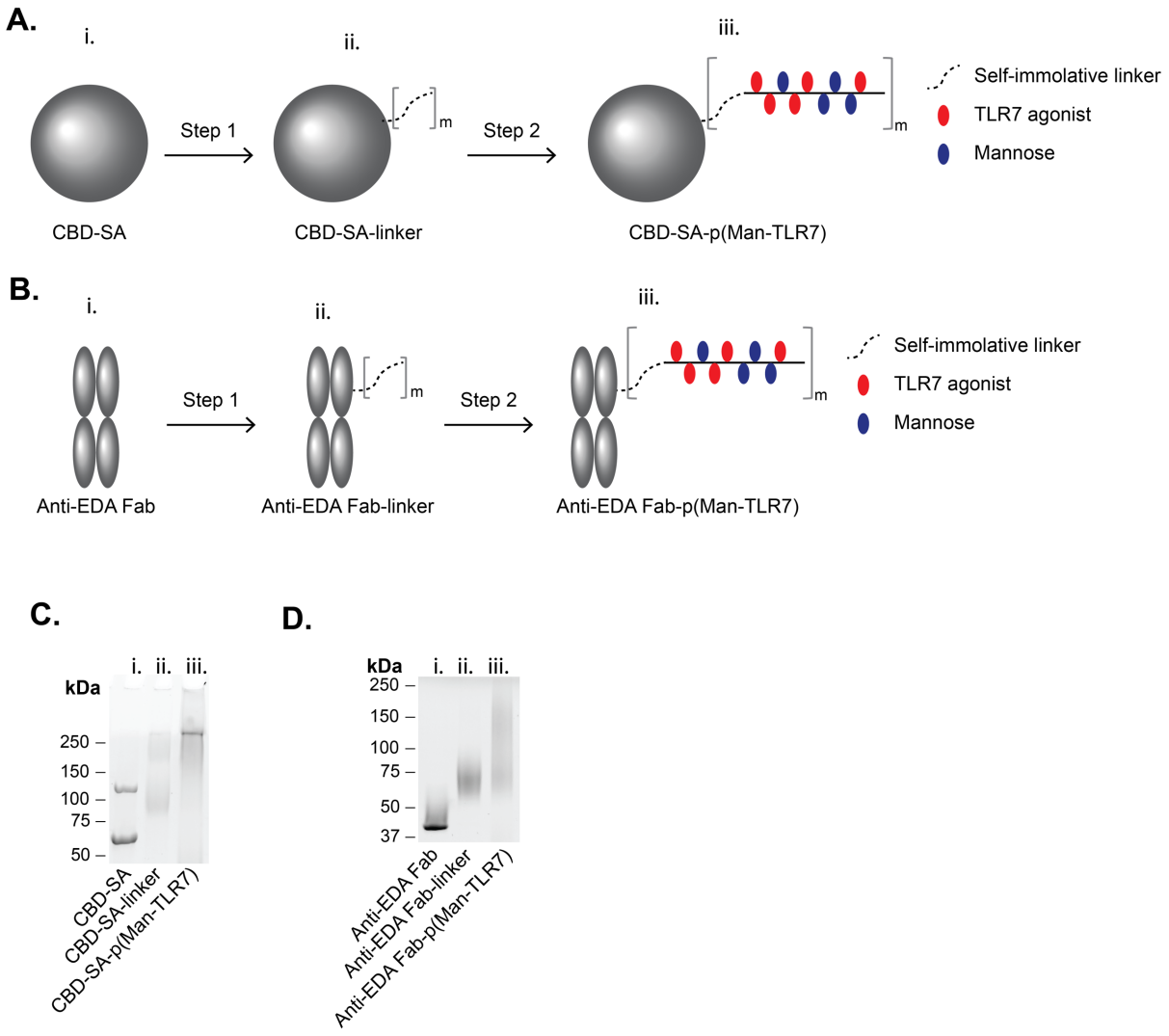

Figure 2.2: Conjugation of CBD-SA anti-EDA Fab to p(Man-TLR7).

(**A**) CBD-SA-p(Man-TLR7) is composed of murine CBD-SA (i.) conjugated, via a self-immolative linker (ii.), to a random copolymer (p(Man-TLR7)) synthesized from monomers that either activate TLR7 (red ovals) or target mannose-binding C-type lectins (blue ovals; iii.). (**B**) Anti-EDA Fab-p(Man-TLR7) is composed of murinized anti-EDA Fab (i.) conjugated to p(Man-TLR7) (ii., iii.). (**C and D**) SDS-PAGE analysis of CBD-SA (C) or anti-EDA Fab (D) before (i.) and after the two step conjugation reaction (ii., iii.).

p(Man-TLR7) (**Fig. 2.2, C and D**). Production of these protein-p(Man-TLR7) conjugates is reproducible and allows for the consistent generation of vaccine materials with little variability.

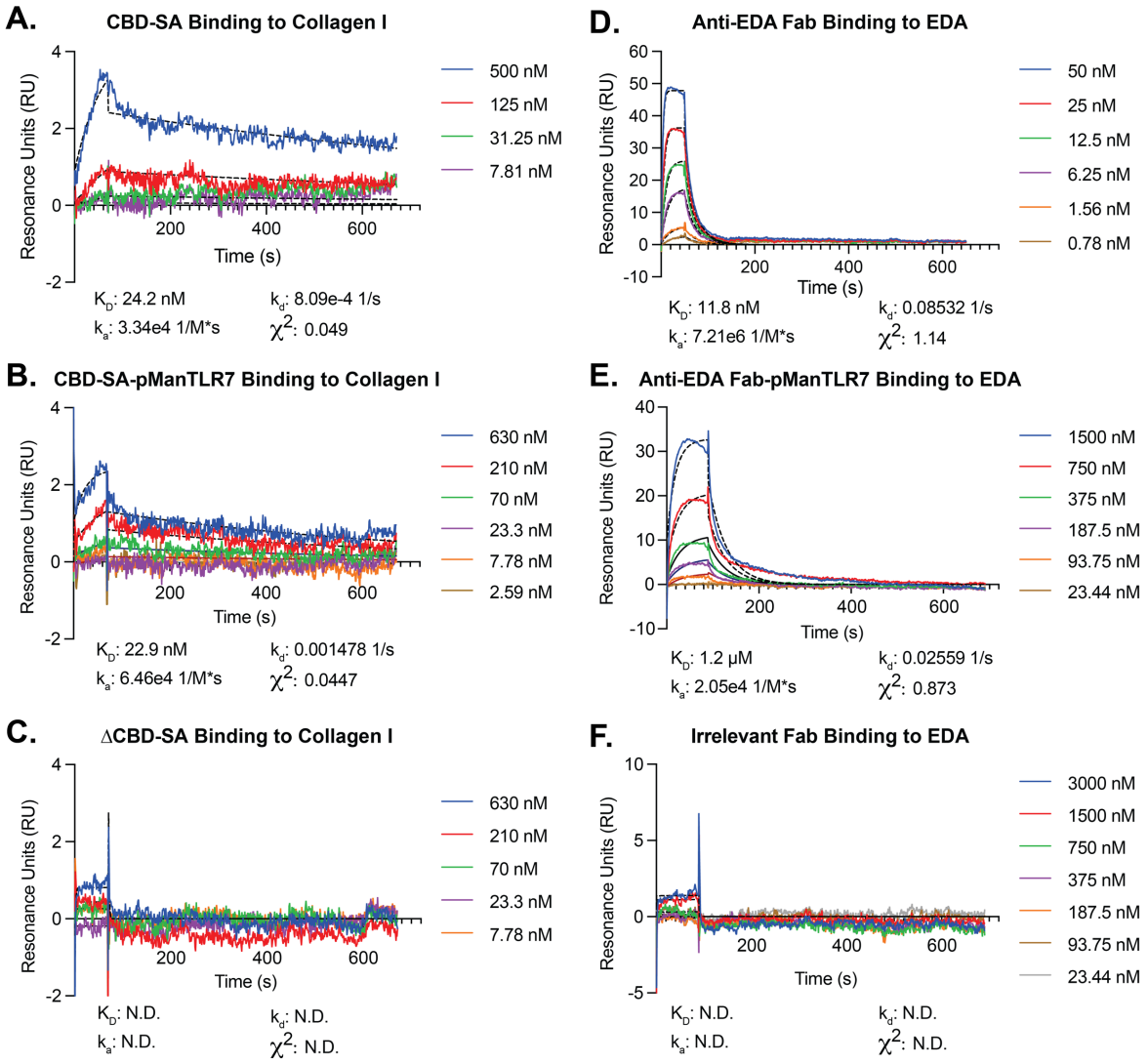

Figure 2.3: p(Man-TLR7) conjugates retain binding to their ligands.

(**A-C**) Characterization of the binding between (A) CBD-SA, (B) CBD-SA-p(Man-TLR7), or (C) ΔCBD-SA and human collagen I via Surface Plasmon Resonance (SPR). (**D-F**) Characterization of the binding between (D) anti-EDA Fab, (E) anti-EDA Fab-p(Man-TLR7), or (F) irrelevant Fab and EDA via SPR. The graphs represent the real-time binding profile for each antigen and calculated K_D, k_a, k_d and χ^2.

Following conjugation, we assessed the ability of the conjugates to bind to their target proteins via surface plasmon resonance (SPR; **Fig. 2.3, A-F**). In the case of CBD-SA-p(Man-TLR7), we observed a similar K_D for binding to human collagen I before and after conjugation to p(Man-TLR7) (24.2 nM and 22.9 nM, respectively; **Fig. 2.3, A and B**). We also assessed the

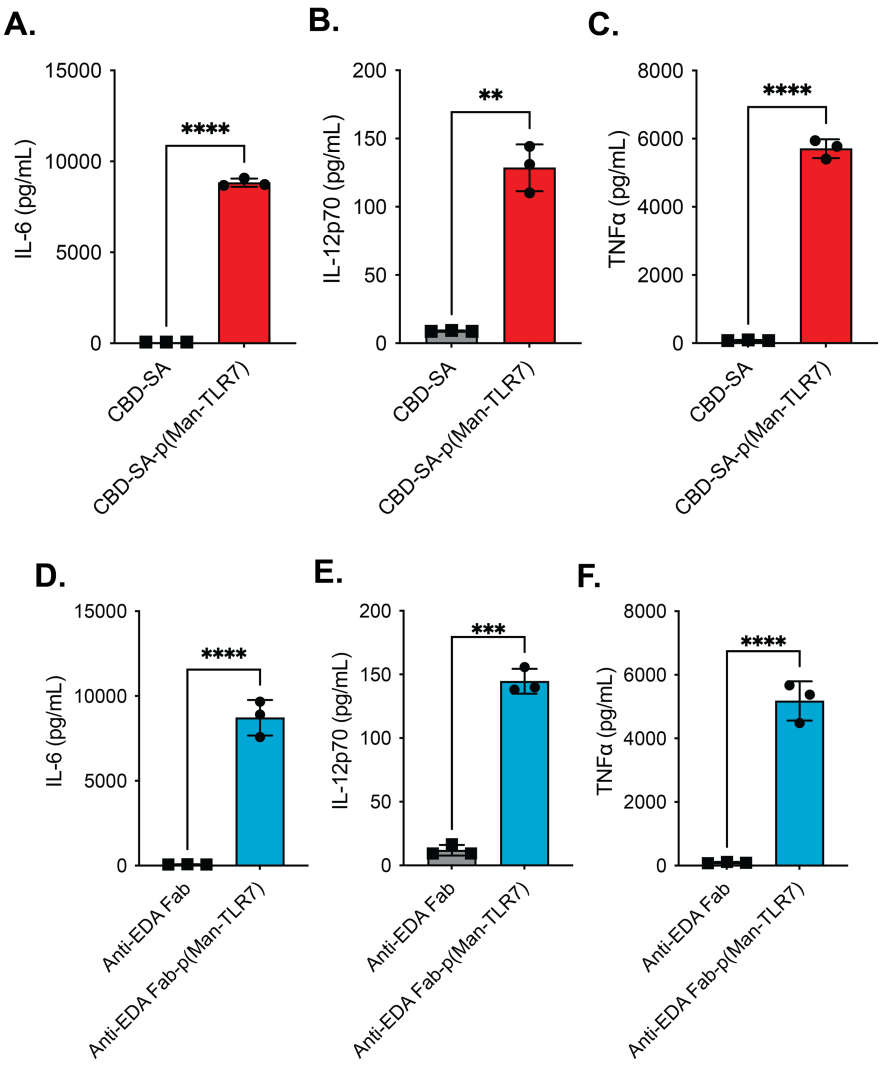

Figure 2.4: CBD-SA- and anti-EDA Fab-p(Man-TLR7) are potent activators of BMDCs.

(**A-F**) Concentration of IL-6 (A and D), IL-12p70 (B and E), and TNFα (C and F) in the supernatant of BMDCs stimulated for 18h with either CBD-SA, CBD-SA-p(Man-TLR7), anti-EDA Fab, or anti-EDA Fab-p(Man-TLR7) at the concentration corresponding to 12.5 μM (A and D) or 50 μM (B, C, E, and F) of the adjuvant, as determined by ELISA. Columns and error bars indicate mean±SD; statistical comparisons are based on one-way ANOVA with Tukey's post-test: **p<0.01,***p<0.001, ****p<0.0001.

collagen I binding ability of a variant of CBD-SA which contains several point mutations within the CBD that have been reported to abrogate binding to collagen (termed ΔCBD-SA) [135,136]. ΔCBD-SA did not exhibit any detectable affinity for collagen I (**Fig. 2.3C**). In the case of anti-EDA Fab-p(Man-TLR7), although we observe about a 100 fold decrease in K_D after conjugation

(11.8 nM before conjugation, as opposed to 1.2 μM after conjugation), ligand-specific binding is still observed (**Fig. 2.3, D and E**). Additionally, we did not observe any detectable binding to EDA for an irrelevant control Fab, which binds the xenoantigen outer surface protein A from *Borrelia burgdorferi* (**Fig. 2.3F**) [137].

Lastly, we observed that the protein-p(Man-TLR7) conjugates both retained the ability to activate bone marrow-derived dendritic cells (BMDCs) *in vitro*, as seen by the secretion of the immunostimulatory cytokines IL-6, IL-12p70, and TNFα by stimulated BMDCs (**Fig. 2.4, A-F**).

2.3.2 CBD-SA-p(Man-TLR7), but not anti-EDA Fab-p(Man-TLR7), exhibits prolonged intratumoral retention

We next asked whether our targeted protein-p(Man-TLR7) conjugates would be retained for longer within the tumor after intratumoral (i.t.) administration as compared to non-targeted protein-p(Man-TLR7) conjugates. To do this, we injected EMT6 tumor-bearing mice with a fluorescently labeled targeted or untargeted p(Man-TLR7) conjugate and used *in vivo* fluorescent imaging (IVIS) to assess retention within the tumor. CBD-SA-p(Man-TLR7) was compared to ΔCBD-SA-p(Man-TLR7), and anti-EDA Fab-p(Man-TLR7) was compared to irrelevant Fab-p(Man-TLR7), as neither ΔCBD-SA nor the irrelevant Fab exhibited binding to the ECM components of interest (**Fig. 2.3, C and F**). In the case of CBD-SA-p(Man-TLR7), we observed a significant improvement in intratumoral half-life as compared to ΔCBD-SA-p(Man-TLR7) (**Fig. 2.5, A and B**). However, in the case of anti-EDA Fab-p(Man-TLR7), we did not observe any difference in the intratumoral half-life between the anti-EDA and irrelevant Fabs conjugated to p(Man-TLR7) (**Fig. 2.5, A and B**).

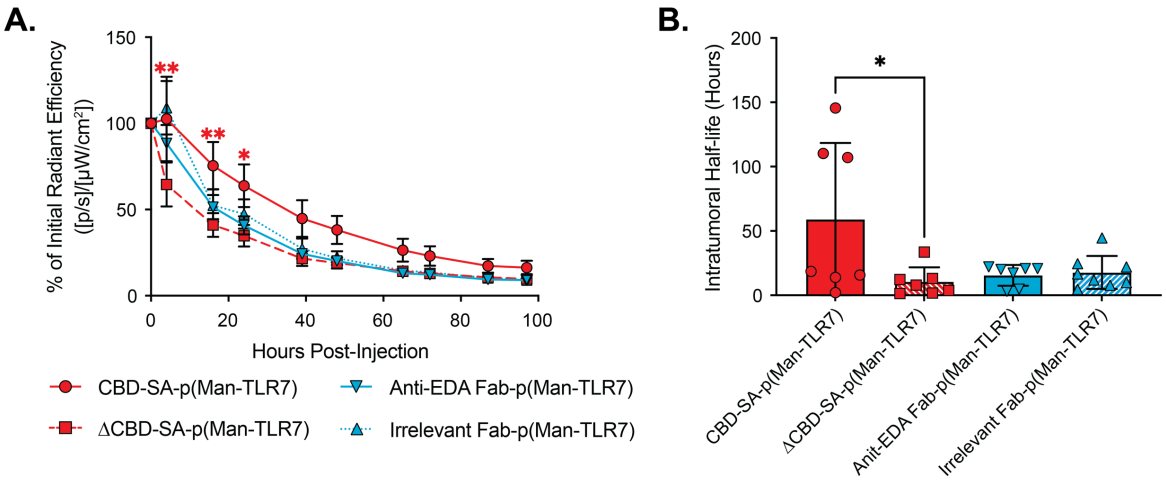

Figure 2.5: CBD-SA-p(Man-TLR7) but not anti-EDA Fab-p(Man-TLR7) shows enhanced intratumoral retention compared to untargeted conjugates.

(**A and B**) EMT6 tumor-bearing mice were injected with fluorescently labeled CBD-SA-p(Man-TLR7), ΔCBD-SA-p(Man-TLR7), anti-EDA Fab-p(Man-TLR7), or irrelevant Fab-p(Man-TLR7) 14 days after tumor inoculation. Mice were then imaged via an IVIS In Vivo imaging system starting immediately after injection. (A) Loss of tumor fluorescence was calculated as % of initial total radiant efficiency. Error bars indicate mean±SEM. (B) Intratumoral half-life was calculated using one phase exponential decay curve fitting. Columns and error bars indicate mean±SEM. Statistical comparisons are based on (A) two-way ANOVA (between CBD-SA- and ΔCBD-SA-p(Man-TLR7) or (B) one-way ANOVA with Tukey's post-test: *$p<0.05$, **$p<0.01$.

2.3.3 Vaccination with p(Man-TLR7) conjugates slows tumor growth and results in improved survival in the B16F10 murine melanoma model

We next wanted to assess the *in vivo* efficacy of both of our p(Man-TLR7) conjugates, even though we only saw prolonged intratumoral retention with CBD-SA-p(Man-TLR7). We decided to first assess efficacy in the B16F10 murine melanoma model, which responds poorly to checkpoint blockade therapy alone [74,85,138]. Despite checkpoint blockade being ineffective as a monotherapy in treating B16F10 tumors, we hypothesized that our vaccines would achieve maximal therapeutic efficacy when combined with checkpoint blockade therapy, as this could help overcome T regulatory cell (T_{reg}) or PD-L1-mediated immunosuppression

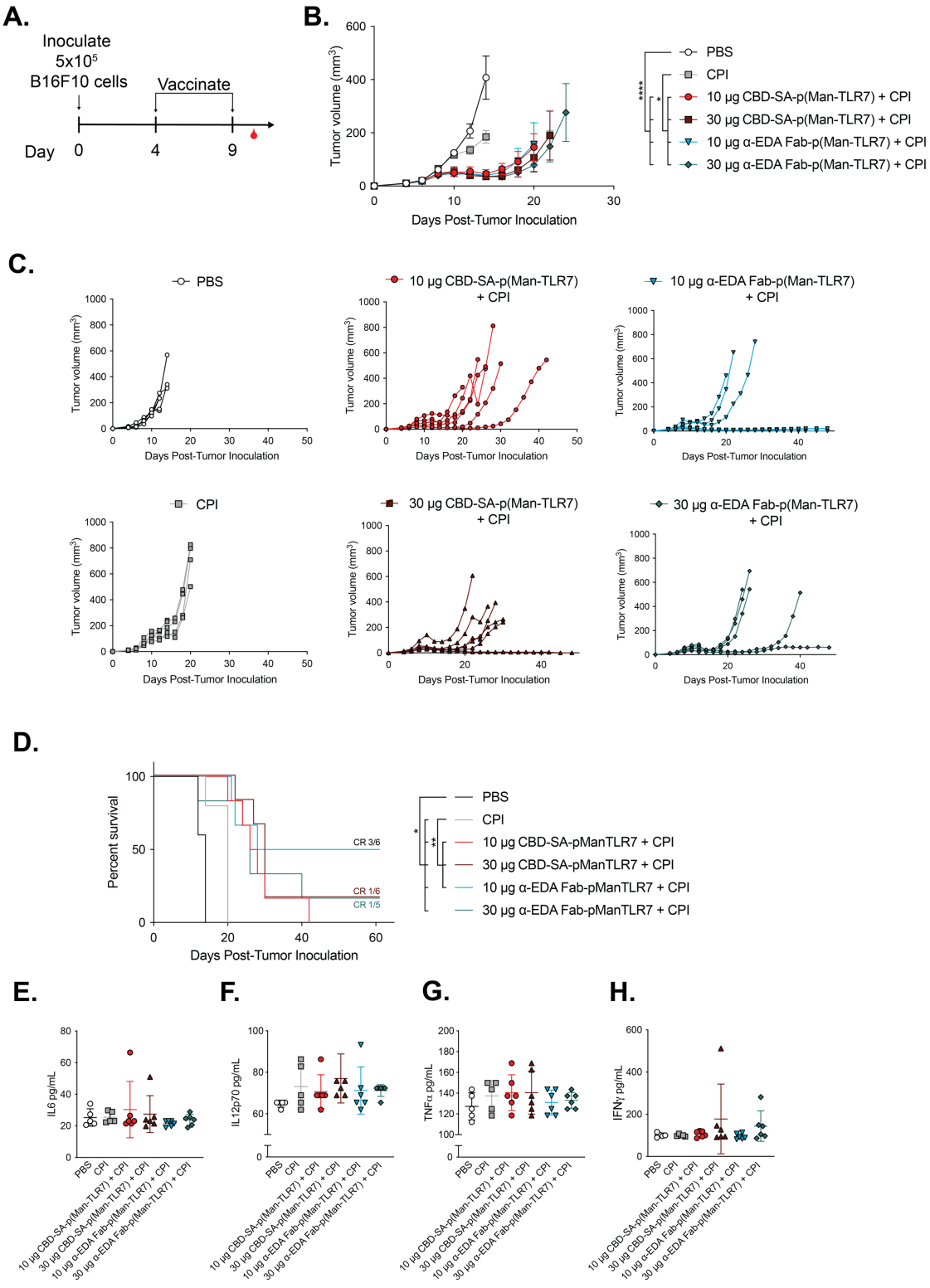

Figure 2.6: Dose study for CBD-SA-p(Man-TLR7) and anti-EDA Fab-p(Man-TLR7).

(Continued on next page)

Fig. 2.6 Cont: (**A**) Mice (n = 5-6) were inoculated with 500,000 B16F10 cells on day 0 and vaccinated at days 4 and 9 post-tumor inoculation with 10 or 30 μg of TLR7 as CBD-SA-p(Man-TLR7) or anti-EDA Fab-p(Man-TLR7) in combination with anti-PD-1 + anti-CTLA-4 antibodies (CPI, 100 μg of each). p(Man-TLR7) conjugates were administered intratumorally. CPI was administered intraperitoneally. Mice that received CPI only, as indicated in the figure, also received intratumoral PBS. (**B**) Tumor volumes over time [mean ± SEM]. (**C**) Tumor volumes over time for all mice individually. (**D**) Percent survival until endpoint. (**E-H**) Blood was collected 11 days post-tumor inoculation, and levels of IL-6 (E), IL-12p70 (F), TNFα (G), and IFNγ (H) in the serum were assessed by ELISA. Columns and error bars indicate mean±SD. Log-rank (Mantel-Cox) test was performed for survival curves. Statistical analysis on tumor growth curves was done using one-way ANOVA followed by Tukey's multiple comparisons test at day 12: *p<0.05, **p<0.01, ****p<0.0001.

within the tumor, mechanisms by which tumors avoid immune recognition and desctruction. As a result, we first performed a dose study, looking at two different doses of each vaccine in combination with both anti-PD-1 and anti-CTLA-4 checkpoint inhibitors (CPI) in order to have the highest chance at observing a therapeutic benefit in this study (**Figure 2.6, A-H**). Both p(Man-TLR7) conjugates in combination with CPI resulted in a significant slowing of tumor growth (**Fig. 2.6, B and C**) and improved survival (**Fig. 2.6D**). Both doses tested, 10 μg and 20 μg TLR7, showed anti-tumor efficacy, and significant differences between the two doses were not observed for either conjugate in terms of slowing of tumor growth (**Fig. 2.6, B and C**), improvement in survival (**Fig. 2.6D**), or expression of systemic inflammatory cytokines, included here as a potential indicator of toxicity (**Fig. 2.6, E-H**). As a result, we decided to proceed with the lower dose of 10 μg TLR7.

After choosing an optimal dose, we next wanted to further investigate treatment of B16F10 tumors with our vaccines in combination with CPI in order to determine if synergy is observed between these two treatment approaches. Upon vaccination of B16F10 tumor-bearing mice with CBD-SA-p(Man-TLR7) or anti-EDA Fab-p(Man-TLR7) alone via i.t. administration, we only observed a modest slowing of tumor growth that was not significant (**Fig. 2.7, A-C**).

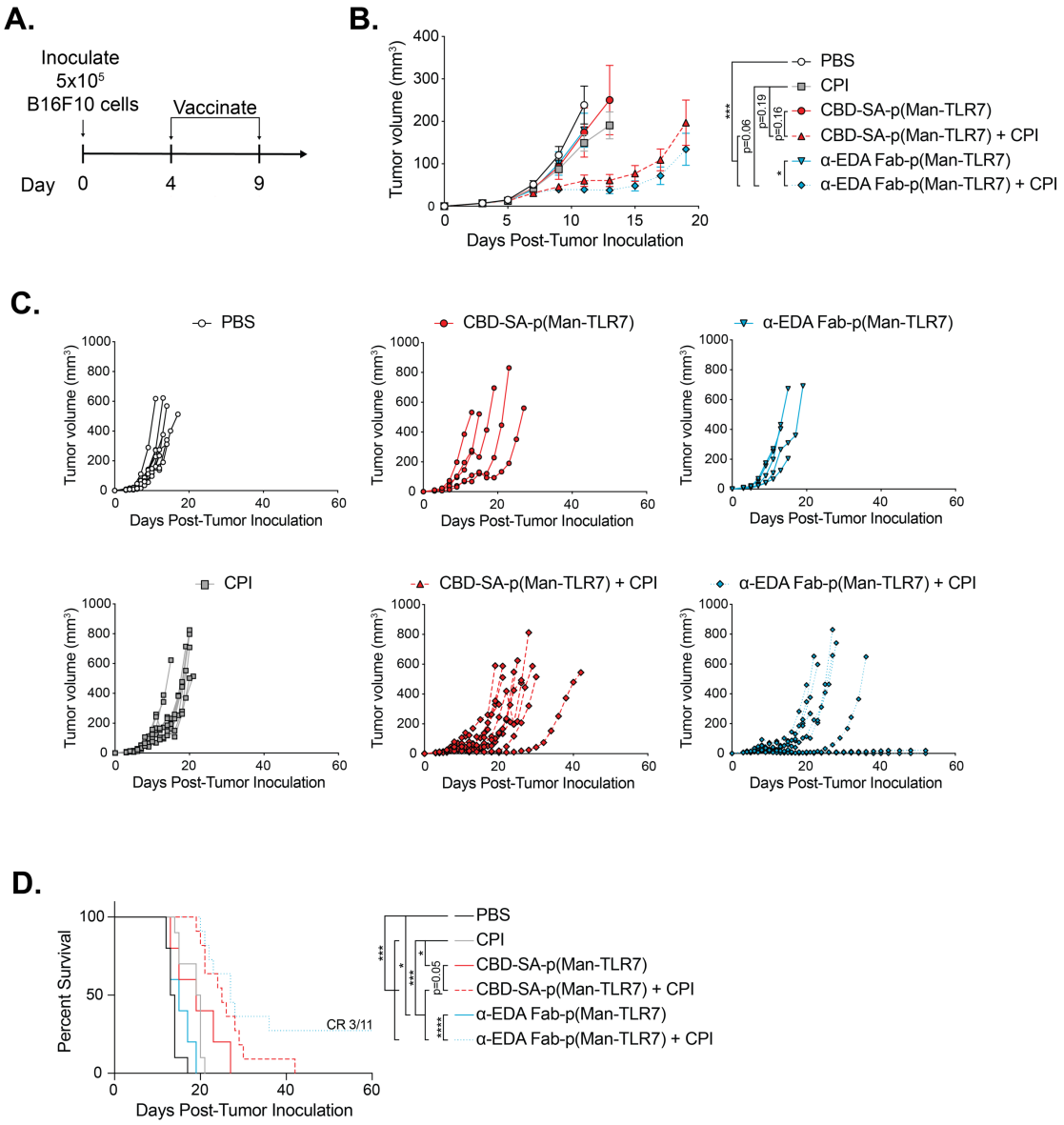

Figure 2.7: Both p(Man-TLR7) vaccine conjugates synergize with checkpoint blockade to significantly slow tumor growth and enhance survival of B16F10 tumor-bearing mice.

(**A**) Mice (n = 6-11) were inoculated with 500,000 B16F10 cells on day 0 and vaccinated at days 4 and 9 post-tumor inoculation with 10 μg of TLR7 as CBD-SA-p(Man-TLR7) or anti-EDA Fab-p(Man-TLR7), alone or in combination with anti-PD-1 + anti-CTLA-4 antibodies (CPI, 100 μg of each). p(Man-TLR7) conjugates were administered intratumorally. CPI was administered intraperitoneally. Mice that received CPI only, as indicated in the figure, also received intratumoral PBS. (**B**) Tumor volumes over time [mean ± SEM]. (**C**) Tumor volumes over time for all mice individually. (**D**) Percent survival until endpoint. Data were pooled from two independent experiments. Log-rank (Mantel-Cox) test was performed for survival curves. Statistical analysis on tumor growth curves was done using one-way ANOVA followed by Tukey's multiple comparisons test at day 11: *p<0.05, ***p<0.001, ****p<0.0001.

However, we observed a significant slowing of tumor growth when targeted-p(Man-TLR7) was combined with anti-PD-1 and anti-CTLA-4 antibodies (**Fig. 2.7, B and C**). Likewise, we observed the greatest improvement in survival when our vaccines were combined with checkpoint blockade therapy (**Fig. 2.7D**). Based on these results, we concluded that i.t. administered CBD-SA-p(Man-TLR7) and anti-EDA Fab-p(ManTLR7) synergize with checkpoint blockade therapy, resulting in therapeutic benefit in treating this poorly immunogenic tumor model.

2.3.4 Matrix-targeted p(Man-TLR7) conjugates control and eradicate EMT6 tumors

After the promising results in the B16F10 melanoma model, we wanted to test our vaccines in an additional tumor model and decided to use the EMT6 breast cancer model, as this is an immune-excluded, or cold, tumor model [74,139]. Here, we vaccinated mice twice intratumorally with CBD-SA-p(Man-TLR7) or anti-EDA Fab-p(Man-TLR7) alone or in combination with anti-PD-1 (**Fig. 2.8A**). We observed the greatest slowing of tumor growth (**Fig. 2.8, B and C**) and significantly improved survival (**Fig. 2.8D**) when both of our vaccines were combined with checkpoint blockade therapy, as observed previously with the B16F10 tumor model. Additionally, CBD-SA-p(Man-TLR7) in combination with anti-PD-1 resulted in 8 out of 11 mice exhibiting a complete response, while 4 out of 11 mice treated with anti-EDA Fab-p(Man-TLR7) with anti-PD-1 exhibited a complete response. This result suggests that collagen-targeted p(Man-TLR7) plus anti-PD-1 may be more effective than EDA-targeted p(Man-TLR7) plus anti-PD-1 ($p = 0.21$). Lastly, all mice exhibiting a complete response from this experiment were rechallenged with a second inoculation of EMT6 cells in the contralateral mammary fat pad. Compared with naïve control mice that were inoculated with EMT6 cells, which all developed tumors, no mice that had cleared their tumor from the previous experiment

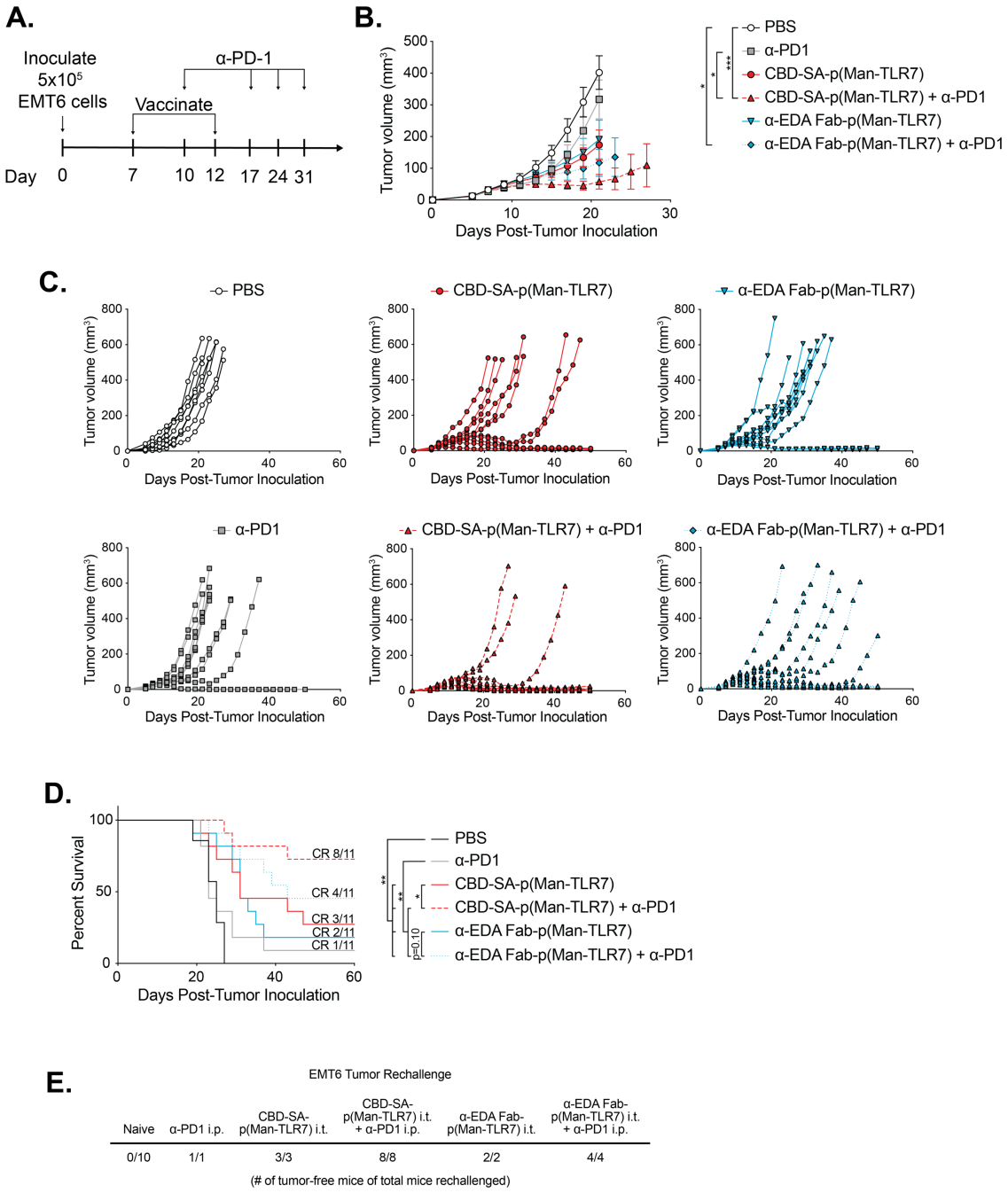

Figure 2.8: Vaccination of EMT6 tumor-bearing mice results in long-lasting anti-tumor memory-responses.

(**A**) Mice (n = 8-11) were inoculated with 500,000 EMT6 cells on day 0 and vaccinated at days 7 and 12 post-tumor inoculation with 10 µg of TLR7 as CBD-SA-p(Man-TLR7) or anti-EDA Fab-p(Man-TLR7). For the groups indicated, mice received an anti-PD-1 antibody (100 µg) starting at day 10 and every 7 days thereafter until day 31. Additional groups assessed include a PBS group, as well as a group only receiving anti-PD-1. The anti-PD-1 antibody was injected intraperitoneally. Other treatments were administered intratumorally. (Continued on next page)

Fig. 2.8, continued: Mice that received anti-PD-1 only also received intratumoral PBS. (**B**) Tumor volumes over time [mean ± SEM]. (**C**) Tumor volumes over time for all mice individually. (**D**) Percent survival until endpoint. (**E**) Surviving mice were re-challenged with 500,000 EMT6 cells, injected in the contralateral mammary fat pad (as compared to the initial tumor inoculation), at day 127 after the initial tumor injection. Tumor growth was monitored, and the number of mice that remained tumor free is listed in the table out of the number that were rechallenged (# tumor free/total # rechallenged). Data were pooled from two independent experiments. Log-rank (Mantel-Cox) test was performed for survival curves. Statistical analysis on tumor growth curves was done using one-way ANOVA followed by Tukey's multiple comparisons test at day 21: *p<0.05, **p<0.01, ***p<0.001.

developed a tumor after the rechallenge, illustrating that our vaccines are able to induce long-term immunologic memory (**Fig. 2.8E**).

2.3.5 CBD-SA-p(Man-TLR7) vaccination increases the proportion of CD8$^+$ effector T cells in the tumor and does not increase exhaustion of T cells

We next wanted to begin to understand the immunological mechanisms behind the observed anti-tumor efficacy. Because of the importance of T cell responses in treating tumors, we first looked at the T cell responses within the tumor, tumor-draining lymph nodes, and spleens of vaccinated mice. Here, we decided to return to the B16F10 melanoma model due to the efficacy we observed previously (**Fig. 2.7**), as well as the availability of various tools that would allow us to further characterize the T cell response. We further decided to focus here on only CBD-SA-p(Man-TLR7) due to the superior tumor retention observed (**Fig. 2.5**), as well as the trend toward improved survival of EMT6 tumor-bearing mice vaccinated with CBD-SA-p(Man-TLR7) plus anti-PD-1, as compared to anti-EDA Fab-p(Man-TLR7) plus anti-PD-1 (**Fig. 2.8D**). Additional control groups consisting of an unconjugated mixture of CBD-SA and p(Man-TLR7) with or without CPI (anti-PD-1 and anti-CTLA-4) were added here, in order to analyze the effect that targeting the p(Man-TLR7) polymer to the ECM has on the cellular responses in vaccinated mice. Mice were vaccinated at days 4 and 9 post-B16F10 tumor inoculation and

euthanized at day 10, at which time the tumor, tumor-draining lymph nodes, and spleen were harvested for flow cyotmetric analysis (**Fig. 2.9A; Fig. A.1a**). Within the tumor, no significant differences were observed in $CD4^+$ T cells, and few differences were observed in the lymph nodes and spleen (**Fig. 2.9, B-D**). However, significant increases in the proportions of $CD8^+$ T cells and $CD8^+$ effector T cells were observed in the tumors of mice treated with CBD-SA-p(Man-TLR7) plus CPI (**Fig. 2.9B**). In the draining lymph nodes of CBD-SA-p(Man-TLR7) plus CPI treated mice, a trend towards a decrease in the percentage of total $CD8^+$ T cells and a significant decrease in the percentage of $CD8^+$ effector T cells were observed, potentially pointing towards a migration of these cells from the lymph nodes to the tumor (**Fig. 2.9C**). Conversely, no change in the proportion of $CD8^+$ T cells but an increase in the proportion of $CD8^+$ effector T cells was observed in the spleen (**Fig. 2.9D**).

We next looked at TOX expression on $CD8^+$ T cells. TOX is a transcription factor that drives a transcriptional program that is associated with T cell exhaustion and dysfunctional intratumoral T cells (T cells that are unable to produce effector cytokines and express increased levels of inhibitory receptors) [140,141]. In mice treated with CPI alone, there was a trend toward increased proportions of TOX^+ $CD8^+$ T cells in the tumor and draining lymph nodes, as compared to saline-treated control mice (**Fig. 2.9, B and C**). This same increase in proportions of TOX^+ $CD8^+$ T cells was not observed in the other treated groups (**Fig 2.9, B and C**). Significant differences were not seen in the spleen for any groups (**Fig.2.9D**).

2.3.6 Antigen-specific immune responses are observed in the tumor and tumor draining lymph nodes following vaccination

The next question we wanted to answer was whether the observed T cell responses are antigen-specific. To answer this question in the tumor, we stained cells (from **Fig. 2.9**) with a

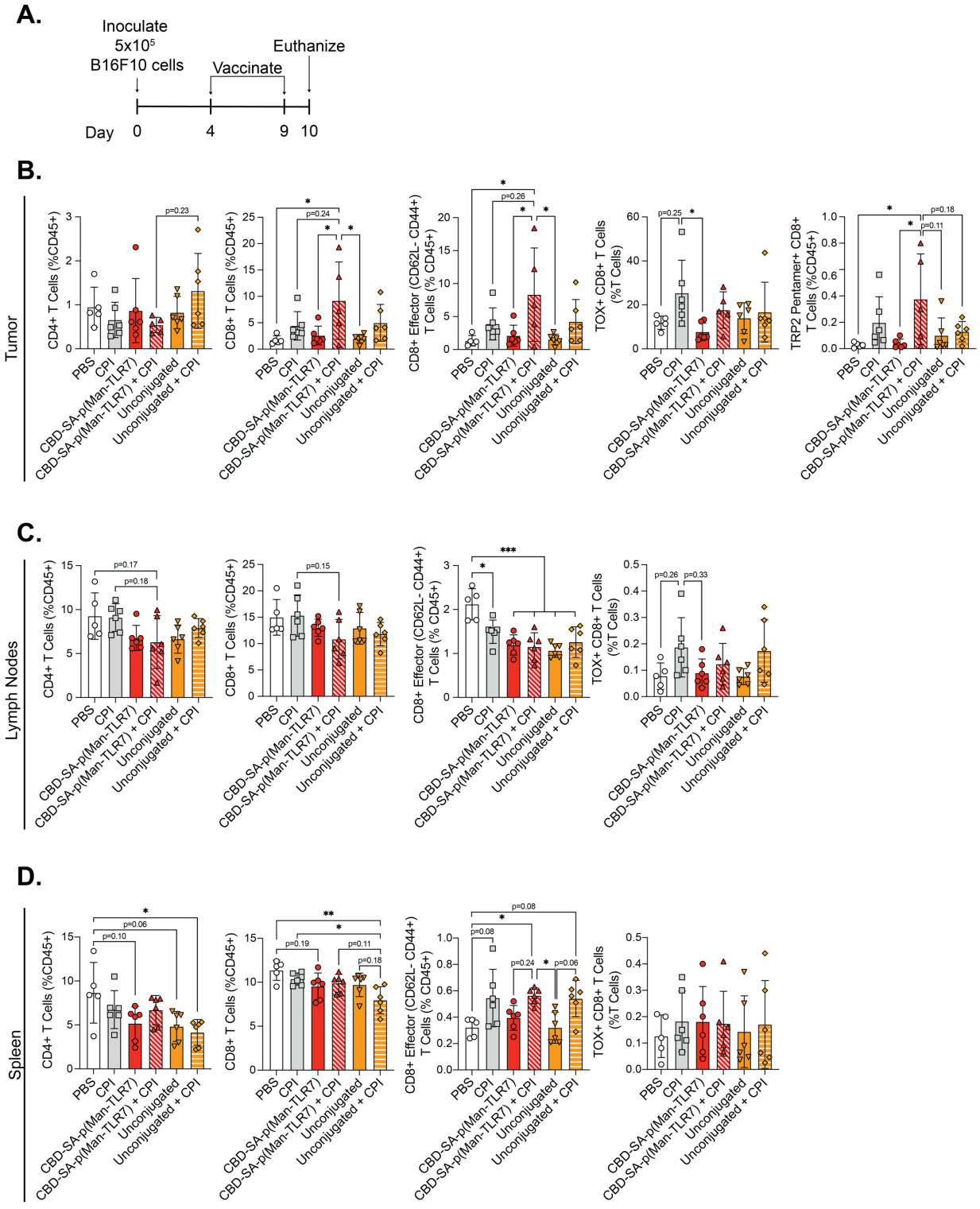

Figure 2.9: CBD-SA-p(Man-TLR7) vaccination increases the number of CD8$^+$ effector T cells in the tumor and does not increase the exhaustion of CD8$^+$ T cells in the tumor, lymph nodes, or spleen.

(Continued on next page)

Fig. 2.9, continued: (**A**) Mice (n = 5-6) were inoculated with 500,000 B16F10 cells on day 0 and vaccinated at days 4 and 9 post-tumor inoculation with 10 μg of TLR7 as CBD-SA-p(Man-TLR7) or an unconjugated mixture of CBD-SA and p(Man-TLR7). Both of these formulations were tested alone or in combination with anti-PD-1 + anti-CTLA-4 antibodies (CPI, 100 μg of each). Additional groups included mice injected with PBS only and mice injected with CPI (plus intratumoral PBS). CPI was administered intraperitoneally. All other treatments were administered intratumorally. Mice were then euthanized at day 10, and the tumor, tumor-draining lymph nodes, and spleen were harvested for analysis. (**B-D**) Flow cytometric analysis on the (B) tumor, (C) tumor-draining lymph nodes, and (D) spleen of vaccinated mice. Cell types are defined as follows: $CD4^+$ T cells: $CD45^+ CD3^+ CD4^+$; $CD8^+$ T cells: $CD45^+ CD3^+ CD8^+$; $CD8^+$ effector T cells: $CD45^+ CD3^+ CD8^+ CD62L^- CD44^+$; TOX^+ $CD8^+$ T cells: $CD45^+ CD3^+ CD8^+ TOX^+$; TRP2 pentamer$^+$ $CD8^+$ T cells: $CD45^+ CD3^+ CD8^+$ TRP2-pentamer$^+$. Columns and error bars indicate mean±SD. Statistical comparisons are based on one-way ANOVA with Tukey's post-test: *p<0.05, **p<0.01, ***p<0.001.

TRP2 pentamer (H-2K^b-SVYDFFVWL) in order to determine the proportions of $CD8^+$ T cells that are specific to TRP2, an endogenous B16F10 melanocyte antigen. We indeed observed an increase in the percentage of TRP2 pentamer$^+$ $CD8^+$ T cells in the tumors of mice treated with CBD-SA-p(Man-TLR7) + CPI (**Fig. 2.9B; Fig. A.1b**).

Next, to answer this question in the tumor draining lymph nodes, we restimulated cells from the lymph nodes *ex vivo* with a pool of two MHC-I-restricted peptides ($Trp2_{180-188}$ and $hgp100_{25-33}$) from proteins expressed in B16F10 tumors. Cells were restimulated for either 6 hours or 3 days, and then the expression of cytokines on $CD8^+$ T cells (after 6 hours) or the levels of cytokines secreted into the supernatant of cell culture media (after 3 days) were analyzed. After the six hour restimulation, a significantly increased percentage of IFNγ^+ $CD8^+$ T cells was observed in mice vaccinated with CBD-SA-p(Man-TLR7) plus CPI via flow cytometric analysis (**Fig. 2.10A; Fig. A.2**). Trends towards an increased proportion of TNFα^+ $CD8^+$ T cells and polyfunctional IFNγ^+ TNFα^+ CD8+ T cells were also observed in mice vaccinated with CBD-SA-p(Man-TLR7) plus CPI (**Fig. 2.10A**). An increase in polyfunctional T cells producing multiple effector cytokines points toward an improved functionality of these T

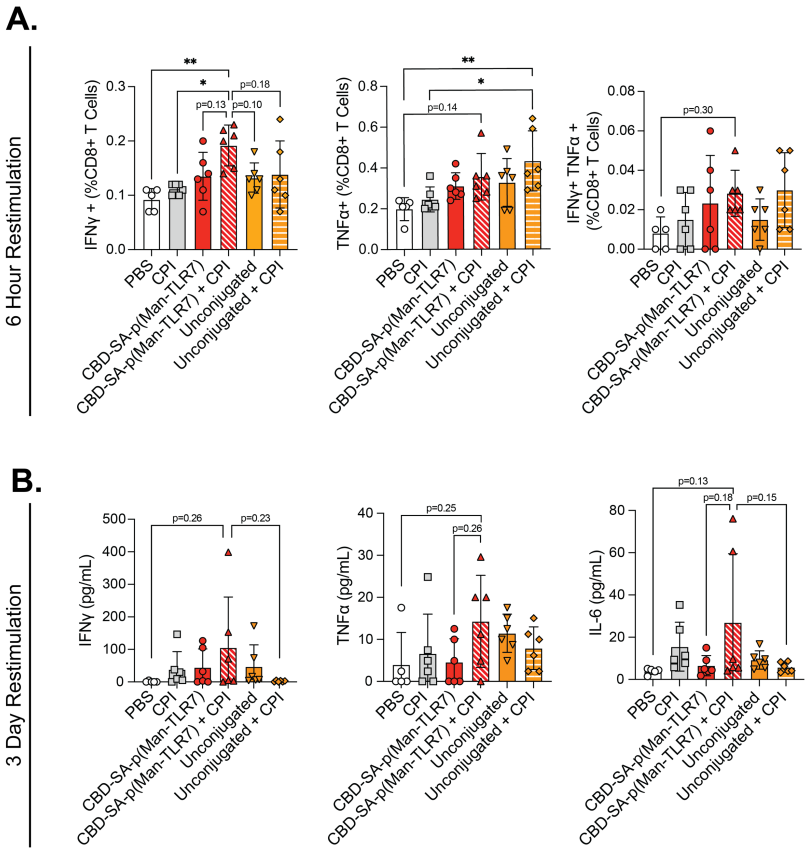

Figure 2.10: CBD-SA-p(Man-TLR7) induces antigen-specific T cell responses in the lymph nodes.

Cells from the tumor-draining lymph nodes of the mice from Fig. 2.9A were restimulated *ex vivo* with a pool of two B16F10 melanoma-associated peptides, mTRP-$2_{180\text{-}188}$ (SVYDFFVWL) and $hgp100_{25\text{-}33}$ (KVPRNQDWL), for either (**A**) 6 hours prior to flow cytometric analysis or (**B**) 3 days prior to multiplexed cytokine analysis. (A) Cytokine-producing $CD8^+$ T cell responses were detected by intracellular staining for IFNγ and TNFα and quantified by flow cytometry. $CD8^+$ T cells were defined as described in Fig. 2.9. (B) Production of IFNγ, TNFα, and IL-6 in the cell culture supernatant after 3 days of *ex vivo* restimulation, as quantified (in pg/mL) via LEGENDplex™ assay. Columns and error bars indicate mean±SD. Statistical comparisons are based on one-way ANOVA with Tukey's post-test: *p<0.05, **p<0.01.

cells, which is important in predicting therapeutic anti-tumor efficacy [142]. Interestingly, vaccination with the unconjugated mixture plus CPI generated a significant increase in the percentage of $TNF\alpha^+$ $CD8^+$ T cells but not $IFN\gamma^+$ $CD8^+$ T cells (**Fig. 2.10A**). Furthermore, the three day restimulation resulted in trends toward an increase in the secretion of IFNγ, TNFα, and

IL-6 from cells isolated from the lymph nodes of mice treated with CBD-SA-p(Man-TLR7) plus CPI (**Fig 2.10B**). These results from both of these assays point towards the induction of antigen-specific cellular immunity against two known B16F10 epitopes.

2.3.7 CBD-SA-p(Man-TLR7) vaccination increases the activation of CD103$^+$ DCs in the tumor

We also looked into differences in the myeloid cell populations within the tumor and tumor draining lymph nodes (**Fig. A.3**). No significant differences in the proportion of DCs are observed in the tumors or lymph nodes of mice vaccinated with CBD-SA-p(Man-TLR7) plus CPI as compared to saline or CPI alone (**Fig. 2.11, A and B**). In the tumor, the percentage of CD103$^+$ DCs is decreased relative to saline-treated control mice. However, of the CD103$^+$ DCs that are present, a significantly higher fraction of these cells express CD80 and there is a trend towards a higher fraction of CD86$^+$ CD103$^+$ DCs in mice vaccinated with CBD-SA-p(Man-TLR7)+CPI, as compared to PBS treated mice (**Fig. 2.11A**). Similar results are observed in the tumors of CPI-treated mice (**Fig. 2.11A**). CD103$^+$ DCs are cross-presenting DCs that play a critical role in the priming of CD8$^+$ T cell responses in order to mount anti-tumor immune responses [143]. This increase in activation observed in these cross-presenting cells within the tumor is very promising. This trend, however, is not observed in CD103$^+$ DCs or lymph node-resident CD8$^+$ DCs (which are also known to prime CD8$^+$ T cell responses [144]) within the draining lymph nodes (**Fig. 2.11, A and B**). Additionally, significant differences were not observed in the proportion of CD11b$^+$ DCs in the tumors or lymph nodes of mice vaccinated with CBD-SA-p(Man-TLR7) alone or with CPI as compared to saline or CPI alone, although there is a trend towards a decrease in these cells in the tumor (**Fig. 2.11, A and B**).

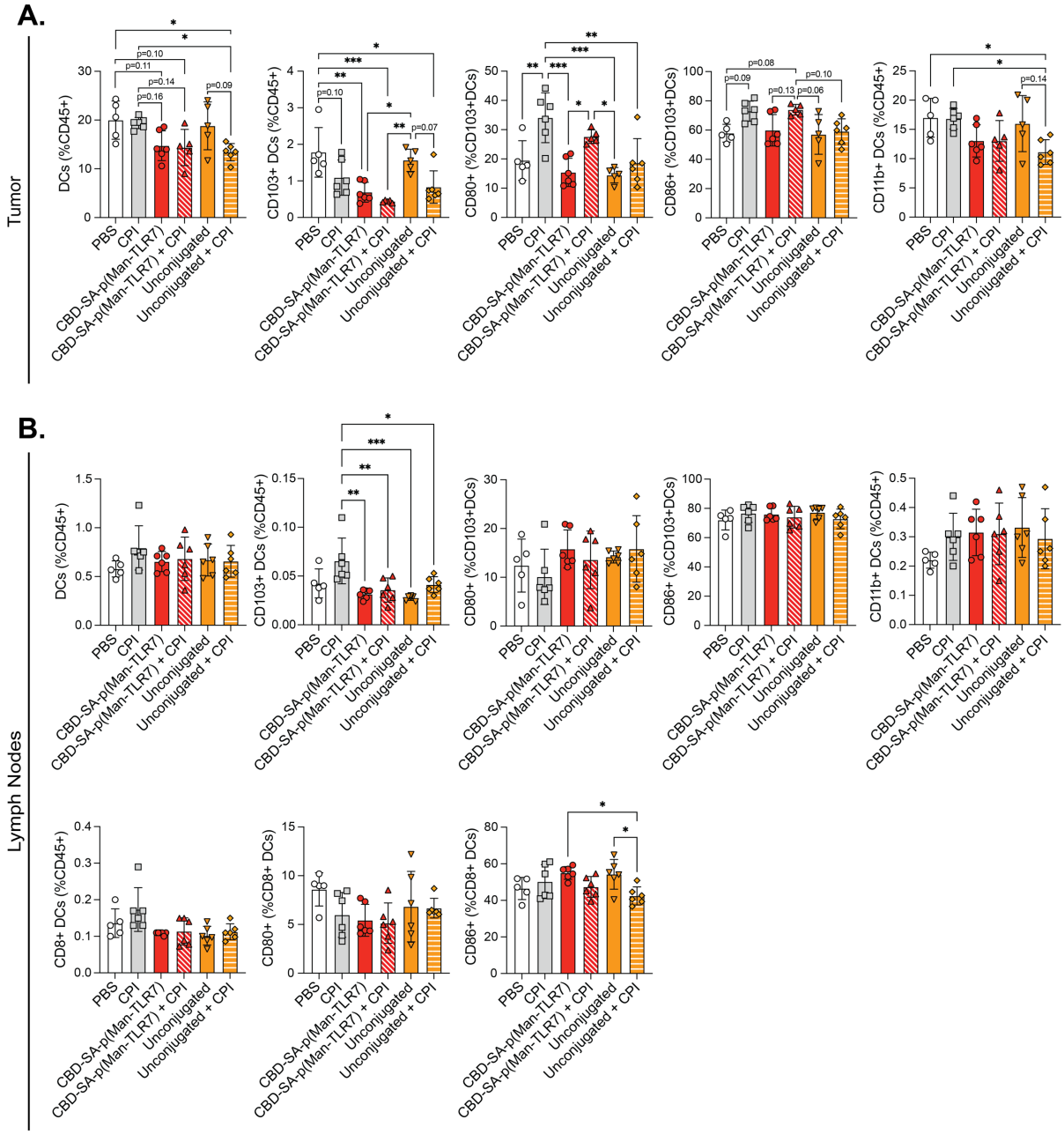

Figure 2.11: Vaccination with CBD-SA-p(Man-TLR7) increases the activation of CD103$^+$ DCs in the tumor.

(**A and B**) Flow cytometric analysis of DCs from the (A) tumors and (B) tumor-draining lymph nodes of mice from Fig. 2.9A. DCs are defined as follows: CD45$^+$ B220$^-$ MHCII$^+$ CDllc$^+$. DCs were further classified by expression of (A and B) CD103, (A and B) CD11b, and (B) CD8. Additionally, expression of the activation markers CD80 and CD86 was assessed on CD103$^+$ DCs and CD8$^+$ DCs. Columns and error bars indicate mean±SD. Statistical comparisons are based on one-way ANOVA with Tukey's post-test: *p<0.05, **p<0.01,***p<0.001.

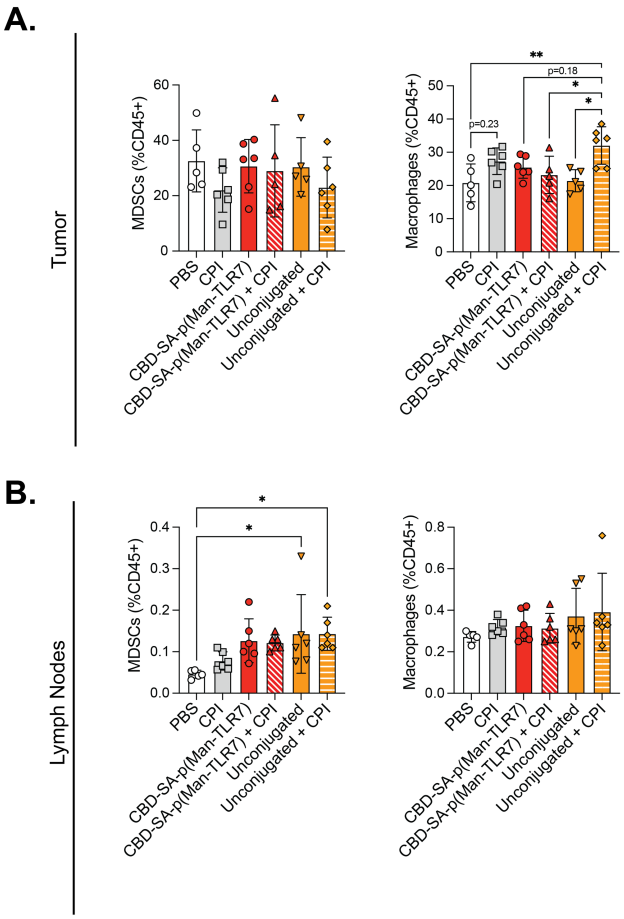

Figure 2.12: Few changes are observed in MDSC and macrophage numbers in the tumor and lymph nodes after vaccination.

(**A and B**) Flow cytometric analysis of MDSCs and macrophages from the (A) tumors and (B) tumor-draining lymph nodes of mice from Fig. 2.9A. Cell types are defined as follows: MDSCs: $CD45^+$ $B220^-$ $MHCII^-$; macrophages: $CD45^+$ $B220^-$ $MHCII^+$ $CD11c^-$ $CD11b^+$. Columns and error bars indicate mean±SD. Statistical comparisons are based on one-way ANOVA with Tukey's post-test: *p<0.05, **p<0.01.

Furthermore, we also looked at percentages of myeloid-derived suppressor cells (MDSCs) and macrophages within the tumor and lymph nodes of vaccinated mice. Significant changes in the proportions of these cells were not observed in mice vaccinated with CBD-SA-p(Man-TLR7) with or without CPI versus saline- or CPI-treated mice (**Figure 2.12, A and B**). Interestingly, however, in both the tumors and draining lymph nodes of mice vaccinated with CBD-SA-p(Man-TLR7) alone or in combination with CPI, an increase in PDL1 expression is observed in DCs,

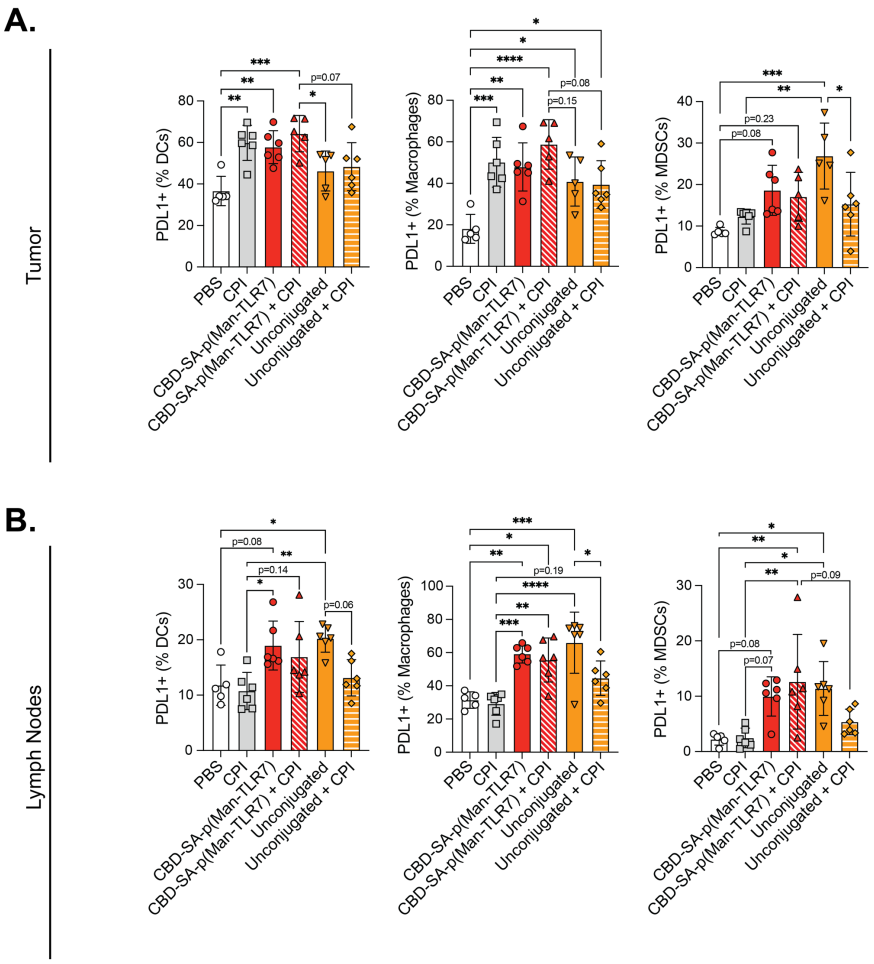

Figure 2.13: An increase in PDL1-expressing cells is observed across myeloid cell populations in both the tumor and lymph nodes of mice vaccinated with CBD-SA-p(Man-TLR7).

(**A and B**) PDL1 expression on DCs, macrophages, and MDSCs from the the (A) tumors and (B) tumor-draining lymph nodes of mice from Fig. 2.9A, as determined via flow cytometry. Cells types were defined as described in Fig. 2.11 and 2.12. Columns and error bars indicate mean±SD. Statistical comparisons are based on one-way ANOVA with Tukey's post-test: *p<0.05, **p<0.01,***p<0.001, ****p<0.0001.

macrophages, and MDSCs (**Fig. 2.13, A and B**). This increase in PDL1 expression could potentially point towards a mechanism behind the observed synergy between our vaccine and checkpoint blockade therapy that results in a therapeutic benefit.

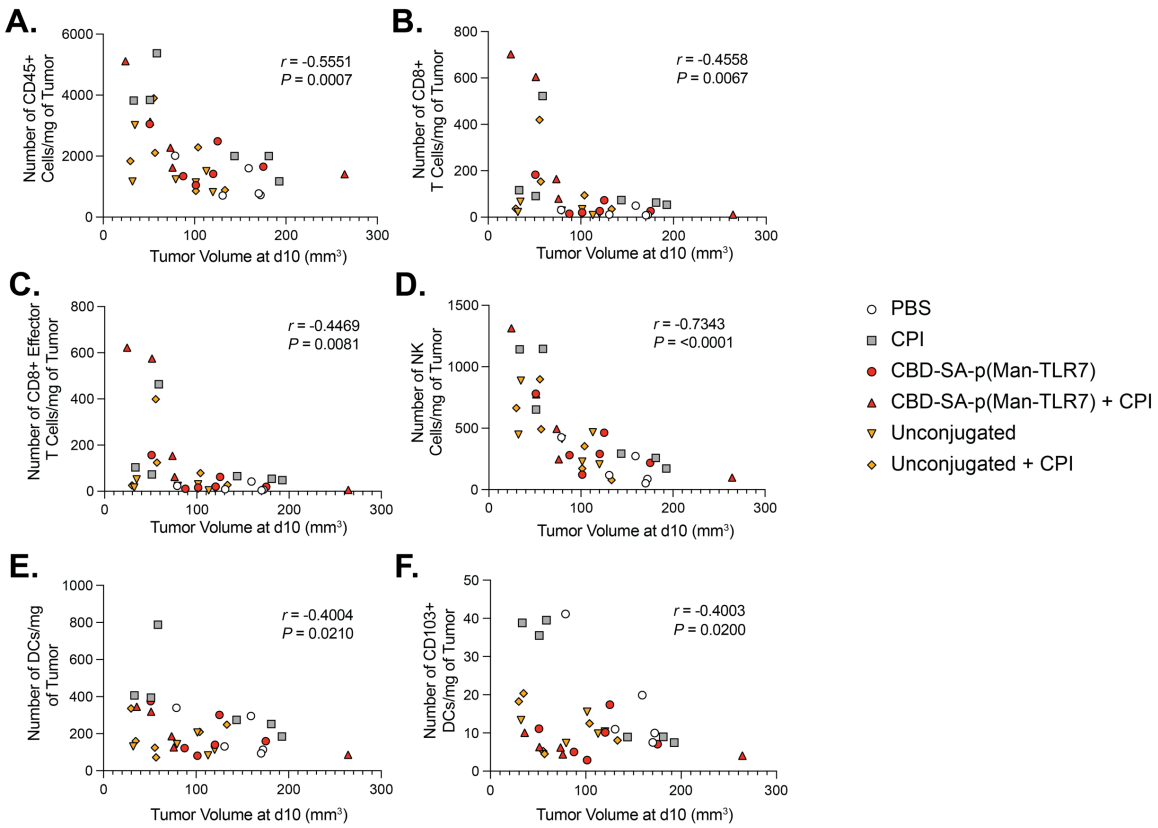

Figure 2.14: Immune cell infiltrates are negatively correlated with tumor growth.

(**A-F**) Linear regression analysis comparing the number of tumor-infiltrating cells with tumor volume was performed using the results obtained in Fig. 2.9, 2.11, and 2.12. Correlations between tumor volume at day 10 (d10) and the number per mg of tumor tissue of (A) $CD45^+$ cells, (B) $CD8^+$ T cells, (C) $CD8^+$ effector T cells, (D) natural killer (NK) cells, (E) DCs, or (F) $CD103^+$ DCs are shown. Previously mentioned cell types were defined as in Fig. 2.9, 2.11, and 2.12, and NK cells were defined as $CD45^+NK1.1^+CD3^-$.

2.3.8 Numbers of immune cells present within the tumor are negatively correlated with tumor volume

We next performed a correlation analysis between numbers various immune cells within the tumor and the tumor volume the time mice were euthanized. A negative correlation between the number of $CD45^+$ cells, $CD8^+$ T cells, $CD8^+$ effector T cells, NK cells, DCs, and $CD103^+$ DCs versus tumor volume was observed (**Fig. 2.14, A-F**). Interestingly, the strongest correlation was observed between the number of NK cells and tumor volume ($P<0.001$; **Fig. 2.14B**). The

next strongest correlation was observed between numbers of $CD45^+$ cells and tumor volume, pointing towards immune infiltration alone being important for driving antitumor immunity (P – 0.0007; **Fig. 2.14A**). Unsurprisingly, strong correlations between $CD8^+$ T cells or $CD8^+$ effector T cells (P = 0.0067 and 0.0081, respectively) and tumor volume were observed, emphasizing the importance of these cells in the antitumor immune response (**Fig. 2.14, B and C**).

2.3.9 Pro-inflammatory cytokines and chemokines are present within the tumor following vaccination

In order to further understand the immune response, we then looked into cytokine and chemokine expression within tumors after vaccination. The mice were vaccinated as in **Fig. 2.9A** and euthanized at day 10, at which time the tumors were homogenized in order to assess the expression levels of various pro-inflammatory cytokines and chemokines. A significant increase in IFNγ expression was seen following vaccination with CBD-SA-p(Man-TLR7) plus CPI, as compared to vaccination with CBD-SA-p(Man-TLR7) alone or saline-treated control animals (**Fig. 2.15A**). Similar trends were observed with TNFα (**Fig. 2.15B**). Additionally, CBD-SA-p(Man-TLR7) plus CPI induced an increase in the expression of the pro-inflammatory chemokines CCL2, CCL5, CXCL9, CXCL10, CCL3, CCL4, and CXCL13, as compared to PBS treatment (**Fig. 2.15, C-I**). These chemokines are likely helping to drive the observed antitumor immunity. For example, CXCL10 is important for recruiting effector T cells [145], and CCL4 has been shown to recruit $CD103^+$ DCs and enhance the efficacy of checkpoint blockade therapy [146]. In the case of CCL22, however, vaccination with CBD-SA-p(Man-TLR7) plus CPI resulted in a decrease as compared to CPI-treated mice (**Fig. 2.15J**). This decrease may be a positive indicator for the antitumor efficacy of our vaccine, as CCL22 has been shown to be

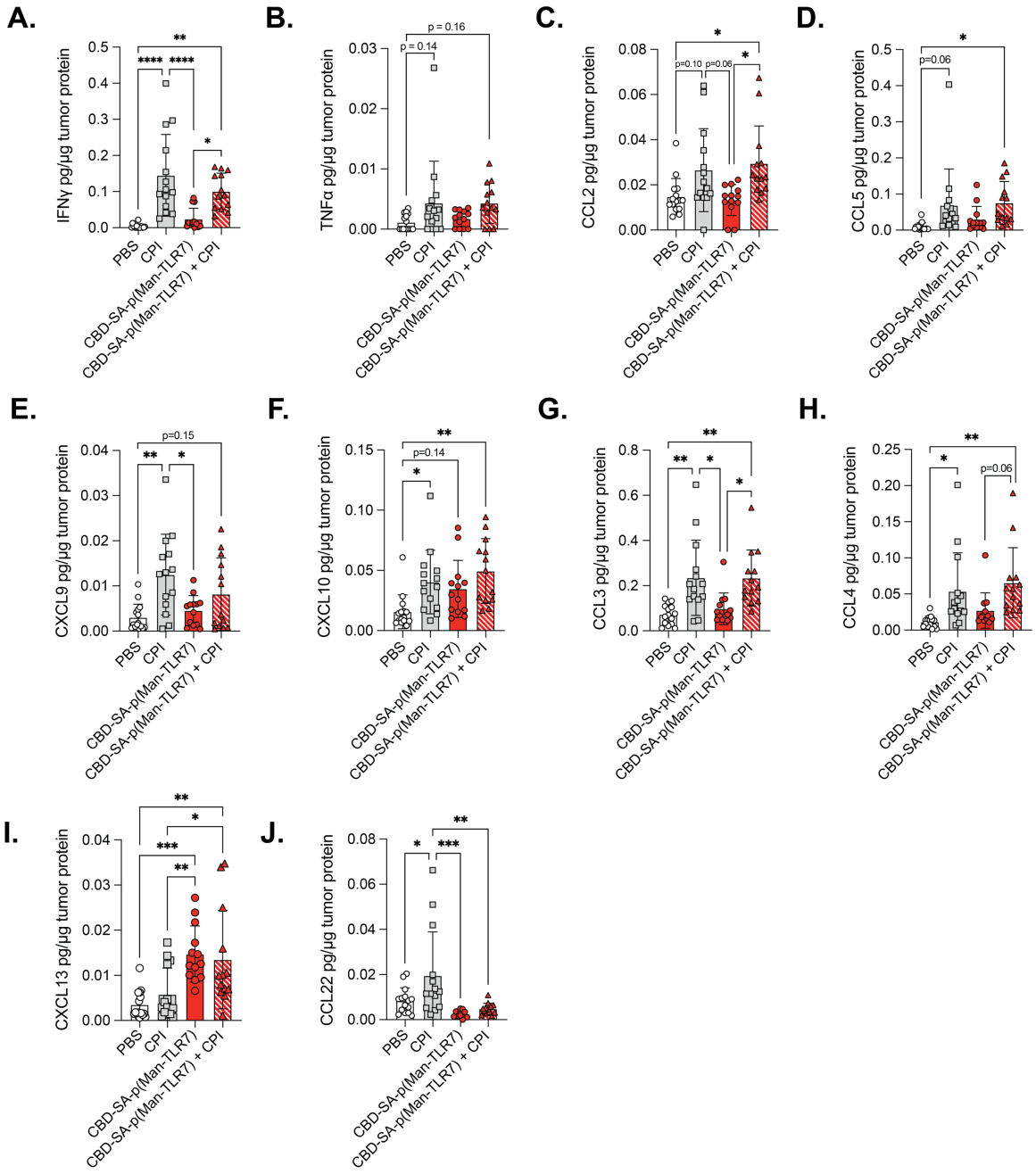

Figure 2.15: An increase in various proinflammatory cytokines and chemokines is observed within the tumor following vaccination.

B16F10 tumor-bearing mice (n = 13-15) were vaccinated at days 4 and 9 and euthanized at day 10 as in Figure 2.8, except the unconjugated and unconjugated + CPI groups were not included here. (**A-J**) Tumors were homogenized, and the concentration of (A) IFNγ, (B) TNFα, (C) CCL2, (D) CCL5, (E) CXCL9, (F) CXCL10, (G) CCL3, (H) CCL4, (I) CXCL13, and (J) CCL22 in the tumor lysates was determined via LEGENDplex™ assays. Concentrations of these cytokines and chemokines was normalized to the total protein content with the tumor. Data were compiled from two independent experiments. (Continued on next page)

Fig. 2.15, continued: Columns and error bars indicate mean±SD. Statistical comparisons are based on one-way ANOVA with Tukey's post-test: *p<0.05, **p<0.01,***p<0.001, ****p<0.0001.

important in the interaction of T_{reg} cells with DCs, helping to promote the immune escape of tumors [147].

2.3.10 Toxicity markers are not increased following vaccination

Next, we wanted to investigate the toxicity of our vaccine. To do this, we collected serum from B16F10 and EMT6 tumor-bearing mice two days after their second vaccination (**Fig. 2.16, A and B**). Here, we compared our targeted i.t. vaccinations with and without checkpoint blockade (anti-PD-1 only for EMT6 tumors and a combination of anti-PD-1 and anti-CTLA-4 for B16F10 tumors) to a clinically available TLR9 agonist, CpG, as a benchmark. For both B16F10 and EMT6 tumor-bearing mice, CpG resulted in the highest levels of alanine transaminase (ALT), a measure of liver toxicity (**Fig. 2.16, A and B**). Meanwhile, treatment with our vaccine alone or in combination with checkpoint blockade did not result in significantly increased ALT levels as compared to PBS-treated control mice (**Fig. 2.16, A and B**). No significant changes in blood urea nitrogen (BUN), a measure of kidney and liver toxicity, were observed for any of the groups in both B16F10 and EMT6 tumors (**Fig. 2.16, A and B**). CpG-treated mice exhibited a decrease in total bilirubin (T. bili) levels, another marker for liver toxicity, compared to PBS and anti-PD-1-treated mice in EMT6 tumors, but no significant differences were observed in B16F10 tumors (**Fig. 2.16, A and B**). This lack of significantly increased levels of these systemic toxicity markers points toward a promising safety profile for our targeted-p(Man-TLR7) vaccines.

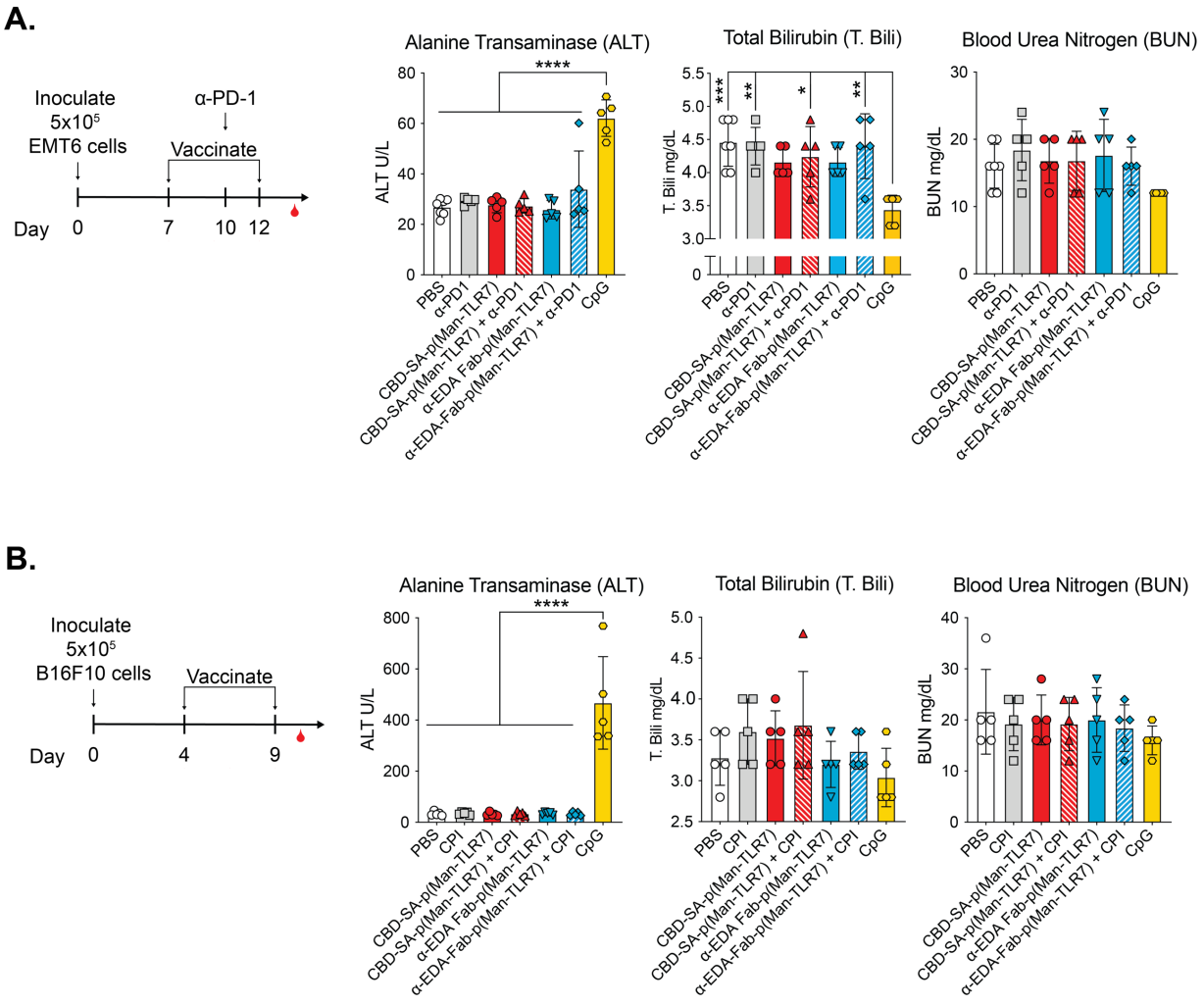

Figure 2.16: Vaccination with p(Man-TLR7) conjugates does not result in increased systemic toxicity.

(**A**) Mice (n = 5-7) were inoculated with 500,000 EMT6 cells on day 0 and vaccinated at days 7 and 12 post-tumor inoculation with 10 µg of TLR7 as murine CBD-SA-p(Man-TLR7) or murinized anti-EDA Fab-p(Man-TLR7), 20 µg CpG, or PBS. An anti-PD-1 antibody (100 µg) was injected intraperitoneally at day 10 post-tumor inoculation for the groups indicated. All other treatments were administered intratumorally, as indicated. Mice that received anti-PD-1 only also received intratumoral PBS. Blood was collected at day 11 post-tumor inoculation, and the serum was analyzed for the presence of alanine transaminase, total bilirubin, or blood urea nitrogen. (**B**) Mice (n = 5) were inoculated with 500,000 B16F10 cells on day 0 and vaccinated at days 4 and 9 post-tumor inoculation with 10 µg of TLR7 as murine CBD-SA-p(Man-TLR7) or murinized anti-EDA Fab-p(Man-TLR7) alone or in combination with anti-PD-1 + anti-CTLA-4 antibodies (CPI, 100 µg of each), 20 µg CpG, CPI alone, or intratumoral PBS. Checkpoint antibodies were administered intraperitoneally. Other treatments were administered intratumorally, as indicated. Mice that received CPI only also received intratumoral PBS. Blood was collected at day 11 post-tumor inoculation, and the serum was analyzed for the presence of alanine transaminase, total bilirubin, or blood urea nitrogen. (Continued on next page)

Fig. 2.16, continued: Columns and error bars indicate mean±SD. Statistical analysis was done using one-way ANOVA followed by Tukey's multiple comparisons test: *p<0.05, **p<0.01, ***p<0.001, ****p<0.0001.

2.3.11 Intravenous administration of p(Man-TLR7) conjugates significantly slows B16F10 tumor growth

Because i.t. administration is limited to tumors that are accessible for injection, we next wanted to assess the efficacy of our vaccines upon intravenous administration in the B16F10 melanoma model (**Fig. 2.17A**). A significant slowing of tumor growth (**Fig. 2.17, B and C**) and improved survival (**Fig. 2.17D**) were observed with both intravenous (i.v.) and i.t. administration of the two p(Man-TLR7) conjugates in combination with anti-PD-1 and anti-CTLA-4 antibodies. However, i.t. administration of the vaccine resulted in trends toward improved slowing of tumor growth and significantly improved survival as compared to i.v. administration (**Fig. 2.17, B-D**). With i.t. administration, we saw complete responses in three out of six mice vaccinated with 10 μg anti-EDA Fab-p(Man-TLR7) in combination with checkpoint blockade (**Fig. 2.17D**). In order to see if we observed any potential differences in toxicity, we looked at systemic levels of several proinflammatory cytokines in the serum after vaccination. Systemic levels of the cytokines IL-6, IL-12p70, TNFα, and IFNγ were not significantly increased in the serum after vaccination via either administration route (**Fig. 2.17, E-H**). This may indicate that intravenous injection does not result in increased toxicity of our vaccines versus intratumoral injection. However, further work is necessary to fully determine differences in toxicity observed with the two different injection routes.

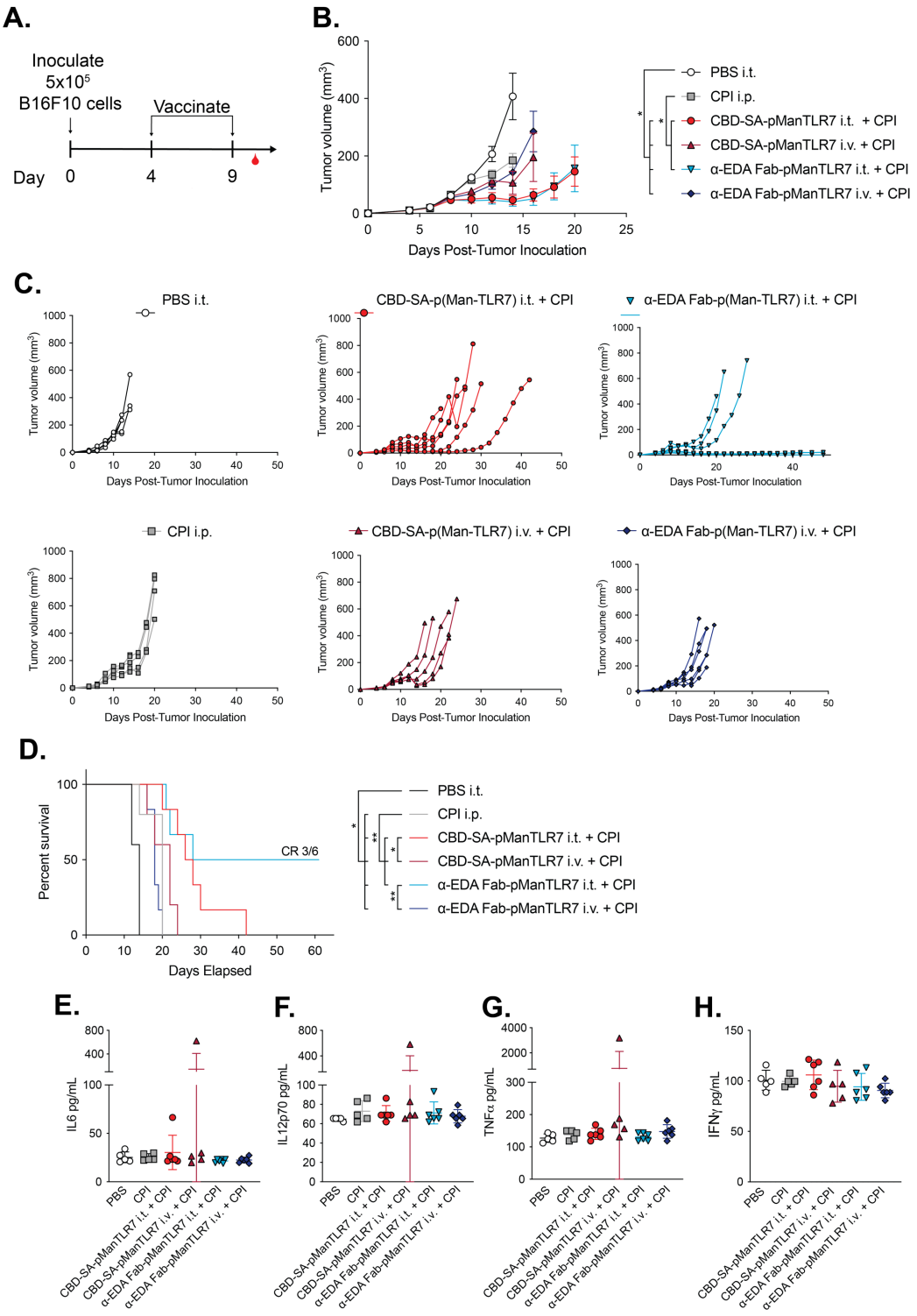

Figure 2.17: Both intratumoral and intravenous administration of p(Man-TLR7) conjugates results in a significant slowing of tumor growth and improved survival, but intratumoral administration is superior.

(Continued on next page)

Fig. 2.17, continued: (**A**) Mice (n=5-6) were inoculated with 500,000 B16F10 cells on day 0 and vaccinated at days 4 and 9 post-tumor inoculation with 10 or 30 μg of TLR7 as murinized anti-EDA Fab-p(Man-TLR7) in combination with anti-PD-1 + anti-CTLA-4 antibodies (CPI, 100 μg of each), murine CBD-SA-p(Man-TLR7) in combination with CPI, CPI alone, or intratumoral PBS. CPI was administered intraperitoneally. Other treatments were administered intravenously or intratumorally, as indicated in the figure. Mice that received CPI only also received intratumoral PBS. (**B**) Tumor volumes over time until the first mouse died in each group [mean ± SEM]. (**C**) Tumor volumes over time for all mice individually. (**D**) Percent survival until endpoint. (**E-H**) Blood was collected 11 days post-tumor inoculation, and levels of IL-6 (E), IL-12p70 (F), TNFα (G), and IFNγ (H) in the serum were assessed by ELISA. Columns and error bars indicate mean±SD. Log-rank (Mantel-Cox) test was performed for survival curves. Statistical analysis on tumor growth curves was done using one-way ANOVA followed by Tukey's multiple comparisons test at day 12: *$p<0.05$, **$p<0.01$.

2.3.12 p(Man-TLR7) conjugated to human targeting proteins synergizes with checkpoint blockade therapy, resulting in a slowing of B16F10 tumor growth

Based on the translational advantages of intravenous injection, we then decided to further investigate this administration route for our vaccines. We additionally used human anti-EDA Fab and human CBD-SA in order to further increase the translation potential. After recombinantly producing these proteins, conjugating them to p(Man-TLR7), and checking for binding to their targets (**Fig. 2.18, A-D**), we performed a dose study, vaccinating B16F10 tumor-bearing mice with varying doses of both vaccines via intravenous injection (**Fig. 2.19A**). We increased the number of doses of our vaccines here to three doses as compared to two doses (used previously with the murine protein-p(Man-TLR7) conjugates) to try to further improve our vaccines' therapeutic potential. Overall, we observed a significant slowing of tumor growth upon vaccination with human anti-EDA Fab-p(Man-TLR7) compared to untreated tumor-bearing mice (**Fig. 2.19, B and C**). However, there were no differences in efficacy when mice were treated with the varying doses, ranging from 10 μg to 100 μg TLR7 for human anti-EDA Fab-p(Man-TLR7) or from 1 μg to 50 μg for human CBD-SA-p(ManTLR7) (**Fig. 2.19, B-E**). Based on these results and in order to be able to compare between our two vaccines, we decided to move

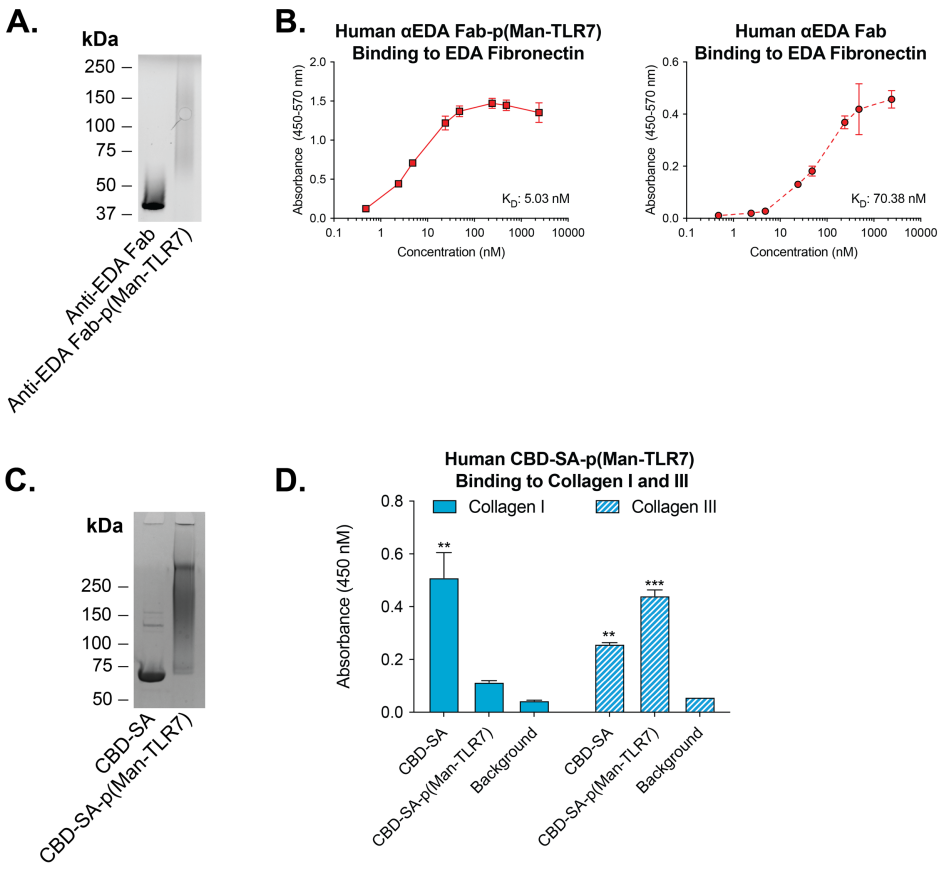

Figure 2.18: Human CBD-SA-p(Man-TLR7) and human anti-EDA Fab-p(Man-TLR7) retain binding to their antigens.

Human CBD-SA-p(Man-TLR7) and human anti-EDA Fab-p(Man-TLR7) conjugates were made as described above. (**A**) SDS-PAGE analysis of human anti-EDA Fab-p(Man-TLR7) before and after conjugation. (**B**) ELISA testing binding of human anti-EDA Fab-p(Man-TLR7) (left) and human anti-EDA Fab to EDA. Error bars indicate mean±SD. (**C**) SDS-PAGE analysis of human CBD-SA-p(Man-TLR7) before and after conjugation. (**D**) ELISA testing binding of human CBD-SA and human CBD-SA-p(Man-TLR7) to human collagen I and III. Columns and error bars indicate mean±SD. Statistical comparisons are based on one-way ANOVA with Tukey's post-test: **p<0.01, ***p<0.001.

forward with the 10 μg TLR7 dose for both vaccine conjugates. Additionally, we decided to only vaccinate mice twice going forward due to the observation of adverse reactions at the administration of the third dose (mice became hunched with ruffled fur).

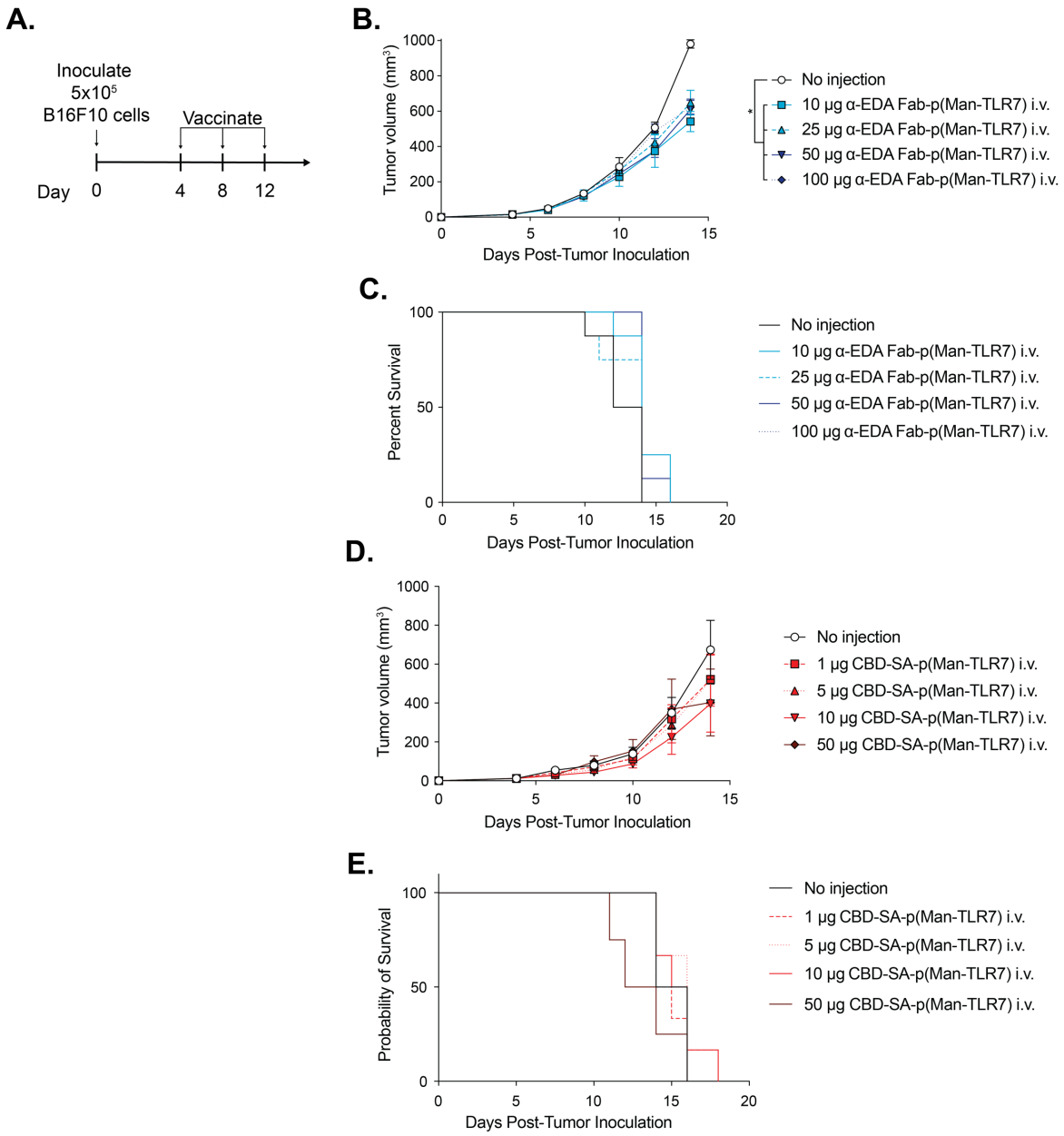

Figure 2.19: Dose study for human CBD-SA-p(Man-TLR7) and human anti-EDA Fab-p(Man-TLR7).

(**A**) Mice were inoculated with 500,000 B16F10 cells on day 0 and vaccinated intravenously at days 4, 8, and 12 post-tumor inoculation with (**B-C**) 10, 25, 50, or 100 µg of TLR7 as human anti-EDA Fab-p(Man-TLR7) (n = 8) or (**D-E**) 1, 5, 10, or 50 µg of TLR7 as human CBD-SA-p(Man-TLR7) (n = 4-6). (B and D) Tumor volumes over time [mean ± SEM]. (C and E) Percent survival until endpoint. Log-rank (Mantel-Cox) test was performed for survival curves. Statistical analysis on tumor growth curves was done using one-way ANOVA followed by Tukey's multiple comparisons test calculated at day 14: *p<0.05.

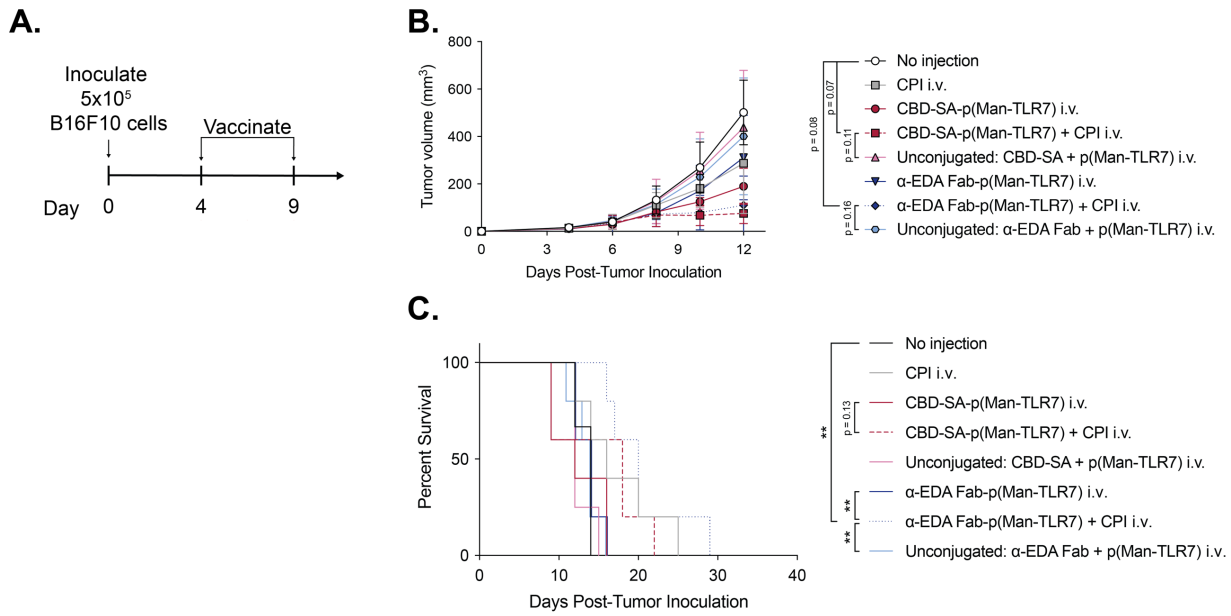

Figure 2.20: Intravenous administration of p(Man-TLR7) conjugates synergizes with checkpoint blockade therapy to result in trends toward slowing of B16F10 tumor growth and improved survival.

(**A**) Mice were inoculated with 500,000 B16F10 cells on day 0 and vaccinated at days 4 and 9 post-tumor inoculation with 10 μg of TLR7 as human anti-EDA Fab-p(Man-TLR7) alone (n = 4) or in combination with anti-PD-1 + anti-CTLA-4 antibodies (100 μg of each, administered intravenously), equivalent amounts of an unconjugated mix of human anti-EDA Fab and p(Man-TLR7), or anti-PD-1 + anti-CTLA-4 alone. Alternatively, mice were vaccinated with 10 μg of TLR7 as human CBD-SA-p(Man-TLR7) alone (n = 3) or in combination with anti-PD-1 + anti-CTLA-4 antibodies (n=3), or equivalent amounts of an unconjugated mix of human CBD-SA (n =4) and p(Man-TLR7). Additionally, one group of mice was left untreated as a control (n = 3). All treatments were administered intravenously via the tail vein. n=5 for all groups, except where noted. (**B**) Tumor volumes over time until the first mouse died [mean ± SD]. (**C**) Percent survival until endpoint. Log-rank (Mantel-Cox) test was performed for survival curves. Statistical analysis on tumor growth curves was done using one-way ANOVA followed by Tukey's multiple comparisons test at day 12: **p<0.01

After deciding on a dose, we decided to assess the anti-tumor efficacy of our vaccinations in combination with checkpoint antibody therapy. Treatment of B16F10 tumor-bearing mice with i.v.-delivered human anti-EDA Fab-p(Man-TLR7) or human CBD-SA-p(Man-TLR7) resulted in slightly reduced tumor size compared to untreated control animals, whereas treatment with unconjugated mixtures of these vaccine formulations did not result in slowed tumor growth

(**Fig. 2.20, A and B**). When we then combined our human anti-EDA Fab-p(Man-TLR7) or human CBD-SA-p(Man-TLR7) vaccination with anti-PD-1 and anti-CTLA-4 antibodies, we observed improved anti-tumor efficacy with both vaccines ($p = 0.08$ and $p = 0.07$, respectively) and significantly improved overall survival upon vaccination with human anti-EDA Fab-p(Man-TLR7), as compared to the unvaccinated control group (**Fig. 2.20, B and C**). This data shows that systemically administered targeted-p(Man-TLR7) vaccination synergizes with checkpoint blockade therapy to provide a therapeutic benefit in treating B16F10 tumors.

In order to begin to assess the immunological mechanisms underlying the anti-tumor efficacy observed, we next looked at the cell types present within the tumor after vaccination with i.v.-delivered human anti-EDA Fab-p(Man-TLR7) (**Fig. 2.21A**). We chose to only focus on human anti-EDA Fab-p(Man-TLR7) here due to the significant improvement in survival of mice treated with human anti-EDA Fab-p(Man-TLR7) plus CPI we observed in **Fig. 2.20C**. Similar to previous results (**Fig. 2.20B**), vaccination with human anti-EDA Fab-p(Man-TLR7) in combination with CPI significantly slowed B16F10 tumor growth (**Fig. 2.21B**). Upon euthanizing the mice, we did not observe any significant differences in the proportions of $CD8^+$ T cells in the tumor (**Fig. 2.21C**). However, we did see a significant decrease in $CD4^+$ T cells and $CD4^+$ $CD25^+$ $FoxP3^+$ T_{reg} cells, as well as an increase in the ratio of $CD8^+$ T cells to T_{reg} cells, in the tumor (**Fig. 2.21, D-F**). Additionally, a significant increase in the percentage of NK cells in the tumor was observed (**Fig. 2.21G**), as was a decrease in macrophages within the tumor (**Fig. 2.21H**). Further studies are required to fully elucidate the immunological mechanisms behind the observed antitumor efficacy. However, these results still provide an insight into cellular responses within the tumor after vaccination.

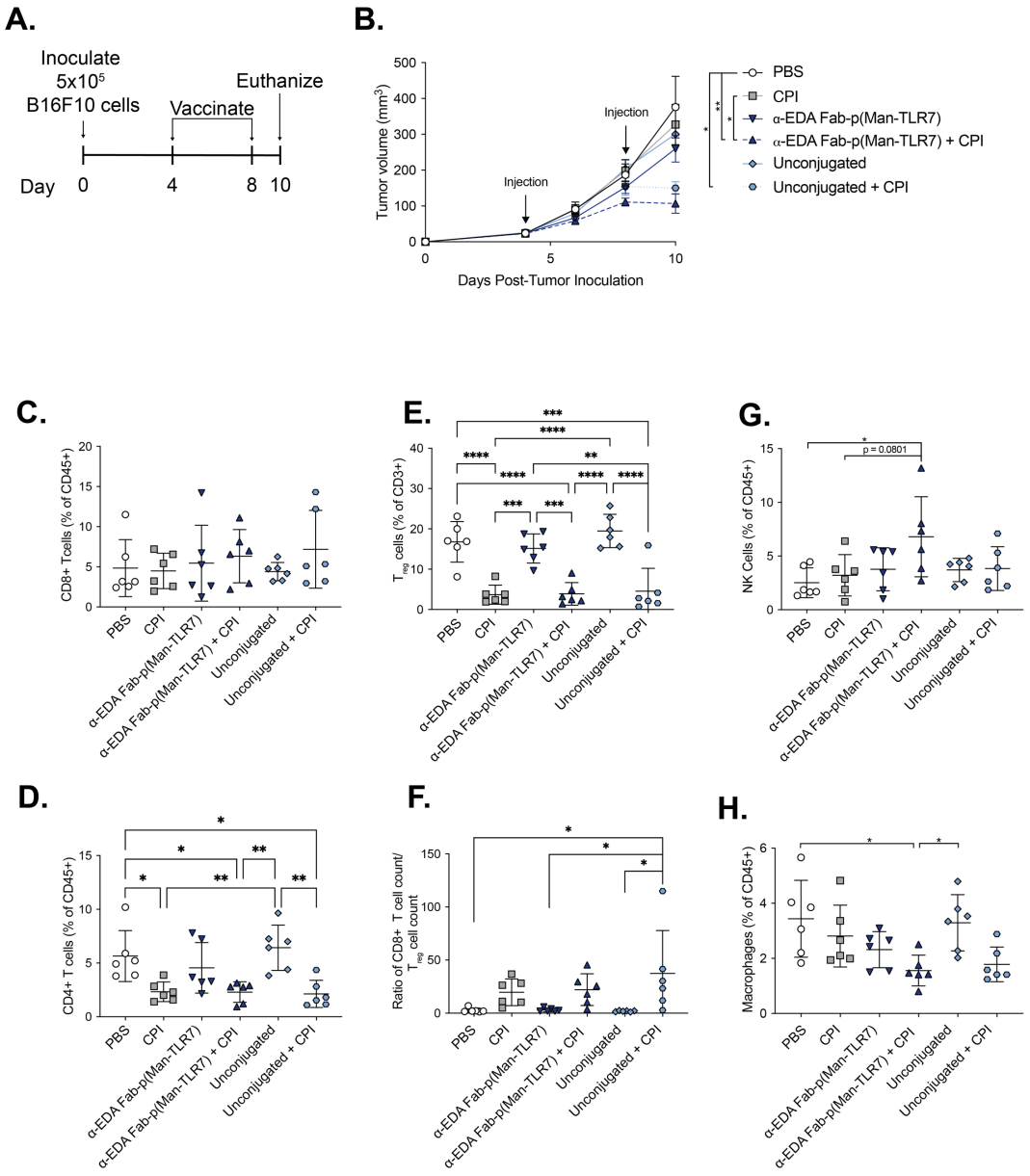

Figure 2.21: Vaccination with human anti-EDA Fab-p(Man-TLR7) results in decreased proportions of T_{reg} cells, increased proportions of NK cells, and no change in proportions of $CD8^+$ T cells.

(**A**) Mice (n=6) were inoculated with 500,000 B16F10 cells on day 0 and vaccinated at days 4 and 8 post-tumor inoculation with 30 µg of TLR7 as human anti-EDA Fab-p(Man-TLR7) alone or in combination with anti-PD-1 + anti-CTLA-4 antibodies (100 µg of each), equivalent amounts of an unconjugated mix of human anti-EDA Fab and p(Man-TLR7) with or without the checkpoint antibodies, anti-PD-1 + anti-CTLA-4 alone, or PBS. Checkpoint antibodies were administered intraperitoneally. All other treatments were administered intravenously. Mice were then euthanized at day 10, and the tumors were harvested. (**B**) Tumor volumes over time [mean ± SEM]. (**C-H**)**.** Flow cytometric analysis on the harvested tumors. Cell types are defined as follows: (C) $CD8^+$ T cells: $CD45_+ CD3^+ CD8^+$; (Continued on next page)

Fig. 2.21, continued: (D) $CD4^+$ T cells: $CD45^+$ $CD3^+$ $CD4^+$; (E) T_{reg} cells: $CD45^+$ $CD3^+$ $CD4^+$ $CD25^+$ $Foxp3^+$; (G) NK cells: $CD45^+$ $CD3^-$ $NK1.1^+$; (H) Macrophages: $CD45^+$ $CD19^-$ $Gr1^-$ $F4/80^+$. Error bars indicate mean±SD All statistical analyses were done using one-way ANOVA with Tukey's test. *p<0.05, **p<0.01, ***p<0.001, ****p<0.0001.

2.3.13 Anti-drug antibodies are induced against the protein component of p(Man-TLR7) conjugate vaccines

Lastly, because we previously had observed adverse reactions after multiple doses of both CBD-SA-p(Man-TLR7) and anti EDA Fab-p(Man-TLR7), we wanted to see if anti-drug antibodies (ADAs) were being induced upon vaccination. To do this, we collected plasma from B16F10 tumor-bearing mice two days after the second administration of each of our p(Man-TLR7) vaccines (**Fig 2.22A**). When human targeting proteins are used for intravenous vaccination, we observe a dose-dependent ADA response for both the human CBD and human anti-EDA Fab (**Fig. 2.22, B and C**). When murine or murinized (in the case of the anti-EDA Fab) proteins are used, there are still detectable levels of antibodies present after intratumoral administration in some mice, but the levels are not significant compared to PBS- or CPI-treated mice (**Fig. 2.22, D and E**). We do still observe a dose-dependent ADA response upon intravenous injection of our murine or murininized protein-p(Man-TLR7) conjugates, though, with antibodies present in all mice treated with 30 μg murinized anti-EDA Fab-p(Man-TLR7) or murine CBD-SA-p(Man-TLR7) (**Fig. 2.22, D and E**). These results point to intratumoral administration being more favorable than intravenous administration not only because i.t. administration results in improved anti-tumor efficacy (**Fig. 2.17**), but also because fewer ADAs are observed as compared to i.v. administration (**Fig. 2.22, D and E**). Despite some promising results, further optimization is required for intravenous administration of our targeted-p(Man-TLR7) vaccines.

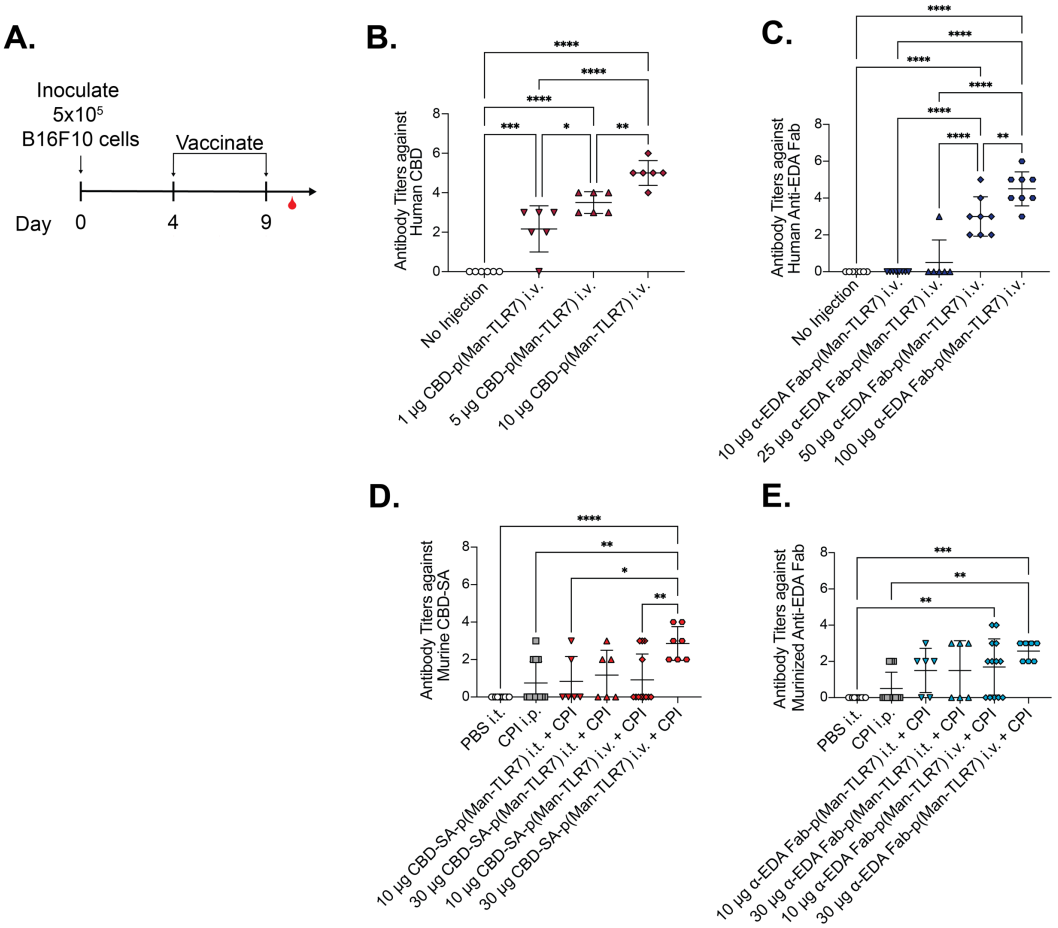

Figure 2.22: Anti-drug antibodies are induced following vaccination with human protein-p(Man-TLR7) conjugates.

(**A-E**) B16F10 tumor-bearing mice (n = 6-13) were vaccinated at days 4 and 9 post-tumor inoculation with the indicated doses of (B) human CBD-p(Man-TLR7), (C) human anti-EDA Fab-p(Man-TLR7), (D) murine CBD-SA-p(Man-TLR7) plus anti-PD-1 + anti anti-CTLA-4 antibodies (CPI, 100 µg of each), or (E) murinized anti-EDA Fab-p(Man-TLR7) plus CPI. Doses are TLR7 based. Additional groups include (B and C) mice that did not receive any injection, (D and E) mice treated with PBS, and (D and E) mice treated with CPI (plus intratumoral PBS). CPI was administered intraperitoneally. All other treatments were administered as indicated. (B-E) Blood was collected 11 days post-tumor inoculation, and titers of IgGs against the human CBD (B), human anti-EDA Fab (C), murine CBD-SA (D), or murinized anti-EDA Fab in the plasma were assessed by ELISA. Error bars indicate mean±SD. Statistical analyses were done using one-way ANOVA with Tukey's test. *p<0.05, **p<0.01, ***p<0.001, ****p<0.0001.

2.4 Discussion

Tumor immunotherapy via checkpoint blockade is having a tremendous impact in the clinic, yet this therapy works well in only a subset of patients [12,148,149]. In the work presented here, we have sought to enhance the endogenous anti-tumor response by supplementing checkpoint blockade with our matrix-targeted polymeric glyco-adjuvant vaccine.

Our vaccine described here consists of two main components. First, our vaccine contains a tumor targeting component. For this, we chose to use a tumor extracellular matrix-targeting approach for our vaccine, specifically targeting EDA fibronectin or collagen I and III. Previous work has shown that antibody fragments that bind EDA are able to preferentially localize to the tumor after intravenous injection [50] and are able to deliver various immunomodulatory agents to the tumor for effective cancer treatment [150–155]. This targeting approach is advantageous because EDA has been shown to be expressed in many different cancer types [51], which may allow our vaccine to be broadly applicable to many tumor types. Collagen targeting is a promising approach, as well, as this approach has been shown previously to improve the efficacy and decrease the toxicity of multiple cancer therapeutics [74,146,156]. Furthermore, many tumors have been shown to express increased amounts of collagen relative to normal tissues [157,158]. We hypothesized that incorporating these ECM-binding proteins would increase the tumor-retention of our vaccines when injected intratumorally. This may allow the tumor extracellular matrix to act as a depot for our vaccine, increasing the time over which it can activate APCs. Indeed, we observed an increase in the intratumoral half-life of CBD-SA-p(Man-TLR7) as compared to an untargeted p(Man-TLR7) conjugate (**Fig. 2.5**). This same improvement was not observed for anti-EDA Fab-p(Man-TLR7) (**Fig. 2.5**). However, this could potentially be an artefact of the assay used, and intratumoral retention may be improved if the

Fab were replaced with a full-length antibody, thereby increasing the avidity of the interaction of the conjugate with EDA. Lastly, the ECM may be a more stably and consistently expressed target within the tumor as compared to tumor cell surface receptors, which are subject to receptor endocytosis and potentially down-regulation due to tumor cell mutations.

The second component of our vaccine is the p(Man-TLR7) polymer. In previous work, we have shown that vaccination with p(Man-TLR7) induces potent $CD8^+$ T cell responses in several vaccination models [97]. The mannose portion of the polymer promotes APC targeting and uptake [116,129], while the TLR7 agonist portion can activate those APCs and promote the priming of $CD8^+$ T cell responses [130,131]. Because of the critical role that $CD8^+$ T cells play in anti-tumor immune responses and that fact that many cancer vaccines have failed to elicit a sufficient $CD8^+$ T cell response [122,123,126–128], in the work presented here, we extended the use of this polymer to cancer vaccination. We observed anti-tumor efficacy with both i.t.-administered CBD-SA-p(Man-TLR7) and anti-EDA-Fab-p(Man-TLR7) in combination with checkpoint blockade therapy in multiple cold tumor models (**Fig. 2.7; Fig 2.8**). Additionally, we observed an increase in the proportion $CD8^+$ effector T cells within B16F10 tumors after treatment with CBD-SA-p(Man-TLR7) plus checkpoint blockade, as well as an increase in the percentage of cross-presenting $CD103^+$ DCs expressing activation markers and an increase in expression of a number of proinflammatory cytokines and chemokines (**Fig 2.9B; Fig 2.11A; Fig. 2.15**). Furthermore, these T cell responses were antigen-specific in both the tumor and tumor-draining lymph nodes (**Fig. 2.9B; Fig. 2.10**). Antitumor efficacy was also observed when our vaccines were administered intravenously; however, intratumoral administration appeared to be more favorable (**Fig. 2.17; Fig. 2.20**). Future work is needed to optimize intravenous delivery of these vaccines if that approach is desired.

Synergy of our targeted-p(Man-TLR7) vaccines with checkpoint blockade therapy was observed in treating established B16F10 and EMT6 tumors. One potential mechanism for this was explained by the increase in the proportion of PDL1-expressing myeloid cells (DCs, macrophages, and MDSCs) observed after vaccination of B16F10 tumors with CBD-SA-p(Man-TLR7) alone or in combination with CPI (**Fig. 2.13**). These results suggest that our p(Man-TLR7) conjugate vaccines increase the expression of this ligand for the inhibitory receptor, PD-1. Therefore, when tumor-bearing mice are treated with our vaccine alone, this increase in this inhibitory pathway diminishes the antitumor immunity caused by our vaccine, resulting in only modest slowing of tumor growth and improvement in survival (**Fig. 2.7; Fig. 2.8**). However, by administering an anti-PD-1 antibody in combination with our vaccine, we are able to block this inhibitory axis and overcome the negative effects, resulting in significant slowing of tumor growth and improved survival (**Fig. 2.7; Fig. 2.8**).

One potential drawback of our approach is that p(Man-TLR7), as a strong adjuvant, is able to drive antibody responses against the protein component of our vaccine (**Fig. 2.22**). However, we were able to decrease the ADAs observed by lowering the dose of our vaccines and administering them intratumorally, as compared to intravenously. Additionally, we still observed anti-tumor efficacy (**Fig. 2.7; Fig. 2.8; Fig. 2.17; Fig. 2.20**) and did not see increased levels of systemic toxicity markers (**Fig. 2.16**), despite the presence of ADAs. Another potential limitation to our approach here is the fact that we see the best anti-tumor efficacy when our vaccine is injected intratumorally. This would limit our vaccine to solid tumors that are accessible for injection. However, we did see some promising results with intravenous injections, and we hypothesize that the anti-tumor effect could be optimized for this delivery route, perhaps by altering the formulation of our vaccine. One final potential limitation of our vaccine is that both

collagen and EDA are expressed in other contexts. Collagen is expressed in almost all mammalian tissues [159], and EDA is expressed particularly in sites of wound healing and where angiogenesis is occurring [160–162]. As such, EDA targeting has been used in targeted-delivery of therapeutics to different diseases including, arthritis [163,164], endometriosis [165], chronic skin inflammation [166], atherosclerosis [167], and colitis [168,169]. Therefore, our vaccine has the potential to target sites other than the tumor. However, since our most promising results have come from administration of our vaccine directly into the tumor, we hypothesize that any off-target effects should be minimal. Furthermore, even if intravenous administration is further optimized in the future, anti-EDA antibody fragments and the CBD have both been reported to primarily accumulate in the tumor as compared to other sites in tumor-bearing mice [50,74].

Unlike traditional cancer vaccines, our approach here relies on endogenous antigens already present within the tumor. In general, a significant challenge for cancer vaccines is the source of antigen. One approach is to use exogenous antigens in the form of proteins or peptides. However, choosing the antigens that will generate a robust immune response is challenging, especially when the heterogeneity of even a single patient's tumor is considered. Another approach is to deliver cancer cells themselves as a source of antigens. This presents a number of clinical translation challenges, though, from finding non-immunogenic sources of tumor cells to manufacturing difficulties associated with working with cells. Therefore, by relying on endogenous TAAs, our vaccination approach overcomes these challenges. This means that using our vaccination strategy, there is no longer a need to pre-identify antigens to use for vaccination or to have to change the vaccination strategy between patients. Instead, our approach utilizes the biology of each patient's tumor without requiring adaptation to each patient. Thus, our approach

may hold significant clinical translational potential as a personalized and effective therapeutic cancer vaccine.

In conclusion, we have shown that vaccination with CBD-SA-p(Man-TLR7) or anti-EDA Fab-p(Man-TLR7) synergizes with checkpoint blockade therapy to slow tumor growth and improve survival in both the B16F10 and EMT6 murine cold tumor models. Increased proportions of $CD8^+$ effector T cells and antigen-specific $CD8^+$ T cells are observed upon vaccination of B16F10 tumor-bearing mice with CBD-SA-p(Man-TLR7) in combination with checkpoint blockade. These T cell responses are accompanied by an increase in the proportion of activated cross-presenting $CD103^+$ DCs, as well as an increase in the expression of proinflammatory cytokines and chemokines, in the tumor. Furthermore, this observed anti-tumor efficacy occurs without an increase in multiple systemic markers of toxicity. Overall, the observed synergy with checkpoint blockade therapy and the efficacy of our vaccine in multiple tumor models highlight the potential for clinical translation of our targeted-p(Man-TLR7) vaccine.

2.5 Materials and Methods

2.5.1 Study design

This study was designed to test the anti-tumor efficacy of two extracellular matrix-targeted vaccines, consisting of targeting proteins conjugated to the polymeric glyco-adjuvant p(Man-TLR7). In the study, efficacy was assessed in multiple tumor models (B16F10 and EMT6) by analyzing changes in tumor growth and survival, as well as differences in important cellular readouts. Both CBD-SA-p(Man-TLR7) and anti-EDA Fab-p(Man-TLR7) were tested alone and in combination with checkpoint blockade therapy (anti-PD-1 or anti-PD-1 plus anti-CTLA-4).

All treatments were performed on the same days, unless stated otherwise. Statistical methods were not used to predetermine necessary sample size, but sample sizes were chosen on the basis of estimates from pilot experiments and previously published results such that appropriate statistical tests could yield statistically significant results. In animal studies, all mice were treated in the same manner. Animals were randomized into treatment groups within cages before vaccination, and analyses were performed in a blinded fashion. Production of the studied conjugates was performed multiple times to ensure reproducibility. Samples were excluded from analysis only when an animal developed a health problem for a nontreatment-related reason, according to the animal care guidelines. All tumor experiments were considered to have reached their end point when tumor volumes exceeded 500 mm^3. The proteins used in the p(Man-TLR7) conjugates are murine/murinized unless stated otherwise. Doses for p(Man-TLR7) conjugates are TLR7-based, unless otherwise noted. CPI indicates anti-PD-1 plus anti-CTLA-4, unless indicated otherwise. Statistical methods are described in the "Statistical analysis" section.

2.5.2 Synthesis and characterization of p(Man-TLR7) polymer

The polymeric glyco-adjuvant p(Man–TLR7) was synthesized via a reversible addition–fragmentation chain transfer (RAFT) polymerization using an azide-modified RAFT agent, a biologically inert comonomer (N-(2-hydroxypropyl) methacrylamide, HPMA) and two functional monomers: one synthesized from D-mannose, and the other from a potent TLR7 ligand (mTLR7) (**Fig. 1.1A**), as described previously [97]. Molecular weight and polydispersity of the p(Man–TLR7) construct were measured by size exclusion chromatography (molecular weight target at ~20 kDa), and was composed of a 1:2.1:3.5 molar ratio of mTLR7:mannose monomer:HPMA, as measured by mTLR7-specific UV absorbance and ^{1}H NMR.

2.5.3 Production and purification of proteins

The sequences encoding the human or murinized anti-EDA Fab or the irrelevant murine Fab (Table 2.1) were synthesized and subcloned into the mammalian expression vector pSecTag A. The murinized anti-EDA Fab is a chimeric Fab composed of murine constant regions and human variable regions. The sequences encoding murine or human CBD-SA or murine ΔCBD-SA (Table 2.1) were synthesized and subcloned into the mammalian expression vector pcDNA3.1(+) by GenScript. Suspension-adapted HEK-293F cells were routinely maintained in serum-free FreeStyle 293 Expression Medium (Gibco). On the day of transfection, cells were inoculated into fresh medium at a density of 1 x 10^6 cells/mL, and then 2 μg/mL plasmid DNA, 2 μg/ml linear 25 kDa polyethylenimine (Polysciences), and OptiPRO SFM medium (4% final concentration, Thermo Fisher) were sequentially added. The culture flask was agitated by orbital shaking at 135 rpm at 37°C in the presence of 5% CO2. 7 days after transfection, the cell culture medium was collected by centrifugation and filtered through a 0.22 μm filter. For the anti-EDA Fab, cell culture medium was loaded onto a HiTrap MabSelect 5 mL column (GE Healthcare), using an ÄKTA Pure 25 (GE Healthcare). After washing the column with PBS, protein was eluted with 0.1 M sodium citrate (pH 3.0). For CBD-SA, cell culture medium was loaded onto a HisTrap HP 5 mL column (GE Healthcare). After washing the column with wash buffer (20 mM imidazole, 20 mM NaH_2PO_4, and 0.5 M NaCl, pH 7.4), the protein was eluted with a gradient of 500 mM imidazole (in 20 mM NaH_2PO_4 and 0.5 M NaCl, pH 7.4). The CBD-SA was further purified using size exclusion chromatography with a HiLoad Superdex 200 pg column (GE Healthcare). EDA protein was recombinantly expressed and purified as described previously [170]. All purification steps were carried out at 4°C. The proteins were verified as >90% pure by SDS-PAGE (performed on 4-20% gradient gels (Bio-Rad)).

Table 2.1: Amino acid sequences of targeting proteins.

Murinized anti-EDA Fab
Heavy chain: EVQLLESGGGLVQPGGSLRLSCAASGFTFSVMKMSWVRQAPGKGLEWVSAISGSGGS TYYADSVKGRFTISRDNSKNTLYLQMNSLRAEDTAVYYCAKSTHLYLFDYWGQGTL VTVSSAKTTPPSVYPLAPGSAAQTNSMVTLGCLVKGYFPEPVTVTWNSGSLSSGVHTF PAVLQSDLYTLSSSVTVPSSTWPSETVTCNVAHPASSTKVDKKIVPRDCGS* Light chain: EIVLTQSPGTLSLSPGERATLSCRASQSVSNAFLAWYQQKPGQAPRLLIYGASSRATGI PDRFSGSGSGTDFTLTISRLEPEDFAVYYCQQMRGRPPTFGQGTKVEIKRADAAPTVSI FPPSSEQLTSGGASVVCFLNNFYPKDINVKWKIDGSERQNGVLNSWTDQDSKDSTYS MSSTLTLTKDEYERHNSYTCEATHKTSTSPIVKSFNRNEC*
Human anti-EDA Fab
Heavy chain: EVQLLESGGGLVQPGGSLRLSCAASGFTFSVMKMSWVRQAPGKGLEWVSAISGSGGS TYYADSVKGRFTISRDNSKNTLYLQMNSLRAEDTAVYYCAKSTHLYLFDYWGQGTL VTVSSASTKGPSVFPLAPSSKSTSGGTAALGCLVKDYFPEPVTVSWNSGALTSGVHTF PAVLQSSGLYSLSSVVTVPSSSLGTQTYICNVNHKPSNTKVDKRVEPKSCGS* Light chain: EIVLTQSPGTLSLSPGERATLSCRASQSVSNAFLAWYQQKPGQAPRLLIYGASSRATGI PDRFSGSGSGTDFTLTISRLEPEDFAVYYCQQMRGRPPTFGQGTKVEIKRTVAAPSVFI FPPSDEQLKSGTASVVCLLNNFYPREAKVQWKVDNALQSGNSQESVTEQDSKDSTYS LSSTLTLSKADYEKHKVYACEVTHQGLSSPVTKSFNRGEC*
Irrelevant Murine Fab
Heavy chain: QIQLVQSGPELKKPGETVKISCKASGYTFTDYSMYWVKQAPGKGLKRMGWINTETGE PTYADDFKGRFALSLDTSASTAYLHISNLKNEDTATYFCARGLDSWGQGTSVTVSSA KTTPPSVYPLAPGSAAQTNSMVTLGCLVKGYFPEPVTVTWNSGSLSSGVHTFPAVLQS DLYTLSSSVTVPSSTWPSETVTCNVAHPASSTKVDKKIVPRDCGS* Light chain: DIQMTQSPSSLSATLGGKVTITCKASQDINKYIAWYQHKPGKGPRLLIHYTSTLQPGNP SRFSGSGSGRDYSFSISNLEAEDIAIYYCLQYDNLQRTFGGGTKVEIKRADAAPTVSIFP PSSEQLTSGGASVVCFLNNFYPKDINVKWKIDGSERQNGVLNSWTDQDSKDSTYSMS STLTLTKDEYERHNSYTCEATHKTSTSPIVKSFNRNEC*
Murine CBD-SA
CSQPLDVVLLLDGSSSLPESSFDKMKSFAKAFISKANIGPHLTQVSVIQYGSINTIDVPW NVVQEKAHLQSLVDLMQQEGGPSQIGDALAFAVRYVTSQIHGARPGASKAVVIIIMD TSLDPVDTAADAARSNRVAVFPVGVGDRYDEAQLRILAGPGASSNVVKLQQVEDLST MATLGNSFFHKLCSGFSGVGGGSGGGSEAHKSEIAHRYNDLGEQHFKGLVLIAFSQY LQKCSYDEHAKLVQEVTDFAKTCVADESAANCDKSLHTLFGDKLCAIPNLRENYGEL ADCCTKQEPERNECFLQHKDDNPSLPPFERPEAEAMCTSFK…(Continued on next page)

Table 2.1, continued:

Murine CBD-SA Continued
(Continued from previous page)…ENPTTFMGHYLHEVARRHPYFYAPELLYYAEQYNEI LTQCCAEADKESCLTPKLDGVKEKALVSSVRQRMKCSSMQKFGERAFKAWAVARLS QTFPNADFAEITKLATDLTKVNKECCHGDLLECADDRAELAKYMCENQATISSKLQT CCDKPLLKKAHCLSEVEHDTMPADLPAIAADFVEDQEVCKNYAEAKDVFLGTFLYEY SRRHPDYSVSLLLRLAKKYEATLEKCCAEANPPACYGTVLAEFQPLVEEPKNLVKTN CDLYEKLGEYGFQNAILVRYTQKAPQVSTPTLVEAARNLGRVGTKCCTLPEDQRLPC VEDYLSAILNRVCLLHEKTPVSEHVTKCCSGSLVERRPCFSALTVDETYVPKEFKAETF TFHSDICTLPEKEKQIKKQTALAELVKHKPKATAEQLKTVMDDFAQFLDTCCKAADK DTCFSTEGPNLVTRCKDALAHHHHHH**
Human CBD-SA
CSQPLDVILLLDGSSSFPASYFDEMKSFAKAFISKANIGPRLTQVSVLQYGSITTIDVPW NVVPEKAHLLSLVDVMQREGGPSQIGDALGFAVRYLTSEMHGARPGASKAVVILVTD VSVDSVDAAADAARSNRVTVFPIGIGDRYDAAQLRILAGPAGDSNVVKLQRIEDLPT MVTLGNSFLHKLCSGFVRIGGGSGGGSEAHKSEIAHRYNDLGEQHFKGLVLIAFSQYL QKCSYDEHAKLVQEVTDFAKTCVADESAANCDKSLHTLFGDKLCAIPNLRENYGELA DCCTKQEPERNECFLQHKDDNPSLPPFERPEAEAMCTSFKENPTTFMGHYLHEVARR HPYFYAPELLYYAEQYNEILTQCCAEADKESCLTPKLDGVKEKALVSSVRQRMKCSS MQKFGERAFKAWAVARLSQTFPNADFAEITKLATDLTKVNKECCHGDLLECADDRA ELAKYMCENQATISSKLQTCCDKPLLKKAHCLSEVEHDTMPADLPAIAADFVEDQEV CKNYAEAKDVFLGTFLYEYSRRHPDYSVSLLLRLAKKYEATLEKCCAEANPPACYGT VLAEFQPLVEEPKNLVKTNCDLYEKLGEYGFQNAILVRYTQKAPQVSTPTLVEAARN LGRVGTKCCTLPEDQRLPCVEDYLSAILNRVCLLHEKTPVSEHVTKCCSGSLVERRPC FSALTVDETYVPKEFKAETFTFHSDICTLPEKEKQIKKQTALAELVKHKPKATAEQLKT VMDDFAQFLDTCCKAADKDTCFSTEGPNLVTRCKDALAHHHHHH**
Murine ΔCBD-SA
CSQPLDVVLLLDGSSSLPESSFDKMKSFAKAFISKANIGPHLTQVSVIQYGSINTIAVPS NVVQEKAHLQSLVDLMQQEGGPSQIGDALAFAVRYVTAQIAGARPGASKAVVIIIMD TSLDPVDTAADAARSNRVAVFPVGVGDRYDEAQLRILAGPGASSNVVKLQQVEDLST MATLGNSFFHKLCSGFSGVGGGSGGGSEAHKSEIAHRYNDLGEQHFKGLVLIAFSQY LQKCSYDEHAKLVQEVTDFAKTCVADESAANCDKSLHTLFGDKLCAIPNLRENYGEL ADCCTKQEPERNECFLQHKDDNPSLPPFERPEAEAMCTSFKENPTTFMGHYLHEVAR RHPYFYAPELLYYAEQYNEILTQCCAEADKESCLTPKLDGVKEKALVSSVRQRMKCS SMQKFGERAFKAWAVARLSQTFPNADFAEITKLATDLTKVNKECCHGDLLECADDR AELAKYMCENQATISSKLQTCCDKPLLKKAHCLSEVEHDTMPADLPAIAADFVEDQE VCKNYAEAKDVFLGTFLYEYSRRHPDYSVSLLLRLAKKYEATLEKCCAEANPPACYG TVLAEFQPLVEEPKNLVKTNCDLYEKLGEYGFQNAILVRYTQKAPQVSTPTLVEAAR NLGRVGTKCCTLPEDQRLPCVEDYLSAILNRVCLLHEKTPVSEHVTKCCSGSLVERRP CFSALTVDETYVPKEFKAETFTFHSDICTLPEKEKQIKKQTALAELVKHKPKATAEQL KTVMDDFAQFLDTCCKAADKDTCFSTEGPNLVTRCKDALAHHHHHH**

2.5.4 Production of p(Man-TLR7) conjugates

CBD-SA or anti-EDA Fab was mixed with 20 molar equivalents of 2 kDa self-immolative PEG linker in 500 μL phosphate buffer (pH 7.7) and reacted for 1 hour mixing at RT. The reaction solution was then purified twice via Zeba spin desalting columns with 7 kDa cutoff to remove unreacted linker (Thermo Fisher). Successful linker conjugation was confirmed using gel electrophoresis and comparison to a size standard of the unmodified proteins. Protein-linker constructs in PBS (pH 7.4) were then reacted with 10 molar excess of p(Man-TLR7) polymer in an endotoxin-free Eppendorf tube for 2 hours, mixing, at RT. Excess p(Man-TLR7) polymer was removed using FPLC size-exclusion chromatography Superdex 200 column (GE). Fractions containing species with MW higher than 75 kDa (as assessed by gel electrophoresis) were then pooled and concentrated in 30 kDa Amicon centrifuge unit (Millipore Sigma). TLR7 content was then determined via absorbance at 327nm and Fab content was determined via gel electrophoresis.

2.5.5 Determination of TLR7 content in p(Man-TLR7) conjugates

To determine the concentration of TLR7 content in the polymer and polymer-Fab conjugates, the absorbance at 327nm was measured. Known quantities of mTLR7 in saline was measured (n=3 independent samples) at 327nm in several concentrations ranging from 8 mg/mL to 1 mg/mL to calculate a standard curve as previously published by Wilson et al [97]. The determined standard curve [TLR7 (mg/mL) = 1.9663* A_{327} + 0.0517] was then used to calculate TLR7 concentration in the prepared p(Man-TLR7) conjugate.

2.5.6 Determination of protein content in p(Man-TLR7) conjugates

SDS-PAGE was performed on 4-20% gradient gels (Bio-Rad) using a standard curve of desired protein (2, 1.5, 1, and 0.5 mg/mL of CBD-SA or anti-EDA Fab) and two dilutions of protein-p(Man-TLR7) conjugate samples were reduced with 10mM dithiothreitol. Reducing conditions liberates conjugated p(Man-TLR7) allowing for the reduced protein band intensity to be analyzed. Band density of the reduced sample and protein standard curve was then analyzed using ImageJ and the protein concentration of the sample was calculated using the standard curve generated.

2.5.7 Surface Plasmon Resonance (SPR) Analysis for CBD-SA and CBD-SA-p(Man-TLR7) binding to Collagen I

SPR measurements were made using a Biacore X100 SPR system (Cytiva, Marlborough, MA). Human collagen I (EMD Millipore) was immobilized via amine coupling on a CM5 chip (Cytiva) according to the manufacturer's instructions, resulting in ~580 resonance units corresponding to ligand coating. CBD-SA, CBD-SA-p(Man-TLR7), or ΔCBD-SA was then flowed at increasing concentrations (as indicated in **Fig. 2.3**) in PBS with 0.05% Tween 20 for a contact time of 70 seconds at 30 μL min^{-1}, followed by running buffer for a dissociation time of 600 seconds. At the end of each cycle, the sensor chip surface was regenerated with a 30-second pulse of 50 mM NaOH at 10 μL min^{-1}. Specific binding of CBD-SA, CBD-SA-p(Man-TLR7), or ΔCBD-SA was calculated by comparison to a channel with BSA (Sigma) immobilized on the surface as a reference (BSA immobilization resulted in ~1300 resonance units). The experimental results were fitted with Langmuir binding kinetics (1:1 binding) using the BIAevaluation software (Cytiva, version 2.0.2.).

2.5.8 SPR Analysis for anti-EDA Fab and anti-EDA Fab-p(Man-TLR7) binding to EDA

SPR measurements were made using a Biacore X100 SPR system (Cytiva, Marlborough, MA). At the beginning of each cycle, the surface of an NTA chip (Cytiva) was conditioned with EDTA according to the manufacturer's instructions. Then, 2 μg mL^{-1} EDA in PBS with 0.05% Tween 20 was flowed at a flowrate of 5 μL min^{-1} for 120 seconds, resulting in ~30-60 resonance units corresponding to ligand coating. Anti-EDA Fab, anti-EDA Fab-p(Man-TLR7), or irrelevant Fab was then flowed at increasing concentrations (as indicated in **Fig. 2.3**) in PBS with 0.05% Tween 20 for a contact time of 50 seconds (anti-EDA Fab) or 90 seconds (anti-EDA Fab-p(Man-TLR7) and irrelevant Fab) at 30 μL min^{-1}, followed by running buffer for a dissociation time of 600 seconds. At the end of each cycle, the sensor chip surface was regenerated with one 60-second pulse of 0.35M EDTA followed by a 30-second pule of 50 mM NaOH at 30 μL min^{-1}. Specific binding of anti-EDA Fab, anti-EDA Fab-p(Man-TLR7), or irrelevant was calculated by comparison to a nonfunctionalized channel used as a reference. The experimental results were fitted with Langmuir binding kinetics (1:1 binding) using the BIAevaluation software (Cytiva, version 2.0.2.).

2.5.9 Binding of human CBD-SA and CBD-SA-p(Man-TLR7) to Collagen I and III

Affinity measurements were performed using enzyme-linked immunosorbent assay (ELISA). 96-well medium-binding ELISA plates (Greiner Bio-One) were coated with 10 μg/mL human collagen I or III (EMD Millipore) in PBS overnight at 4°C. The following day, plates were washed in PBS with 0.05% Tween 20 (PBS-T) and then blocked with 2% BSA in PBS-T for 2 hours at room temperature. Then, wells were washed with PBS-T and further incubated with CBD-SA or CBD-SA-p(Man-TLR7) for 2 hours at room temperature. After 6 washes with PBS-

T, wells were incubated for 1 hour at room temperature with biotin-conjugated anti-mouse serum albumin (Abcam). Subsequently, wells were washed again 6 times with PBS-T and incubated for 30 minutes at room temperature with HRP-conjugated streptavidin (Thermo Scientific). Lastly, wells were washed 6 more times with PBS-T, and bound CBD-SA or CBD-SA-p(Man-TLR7) was detected with tetramethylbenzidine substrate by measurement of the absorbance at 450 nm with subtraction of the measurement at 570 nm.

2.5.10 Binding of human anti-EDA Fab and anti-EDA Fab-p(Man-TLR7) to EDA

Affinity measurements were performed using ELISA. 96-well ELISA plates (Nunc MaxiSorp flat-bottom plates, Thermo Fisher) were coated with 10 μg/mL EDA (produced in our lab) in PBS overnight at 4°C. The following day, plates were washed in PBS with 0.05% Tween 20 (PBS-T) and then blocked with 1x casein (Sigma) diluted in PBS for 2 hours at room temperature. Then, wells were washed with PBS-T and further incubated with various dilutions of anti-EDA Fab or anti-EDA Fab-pManTLR7 for 2 hours at room temperature. After 6 washes with PBS-T, wells were incubated for 1 hour at room temperature with horseradish peroxide (HRP)-conjugated antibody against human IgG (Jackson ImmunoResearch). After 6 washes with PBS-T, bound anti-EDA Fab or anti-EDA Fab-p(Man-TLR7) was detected with tetramethylbenzidine substrate by measurement of the absorbance at 450 nm with subtraction of the measurement at 570 nm. The apparent dissociation constant (K_D) values were obtained by nonlinear regression analysis in Prism software (v7, GraphPad Software) assuming one-site specific binding.

2.5.11 In vitro activation of p(Man-TLR7) Conjugates

BMDCs were prepared from C57Bl/6 mice (Jackson Laboratory) as previously described

[171] and used on day 8–9. For BMDC activation studies, 1×10^5 cells per well were seeded in round-bottom 96-well plates (Fisher Scientific) in RPMI 1640 with 10% fetal bovine serum (FBS, Gibco) and 2% Penicillin-Streptomycin (Invitrogen), treated with CBD-SA, CBD-SA-p(Man-TLR7), anti-EDA Fab, or anti-EDA Fab-p(Man-TLR7), and then incubated at 37°C. The samples were allowed to culture for 18h at 37°C and cytokine concentration was measured in the media by Ready-Set-Go™ ELISA kits (Thermo Fisher) as detailed in the manufacturer's instructions.

2.5.12 Reagents for in vivo studies

Rat anti-mouse PD-1 (Clone 29F.1A12, Bio X Cell) and hamster anti-mouse CTLA-4 (clone 9H10, Bio X Cell) were used for checkpoint blockade antibody studies. VacciGrade CpG ODN 1826 was used for toxicity studies (InvivoGen). Before administration to mice, endotoxin levels of all formulations were tested via HEK-Blue hTLR4 cells from InvivoGen.

2.5.13 Cell culture

B16F10 cells (ATCC) were cultured in DMEM (Gibco) with 10% FBS (Gibco) and 1% Penicillin-Streptomycin (Invitrogen) . EMT6 cells (ATCC) were cultured in RPMI 1640 (Gibco) with 10% FBS (Gibco) and 1% Penicillin-Streptomycin (Invitrogen). Cell lines were tested to confirm a lack of murine pathogens via IMPACT I PCR testing (IDEXX Laboratories).

2.5.14 Animals

All studies with animals were carried out in accordance to procedures approved by the Institutional Animal Care and Use Committee at the University of Chicago and housed in a specific pathogen-free environment at the University of Chicago. C57BL/6 or BALB/c female mice aged between 8-12 weeks were obtained from Charles River or The Jackson Laboratory.

2.5.15 B16F10 and EMT6 tumor inoculation, treatment, and measurement

$5x10^5$ B16F10 cells resuspended in 30 μL of PBS were inoculated intradermally on the left side of the back of each C57BL/6 mouse. Alternatively, $5x10^5$ EMT6 cells resuspended in 30 μL of PBS were inoculated into the lower right mammary fat pad on each BALB/s mouse. Tumors were measured every other day starting between days 3 and 5 after tumor inoculation with digital calipers. Volumes were calculated as volume V= length x width x height x π/6. Mice were sacrificed when tumor volume reached over 500 mm^3 or early endpoint criteria were reached. Treatments were performed on days described in figures and in figure legends. p(Man-TLR7) conjugate vaccination or control treatment was administered in described doses and treatments via intravenous injection in a total volume of 100 μL or via intratumoral injection in a total volume of 30 μL. Treatment with 100 μg of anti-PD-1 with or without 100 μg of anti-CTLA-4 was administered intraperitoneally or intravenously. Prior to initial treatment, mice were randomized into treatment groups with each treatment group split between cages to reduce cage effects.

2.5.16 Intratumoral retention of p(Man-TLR7) conjugates

Fluorescently-labeled CBD-SA-, ΔCBD-SA-, anti-EDA Fab-, or irrelevant Fab-p(Man-TLR7) conjugates were prepared by first labeling the proteins with Alexa Fluor 647 NHS Ester (Invitrogen) according to the manufacturer's instructions and then carrying out the conjugation to p(Man-TLR7), as described above. EMT6 tumor-bearing mice were then injected intratumorally at day 14 post-tumor inoculation with the fluorescently labeled conjugates. The doses used were based on the protein content in the conjugates and were equivalent to a 10 μg TLR7-based dose. Mice were then imaged via an IVIS Spectrum In Vivo Imaging System (Perkin Elmer), starting

immediately after injection. Mice were imaged at multiple time points until the fluorescent signal was undetectable over the background. Images were processed using Living Image 4.5.5 software (Perkin Elmer). Total radiant efficiency, measured in (photons/s)/(μW/cm2), was quantified for a region of interest (ROI) that encompassed the tumor area. All imaging parameters were kept consistent between all images taken. Background radiant efficiency (using an ROI from the sample stage) was subtracted from all measurements. The percent of initial (0 hr timepoint) total radiant efficiency was then calculated for all timepoints in order to account for any differences in the degree of fluorescent labeling across the conjugate groups assessed. Intratumoral half-life was calculated using one phase exponential decay (dissociation) curve fitting in GraphPad Prism v9.

2.5.17 Serum cytokine concentration analysis

B16F10 melanoma tumors were inoculated as described above, and mice were vaccinated as described above. On day 11 post-tumor inoculation, 50 μL of blood was collected in heparin-coated tubes, and serum was separated by centrifugations and stored at -20℃. Serum was assessed for IL-6, IL-12p70, TNFα, and IFNγ using Ready-Set-Go (Thermo Fisher) or Quantikine (R&D) ELISA kits, following the manufacturer's instructions.

2.5.18 Preparation of single cell suspensions from organs

Tumors, spleens, and/or tumor-draining lymph nodes were collected at the time point indicated in the figure legends and stored in ice-cold DMEM (Gibco) until further steps. Spleens were processed into a single-cell suspension via mechanical disruption and passage through a 70μm filter. The splenocytes were washed with PBS and then exposed to ACK lysis buffer (0.155 M NH_4Cl, Gibco) for 5 minutes at room temperature to lyse red blood cells. The lymph nodes and

tumors were mechanically disrupted, then digested at 37°C for 45 min in DMEM with 3.5 mg/mL collagenase D (Roche), 1 mg/mL collagenase IV (Worthington), 1.2 mM $CaCl_2$ (Sigma), 1% Penicillin-Streptomycin (Invitrogen), and 2% FBS before being passed through a 70 μm filter. Single cell suspensions were then washed with PBS and resuspended in IMDM (Gibco) with 10% FBS and 1% Penicillin-Streptomycin.

2.5.19 Flow cytometric analysis

The following procedures were all performed at 4˚C in the dark. Prepared cells were stained for viability using fixable dyes (**Table 2.2**) at 1:500 dilution in PBS with anti-CD16/32 included (1:100 dilution) for 15 minutes. Surface staining was performed in Brilliant Stain buffer (BD Biosciences) using monoclonal antibodies against the murine targets indicated in **Table 2.2**. All antibodies were titrated to determine optimal working dilutions which often was 1:100 or 1:200. Cells were incubated with the surface stain cocktail for 20 minutes before washing in PBS, followed by fixation. Fixation was performed using the following buffers: for assays without intracellular staining, cells were fixed for 20 minutes using a 2% paraformaldehyde solution; for assays with transcription factor staining, cells were fixed and permeabilized using the Invitrogen FoxP3/Transcription factor kit (eBioscience) according to manufacturer instructions; for assays which required non-transcription factor internal staining (cytokines alone) fixation and permeabilization was performed using the Cytofix/Cytoperm kit (BD Biosciences) according to manufacturer instructions. Assays requiring intracellular staining were performed using antibodies against the murine targets at 1:200 dilution in the corresponding kit permeabilization buffer, according to manufacturer instructions (**Table 2.2**). Following fixation and/or intracellular staining, cells were resuspended in FACS buffer (PBS pH 7.4 with 2mM EDTA and 2% FBS, made in house) prior to flow cytometric analysis. Tumor samples were also stained

with a TRP2 pentamer (H-2K^b-SVYDFFVWL, ProImmune). Pentamer staining was conducted after the viability staining. Cells were first incubated at 37°C for 30 minutes in 50 mM dasatinib. The pentamer (at a dilution of 1:10) was then added directly to the cells in dasatinib, and the cells were stained for 1 hour at room temperature. Following the pentamer staining, the cells were washed and surface stained as described above. Flow cytometry measurements were performed using a LSR Fortessa flow cytometer (BD Biosciences), and data were analyzed using FlowJo software (Tree Star).

Table 2.2: Probes and markers used to characterize cell populations using flow cytometry.

Immune cell panel for Fig. 2.9			
Marker	**Fluorophore**	**Vendor**	**Clone**
Viability Dye	eFluor 455 (UV)	Invitrogen	-
CD45	BV786	BD Horizon	30-F11
CD3	APC-Cy7	BD Pharmingen	145-2C11
CD4	BUV395	BD Horizon	GK1.5
CD8	BUV737	BD Horizon	53-6.7
CD44	PE-Cy7	Biolegend	IM7
CD62L	BV711	Biolegend	MEL-14
TOX	eFluor 660	Invitrogen	TXRX10
TRP2 Pentamer	PE	ProImmune	H-2K^b SVYDFFVWL
NK1.1	BV605	Biolegend	PK136
Anti-PE	unlabeled	Biolegend	PE001
Myeloid cell panel for Fig. 2.11, 2.12, and 2.13			
Marker	**Fluorophore**	**Vendor**	**Clone**
Viability Dye	eFluor 455 (UV)	Invitrogen	-
CD45	BV786	BD Horizon	30-F11
CD8	APC-Cy7	Biolegend	53-6.7
CD11b	BV605	Biolegend	M1/70
CD11c	PE-Cy7	BD Pharmingen	HL3
CD80	BUV737	BD Horizon	16-10A1
CD86	BUV395	BD Horizon	GL1
CD103	PE	BD Pharmingen	M290
B220	BV421	Biolegend	RA3-6B2
I-A/E	PerCP-Cy5.5	Biolegend	M5/114.15.2
PD-L1	BV711	BD Horizon	MIH5

(Continued on next page)

Table 2.2, continued:

Restimulation panel for Fig. 2.10			
Marker	**Fluorophore**	**Vendor**	**Clone**
Viability Dye	eFluor 455 (UV)	Invitrogen	-
CD3	BUV395	BD Horizon	145-2C11
CD4	BV786	BD Horizon	GK1.5
CD8	BV421	BD Horizon	53-6.7
IFNγ	APC	Biolegend	XMG1.2
TNFα	BV605	Biolegend	MP6-XT22
Immune cell panel for Fig. 2.21			
CD45	APC-Cy7	Biolegend	30-F11
CD3	BUV395	BD Horizon	145-2C11
CD4	BV786	BD Optibuild	RM4-4
CD8	FITC	Biolegend	53-6.7
CD25	PE	Biolegend	3C7
FoxP3	AF647	BD Pharmingen	MF23
NK1.1	BV421	Biolegend	PK136
Myeloid cell panel for Fig. 2.21			
CD45	APC-Cy7	Biolegend	30-F11
CD19	BUV395	BD Horizon	1D3
Ly6G	AF488	Biolegend	1A8
Ly6C	BV605	Biolegend	HK1.4
F4/80	APC	Biolegend	BM8

2.5.20 Ex vivo restimulations

Cells from the tumor-draining lymph nodes were restimulated *in vitro* with mTRP-$2_{180\text{-}188}$ (SVYDFFVWL) and $hgp100_{25\text{-}33}$ (KVPRNQDWL) peptides (Genscript, both peptides were pooled, each peptide was used at 2μg/mL) for 6 hours or 3 days. For 3 day restimulations, $5x10^5$ cells were incubated with peptides for 3 days in complete IMDM at 37°C. After 3 days, the cells were spun down, and the supernatant was used to measure secreted cytokines using a LEGENDplex™ Mouse Th Cytokine Panel kit (BioLegend) according to the manufacturer's instruction. Approximately 500 events per cytokine were acquired using a LSR Fortessa flow cytometer (BD Biosciences), and analyzed with LEGENDplex v8.0 software.

For 6 hour restimulations, $1x10^6$ cells from the tumor-draining lymph nodes were incubated with peptides for 6 hours in complete IMDM at 37°C. After 2 hours of *in vitro* restimulation, GolgiPlug and GolgiStop (BD) were added according to manufacturer's instructions. Cells were then incubated for 4 more hours, stained for intracellular cytokines, and analyzed via flow cytometry, as described.

2.5.21 Analysis of intratumoral cytokines and chemokines after vaccination

B16F10 tumor bearing mice were treated at days 4 and 9 with intratumorally-delivered PBS, CPI, CBD-SA-p(Man-TLR7), or CBD-SA-p(Man-TLR7)+CPI and euthanized at day 10. Tumors were collected and homogenized as described previously [156]. Briefly, after the tumors were collected, they were snap-frozen in liquid nitrogen and stored at -80°C. Tumors were then homogenized in Tissue Protein Extraction buffer (T-PER, Thermo Fisher Scientific) containing protease inhibitor tablets (Roche). Tumors were then placed in Lysing Matrix D tubes (MP Bio) and homogenized using a FastPrep tissue homogenizer (MP Bio). Multiplex analysis was then performed on the homogenized tumors using LEGENDplex™ Mouse Inflammation Panel and Mouse Proinflammatory Chemokine Panel kits (Biolegend) according to the manufacturer's instructions in order to quantify the cytokines and chemokines present within the tumor. Approximately 500 events per cytokine or chemokine were acquired using a LSR Fortessa flow cytometer (BD Biosciences), and the data was analyzed with LEGENDplex v8.0 software. The concentrations of cytokines and chemokines were then normalized to the total protein content of the tumor, as measured via Pierce BCA Protein Assay (Thermo Fisher Scientific).

2.5.22 Toxicity assessments

Blood samples from treated mice (as in **Fig. 2.16**) were collected into protein low-bind tubes (Eppendorf) two days after the second treatment injection. The blood was allowed to clot for two hours at 4℃ and then was spun down at 10,000 x g for 10 minutes. The serum was collected and then analyzed using a Biochemistry Analyzer (Alfa Wassermann Diagnostic Technologies) according to the manufacturer's instructions.

2.5.23 Anti-Fab or anti-CBD-SA IgG concentration analysis

B16F10 melanoma tumors were inoculated as described above, and mice were vaccinated as described above. On day 11 post-tumor inoculation, 50 μL of blood was collected in heparin-coated tubes, and plasma was separated by centrifugation and stored at -20℃. Plasma was assessed for anti-Fab or anti-CBD-SA IgGs by ELISA. 96-well ELISA plates (Nunc MaxiSorp flat-bottom plates, Thermo Fisher) were coated with 10 μg/mL anti-EDA Fab or CBD-SA in PBS overnight at 4°C. The following day, plates were washed in PBS with 0.05% Tween 20 (PBS-T) and then blocked with 1x casein (Sigma) diluted in PBS for 1 hour at room temperature. Then, wells were washed with PBS-T and further incubated with various dilutions of plasma for 2 hours at room temperature. After 6 washes with PBS-T, wells were incubated for 1 hour at room temperature with horseradish peroxide (HRP)-conjugated antibody against mouse IgG (Fc region specific, Jackson ImmunoResearch,). After 6 washes with PBS-T, bound anti-Fab or anti-CBD-SA IgGs were detected with tetramethylbenzidine substrate by measurement of the absorbance at 450 nm with subtraction of the measurement at 570 nm.

2.5.24 Statistical analysis

Statistical analysis was performed using GraphPad Prism v9. Multiple group comparisons used one-way ANOVA with Tukey's post-hoc correction or two-way ANOVA with Tukey's multiple comparisons test. Differences in survival curves were analyzed using log-rank (Mantel Cox) test. Group size (*n*) used to calculate significance is indicated in figure legend. For showing statistical significance: *p<0.05, **p<0.01, ***p<0.001, ****p<0.0001, unless otherwise stated.

2.6 Author Contributions

2.6.1 Author list

Laura T. Gray[1], Aaron T. Alpar[1], Michal M. Raczy[1], Koichi Sasaki[1,2], Aslan Mansurov[1], Tiffany M. Marchell[3], Joseph W. Reda[1], Suzana Gomes[1], Ani Solanki[4], Mindy Nguyen[1], Elyse A. Watkins[1], John-Michael Williford[1], Rachel P. Wallace[1], Anna Slezak[1], Kirsten Refvik[1], Lisa R. Volpatti[1], Benjamin T. Nicholson[5], Jun Ishihara[1,2], D. Scott Wilson[1,6], Melody A. Swartz[1,3,5,7], Jeffrey A. Hubbell[1,3,5]

2.6.2 Affiliations

[1]Pritzker School of Molecular Engineering, University of Chicago; Chicago, IL 60637, United States.

[2]Department of Bioengineering, Imperial College London; London, United Kingdom.

[3]Committee on Immunology, University of Chicago; Chicago, IL 60637, United States.

[4]Animal Resources Center, University of Chicago; Chicago, IL 60637, United States.

[5]Committee on Cancer Biology, University of Chicago; Chicago, IL 60637, United States.

[6]Department of Biomedical Engineering, Johns Hopkins School of Medicine; Baltimore, MD 21231, United States.

[7]Ben May Department of Cancer Research, University of Chicago; Chicago, IL 60637, United States.

2.6.3 Contributions

Jeffrey A. Hubbell, Melody A. Swartz, D. Scott Wilson, and Jun Ishihara oversaw all research; Laura T. Gray, Michal M. Raczy, and D. Scott Wilson performed the synthesis and characterization of the conjugates; Laura T. Gray, Koichi Sasaki, Elyse Watkins, and John-Michael Williford performed protein expression and purification; Joseph W. Reda assisted with SPR analysis; Suzana Gomes cultured all cancer cell lines used and performed endotoxin testing. Laura T. Gray, Jeffrey A. Hubbell, D. Scott Wilson, Jun Ishihara, Aaron T. Alpar, and Aslan Mansurov designed animal studies. Laura T. Gray, Aaron T. Alpar, Koichi Sasaki, Aslan Mansurov, Tiffany M. Marchell, Ani Solanki, Mindy Nguyen, Rachel P. Wallace, Anna Slezak, Kirsten Refvik, Lisa R. Volpatti, Benjamin T. Nicholson, Jun Ishihara, and D. Scott Wilson assisted with animal studies; Laura T. Gray wrote the manuscript.

2.7 Acknowledgements

We would like to acknowledge helpful conversations with Claudia Battistella, Abbey Lauterbach, Ako Ishihara, and Levi Bennish, as well as technical assistance from Yue Wang, that contributed to this work. Parts of this work were carried out at the Cytometry and Antibody

Technology Core Facility (Cancer Center Support Grant P30CA014599), the Soft Matter Characterization Facility, the Mass Spectrometry Facility (NSF instrumentation grant CHE-1048528), the Nuclear Magnetic Resonance Facility, the Human Tissue Resource Center, the Integrated Light Microscopy Core, the Optical Imaging Core Facility, and the Comprehensive Cancer Center DNA Sequencing and Genotyping at the University of Chicago. We would also like to thank the University of Chicago Animal Resources Center for help and guidance on animal work.

2.8 Funding

This work was supported by AbbVie; the National Institute of Allergy and Infectious Disease (NIAID) [grant T32-AI007090 – Tiffany M. Marchell]; and the Chicago Immunoengineering Innovation Center at the University of Chicago.

2.9 Data Availability

All data are available within the text, or can be obtained from the authors upon request.

2.10 Conflicts of Interest

The University of Chicago has filed for patent protection on the p(Man-TLR7) delivery platform, and Jeffrey A. Hubbell, D. Scott Wilson, Laura T. Gray, and Tiffany M. Marchell are named as co-inventors on one or more of these patents.

CHAPTER 3

GENERATION OF POTENT CELLULAR AND HUMORAL IMMUNITY AGAINST SARS-COV-2 ANTIGENS VIA CONJUGATION TO A POLYMERIC GLYCO-ADJUVANT

3.1 Abstract

The SARS-CoV-2 virus has caused an unprecedented global crisis, and curtailing its spread requires an effective vaccine which elicits a diverse and robust immune response. We have previously shown that vaccines made of a polymeric glyco-adjuvant conjugated to an antigen were effective in triggering such a response in other disease models and hypothesized that the technology could be adapted to create an effective vaccine against SARS-CoV-2. The core of the vaccine platform is the copolymer p(Man-TLR7), composed of monomers with pendant mannose or a toll-like receptor 7 (TLR7) agonist. Thus, p(Man-TLR7) is designed to target relevant antigen-presenting cells (APCs) via mannose-binding receptors and then activate TLR7 upon endocytosis. The p(Man-TLR7) construct is amenable to conjugation to protein antigens such as the Spike protein of SARS-CoV-2, yielding Spike-p(Man-TLR7). Here, we demonstrate Spike-p(Man-TLR7) vaccination elicits robust antigen-specific cellular and humoral responses in mice. In adult and elderly wild-type mice, vaccination with Spike-p(Man-TLR7) generates high and long-lasting titers of anti-Spike IgGs, with neutralizing titers exceeding levels in convalescent human serum. Interestingly, adsorbing Spike-p(Man-TLR7) to the depot-forming adjuvant alum, amplified the broadly neutralizing humoral responses to levels matching those in mice vaccinated with formulations based off of clinically-approved adjuvants. Additionally, we observed an increase in germinal center B cells, antigen-specific antibody secreting cells,

activated T follicular helper cells, and polyfunctional Th1-cytokine producing $CD4^+$ and $CD8^+$ T cells. We conclude that Spike-p(Man-TLR7) is an attractive, next-generation subunit vaccine candidate, capable of inducing durable and robust antibody and T cell responses.

3.2 Introduction

Since December 2019, coronavirus disease 2019 (COVID-19), caused by severe acute respiratory syndrome coronavirus 2 (SARS-CoV-2), has evolved into a major global public health crisis. COVID-19 has overwhelmed global health systems due to its ease of transmission, considerable caseloads requiring hospitalization, long in-clinic recuperation times, and a confirmed case-mortality rate at around 1-5% (with significantly higher rates in patients with comorbidities and of older age) [172–174]. As of September 2021, more than 200 million COVID-19 cases and more than 4.5 million deaths have been reported worldwide [175]. These features highlight an urgent need for a vaccine against SARS-CoV-2.

SARS-CoV-2 infections begin through viral recognition of angiotensin-converting enzyme-2 (ACE2) on target cells [176,177], mediated by the Spike glycoprotein that decorates the viral surface [178,179]. Spike typically exists as a homotrimer of 120 kDa proteins (>1100 residues each), of which the ACE2-binding function has been pinpointed to the receptor-binding domain (RBD) occurring around residues 319-541 [180–182]. Therefore, interfering with this binding interaction, by generating antibodies against Spike and/or RBD, represents a promising strategy to limit viral infectivity [183], and in fact, has been the predominant approach used in today's approved vaccines [184–187].

The urgent need for a vaccine has led to an immense number of vaccine candidates under

various stages of development worldwide. As of September 2021, there were over 224 SARS-CoV-2 vaccine candidates under pre-clinical development and around 107 candidates in clinical trials [188]. These numbers are the product of the inherent riskiness in the vaccine development process and include a wide range of technologies, such as DNA vaccines [189], vectored vaccines [190,191], inactivated vaccines [192] and protein subunit vaccines [193,194]. As a result of these development efforts, two mRNA-loaded lipid nanoparticle formulations, developed by Pfizer-BioNTech [2] and Moderna [3], and one viral vector-based vaccine by Johnson&Johnson [191,195] were granted emergency use authorizations in the US by the Food and Drug Administration (FDA) in December 2020 and February 2021, respectively. Since then, the Pfizer-BioNTech vaccine has gone on to receive FDA approval (August 2021) [196]. Beyond the successes, there have also been notable disappointments in the race toward vaccine development, including Sanofi/GSK's [197] and Merck's [198] vaccine candidates that failed to elicit satisfactory immune responses in Phase 1/2 clinical trials. Given the continuing global pandemic, it is likely that more vaccine candidates will be explored and tested in continued efforts to control additional outbreaks, reduce hospitalization and mortality related to infection, reduce vaccine related adverse events, and address newly-emerging strains of SARS-CoV-2.

Ultimately, a successful vaccine against SARS-CoV-2 will provide protection from infection and effectively block the development of severe COVID-19. To do that, it must not only generate high neutralizing antibody titers that can prevent the virus from binding to host cells [199,200], but it should also induce robust and durable T cell responses [201,202]. In fact, elevated T cell levels have been shown to be important in fighting SARS-CoV-2 infection in recovering patients, while reduced T cell numbers have been observed in patients who had severe disease [203–205]. In addition, a vaccine candidate should also favor the production of T

helper cell type 1 (Th1) over T helper cell type 2 (Th2) responses, as the latter have been associated with side effects including lung disease and vaccine-associated enhanced respiratory disease [206,207]. Conversely, Th1-biased immune responses have been shown to be associated with enhanced protection against viral infection [208–210]. Finally, because COVID-19 is disproportionately lethal for elderly patients (age > 65 years), an ideal vaccine must be effective in this age group, even though many vaccine candidates have decreased efficacy within this demographic [211].

Addressing these requirements, our group recently described a modular vaccine platform that incorporates a random co-polymer of mannose and imidazoquinoline toll-like receptor 7 (TLR7) agonist monomers (p(Man-TLR7)) with an antigen on the same macromolecule. This platform leverages the dendritic cell (DC)-targeting properties of mannose-binding C-type lectins to efficiently co-deliver antigens and a potent polymeric adjuvant to these cells, eliciting broad lymphocyte-driven responses [97]. The simplicity of our platform design allows the reversible conjugation of amine-containing antigens to the synthetic polymer p(Man-TLR7) in a manner such that the native antigen is released after reduction and self-immolation of the linker in response to intracellular signals. Following administration, the immunogenic conjugates are successfully taken up by DCs, resulting in antigen processing, cross-presentation, and activation. p(Man-TLR7) successfully adjuvanted ovalbumin and the malaria circumsporozoite protein (CSP), eliciting robust and high-quality humoral and cellular immune responses [97]. Moreover, vaccination with CSP-p(Man-TLR7) generated neutralizing antibodies that inhibited the invasion of *P. falciparum* sporozoites into human hepatocytes *ex vivo* [97].

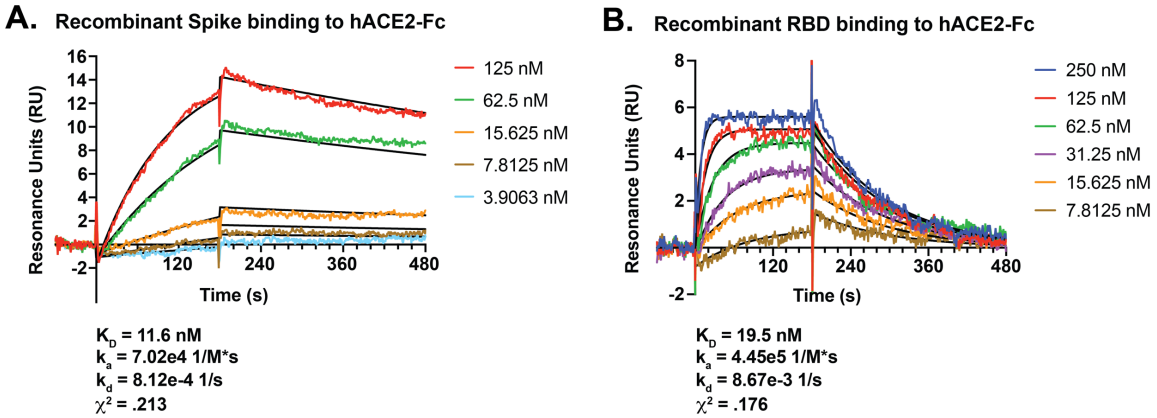

Figure 3.1: Surface Plasmon Resonance (SPR) analysis of binding of SARS-CoV-2 antigens to human ACE2 (hACE2).

Characterization of the binding between (**A**) Spike or (**B**) RBD and hACE2-Fc was conducted using SPR. The graphs represent the real-time binding profile for each antigen and calculated K_D, k_a, k_d and χ^2.

In this work, we hypothesized that the success of p(Man-TLR7) as a vaccine platform in other disease models would translate to SARS-CoV-2, resulting in robust neutralizing antibody responses and T cell responses against a conjugated viral antigen. To explore this, p(Man-TLR7) was conjugated to either the prefusion-stabilized Spike protein or its RBD. To place our preclinical work into broader context, we also evaluated our Spike-p(Man-TLR7) vaccine against benchmark formulations based on the most clinically advanced subunit vaccine adjuvants.

3.3 Results

3.3.1 In vitro characterization of antigen-p(Man-TLR7) conjugates

We first produced both Spike and RBD antigens and verified their binding ability to the ACE2 receptor via surface plasmon resonance (SPR; **Fig. 3.1, A and B**). The dissociation constants (K_D) were quantified at 11.6 nM and 19.5 nM, respectively, which corresponded with reported values of 2.9-14.7 nM [182,212] and 4.7-44.2 nM [179,180], respectively. These

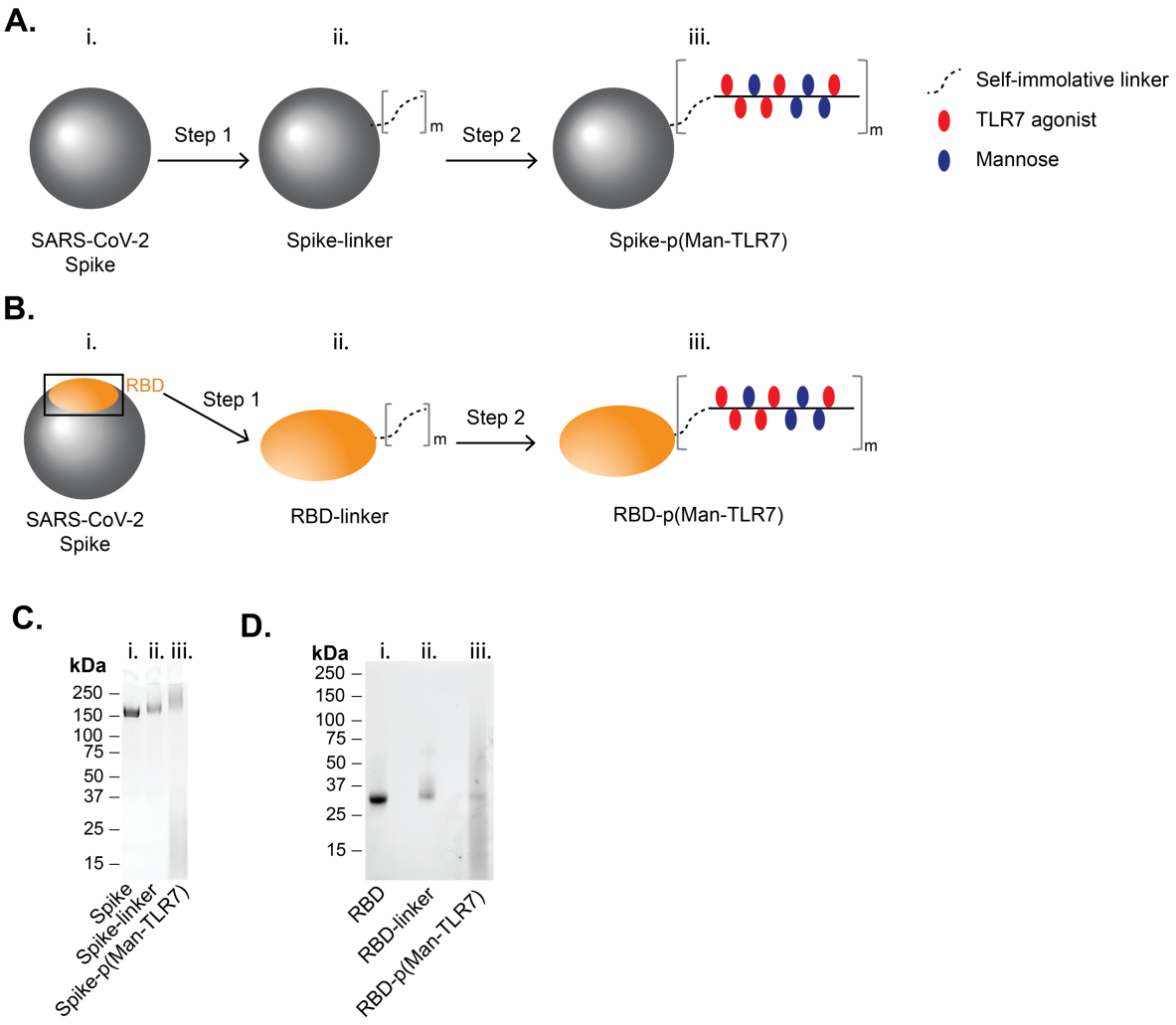

Figure 3.2: Generation of Spike-p(Man-TLR7) and RBD-p(Man-TLR7).

(**A**) Spike-p(Man-TLR7) is composed of Spike antigen (i.) conjugated, via a self-immolative linker (ii.), to p(Man-TLR7), a random copolymer synthesized from monomers that either activate TLR7 (red ovals) or target mannose-binding C-type lectins (blue ovals; iii.). (**B**) RBD-p(Man-TLR7) is composed of RBD antigen (i.) conjugated, via a self-immolative linker (ii.), to p(Man-TLR7) (iii.). (**C**) SDS-PAGE analysis of Spike before (i.) and after the two step conjugation reaction (ii., iii.). (**D**) SDS-PAGE analysis of RBD before (i.) and after the two step conjugation reaction (ii., iii.). The observed band between 15 and 25kDa comes from the free p(Man-TLR7) polymer in both (C and D).

antigens were then conjugated to the p(Man-TLR7) construct, yielding two subunit vaccine candidates: RBD-p(Man-TLR7) and Spike-p(Man-TLR7) (**Fig. 3.2, A and B**). The conjugation of the p(Man-TLR7) polymer to antigen via covalent self-immolative linkage was confirmed via

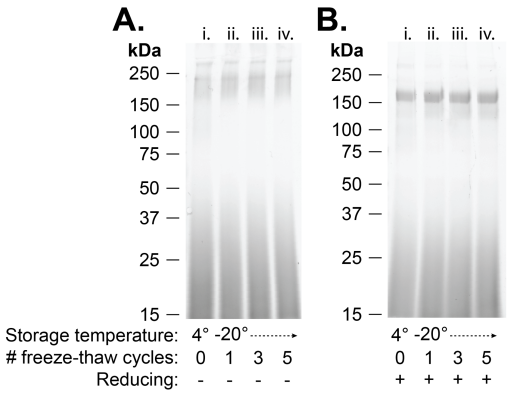

Figure 3.3: Spike-p(Man-TLR7) conjugates remain conjugated when stored at different temperatures long term and after multiple freeze-thaw cycles.

(**A and B**) SDS-PAGE analysis of Spike-p(Man-TLR7) after storage at 4°C for greater than 9 months (i.), or after storage at -20°C for greater than 9 months, followed by one (ii.), three (iii.), or five (i.v.) freeze-thaw cycles. The gels were run under non-reducing (A) or reducing (B) conditions. In both (A) and (B), the band observed between about 15 and 25 kDa in all lanes is free p(Man-TLR7).

sodium dodecyl sulfate-polyacrylamide gel electrophoresis (SDS-PAGE), as indicated by an increase in molecular weight (**Fig. 3.2, C and D**). The number of polymer molecules attached to antigen was estimated to be between 1 and 5 based on the SDS-PAGE results. Because long-term stability of vaccine formulations at different storage conditions is important for their practical worldwide distribution, especially to low-income countries, we also tested the stability of our vaccine by monitoring the change in molecular weight using SDS-PAGE analysis after long-term storage under several different conditions: storage at 4°C for greater than 9 months and storage at -20°C for greater than 9 months, followed by repeated freeze-thaw cycles. Because both of our vaccine conjugates are produced using the same methods and thus should have similar stability profiles, we chose to only analyze the stability of one vaccine conjugate, Spike-p(Man-TLR7). As evidenced by our analysis in **Fig. 3.3**, Spike-p(Man-TLR7) remained stable for at least 9 months when stored at 4°C, as the molecular weight observed here was consistent with that

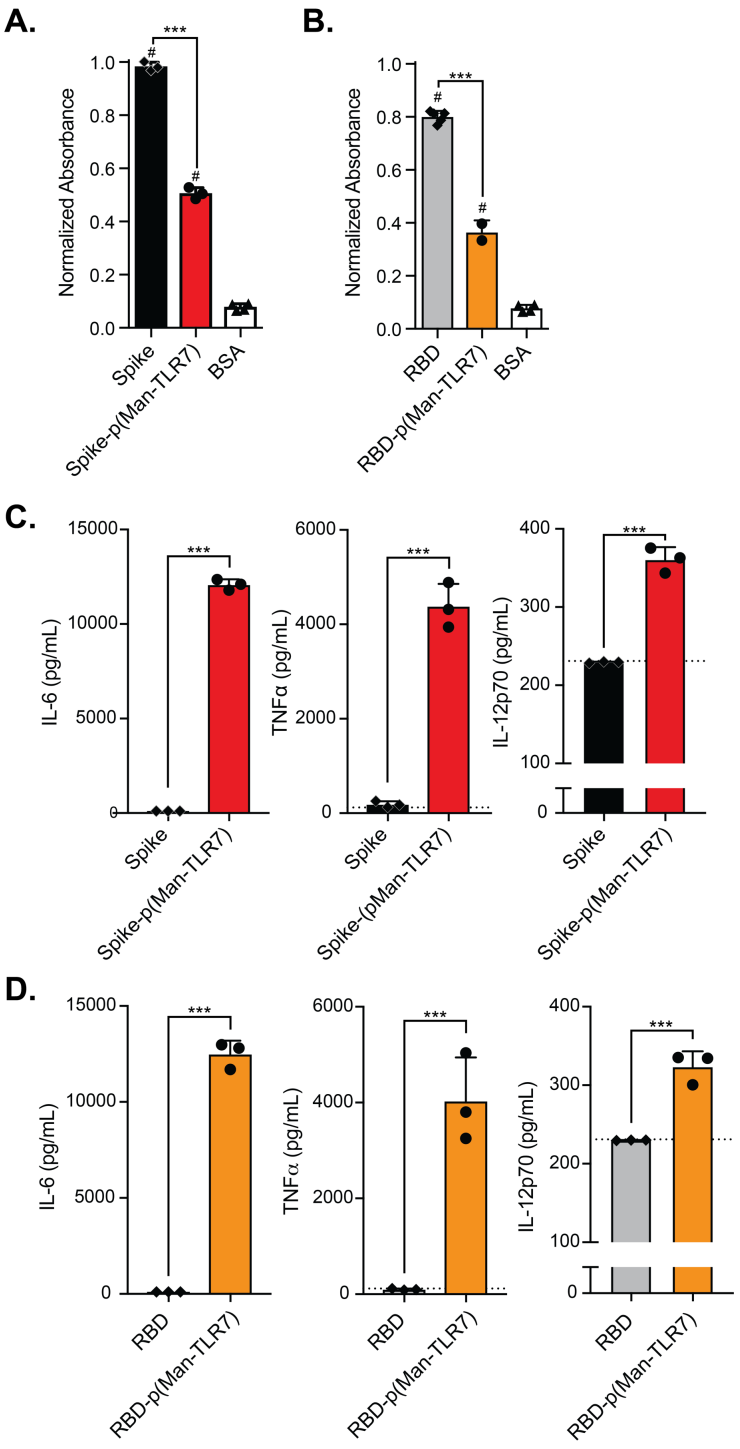

Figure 3.4: Spike- and RBD-p(Man-TLR7) retain binding to ACE2 and are potent activators of BMDCs.

(**A and B**) Analysis of the binding ability of Spike-p(Man-TLR7) (A) or RBD-p(Man-TLR7) (B) to human ACE2 (hACE2) via enzyme-linked immunosorbent assay (ELISA). (**C and D**) Concentration of IL-6, TNFα and IL-12p70 in the supernatant of BMDCs stimulated for 18h with Spike (C), Spike-p(Man-TLR7) (C), RBD (D), (Continued on next page)

Fig. 3.4, continued: or RBD-p(Man-TLR7) (D) at the concentration corresponding to 25μM of the adjuvant, as determined by ELISA. Dotted horizontal lines represent the assay background. In (C and D), columns and error bars indicate mean+SD; statistical comparisons are based on one-way ANOVA with Tukey's post-test: *** $p<0.001$; # $p<0.001$ as compared to bovine serum albumin (BSA).

observed for Spike-p(Man-TLR7) in **Fig. 3.2C**. In addition, after storage at -20°C for greater than 9 months, the conjugate can be thawed and frozen again at least 5 times without affecting the molecular weight (**Fig. 3.3, A and B**).

Because of the nature of this conjugation, the protein's surface accessible lysine residues are modified at random, which could interfere with the binding ability to ACE2. As the ACE2 binding site on Spike and RBD is an important epitope for generating neutralizing antibodies [183], steric hindrance of this site by the p(Man-TLR7) polymer could negatively affect the generation of neutralizing antibodies. Despite these concerns, RBD-p(Man-TLR7) and Spike-p(Man-TLR7) both retained ACE2-binding activity, although at half the levels of unmodified antigens (**Fig. 3.4, A and B**) Furthermore, we validated that antigen-p(Man-TLR7) conjugates activated murine bone marrow-derived dendritic cells (BMDCs) in a manner consistent with previous publications [97]. Unlike unmodified antigens, both RBD-p(Man-TLR7) and Spike-p(Man-TLR7) stimulated BMDCs to secrete the immunostimulatory cytokines IL-12p70, IL-6, and TNFα (**Fig. 3.4, C and D**).

Lastly, one of the commonly observed side effects upon administration of synthetic vaccines and nanomedicines is complement activation-related pseudoallergy (CARPA) [213]. Activation of complement, especially through the lectin pathway, has been reported in the case of intravenously infused nano-formulations, such as pegylated liposomes (i.e. Doxil) [214]. This results in a cascade reaction that leads to the generation of the anaphylatoxins C3a and C5a,

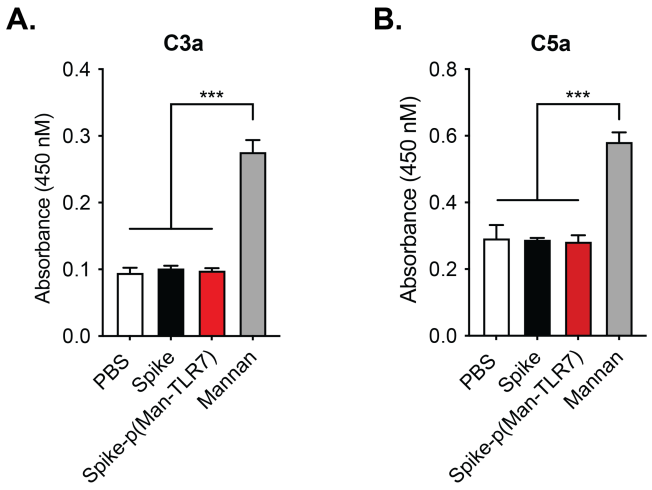

Figure 3.5: Anaphylatoxins are not generated when mouse serum is incubated with Spike-p(Man-TLR7) *ex vivo*.

(**A and B**) Serum isolated from C57Bl/6 mice was incubated for 45 minutes at 37°C with either PBS, Spike, Spike-p(Man-TLR7) or mannan (positive control) adsorbed onto the microwell plate. The concentration of generated mouse anaphylatoxins C3a (A) and C5a (B) was quantified by ELISA. Comparisons were made using one-way ANOVA with Tukey's post-test: ***$p<0.001$.

which bind to anaphylatoxin receptors on immune cells. This triggers intracellular signaling that results in degranulation and release of molecules such as histamines [215]. The presence of PEG and mannose residues in the antigen-p(Man-TLR7) structure could potentially trigger activation of complement through the lectin pathway and the generation of anaphylatoxins. In order to assess whether our vaccine formulations trigger this activation, we incubated serum isolated from C57Bl/6 mice in plates coated with PBS-, Spike-, Spike-p(Man-TLR7)- or mannan. Here, we again chose to focus only on Spike-p(Man-TLR7), as both of our vaccine formulations utilize the same p(Man-TLR7) polymer. Using enzyme-linked immunosorbent assays (ELISA), we discovered that the concentration of the C3a and C5a anaphylatoxins was elevated above the PBS background only in serum incubated with mannan (**Fig. 3.5, A and B**), a polysaccharide that has been shown to activate complement through the lectin pathway [216]. This *ex vivo* assay

confirmed that Spike-p(Man-TLR7) does not activate complement in direct contact with mouse serum, pointing towards a low risk for subcutaneous administration of our conjugates inducing CARPA. Overall, functional recombinant Spike and RBD were successfully expressed in-house and coupled onto p(Man-TLR7) to generate conjugates that retain ACE2 binding activity, show superior DC stimulation compared to unmodified antigen, and do not activate complement via the lectin pathway *ex vivo*.

3.3.2 Vaccination with Spike-p(Man-TLR7) but not RBD-p(Man-TLR7) elicits SARS-CoV-2 neutralizing antibody responses

Next, we asked if the DC immune-stimulatory capacity of the conjugates *in vitro* would translate to superior antibody responses *in vivo*. To evaluate this, healthy adult C57BL/6 mice were vaccinated subcutaneously (s.c., in the hocks) in a prime-boost schedule 3 weeks apart, and sacrificed a week after the boost (**Fig. 3.6A**). We first assessed the humoral response in mice vaccinated with RBD-p(Man-TLR7) compared to mice vaccinated with RBD alone or adjuvanted with a mimic of the clinically-approved adjuvant AS04 (RBD+AS04-L; protein mixed with alum (aluminum hydroxide wet gel suspension) and monophosphoryl lipid A (MPLA); L for 'like'), formulated according to published procedures [217]. AS04 was designated as a positive control adjuvant due to its success in stimulating broad lymphocyte-driven responses against virally-mediated diseases such as those caused by the human papillomavirus [218,219] and Hepatitis B virus [218,219], making it an ideal benchmark for evaluating the efficacy of the p(Man-TLR7) platform.

Vaccination with RBD-p(Man-TLR7) induced circulating levels of RBD-specific IgGs that trended higher than levels observed in mice vaccinated with RBD alone and naïve mice (p =

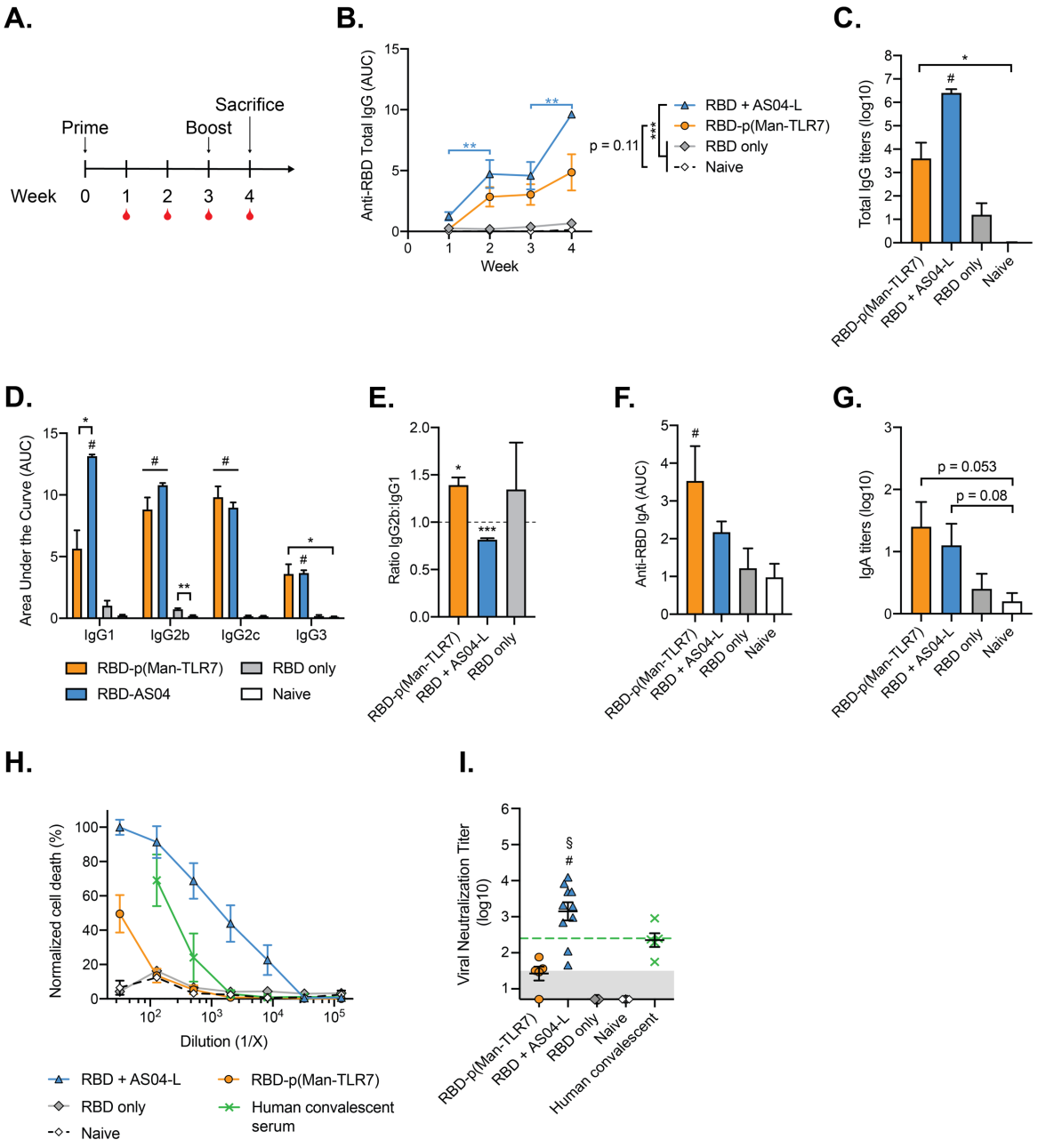

Figure 3.6: RBD-p(Man-TLR7) vaccination generates RBD-specific antibodies, which fail to potently neutralize SARS-CoV-2.

(A) Mice were vaccinated with RBD-p(Man-TLR7), RBD+AS04-L, or RBD at weeks 0 (prime) and 3 (boost) and their plasma was collected weekly up until week 4. Plasma from naïve mice was collected at the same time points. (**B**) Total RBD-specific IgG antibodies over time reported as the area under the log-transformed curve (AUC) of absorbance vs. dilution. (**C**) Titers of total RBD-specific IgG antibodies at week 4. (**D**) Comparison of RBD-specific IgG Isotypes (IgG1, IgG2b, IgG2c and IgG3) and (**E**) corresponding IgG2b:IgG1 ratios at one week post boost (week 4). (**F and G**) Circulating anti-RBD IgA antibodies quantified at week 4 via (F) AUC analysis and (G) titration. (**H**) Neutralization assay of SARS-CoV-2 infection (Continued on next page)

Fig. 3.6, continued: on Vero-E6 cells in vitro. SARS-CoV-2 was pre-incubated with plasma isolated from mice at week 4. Percent neutralization was calculated based on viability of cells that did not receive virus (100%) or virus without plasma preincubation (0%). (**I**) Viral neutralization titers, representing plasma dilution at which 50% of SARS-CoV-2-mediated cells death is neutralized. Shaded area represents the lower limit of detection (titer of 2.11); green dotted horizontal line represents FDA recommendation for "high titer" classification (= 2.40). All data are presented as mean±SEM with n = 5-10 mice per group. Comparisons were made using (B) two-way ANOVA with Tukey's multiple comparison test, (C and D) Brown-Forsythe ANOVA with Dunnet's T3 test, (E) one sample t test (compared to the theoretical value of 1, representing an unbiased Th1/Th2 response), (F and G) one-way ANOVA with Tukey's post-test, or (I) Kruskal-Wallis non-parametric test with Dunn's post-test: * $p<0.05$, ** $p<0.01$, *** $p<0.001$; # $p<0.05$ (for comparison to both RBD and Naïve groups). Additional comparisons were made in (I) using Wilcoxon signed rank test: § $p<0.05$ (as compared to the FDA "high titer" classification). In (B), comparisons noted on the graph in blue are between the indicated timepoints for RBD+AS04-L, and comparisons noted in the legend are between the indicated groups at week 4. In (B), only relevant statistical comparisons are shown.

0.15 and $p = 0.11$, respectively; **Fig. 3.6, B and C**). Although RBD+AS04-L induced even higher levels of RBD-specific antibodies, RBD-p(Man-TLR7)-elicited antibody isotypes were suggestive of Th1-skewing (**Fig. 3.6, D and E**), as observed by comparing the ratio of IgG2b to IgG1 [220,221], as well as increased levels of anti-RBD serum IgA (**Fig. 3.6, F and G**). IgG2 isotypes in mice are known to exhibit potent anti-viral activity [222,223], and SARS-CoV-2-specific serum IgA antibodies have been shown to rapidly increase after the onset of COVID-19 and to have neutralization potential [224,225].

We then asked if vaccine-elicited RBD-specific antibodies could effectively neutralize SARS-CoV-2 virions, preventing their ability to infect Vero-E6 cells *in vitro*. We observed that while plasma from mice vaccinated with RBD-p(Man-TLR7) showed an increase in virus neutralization titer (VNT) compared to mice vaccinated with RBD alone, it failed to meet the FDA-recommended VNT threshold for COVID-19 convalescent plasma therapy (**Fig. 3.6, H and I**) [226]. At the same time, we observed that plasma from mice vaccinated with the RBD+AS04-L formulation protected Vero-E6 cells against viral infection *in vitro* (**Fig. 3.6, H**

and I).

Next, we assessed the humoral responses of mice vaccinated with Spike-p(Man-TLR7), following the same vaccination schedule (**Fig. 3.7A**). We also compared this formulation against additional benchmarks mimicking clinically-approved vaccine formulations based on alum: Spike+alum and Spike-p(Man-TLR7)+alum. Alum has been shown to enhance antigen availability, activation of antigen presenting cells (APCs), and uptake by immune cells through the formation of a depot at the injection site [227–230]. Additionally, alum is commonly used in combination with other adjuvants with direct immunostimulatory activity, as embodied by one COVID-19 vaccine candidate in clinical testing that formulates Spike with alum and the TLR9 agonist CpG [231]. Based on these properties of alum, we hypothesized that it could synergize with Spike-p(Man-TLR7) to produce a strong humoral response. In addition, we compared our formulations with Spike alone and Spike+AS04-L, as well as with Spike+AS03-L (Spike mixed with an oil-in-water emulsion of α-tocopherol, squalene, and polysorbate 80). AS03-L is an analog of the clinical AS03 adjuvant, which has been investigated in clinical trials as a COVID-19 vaccine with the Spike protein as the antigen [232].

In our studies, vaccination with Spike-p(Man-TLR7) elicited higher titers of Spike-specific antibodies versus vaccination with Spike alone ($p<0.001$) or in naïve mice ($p<0.001$, **Fig. 3.7B**). The benchmark vaccine formulations Spike+AS03-L and Spike+AS04-L elicited even higher Spike-specific IgG titers, but these levels were matched by Spike-p(Man-TLR7)+alum (**Fig. 3.7B**). Compared to all of these groups, however, Spike-p(Man-TLR7)-elicited IgG isotypes were more suggestive of Th1 activity, based on the ratio of IgG2b to IgG1 (**Fig. 3.7, C and D**). Notably, this vaccine, with or without alum, also increased levels of Spike-

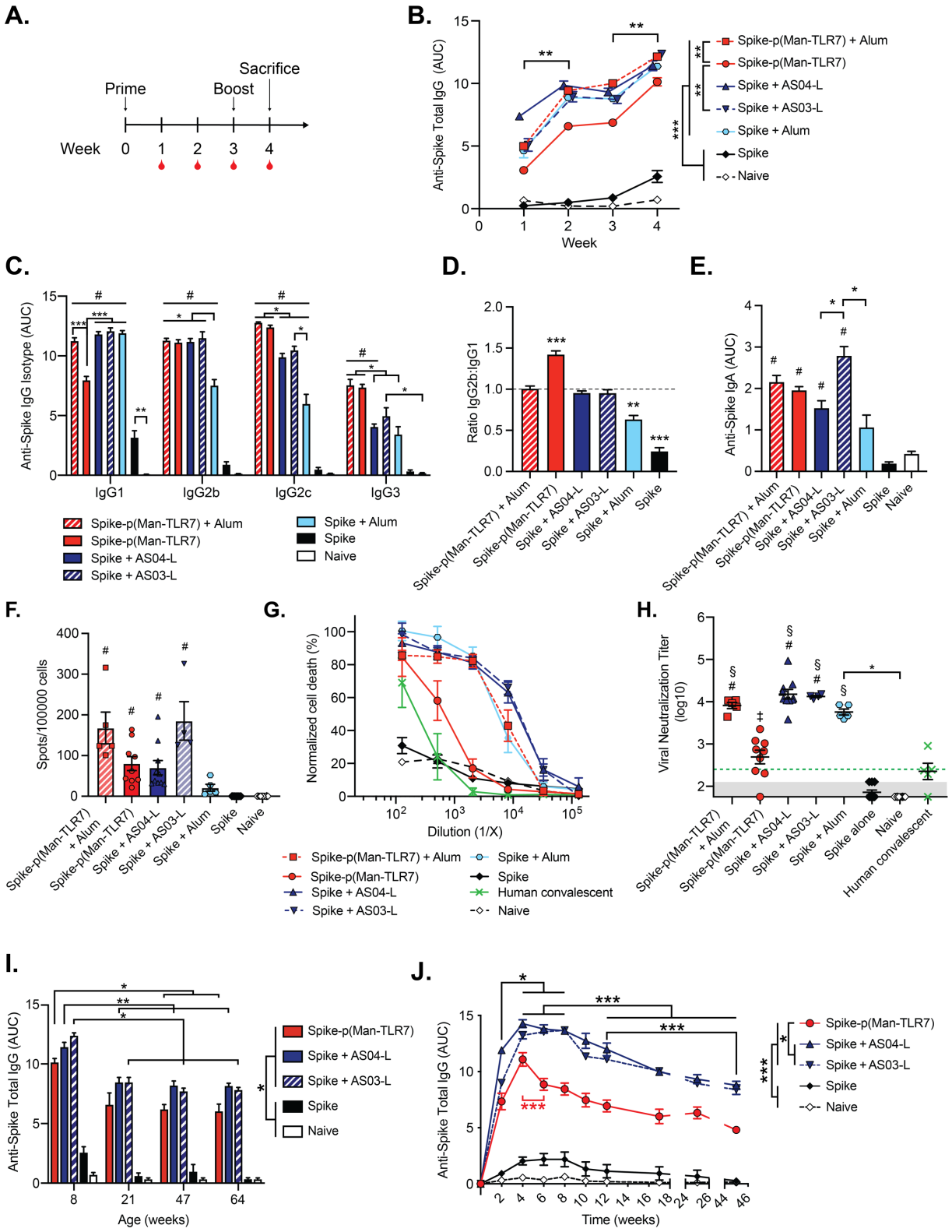

Figure 3.7: Spike-p(Man-TLR7) and Spike-p(Man-TLR7)+alum generate potent humoral responses in mice.

(Continued on next page)

Fig. 3.7, continued: (**A**) Mice were vaccinated with Spike-p(Man-TLR7), Spike-p(Man-TLR7)+alum, Spike+AS04-L, Spike+AS03-L, Spike+alum, or Spike at weeks 0 (prime) and 3 (boost), and their plasma was collected weekly until week 4. Plasma from naïve mice was collected at the same time points. (**B**) Total Spike-specific IgG antibodies over time reported as the area under the log-transformed curve (AUC) of absorbance vs. dilution. (**C**) Comparison of Spike-specific IgG isotypes (IgG1, IgG2b, IgG2c and IgG3) and (**D**) corresponding IgG2b:IgG1 ratios at one week post-boost (week 4). (**E**) Circulating anti-Spike IgA antibodies in the serum of vaccinated mice quantified at week 4 using AUC analysis. (**F**) Quantification of Spike-specific IgG^+ antibody secreting cells by enzyme-linked immunosorbent spot (ELISpot) assay with splenocytes. (**G**) Neutralization assay of SARS-CoV-2 infection on Vero-E6 cells *in vitro*. SARS-CoV-2 was pre-incubated with plasma isolated from mice at week 4. Percent neutralization was calculated based on viability of cells that did not receive virus (100%) or virus without plasma preincubation (0%). (**H**) Viral neutralization titers, representing plasma dilution at which 50% of SARS-CoV-2-mediated cell death is neutralized. Shaded area represents the lower limit of detection (titer of 2.11); green dotted horizontal line represents the FDA recommendation for "high titer" classification (= 2.40). (**I**) Comparison of total Spike-specific IgG antibodies in the plasma of 8, 21, 47 and >64 week old mice that received the indicated vaccines, following the same schedule as in (A). (**J**) Change in total Spike-specific IgG antibodies over time in plasma of mice (n = 5) that received the indicated vaccines, following the same vaccination schedule as in (A). All data are presented as mean±SEM with n = 4-10 mice per group, unless stated otherwise. Comparisons were made using (B and I) two-way ANOVA with Tukey's multiple comparison test, (C and E) Brown-Forsythe ANOVA with Dunnet's T3 test, (D) one sample t test (compared to the theoretical value of 1, representing an unbiased Th1/Th2 response), (F and H) Kruskal-Wallis non-parametric test with Dunn's post-test, or (J) mixed-effects analysis with Tukey's multiple comparison test: * $p<0.05$, **$p<0.01$, *** $p<0.001$; # $p<0.05$ (for comparison to both Spike and naïve groups). Additional comparisons were made in (H) using Wilcoxon signed rank test: § $p<0.05$ and ‡ $p=0.11$ (as compared to the FDA "high titer" classification). In (B), comparisons noted on the graph are between the indicated timepoints for all groups except Spike and Naïve, while comparisons noted in the legend are between the indicated groups at week 4. In (I), comparisons indicated in the legend are true for mice at each age. In (J), comparisons noted on the graph in black are between the indicated timepoints for all groups except Spike and Naïve, and comparisons indicated in red are only for Spike-p(Man-TLR7). Comparisons indicated in the legend of (J) are true for every timepoint. In (B, I, and J), only relevant statistical comparisons are shown.

specific serum IgA, as compared to mice vaccinated with Spike alone, Spike adjuvanted with alum or AS04-L, or naïve mice (**Fig. 3.7E**). However, vaccination with Spike+AS03-L stimulated the highest levels of serum IgA among all groups (**Fig. 3.7E**). In agreement with these Spike-specific antibody responses, all adjuvanted formulations also resulted in an increase in the number of Spike-specific antibody secreting cells (ASCs) as compared to mice vaccinated with Spike alone or naïve mice, with the highest numbers of ASCs observed in mice vaccinated with

Spike-p(Man-TLR7)+alum and Spike+AS03-L (**Fig. 3.7F**).

All adjuvanted vaccine formulations led to demonstrable neutralization of SARS-CoV-2 infection on Vero-E6 cells. In this regard, plasma from mice vaccinated with Spike-p(Man-TLR7) exceeded the FDA-recommended VNT threshold for convalescent plasma therapy, demonstrating superior neutralization activity over human convalescent plasma and 1.6-fold greater neutralization activity versus plasma from mice vaccinated with Spike alone or from naïve mice (**Fig. 3.7, G and H**). While vaccination with either Spike+AS04-L, Spike+AS03-L, or Spike+alum all led to even greater VNTs (**Fig. 3.7, G and H**), co-formulation of Spike-p(Man-TLR7) with alum allowed this platform to match the VNTs elicited by these positive control benchmarks (**Fig. 3.7, G and H**).

We then asked if the efficacy of Spike-p(Man-TLR7) in eliciting strong humoral responses in adult healthy mice would also translate to elderly mice. Four weeks after they received the priming dose, mice of all ages, ranging from 8 to >64 weeks, exhibited high titers of anti-Spike IgGs in all adjuvanted groups assessed (**Fig. 3.7I**). Furthermore, these responses were durable in adult mice, persisting for at least 45 weeks after the priming dose, with area under the curve (AUC) values from log-transformed ELISA absorbance plots for total anti-Spike IgG still exceeding 4.0 at week 45 (**Fig. 3.7J**). The AUC levels peaked at above 10 by week 4, and an initial drop in the levels of antibodies was observed between weeks 4 and 6 for mice vaccinated with Spike-p(Man-TLR7). After 45 weeks, the antibody levels were significantly reduced for mice vaccinated with all adjuvanted formulations as compared to the peak at week 4 (**Fig. 3.7J**). However, the levels of total anti-Spike IgG remained significantly higher in mice vaccinated with all adjuvated formulations than in mice vaccinated with Spike alone up to week 45 (**Fig.**

3.7J).

Taken together, our observations indicate that Spike-p(Man-TLR7) is able to induce a robust humoral response in both adult and elderly mice and that antibodies induced by the p(Man-TLR7) platform persist for at least 45 weeks after the priming dose. Additionally, the humoral response is further increased by the addition of alum to Spike-p(Man-TLR7).

3.3.3 Expansion of epitopic coverage upon Spike-p(Man-TLR7) vaccination

Viruses tend to mutate to evade even the most effective neutralizing antibodies, and as such, a vaccination strategy that can elicit broad epitope coverage might be important to control a mutable virus. We characterized the repertoires of Spike-specific antibodies raised by each vaccine formulation via peptide arrays of linear Spike epitopes. The peptide arrays were constructed based on the full linear amino acid sequence of the SARS-CoV-2 Spike protein (NCBI GenBank accession # QHD43416.1), encompassing 254 unique 15-mer overlapping peptides with 5-amino acid offsets.

While vaccination with unadjuvanted Spike resulted in antibodies that recognized only a limited number of epitopes, p(Man-TLR7) conjugation expanded the epitope coverage to linear epitopes corresponding to the ACE2 binding site of RBD [233] and two previously reported linear Spike epitopes shown to elicit neutralizing antibodies in COVID-19 patients (**Fig. 3.8**) [234,235]. Notably, the addition of alum to Spike-p(Man-TLR7) further expanded the breadth of recognized epitopes, matching or surpassing the breadth of epitopes recognized by antibodies from mice vaccinated with Spike+AS04-L, Spike+AS03-L, or Spike+alum (**Fig. 3.8**).

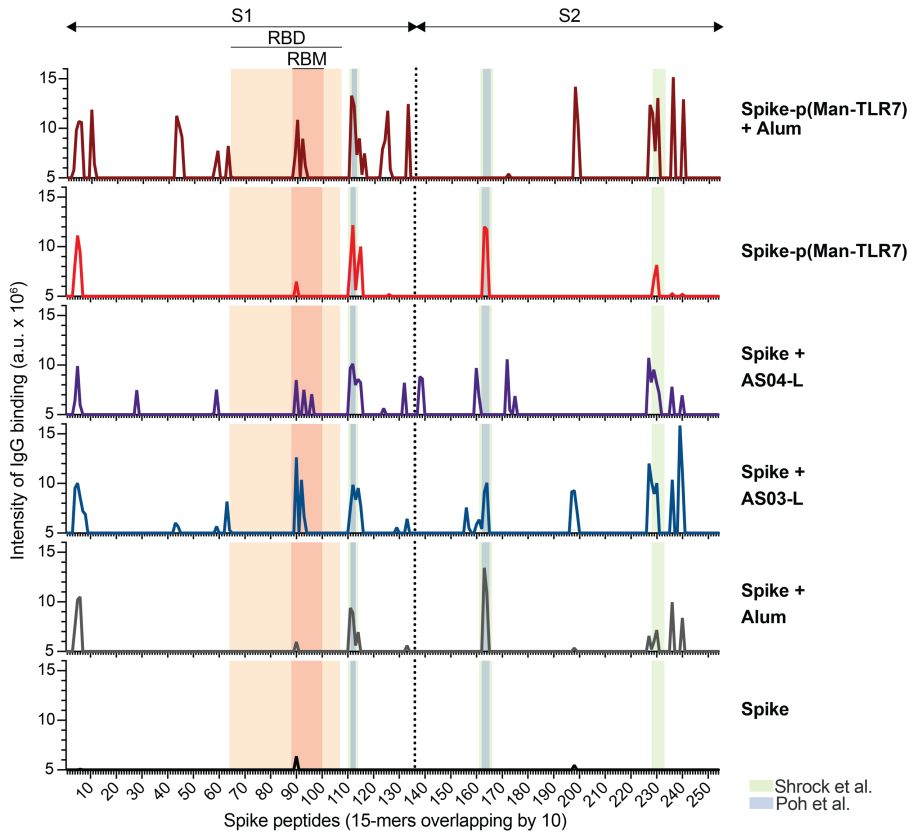

Figure 3.8: Vaccination with Spike-p(Man-TLR7) and Spike-p(Man-TLR7)+alum elicits a broad humoral response targeting the receptor binding motif (RBM) of RBD and other neutralizing linear epitopes.

Mice were vaccinated as in Fig. 3.7A. Plasma was collected at week 4, pooled by vaccination group, and analyzed for binding to linear epitopes using a peptide array. X-axis represents the sequential peptide number within the Spike amino acid sequence (overlapping 15-amino acid peptides with 5-amino acid offsets). Y-axis quantifies the level of antibody binding to each peptide, detected via luminescence (a.u.). Axis begins from the value of the background, which was set at 5 x 10^6 a.u. Several relevant regions of the Spike protein are indicated above the graphs: S1 and S2 subunits, RBD (light orange box), and RBM (dark orange box). Regions corresponding to neutralizing Spike epitopes identified by Shrock et al. [234] and Poh et al. [235] are indicated in light green and light blue boxes, respectively.

3.3.4 Spike-p(Man-TLR7) platforms induce antigen-specific B cell immunity and expansion of T_{fh} cells

Due to the higher neutralizing antibody titers and broader epitope coverage found in the p(Man-TLR7) conjugated group compared to vaccination with Spike alone, we asked how these differences might be reflected in B cell responses in the secondary lymphoid organs. We analyzed the lymph nodes and spleens of vaccinated mice to examine the phenotypes and activation of B cells (**Fig. A.4**) and follicular helper $CD4^+$ T (T_{fh}) cells (**Fig. A.5**), the cells responsible for establishing humoral immunity.

Spike-p(Man-TLR7), both with and without alum, triggered B cell ($CD19^+$ $B220^+$) expansion in the draining lymph nodes and spleen as compared to mice vaccinated with Spike alone or naïve mice (**Fig. 3.9, A and B; Fig. A.4a**). While Spike-p(Man-TLR7) elicited higher frequencies of germinal center (GC) B cells (IgD^- $GL7^+$ $CD38^-$) among splenic and lymph node B cells versus vaccination with Spike alone or in naïve mice, vaccines containing alum were generally even more effective at inducing GC B cells in the lymph nodes. As such, Spike-p(Man-TLR7)+alum triggered fourfold higher frequencies of GC B cells among lymph node B cells versus Spike-p(Man-TLR7) alone (3.4 ± 0.1% vs. 0.8 ± 0.1%) – levels matched by Spike+AS04-L (3.2 ± 0.5%) and Spike+alum (3.7 ± 0.4%) and exceeded by Spike+AS03-L (7.8 ± 0.5%; **Fig. 3.9, A and B**). In contrast, Spike-p(Man-TLR7) and Spike+AS03-L vaccination resulted in the highest frequencies of GC B cells in the spleen (1.2± 0.3% and 1.3± 0.3%, respectively), while the alum-containing formulations (Spike-p(Man-TLR7)+alum, Spike+AS04-L, and Spike+alum) did not result in as high levels of systemic GC responses (**Fig. 3.9B**). Reflective of these trends, the frequency of GC B cells that recognized RBD were elevated in mice treated with Spike-

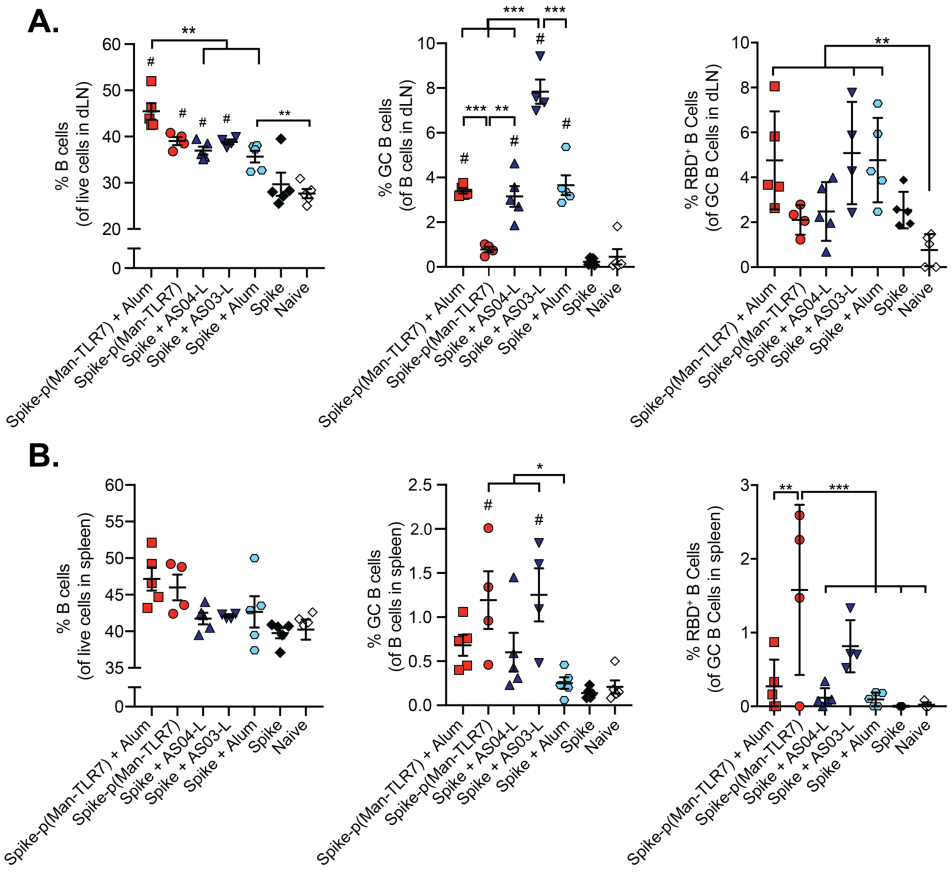

Figure 3.9: Secondary lymphoid organ-resident B cells are activated in mice vaccinated with Spike-p(Man-TLR7) or Spike-p(Man-TLR7)+alum.

(**A and B**) Quantification of B cells resident within the (A) draining LNs (dLNs) of the vaccination site or (B) spleen via flow cytometry at week 4 after vaccination as in Fig. 3.7A. From left to right, total B cells ($CD19^+$ $B220^+$) within live cells, germinal center (GC) B cells ($IgD^-GL7^+CD38^-$) within live B cells, and RBD tetramer reactive GC B cells (RBD^+) as a percentage of GC B cells. Data plotted as mean±SEM with n = 4-5 mice per group. *p<0.05, ** p<0.01, ***p<0.001 by one-way ANOVA with Tukey's post-test; # p<0.05 as compared to both Spike and naïve.

p(Man-TLR7) or Spike-p(Man-TLR7)+alum in the spleen or lymph nodes, respectively (**Fig. 3.9, A and B; Fig. A.4, b and c)**. Additionally, Spike-p(Man-TLR7)+alum increased the frequency of memory B cells (IgD^- $GL7^-$ $CD38^+$) in the draining lymph nodes compared to non-adjuvanted controls and to Spike-p(Man-TLR7) (**Fig. 3.10A**). Moreover, we observed a significant reduction in the naïve B cell population in the draining lymph nodes of mice

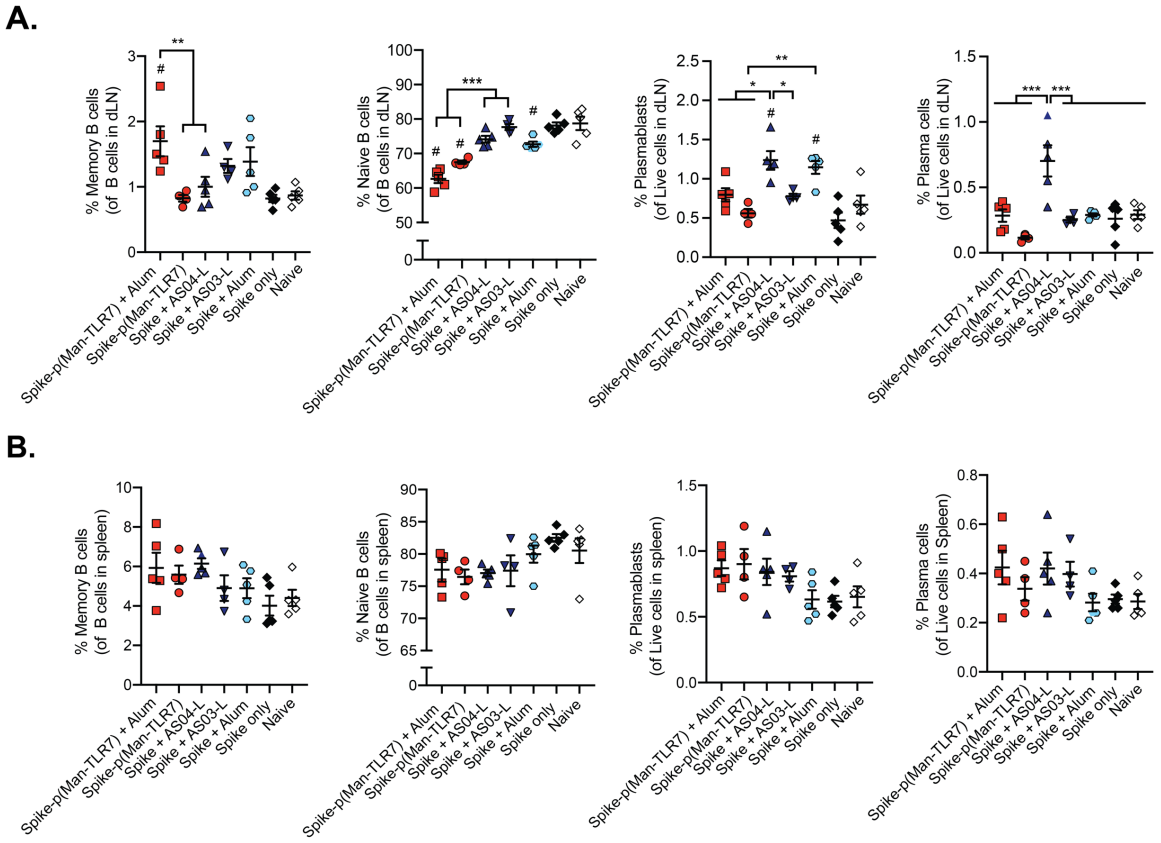

Figure 3.10: Naïve B cells, memory B cells, plasmablasts, and plasma cells in vaccinated mice one week post-boost.

(**A and B**) Characterization of B cells resident within the (A) dLNs of the vaccination site or (B) spleen via flow cytometry at week 4 after vaccination (mice were vaccinated as in Fig. 3.7A). (A-B) From left to right: memory B cells ($IgD^+GL7^-CD38^+$) within all B cells, naïve B cells ($IgM^+IgD^+GL7^-$) within B cells, plasmablasts ($B220^+$ $CD138^+$) within all live cells, and plasma cells ($B220^-CD138^+$) within all live cells. Data presented as mean±SEM with n = 4-5 mice per group; *p<0.05, ** p<0.01, ***p<0.001 via one-way ANOVA with Tukey's post-test; # p<0.05 as compared to both Spike and naïve.

vaccinated with either Spike-p(Man-TLR7) or Spike-p(Man-TLR7)+alum (**Fig. 3.10A**). In the spleen, the different vaccine formulations were not associated with statistically significant differences in memory or naïve B cell composition (**Fig. 3.10B**). Lastly, neither Spike-p(Man-TLR7) nor Spike-p(Man-TLR7)+alum increased the frequencies of plasmablasts ($CD138^+$ $B220^+$) or plasma cells ($CD138^+$ $B220^-$) observed via flow cytometry at one week post-boost in

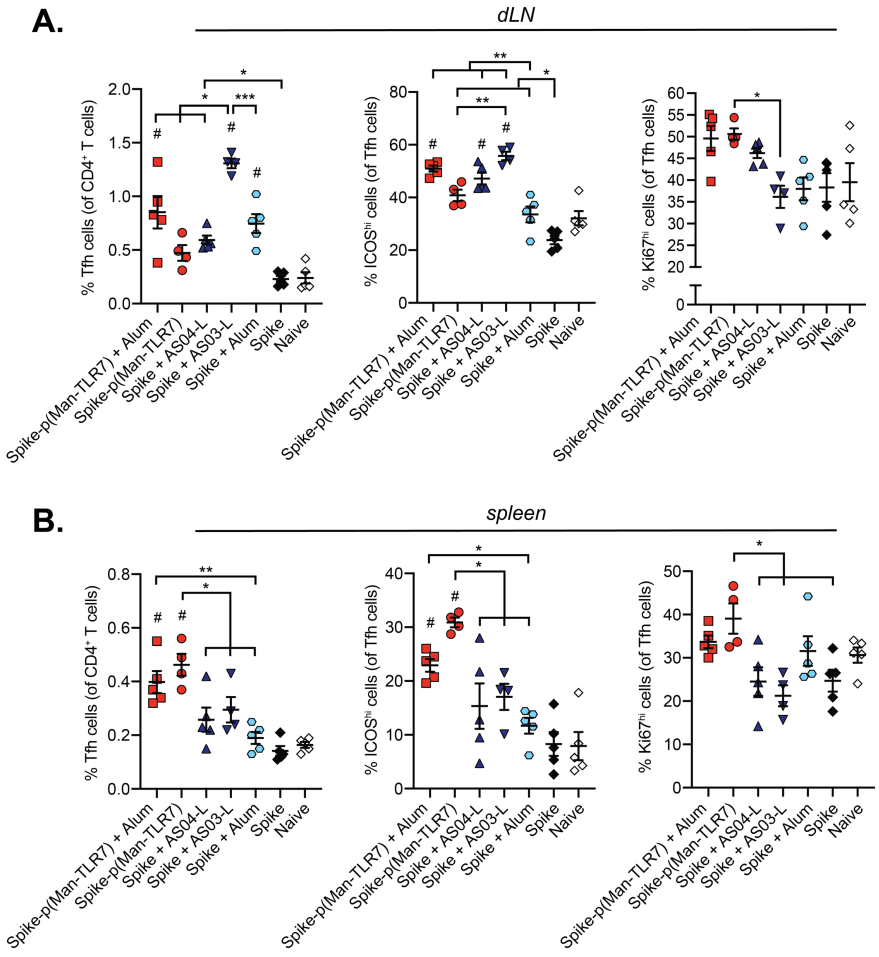

Figure 3.11: CD4$^+$ T follicular helper (T_{fh}) cells are activated in mice vaccinated with Spike-p(Man-TLR7) or Spike-p(Man-TLR7)+alum.

(**A and B**) Activation of CD4$^+$ T_{fh} cells in the dLNs (A) and the spleen (B) was characterized by flow cytometry. T_{fh} cells were defined as CXCR5$^+$BCL6$^+$CD4$^+$ and quantified within CD4$^+$ T cells. ICOS^{hi} T_{fh} cells or Ki67^{hi} T_{fh} cells were quantified within T_{fh} cells. Data plotted as mean±SEM with n = 4-5 mice per group. *p<0.05, ** p<0.01, ***p<0.001 by one-way ANOVA with Tukey's post-test; # p<0.05 as compared to both Spike and naïve.

both the draining lymph nodes and spleen, although a trend towards increased levels was observed in the spleen (**Fig. 3.10, A and B**).

Shifting our focus to the T_{fh} cells (CD4$^+$ Bcl6$^+$ CXCR5$^+$), we observed that animals vaccinated with Spike-p(Man-TLR7)+alum showed an increase in the fraction of T_{fh} cells in both

the spleen and draining lymph nodes compared to mice treated with most other formulations (**Fig. 3.11, A and B; Fig. A.5**). In addition, while a significantly higher fraction of these T_{fh} cells expressed a marker of activation ($ICOS^{hi}$) in both the lymph nodes and spleen compared to unadjuvanted controls, we detected only modest trends towards increased proliferation of these cells, discerned by high expression of Ki67 (**Fig. 3.11, A and B**). In the absence of alum, Spike-p(Man-TLR7) increased frequencies of both total and activated T_{fh} cells in the spleen, but not in the draining lymph nodes, compared to mice treated with other formulations (**Fig. 3.11, A and B**).

Altogether, Spike-p(Man-TLR7) vaccination induced antigen-specific B cell immunity and expansion of activated T_{fh} cells in the spleen, while the addition of the adjuvant alum localized the response to the draining lymph nodes.

3.3.5 Th1 biased cellular responses are observed upon vaccination with Spike-p(Man-TLR7) with and without alum

The establishment of T cell responses plays an essential role in protection against infectious diseases [236]. Some reports indicate that cellular immunity is as crucial as humoral immunity in COVID-19 recovery [237]. Therefore, we characterized the antigen-specific T cell responses in the spleens of mice vaccinated with either Spike-p(Man-TLR7) conjugates or benchmark formulations. One week after the boost, splenocytes from all vaccinated and control mice were restimulated *ex vivo* with Spike peptide pools, and we quantified intracellular levels of the costimulatory cytokines IFNγ, TNFα, and IL-2 (**Fig. A.6**).

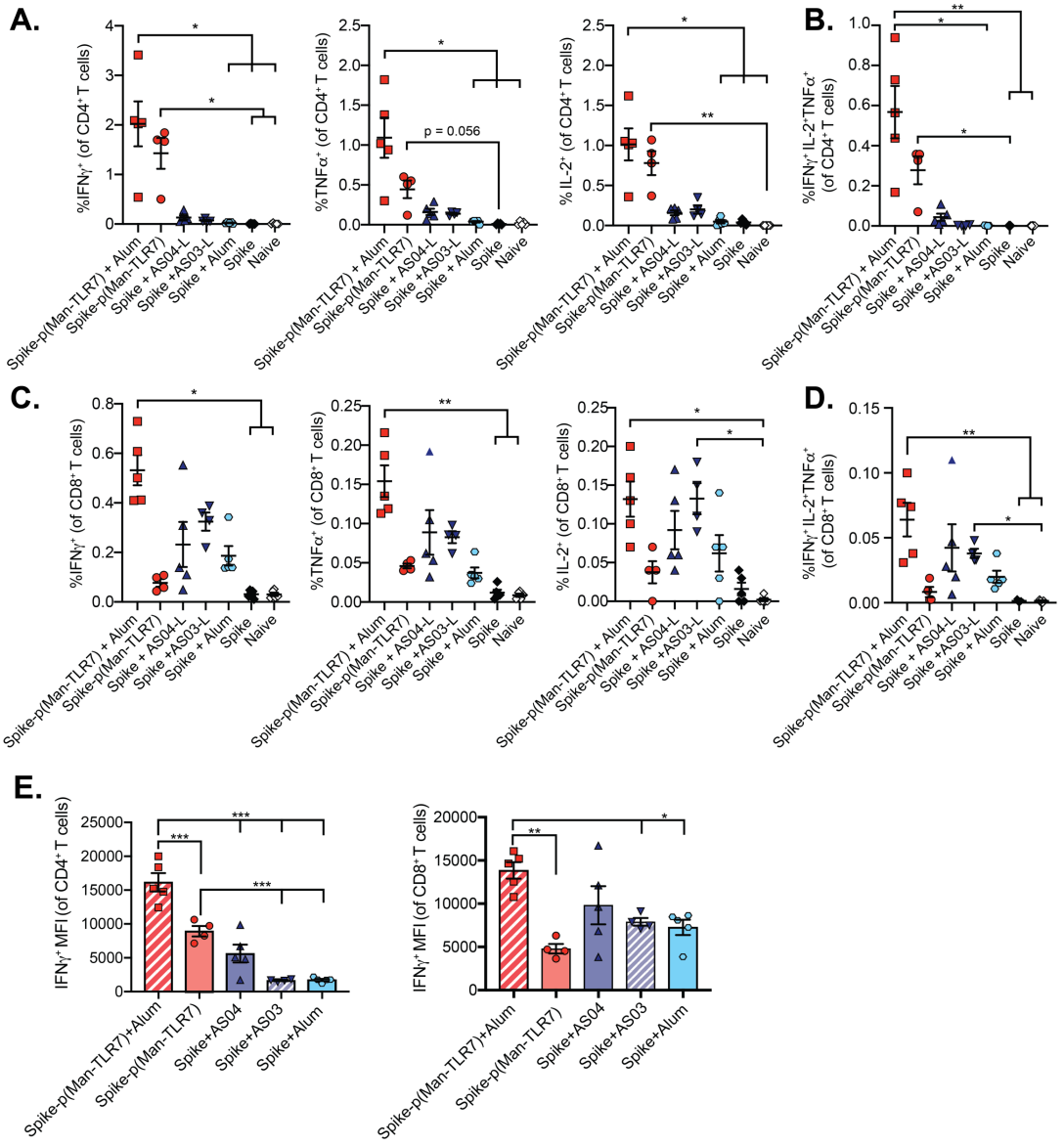

Figure 3.12: Vaccination with Spike-p(Man-TLR7) and Spike-p(Man-TLR7)+alum elicits robust antigen-specific T cell responses.

Splenocytes harvested one week post-boost from vaccinated mice (vaccinated as in Fig. 3.7A) were restimulated *ex vivo* with a Spike-derived peptide pool for 6h prior to flow cytometry analysis. (**A to E**) Cytokine-producing (A and B) $CD4^+$ and (C and D) $CD8^+$ T cell responses were detected by intracellular staining and quantified by flow cytometry. (A) $IFN\gamma^+$, $TNF\alpha^+$ and $IL2^+$ $CD4^+$ T cells quantified within $CD4^+$ T cells. (B) Polyfunctional $CD4^+$ T cells ($IFN\gamma^+$ $TNF\alpha^+$ $IL2^+$ $CD4^+$ T cells) quantified as a percentage of $CD4^+$ T cells. (C) $IFN\gamma^+$, $TNF\alpha^+$ and $IL2^+$ $CD8^+$ T cells, as a percentage of $CD8^+$ T cells. (D) Polyfunctional $CD8^+$ T cells ($IFN\gamma^+$ $TNF\alpha^+$ $IL2^+$ $CD8^+$ T cells), as a percentage of $CD8^+$ T cells. (E) Mean fluorescence intensity (MFI) of $IFN\gamma^+$ $CD4^+$ T cells (left) and $IFN\gamma^+$ $CD8^+$ T cells (right). Data presented as mean±SEM with n = 4-5 mice per group; * $p<0.05$, ** $p<0.01$, ***$p<0.001$ by (A-D) Kruskal-Wallis test with Dunn's post-test or (E) one-way ANOVA with Tukey's post-test.

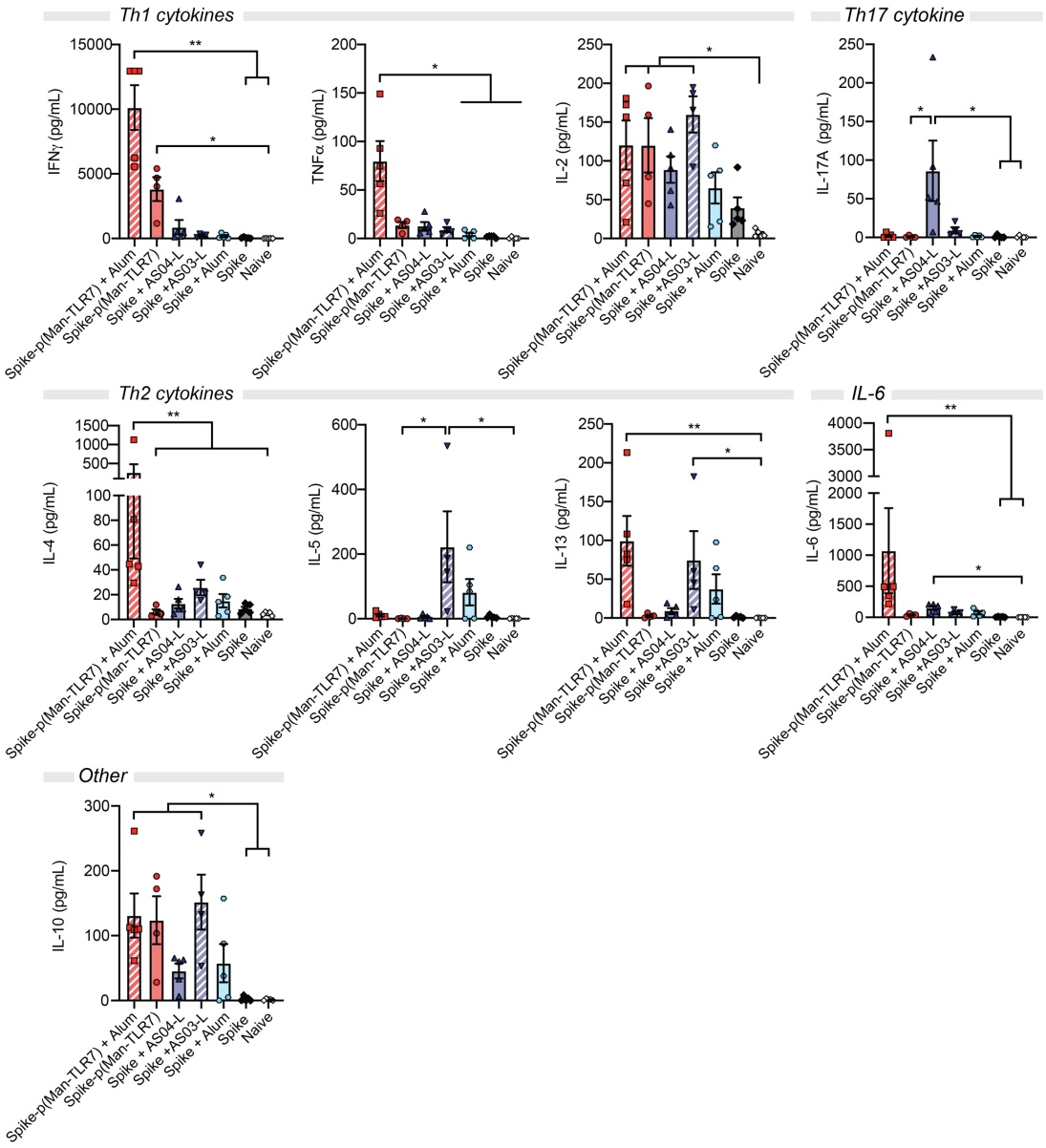

Figure 3.13: *Ex vivo* restimulated splenocytes from mice vaccinated with Spike-p(Man-TLR7) or Spike-p(Man-TLR7)+alum secrete more Th1 cytokines as compared to several other groups.

Splenocytes harvested one week post-boost from vaccinated mice (vaccinated as in Fig. 3.7A) were restimulated *ex vivo* with the full length Spike protein for 3 days prior to multiplexed cytokine analysis. The cytokines quantified (in pg/mL) from the supernatant of restimulated cells include Th1 cytokines (IFNγ, TNFα, IL-2), Th2 cytokines (IL-4, IL-5, IL-13), IL-6, IL-17A (a T helper cell type 17 (Th17) cytokine), and IL-12. Data presented as mean±SEM with n = 4-5 mice per group; * $p<0.05$, ** $p<0.01$ by Kruskal-Wallis test with Dunn's post-test.

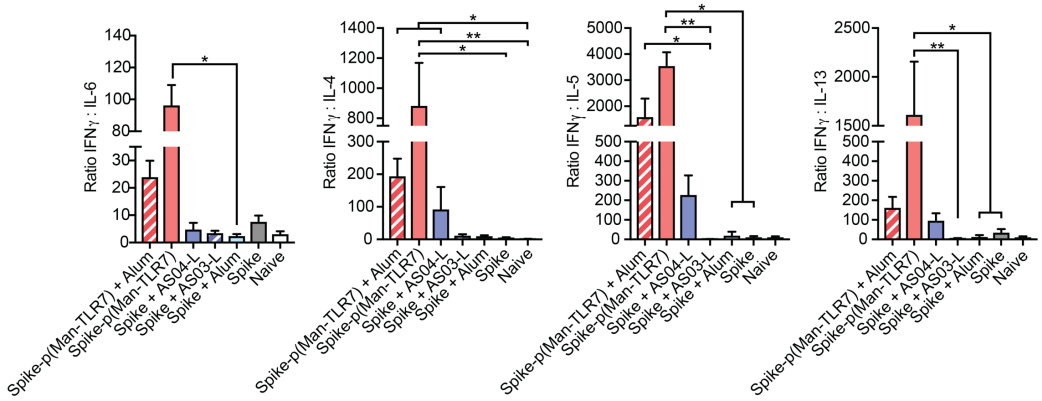

Figure 3.14: Ratio of IFNγ to IL-6 or various Th2 cytokines points towards a Th1-biased response in mice vaccinated with Spike-p(Man-TLR7) or Spike-p(Man-TLR7)+alum.

Ratio (unitless) of IFNγ concentration (pg/mL) to IL-6 or Th2 cytokine (IL-4, IL-5, IL-13) concentration (pg/mL) from Fig. 3.13. From left to right, graphs represent the following ratios: IFNγ/IL-6, IFNγ/IL-4, IFNγ/IL-5 and IFNγ/IL-13. Columns and error bars indicate mean±SEM for n = 4-5 mice per group; *p<0.05, ** p<0.01 via Kruskal-Wallis test with Dunn's post-test.

Vaccination with Spike-p(Man-TLR7) either alone or in combination with alum generated higher frequencies of cytokine$^+$ CD4$^+$ T cells, more polyfunctional CD4$^+$ T cells (producing all three cytokines: IFNγ, TNFα, and IL-2), and higher expression of IFNγ compared to other groups (**Fig. 3.12, A, B, and E**). Splenic CD8$^+$ T cells elicited by Spike-p(Man-TLR7) vaccination trended towards increased intracellular cytokine expression relative to mice treated with Spike alone, but did not reach statistical significance (**Fig. 3.12, C-E**). Spike-p(Man-TLR7)+alum, however, resulted in a superior increase in cytokine$^+$ CD8$^+$ T cells and polyfunctional CD8$^+$ T cells upon restimulation compared to other groups (**Fig. 3.12, C-E**).

To determine the nature of the immune response generated by our glyco-polymer conjugate platform, we quantified the amounts of various cytokines secreted by splenocytes after three days of restimulation with whole Spike protein. Cells collected from the spleens of animals treated with Spike-p(Man-TLR7) and Spike-p(Man-TLR7)+alum produced significantly more

Th1 cytokines, specifically IFNγ and IL-2, compared to most other groups (**Fig. 3.13**). Interestingly, we observed that splenocytes from mice vaccinated with Spike-p(Man-TLR7)+alum also secreted increased levels of IL-6 upon restimulation, as well as Th2 cytokines, specifically IL-4 and IL-13, compared to other groups (**Fig. 3.13**). Nevertheless, the ratio of IFNγ to IL-4, IL-5, IL-13, and IL-6 was significantly higher for Spike-p(Man-TLR7), as well as Spike-p(Man-TLR7)+alum in some cases, compared to benchmark groups (**Fig. 3.14**). Increased secretion of IL-17A was not observed upon restimulation of splenocytes from mice vaccinated with Spike-p(Man-TLR7) or Spike-p(Man-TLR7)+alum (**Fig. 3.13**). At the same time, all adjuvanted groups showed some elevation in IL-10 secretion (**Fig. 3.13**). In summary, we demonstrated that our Spike-p(Man-TLR7) platform induces strong functional Th1-biased T cell responses.

3.4 Discussion

The COVID-19 pandemic has resulted in a global health, economic, and social crisis requiring a rapid response from researchers around the world to develop an effective vaccine against the virus. That urgency led to successful clinical trials, the emergency-use authorization of several vaccine candidates globally, and the FDA approval of one vaccine candidate, although the considerable uncertainties and failure rates inherent in the process are highlighted by high-profile dropouts, as seen in the case of Sanofi/GSK's and Merck's vaccine candidates. Therefore, the global vaccination effort has focused on putting forth as many candidates as possible, in the event that any of the frontrunners failed to live up to their promise in preceding development stages. Based on our recent successful deployment of a synthetic glyco-polymer-based vaccine in addressing the difficulties in the field of malaria vaccination [97], we adapted the vaccine

platform for SARS-CoV-2 by conjugating SARS-CoV-2 viral proteins to the DC-targeted, TLR7 agonist-containing polymer p(Man-TLR7).

Since the beginning of the COVID-19 pandemic, we have learned that the natural responses to SARS-CoV-2 are temporary and decline quickly after recovery. Generation of long-lasting neutralizing antibody responses to components of SARS-CoV-2 is a primary goal of vaccines that would prevent or limit the infection's severity. The Spike protein has been one of the major antigens used in vaccines to elicit potent antibody responses, with some formulations focusing on the full-length Spike protein and others focusing on only the RBD domain of Spike. As such, after successfully formulating two bioactive conjugates, RBD-p(Man-TLR7) and Spike-p(Man-TLR7), we investigated the humoral responses generated in vaccinated mice using a prime-boost regimen. Both RBD-p(Man-TLR7) and Spike-p(Man-TLR7) resulted in high levels of IgGs against the corresponding immunogen. However, with our platform, only Spike-p(Man-TLR7) elicited neutralizing antibodies that exceeded the FDA-recommended VNT. Because RBD is a smaller antigen than the full-length Spike protein, conjugation to p(Man-TLR7) could potentially mask epitopes important for eliciting neutralizing antibodies. In fact, multiple lysine residues available for conjugation are located near the ACE2 binding site on RBD [178,179]. Because the conjugation occurs randomly on sterically-accessible lysine residues, and Spike is a larger protein with more lysine residues available for conjugation, it is statistically less likely for the p(Man-TLR7) polymer to completely mask this site on Spike. Additionally, since there are neutralizing epitopes on Spike outside of the RBD region [183], vaccines using the full-length Spike protein have the potential to elicit neutralizing antibodies against a broader range of epitopes.

Our studies also sought to determine how the combinatorial application of adjuvants may modulate the anatomic localization and efficacy of immune responses. In particular, we explored the use of the depot-forming adjuvant alum, which is commonly seen in other clinical-stage vaccines and COVID-19 vaccine candidates [218,219,231,238]. We observed that alum seemed to have an effect on the anatomic localization of germinal center responses and therefore antibody generation. Vaccination with Spike-p(Man-TLR7) resulted in higher numbers of GC B cells in the spleen, whereas vaccination with Spike-p(Man-TLR7) in combination with alum resulted in higher numbers of GC B cells in the draining lymph nodes (**Fig. 3.9, A and B**). These findings suggest that alum retains vaccines near the site of injection, whereas in its absence, Spike-p(Man-TLR7) can diffuse more systemically. This is in agreement with one of the proposed mechanisms of action for alum being the formation of an antigen depot that results in the slow drainage of antigen from the injection site [227–229]. This slow drainage has important implications for vaccine efficacy, as it has been shown previously that controlled prolonged release of antigen can greatly enhance humoral responses upon vaccination [239]. Although the depot effect of alum has been called into question [240], it is nevertheless consistent with our observations of improved magnitude, breadth, and neutralization activity of the humoral responses elicited by Spike-p(Man-TLR7)+alum, and may be worth a further investigation outside the scope of this study.

Both $CD4^+$ and $CD8^+$ T cells play an important role in the prevention and mitigation of SARS-CoV-2 infection [201,237]. Evidence suggests that patients who recovered from COVID-19 had relatively high T cell levels compared to patients who had severe disease complications and died [204,205]. Notably, T cell responses are more durable than antibody responses which points to their importance in establishing long term protection against the virus [202].

Unfortunately, most reported COVID-19 vaccine candidates induce low T cell responses in mice. In contrast, we observed that immunization with Spike-p(Man-TLR7) with and without alum induced a large fraction of antigen-specific polyfunctional $CD4^+$ T cells, much higher than that observed for clinical benchmark formulations. Surprisingly, Spike-p(Man-TLR7)+alum also induced large numbers of antigen-specific $CD8^+$ T cells. Although alum is often considered a poor $CD8^+$ T cell adjuvant [241,242], studies have shown that antigen-specific $CD8^+$ T cells can be generated after vaccination with antigen and alum [243].

A preferential Th1-biased immune response, as opposed to a Th2-biased response is also desirable from COVID-19 vaccines [206–210]. Here, a Th1 bias was observed in both the IgG isotypes (an increased IgG2b:IgG1 ratio, **Fig. 3.7, C and D**) and cytokines secreted from splenocytes harvested from mice vaccinated with Spike-p(Man-TLR7) (**Fig. 3.13; Fig. 3.14**). While alum synergistically enhanced some of the humoral responses seen with Spike-p(Man-TLR7) vaccination, it decreased the Th1-biased responses observed. This is unsurprising, as alum is known to preferentially induce a Th2 response [244]. As such, when deciding whether to use our p(Man-TLR7) platform alone or in combination with alum, this balance between favorable humoral responses and a skewing away from a Th1 bias must be considered.

There are several translational advantages to our approach for an effective and safe next-generation vaccine. First, the conjugation strategy employed can be performed on any amine-containing antigen, including whole proteins and peptides. This means that, as viral protein mutations emerge, our platform can be easily adapted, and the conjugation can be conducted on newly identified variants. In addition, the APC-directed components of p(Man-TLR7), mannose and the TLR7 agonist, are universally advantageous across species. The pattern recognition

receptors recognizing mannose residues are expressed by APCs in both mice and humans and have been shown to play a significant role in antigen capture and processing [112,245,246], while the TLR7 agonist can also be swapped for other TLR agonists. This is particularly pertinent in human immunology, as not only TLR7 (present mostly in plasmacytoid DCs) but also Toll-like receptor 8 (TLR8, expressed by myeloid DC, monocytes and monocyte-derived DCs) agonists have been shown to be necessary to drive strong B and T cell-mediated immune responses [247]. Lastly, the conjugate formulation can be stably refrigerated for several months and thawed multiple times after storage in a freezer without affecting the structure of the conjugate which has important implications for effective vaccine distribution.

Despite the advantages of the flexible antigen-adjuvant conjugation chemistry, this is also the source of the primary limitation of the p(Man-TLR7) vaccine platform. Although the conjugation of antigen to the polymer is via a self-immolative linker, we observed that this may lead to reduced activity of the antigen, in terms of recognition of its target receptor (**Fig. 3.4, A and B**). This suggests that the smaller the antigen, the fewer the number of potential epitopes, and the higher the chances that conjugation to p(Man-TLR7) may lead to steric blockade of the receptor-binding site. This may adversely affect the quality of resultant antigen-specific humoral responses, as seen in the case of RBD-p(Man-TLR7) (**Fig. 3.6**). This is because intracellular processing in the endosomes of APCs is required for release of the antigen from the rest of the construct, whereas humoral responses are partly dependent on extracellular interactions with B cell receptors in the germinal centers of secondary lymphoid organs. For most antigens, however, this will not be a relevant issue, and it may be possible to optimize the polymer to protein ratio if this issue does arise.

In conclusion, to address a global need for next-generation vaccines against SARS-CoV-2, we have developed the Spike-p(Man-TLR7) vaccine platform and demonstrated its efficacy in mice. We found that conjugating the Spike protein to our polymeric glyco-adjuvant improves Spike's immunogenicity through inducing both potent neutralizing humoral and high-quality cellular responses. We demonstrated that Spike-p(Man-TLR7) is efficacious in elderly mice, and antibody responses are long-lasting. In addition, we determined that combining Spike-p(Man-TLR7) with alum further enhanced immune responses, often exceeding those elicited by mimics of clinical-stage vaccine candidates. Whether in the global fight against SARS-CoV-2 or another pathogen, these studies highlight the adaptability of the modular p(Man-TLR7) platform and reinforce the translational potential of our polymeric glyco-adjuvant to be used in next-generation vaccines.

3.5 Materials and Methods

3.5.1 Study design

This study was designed to test the immunogenicity of an APC-targeting vaccine platform consisting of either the prefusion-stabilized Spike protein or its RBD, conjugated to the polymeric glyco-adjuvant p(Man-TLR7). The goal was to develop a next-generation vaccine platform in response to the ongoing COVID-19 pandemic. In the study, the humoral response in mice vaccinated with Spike-p(Man-TLR7), Spike-p(Man-TLR7)+alum, or RBD-p(Man-TLR7) was characterized by evaluating the antibody titers (IgG and IgA) via ELISA, as well as through a viral peptide array and virus neutralization assay. The lymphocyte responses were characterized by flow cytometry, and B and T cellular reactivity were assessed by quantification of antibody or cytokine expression following antigen restimulation. The studied platform's

immunogenicity was compared to that of the following clinically relevant vaccine formulations: Spike+AS04-L, Spike+AS03-L and Spike+alum. In two experiments (**Fig. 3.7, I and J**), we had to prioritize and limit the number of groups, and as a result, groups treated with Spike-p(Man-TLR7)+alum or Spike+alum were not included. In **Fig. 3.7I**, this was due to a limited availability of elderly mice, and in **Fig. 3.7J**, this was due the extensiveness of the work required in the experiment. Statistical methods were not used to predetermine necessary sample size, but sample sizes were chosen on the basis of estimates from pilot experiments and previously published results such that appropriate statistical tests could yield statistically significant results. All experiments were replicated at least twice except for **Figs. 3.7I, 3.7J, 3.8**, as well as the experimental groups Spike+AS03-L, Spike+alum, and Spike-p(Man-TLR7)+alum (once). In animal studies, all mice were treated in the same manner. Animals were randomly assigned to a treatment group, and analyses were performed in a blinded fashion. Production of the studied conjugates was performed multiple times to ensure reproducibility. Samples were excluded from analysis only when an animal developed a health problem for a nontreatment-related reason, according to the animal care guidelines. Statistical methods are described in the "Statistical analysis" section.

3.5.2 Animals

All studies with animals were carried out in accordance with procedures approved by the Institutional Animal Care and Use Committee at the University of Chicago (protocol # 72551) and housed in a specific pathogen-free environment at the University of Chicago. C57Bl/6 female mice aged 8, 21, 47 or greater than 64 weeks were obtained from The Jackson Laboratory.

3.5.3 Synthesis and characterization of p(Man-TLR7) polymer

The polymeric glyco-adjuvant p(Man–TLR7) was synthesized via a reversible addition–fragmentation chain transfer (RAFT) polymerization using an azide-modified RAFT agent, a biologically inert comonomer (N-(2-hydroxypropyl) methacrylamide, HPMA) and two functional monomers: one synthesized from D-mannose, and the other from a potent TLR7 ligand (mTLR7) (**Fig. 1.1A**), as described previously [97]. Molecular weight and polydispersity of the p(Man–TLR7) construct were measured by size exclusion chromatography (molecular weight target at ~20 kDa), and was composed of a 1:2.1:3.5 molar ratio of mTLR7:mannose monomer:HPMA, as measured by mTLR7-specific UV absorbance and ^{1}H NMR.

3.5.4 Sodium dodecyl sulfate-polyacrylamide gel electrophoresis (SDS-PAGE)

SDS-PAGE was performed on stain-free 4-20% gradient gels (Bio-Rad). Samples run under reducing conditions were incubated for 15 min at 95°C with 710 mM 2-Mercaptoethanol. After electrophoresis, gel images were acquired with the ChemiDoc XRS+ system (Bio-Rad).

3.5.5 Spike and RBD protein production

Plasmids encoding $(His)_6$-tagged pre-fusion stabilized Spike protein or RBD protein (sequences in **Table 3.1**) were obtained from the laboratory of Florian Krammer (Mount Sinai School of Medicine, New York, NY). Suspension-adapted HEK-293F were maintained in serum-free FreeStyle 293 Expression Medium (Gibco). On the day of transfection, cells were inoculated into at a concentration of $1x10^6$ cells/mL. 1 mg/mL plasmid DNA was mixed with 2 mg/mL linear 25 kDa polyethyleneimine (Polysciences) and transfected in OptiPRO SFM medium (4% final volume). After 7 days of culture, supernatants were harvested, and purification was performed as

described previously [156]. Purified proteins were tested for endotoxin via HEK-Blue TLR4 reporter cell line (Invivogen, San Diego, CA) and endotoxin levels were confirmed to be less than 0.01 EU/mL. Protein purity was assessed by SDS-PAGE as described previously [156]. Protein concentration was determined through absorbance at 280 nm using NanoDrop (Thermo Scientific).

Table 3.1: Amino acid sequences of Spike and RBD antigens.

Spike
VNLTTRTQLPPAYTNSFTRGVYYPDKVFRSSVLHSTQDLFLPFFSNVTWFHAIHVSGT NGTKRFDNPVLPFNDGVYFASTEKSNIIRGWIFGTTLDSKTQSLLIVNNATNVVIKVCE FQFCNDPFLGVYYHKNNKSMESEFRVYSSANNCTFEYVSQPFLMDLEGKQGNFKNLR EFVFKNIDGYFKIYSKHTPINLVRDLPQGFSALEPLVDLPIGINITRFQTLLALHRSYLTP GDSSSGWTAGAAAYYVGYLQPRTFLLKYNENGTITDAVDCALDPLSETKCTLKSFTV EKGIYQTSNFRVQPTESIVRFPNITNLCPFGEVFNATRFASVYAWNRKRISNCVADYSV LYNSASFSTFKCYGVSPTKLNDLCFTNVYADSFVIRGDEVRQIAPGQTGKIADYNYKL PDDFTGCVIAWNSNNLDSKVGGNYNYLYRLFRKSNLKPFERDISTEIYQAGSTPCNGV EGFNCYFPLQSYGFQPTNGVGYQPYRVVVLSFELLHAPATVCGPKKSTNLVKNKCVN FNFNGLTGTGVLTESNKKFLPFQQFGRDIADTTDAVRDPQTLEILDITPCSFGGVSVITP GTNTSNQVAVLYQDVNCTEVPVAIHADQLTPTWRVYSTGSNVFQTRAGCLIGAEHVN NSYECDIPIGAGICASYQTQTNSPASVASQSIIAYTMSLGAENSVAYSNNSIAIPTNFTIS VTTEILPVSMTKTSVDCTMYICGDSTECSNLLLQYGSFCTQLNRALTGIAVEQDKNTQ EVFAQVKQIYKTPPIKDFGGFNFSQILPDPSKPSKRSFIEDLLFNKVTLADAGFIKQYGD CLGDIAARDLICAQKFNGLTVLPPLLTDEMIAQYTSALLAGTITSGWTFGAGAALQIPF AMQMAYRFNGIGVTQNVLYENQKLIANQFNSAIGKIQDSLSSTASALGKLQDVVNQN AQALNTLVKQLSSNFGAISSVLNDILSRLDPPEAEVQIDRLITGRLQSLQTYVTQQLIRA AEIRASANLAATKMSECVLGQSKRVDFCGKGYHLMSFPQSAPHGVVFLHVTYVPAQ EKNFTTAPAICHDGKAHFPREGVFVSNGTHWFVTQRNFYEPQIITTDNTFVSGNCDVV IGIVNNTVYDPLQPELDSFKEELDKYFKNHTSPDVDLGDISGINASVVNIQKEIDRLNE VAKNLNESLIDLQELGKYEQYIKWPSGRLV PRGSPGSGYIPEAPRDGQAYVRKDGEWVLLSTFLGHHHHHH*
RBD
RVQPTESIVRFPNITNLCPFGEVFNATRFASVYAWNRKRISNCVADYSVLYNSASFSTF KCYGVSPTKLNDLCFTNVYADSFVIRGDEVRQIAPGQTGKIADYNYKLPDDFTGCVIA WNSNNLDSKVGGNYNYLYRLFRKSNLKPFERDISTEIYQAGSTPCNGVEGFNCYFPLQ SYGFQPTNGVGYQPYRVVVLSFELLHAPATVCGPKKSTNLVKNKCVNFHHHHHH**

3.5.6 Surface plasmon resonance (SPR) measurements

SPR measurements were made using a Biacore X100 SPR system (Cytiva, Marlborough, MA). At the beginning of each cycle, 2 μg mL^{-1} recombinant human ACE2-Fc (Sino Biologicals, Beijing, China) in running buffer (0.01 M HEPES pH 7.4, 0.15 M NaCl, 0.005% v/v Surfactant P20) was flowed over a Protein A coated sensor chip (Cytiva) at a flowrate of 5 μL min^{-1} for 780 seconds, resulting in ~700-1100 resonance units corresponding to ligand coating. Spike or RBD protein was then flowed at decreasing concentrations (ranging from 250 nM to 3.9063 nM) in running buffer for contact time of 180 seconds at 30 μL min^{-1}, followed by running buffer for a dissociation time of 300 seconds. At the end of each cycle, the sensor chip surface was regenerated with two 30-second pulses of 10 mM glycine pH 1.5 at 30 μL min^{-1}. Specific binding of Spike and RBD proteins to ACE2 was calculated by comparison to a non-functionalized channel used as a reference. The experimental results were fitted with Langmuir binding kinetics using the BIAevaluation software (Cytiva, version 2.0.2.).

3.5.7 Production of RBD-p(Man-TLR7) conjugate

RBD was mixed with 5 molar equivalents of 2 kDa self-immolative PEG linker in a phosphate buffer (pH 7.7) and reacted for 1 hour in an endotoxin-free Eppendorf tube mixing at RT. The reaction solution was then purified via Zeba spin desalting columns with 7 kDa cutoff to remove unreacted linker (Thermo Fisher). Successful linker conjugation was confirmed using gel electrophoresis and comparison to a size standard of the unmodified RBD. RBD-linker construct in PBS (pH 7.4) was then reacted with 30 fold molar excess of p(Man-TLR7) polymer in an endotoxin-free Eppendorf tube for 2 hours, mixing, at RT. Conjugation was confirmed via gel electrophoresis, and conjugates were stored at 4°C.

3.5.8 Production of Spike-p(Man-TLR7) conjugate

Spike was mixed with 10 molar equivalents of 2 kDa self-immolative PEG linker in a phosphate buffer (pH 7.7) with 0.1% Tween 80 (Sigma) and reacted for 1 hour in an endotoxin-free Eppendorf tube mixing at RT. The reaction solution was then purified via Zeba spin desalting columns with 7 kDa cutoff to remove unreacted linker (Thermo Fisher). Successful linker conjugation was confirmed using gel electrophoresis and comparison to a size standard of the unmodified Spike. Spike-linker construct in PBS (pH 7.4) was then reacted with 30 fold molar excess of p(Man-TLR7) polymer in an endotoxin-free Eppendorf tube for 2 hours, mixing, at RT. Conjugation was confirmed via gel electrophoresis, and conjugates were stored at 4°C.

3.5.9 Determination of TLR7 content in p(Man-TLR7) conjugates

To determine the concentration of TLR7 content in the polymer and RBD- or Spike- polymer conjugates, the absorbance at 327nm was measured. Known quantities of TLR7 monomer in saline were measured (n=3 independent samples) at 327nm in several concentrations ranging from 8 mg/mL to 1 mg/mL to calculate a standard curve as previously published [97]. The determined standard curve [TLR7 (mg/mL) = 1.9663* A_{327}+0.0517] was then used to calculate TLR7 concentration in the prepared p(Man-TLR7) conjugate.

3.5.10 Determination of RBD or Spike content in p(Man-TLR7) conjugates

SDS-PAGE was performed as previously stated using a standard curve of RBD or Spike protein and two dilutions of RBD- or Spike-p(Man-TLR7) conjugate samples reduced with 710 mM 2-Mercaptoethanol. Reducing conditions liberate conjugated linker-p(Man-TLR7) from the antigen, allowing for reduced antigen band intensity to be analyzed. The band density of the

reduced samples and RBD or Spike standard curve was then analyzed using ImageJ and the RBD or Spike concentration of the samples was calculated using the standard curve generated.

3.5.11 In vitro activity of p(Man-TLR7) conjugates

BMDCs were prepared from C57Bl/6 mice (Jackson Laboratory) as previously described [171] and used on day 8–9. For BMDC activation studies, 2×10^5 cells per well were seeded in round-bottom 96-well plates (Fisher Scientific) in RPMI 1640 with 10% FBS (Gibco) and 2% Penicillin-Streptomycin (Invitrogen), and treated with either Spike or Spike-p(Man-TLR7), then incubated at 37°C. The samples were allowed to culture for 12h at 37°C and cytokine concentration was measured in the media by Ready-Set-Go™ ELISA kits (Thermo Fisher) as detailed in the manufacturer's instructions.

3.5.12 ELISA for ACE2 binding

96-well ELISA plates (Nunc MaxiSorp flat-bottom plates, Thermo Fisher) were coated with 10 nM RBD, RBD-p(Man-TLR7), Spike, Spike-p(Man-TLR7), or bovine serum albumin (BSA, Sigma) in PBS overnight at 4°C. The following day, plates were washed in PBS with 0.05% Tween 20 (PBS-T) and then blocked with 2% BSA (Sigma) diluted in PBS for 1 hour at room temperature. Then, wells were washed with PBS-T and further incubated with human ACE2-Fc (Sino Biological) for 2 hours at room temperature. After 6 washes with PBS-T, wells were incubated for 1 hour at room temperature with horseradish peroxide (HRP)-conjugated antibody against human IgG (Jackson ImmunoResearch). After 6 washes with PBS-T, tetramethylbenzidine substrate was added, followed by 10% H_2SO_4 after 15 min. Subsequently, the absorbance was measured at 450 nm and 570 nm (Epoch Microplate Spectrophotometer,

BioTek).

3.5.13 Complement activation analysis

The complement activation analysis was conducted based on published protocols [216]. First, blood was collected by cardiac puncture from euthanized C57Bl/6 mice using a 1 ml syringe attached to a 25G needle and transferred to a microcentrifuge tube. The blood was incubated at room temperature for 1 h and then spun at 10,000 rpm for 10 min. The supernatant (serum) was transferred to a new microcentrifuge tube to be used in the assay. In the meantime, high binding surface plates (Corning) were coated with either mannan (100µg/ml), Spike (10µM), Spike-p(Man-TLR7) (10µM Spike equivalent), or were left uncoated (n = 4 per group) by incubating 100 µl of each solution per well overnight at 4°C. Then, the wells were emptied, and 1x casein solution (100 µl) was added to block the plate from nonspecific binding and incubated for 1 h at room temperature. After that time, the plates were washed with PBS-T, and previously isolated mouse serum (50 µl) was added to each well and incubated for 45 minutes at 37°C. The serum was then aspirated from the plate and diluted 100x in the blocking buffer to stop the reaction. The concentration of C3a and C5a anaphylatoxins in diluted serum was then determined by mouse complement C3a (Novus Biologicals) and Complement C5a mouse (Invitrogen) colorimetric ELISA kits, respectively, following manufacturers' instructions.

3.5.14 Reagents for in vivo studies

AS03-like squalene-based adjuvant (AddaS03, InvivoGen), Synthetic Monophosphoryl Lipid A (MPLA, Avanti 699800), and Alhydrogel adjuvant 2% (alum, InvivoGen) were used for vaccination studies. All purchased reagents were used as provided by the manufacturer.

3.5.15 Vaccination scheme

Mice were vaccinated via s.c. injections into the front two hocks on days 0 and 21. For all vaccine formulations assessed, 10μg of RBD or Spike protein were used. The following amounts of adjuvant were used: 20 μg TLR7 as p(Man-TLR7), 20 μg TLR7 as p(Man-TLR7) + 50 μg alum, 5 μg MPLA + 50 μg alum, 25 μL AS03-L, or 50 μg alum. Excess free p(Man-TLR7) was added to RBD-p(Man-TLR7) and Spike-p(Man-TLR7) conjugates to achieve an exact dose of 20 μg TLR7 per mouse.

3.5.16 Anti-RBD and anti-Spike antibody analysis

Blood was collected from vaccinated mice weekly or every two weeks into EDTA-K2-coated tubes (Milian). Plasma was separated by centrifugation at 1000 x g for 10 min and stored at -80°C. Plasma was assessed for anti-RBD or anti-Spike IgGs by ELISA. 96-well ELISA plates (Costar high binding assay plates, Corning) were coated with 10 μg/mL RBD or Spike in 50 mM sodium carbonate/sodium bicarbonate pH 9.6 overnight at 4°C. The following day, plates were washed in PBS with 0.05% Tween 20 (PBS-T) and then blocked with 1x casein (Sigma) diluted in PBS for 1 hour at room temperature. Then, wells were washed with PBS-T and further incubated with various dilutions of plasma for 2 hours at room temperature. After 6 washes with PBS-T, wells were incubated for 1 hour at room temperature with horseradish peroxide (HRP)-conjugated antibody against mouse IgG, IgG1, IgG2b, IgG2c, IgG3, or IgA (Southern Biotech). After 6 washes with PBS-T, bound anti-RBD or anti-Spike antibodies were incubated with tetramethylbenzidine substrate for 18 min. 3% H_2SO_4 with 1% HCl was added at that time, and the absorbances at 450 nm and 570 nm were immediately measured (Epoch Microplate Spectrophotometer, BioTek). For all subsequent analysis, the absorbance at 570 nm was

subtracted from the absorbance at 450 nm. For titer analysis, the average background plus four times the standard deviation of the background was subtracted from the absorbance values. Titers were calculated as reciprocal dilutions giving values > 0.01. The assay was able to detect titers ranging between 10^{-2} and 10^{-7}. An arbitrary value of 0 was assigned to the samples with absorbances below the limit of detection for which it was not possible to detect the titer. For AUC analysis, the fold over the median background absorbance was calculated for each sample, and GraphPad Prism (version 8) was then used to calculate the AUC of the log-transformed plot.

3.5.17 Antibody epitope breadth determination via peptide array

Antibody specificity to linear epitopes of the Spike protein was analyzed using a CelluSpots™ Covid19_hullB Peptide Array (Intavis Peptide Services, Tubingen, Germany) according to the manufacturer's protocol. The array comprises 254 peptides spanning the full-length sequence of the Spike protein (NCBI GenBank accession # QHD43416.1), with each 15-mer peptide offset from the previous one by 5 amino acids. Briefly, peptide arrays were blocked in casein blocking solution at 4 °C overnight. Arrays were then incubated with pooled serum diluted 1:200 in blocking buffer for 6 h at room temperature (RT) on an orbital shaker (60 rpm) and then washed 4 times with PBS with 0.05% Tween 20 (PBS-T). Following the fourth wash, arrays were incubated for an additional 2 h at RT and 60 rpm with goat anti-mouse IgG conjugated to HRP (Southern Biotech) diluted 1:5000 in blocking solution. Arrays were washed another 4 times with PBS-T. Spots were detected with Clarity™ Western ECL Substrate (Bio-Rad), and chemiluminescence was measured using a ChemiDoc XRS+ system Gel Documentation System (Bio-Rad). Spots were analyzed using Spotfinder software (version v3.2.1).

3.5.18 SARS-CoV-2 virus neutralization assay

Heat-inactivated plasma from vaccinated or control mice were serially diluted in DMEM with 2% FBS (Gibco), 1% Penicillin-Streptomycin (Invitrogen), and 10mM Non-Essential Amino Acids (Gibco; mixture of glycine, L-alanine, L-asparagine, L-aspartic acid, L-glutamic acid, L-proline, & L-serine)), and subsequently incubated with 400 plaque-forming units of SARS-CoV-2 virus (strain nCov/Washington/1/2020, provided by the National Biocontainment Laboratory, Galveston TX, USA) for 1 h at 37°C. These mixtures were then applied to Vero-E6 cells, which endogenously express ACE2 at high levels and show ACE-2 dependent SARS-CoV-2 infection [177,248]. These mixtures were maintained with the Vero-E6 cells until > 90% cell death occurred in the “no serum" control condition (about 4-5 days). After that, cells were washed with PBS and fixed with 10% formalin, before being stained with crystal violet. Viability was then quantified using a Tecan infinite m200 microplate reader (absorbance 595 nm). Viral neutralization titer represents the greatest plasma dilution at which 50% of SARS-CoV-2-induced cell death is inhibited (EC50). To determine the EC50, data were fit using a least squares variable slope four- parameter model. To ensure realistic EC50 values, we considered a dilution (1/X) of X = 10-1 to be 100% neutralizing and a dilution of X = 108 to be 0% neutralizing and constrained EC50 > 0. Plasma from convalescent human COVID-19 patients were provided by Ali Ellebedy (Washington University School of Medicine, St. Louis, MO; Catalog # NR-53661, NR-53662, NR-53663, NR- 53664, and NR-53665).

3.5.19 Preparation of single cell suspensions from organs

Spleens and injection dLNs were collected on day 28 (7 days post-boost) and stored in ice-cold IMDM (Gibco) until further steps. Spleens were processed into a single-cell suspension via

mechanical disruption and passage through a 70µm filter. The splenocytes were washed with PBS and then exposed to ACK lysis buffer (0.155 M NH4Cl, Gibco) for 5 minutes at room temperature to lyse red blood cells. The lymph nodes were mechanically disrupted, then digested at 37°C for 45 min in IMDM with 3.5 mg/mL collagenase D (Roche) before being passed through a 70µm filter. Single cell suspensions were then washed with PBS and resuspended in IMDM (Gibco) with 10% FBS and 1% Penicillin-Streptomycin.

3.5.20 Anti-Spike IgG enzyme-linked immunosorbent spot (ELISpot) assay

ELISpot plates (Millipore IP Filter plate) were coated with 20µg/mL Spike in sterile PBS overnight at 4°C. Plates were then blocked using ELISpot Media (RPMI 1640, 1% Glutamine, 10% FBS, 1% Penicillin-Streptomycin; Thermo Fisher Scientific) for 2 hours at 37°C. Splenocytes from vaccinated mice were seeded in triplicate at a starting concentration of 6.75×10^5 cell/well and diluted in 3-fold serial dilutions for a total of four dilutions. Plates were incubated for 18 hours at 37°C, 5% CO2 after which the cells were washed off 5x in PBS. Wells were incubated with 100µL IgG-biotin HU adsorbed (Southern Biotech) for 2hr at RT. Next, plates were washed 4x in PBS followed by 100µL HRP-conjugated streptavidin for 1hr at RT. Plates were washed again and incubated with 100µL TMB/well for 5 minutes until distinct spots emerge. Finally, plates are then washed 3x with distilled water and left to dry completely in a laminar flow hood. A CTL ImmunoSpot Analyzer was used to image plates, count spots and perform quality control.

3.5.21 Ex vivo restimulations

Splenocytes were either restimulated *in vitro* with whole Spike protein or Spike peptide pools

(PepMix SARS-CoV-2 Spike Glycoprotein, JPT). For Spike protein restimulations, $5x10^5$ cells were incubated with 100 mg/mL Spike protein for 3 days in complete IMDM. After 3 days, the cells were spun down, and the supernatant was used to measure secreted cytokines using a LEGENDplex™ Mouse Th Cytokine Panel kit (BioLegend) according to the manufacturer's instruction. Approximately 500 events per cytokine were acquired using Attune NxT flow cytometer (ThermoFisher), and analyzed with LEGENDplex v8.0 software.

For Spike peptide restimulations, $2x10^6$ cells were incubated with combined Spike peptide pools (diluted according to manufacturer's instructions) or equivalent amounts of DMSO (as an unstimulated control) for 6 hours in complete IMDM. After 2 hours of *in vitro* restimulation, GolgiPlug (BD) was added according to manufacturer's instructions. Cells were then allowed to incubate for 4 more hours before staining for intracellular cytokines and analyzed via flow cytometry, as described.

3.5.22 Production of RBD protein tetramers

RBD protein expressed with AviTag was purchased from GenScript. Site-specific biotinylation of the AviTag was performed using BirA Biotin-Protein Ligase Reaction kit (Avidity). Next, unconjugated biotin was removed using Zeba spin desalting columns, 7K MWCO (ThermoFisher). The quantification of reacted biotin was performed using the Pierce Biotin Quantification Kit (ThermoFisher). Biotinylated RBD was incubated with either streptavidin-conjugated PE (Biolegend) or streptavidin-conjugated APC fluorophores (Biolegend) for 20 min on ice at a molar ratio of 4:1 of biotin to streptavidin. FITC-labelled Streptavidin (Biolegend) was reacted with excess free biotin to form a non-RBD-specific streptavidin probe as a control. Tetramer formation was confirmed using SDS-PAGE gel. Cells were stained for flow cytometry

with all three streptavidin probes at the same time as other fluorescent surface markers at a volumetric ratio of 1:100 for RBD-streptavidin-PE and 1:200 for RBD-streptavidin-APC and biotin-streptavidin-FITC.

3.5.23 Flow cytometric analysis

The following procedures were all performed at 4˚C in the dark. Prepared cells were stained for viability using fixable dyes (Fixable Viability Dye eFluor455, Invitrogen 65-0868-14; Live/Dead Violet Dead Cell Stain Kit, Invitrogen L34964; Fixable Viability Dye eFluor780, Invitrogen 65-0865-14) at 1:500 dilution in PBS with anti-CD16/32 included (1:100 dilution) for 15 minutes. Surface staining was performed in Brilliant Stain buffer (BD Biosciences) using the made in-house tetramers and monoclonal antibodies against the murine targets (**Table 3.2**). All antibodies and tetramers were titrated to determine optimal working dilutions which often was 1:100 or 1:200. Cells were incubated with the surface stain cocktail for 20 minutes before washing in PBS and fixation. Fixation was performed using the following buffers: for assays without intracellular staining, cells were fixed for 20 minutes using a 2% paraformaldehyde solution; for assays with transcription factor staining, cells were fixed and permeabilized using the Invitrogen FoxP3/Transcription factor kit (eBioscience) according to manufacturer instructions; for assays which required non-transcription factor internal staining (cytokines alone) fixation and permeabilization was performed using the Cytofix/Cytoperm kit (BD Biosciences) according to manufacturer instructions. Assays requiring intracellular staining were performed using antibodies against the murine targets at 1:200 dilution in the corresponding kit permeabilization buffer, according to manufacturer instructions (**Table 3.2**).Following fixation and/or intracellular staining, cells were resuspended in FACS buffer (PBS pH 7.4 with 2mM EDTA and 2% FBS,

made in house) prior to flow cytometric analysis.

Table 3.2: Probes and markers used to characterize cell populations using flow cytometry.

T_{fh} cell panel			
Marker	**Fluorophore**	**Vendor**	**Clone**
Viability Dye	eFluor 780	Invitrogen	-
CD4	BV496	BD Horizon	GK1.5
CD3	BUV737	BD Optibuild	17A2
CD44	PerCP-Cy5.5	Invitrogen	IM7
PD1	BV605	Biolegend	29F.1A12
CXCR5	BV421	Biolegend	L138D7
ICOS	BUV396	BD Horizon	C398.4A
Bcl6	PE-Cy7	Biolegend	7D1
Ki67	PE	Biolegend	16A8
RBD-specific B cell panel			
Marker	**Fluorophore**	**Vendor**	**Clone**
Viability Dye	Violet fluorescent reactive dye	Invitrogen	-
RBD-tetramer	PE	-	-
RBD-tetramer	APC	-	-
F4/80 (Dump)	FITC	Biolegend	BM8
CD11c (Dump)	FITC	Biolegend	N418
Ly6c(Dump)	FITC	Invitrogen	HK1.4
Ly6g (Dump)	FITC	Invitrogen	1A8-Ly6g
CD4 (Dump)	FITC	Biolegend	GK1.5
CD8a (Dump)	FITC	Biolegend	53-6.7
B220	BUV496	BD Horizon	RA3-6B2
CD19	BUV396	BD Horizon	1D3
CD138	BV605	Biolegend	281-2
IgM	BV786	BD Optibuild	II/41
IgD	PE-Cy7	Biolegend	11-26c.2a
CD38	APC-Cy7	Biolegend	90
GL7	PerCP-Cy5.5	Invitrogen	GL-7
Restimulation panel			
Marker	**Fluorophore**	**Vendor**	**Clone**
Viability Dye	eFluor 455 (UV)	Invitrogen	-
CD3	BUV395	BD Horizon	145-2C11
CD4	BV786	BD Horizon	GK1.5
CD8	BV421	BD Horizon	53-6.7
IFNγ	APC	Biolegend	XMG1.2
TNFα	BV605	Biolegend	MP6-XT22
IL-2	PE	BD Pharmingen	JES6-5H4

3.5.24 Statistical analysis

Statistical analysis was performed using GraphPad Prism v8. Multiple group comparisons used one-way ANOVA with Tukey's post-hoc correction, Brown-Forsythe ANOVA with Dunnet's T3 post-test, two-way ANOVA with Tukey's multiple comparisons test, or mixed effects analysis with Tukey's multiple comparisons test. For nonparametric data, the Kruskal-Wallis test, followed by a Dunn's multiple comparison test, was used. For single comparisons to a specific value, a one-sample *t*-test or Wilcoxon signed rank test was used. Data are presented as mean ± SEM, unless otherwise noted. The n values used to calculate statistics are indicated in figure legends. Significance is indicated as follows, unless otherwise noted: * $p<0.05$, ** $p<0.01$, and *** $p<0.001$.

3.6 Author Contributions

3.6.1 Author list

Laura T. Gray[1*], Michal M. Raczy[1*], Priscilla S. Briquez[1*], Tiffany M. Marchell[2*], Aaron T. Alpar[1], Rachel P. Wallace[1], Lisa R. Volpatti[1], Maria Stella Sasso[1], Shijie Cao[1], Mindy Nguyen[1], Aslan Mansurov[1], Erica Budina[1], Elyse A. Watkins[1], Ani Solanki[3], Nikolaos Mitrousis[1], Joseph W. Reda[1], Shann S. Yu[1], Andrew C. Tremain[2], Ruyi Wang[1], Vlad Nicolaescu[4], Kevin Furlong[4], Steve Dvorkin[4], Balaji Manicassamy[5], Glenn Randall[4], D. Scott Wilson[1,6], Marcin Kwissa[1], Melody A. Swartz[1,2,7,8], Jeffrey A. Hubbell[1,2,7]

[*]These authors contributed equally to this work

3.6.2 Affiliations

[1]Pritzker School of Molecular Engineering, University of Chicago; Chicago, IL 60637, United

States.

[2]Committee on Immunology, University of Chicago; Chicago, IL 60637, United States.

[3]Animal Resources Center, University of Chicago; Chicago, IL 60637, United States.

[4]Department of Microbiology, Howard T. Ricketts Laboratory, University of Chicago; Chicago, IL 60637, United States.

[5]Department of Microbiology and Immunology, University of Iowa; Iowa City, IA 52242, United States.

[6]Department of Biomedical Engineering, Johns Hopkins School of Medicine; Baltimore, MD 21231, United States.

[7]Committee on Cancer Biology, University of Chicago; Chicago, IL 60637, United States.

[8]Ben May Department of Cancer Research, University of Chicago; Chicago, IL 60637, United States.

3.6.3 Contributions

Jeffrey A. Hubbell, Melody A. Swartz, and Marcin Kwissa oversaw all research; Laura T. Gray, Michal M. Raczy, Tiffany M. Marchell, and Ruyi Wang performed the synthesis and characterization of the conjugates; Priscilla S. Briquez, Aslan Mansurov, and Erica Budina performed protein expression and purification; Balaji Manicassamy provided materials; Joseph W. Reda conducted the SPR analysis; all authors designed animal studies. Laura T. Gray, Priscilla S. Briquez, Tiffany M. Marchell, Aaron T. Alpar, Rachel P. Wallace, Lisa R. Volpatti,

Maria Stella Sasso, Shijie Cao, Mindy Nguyen, Elyse A. Watkins, Ani Solanki, Nikolaos Mitrousis, Ruyi Wang, and Andrew C. Tremain performed animal studies; Priscilla S. Briquez, Vlad Nicolaescu, Kevin Furlong, Steve Dvorkin, and Glenn Randall designed and performed neutralization assay; Laura T. Gray, Michal M. Raczy, Priscilla S. Briquez, Tiffany M. Marchell, Shann S. Yu, and Aaron T. Alpar wrote the manuscript; all authors proofread the manuscript.

3.7 Acknowledgements

We acknowledge helpful discussions with Patrick C. Wilson, Jenna J. Guthmiller, Anne I. Sperling, and Aaron Esser-Kahn (University of Chicago, Chicago, IL) and with Robert Baker and David Boltz (Illinois Institute of Technology Research Institute, Chicago, IL) that were instrumental to experimental planning and model development. We acknowledge Suzana Gomes and Tera Lavoie for technical assistance. Parts of this work were carried out at the Cytometry and Antibody Technology Core Facility (Cancer Center Support Grant P30CA014599), the Soft Matter Characterization Facility, the Mass Spectrometry Facility (NSF instrumentation grant CHE-1048528), the Nuclear Magnetic Resonance Facility, the Advanced Electron Microscopy Facility (RRID:SCR_019198), and the Human Immunologic Monitoring Facility (RRID:SCR_017916) at the University of Chicago. We would also like to thank the University of Chicago Animal Resources Center for help and guidance on animal work. We are grateful to the laboratory of Florian Krammer (Icahn School of Medicine at Mount Sinai, New York City, NY) for providing plasmids coding for the Spike RBD, produced with support from the NIH NIAID (Contract # HHSN272201400008C). We are also grateful to the groups of Jesse Bloom (Fred Hutchinson Cancer Research Center, Seattle, WA) and Ali Ellebedy (Washington University School of Medicine, St. Louis, MO) for contributing reagents via the NIH NIAID BEI

Resources repository.

3.8 Funding

This work was supported by the National Heart, Lung, and Blood Institute (NHLBI) [grant T32-HL007605 – Lisa R. Volpatti]; the Canadian Institutes of Health Research [grant 201910MFE-430736-73744 – Nikolaos Mitrousis]; the National Institute of Allergy and Infectious Disease (NIAID) [grant T32-AI007090 – Tiffany M. Marchell and Andrew C. Tremain]; and the Chicago Immunoengineering Innovation Center at the University of Chicago.

3.9 Data Availability

All data are available within the text, or can be obtained from the authors upon request.

3.10 Conflicts of Interest

The University of Chicago has filed for patent protection on the p(Man-TLR7) delivery platform, and Jeffrey A. Hubbell and D. Scott Wilson are named as co-inventors on these patents.

CHAPTER 4

DISCUSSION, FUTURE DIRECTIONS, AND CONCLUSION

4.1 Discussions and Future Directions in the Use of p(Man-TLR7) for Cancer Vaccination

In the first application in which we assessed the efficacy of our polymeric glyco-adjuvant vaccine platform, we showed that tumor ECM-targeted p(Man-TLR7) is able to act as an effective therapeutic cancer vaccine. ECM targeted-p(Man-TLR7) vaccination demonstrated promising antitumor immune responses in two different cold tumor models, particularly when combined with checkpoint blockade therapy. Vaccination with our protein-polymeric glyco-adjuvant conjugates resulted in slowing of tumor growth, improved survival, and the development of immunologic antitumor memory. These results were further accompanied by an increased proportion of $CD8^+$ T cells within the tumor, as well as indications of an antigen-specific immune response occurring.

Further work remains to fully elucidate the mechanisms underlying the antitumor efficacy observed here. In particular, further studies are necessary to fully determine the importance of the targeting component used. Previous studies from our lab indicate that intratumorally delivered p(Man-TLR7) is not effective at treating both B16F10 and EMT6 tumors when it is not tumor-targeted [249]. We also see indications in the work presented here that non-targeted p(Man-TLR7) is not as effective as targeted versions in terms of slowing of tumor growth (**Fig. 2.20; Fig. 2.21**), improving survival (**Fig. 2.20; Fig. 2.21**), recruiting antigen-specific $CD8^+$ T cells to the tumor (**Fig. 2.9**), and increasing the proportion of activated $CD103^+$ DCs within the tumor (**Fig. 2.12**). Based on this previous and current work, we

hypothesize that the ECM-targeting strategy used here is important the antitumor immunity induced by our vaccines. However, a true head-to-head study is needed in order to fully determine the necessity of the ECM-targeting component of our vaccines.

Further work could also be done to maximize the therapeutic potential of our vaccines. One approach would be to alter the targeting strategy we are using. If ECM-targeting is still desired, one strategy could be to switch from using an anti-EDA Fab to using a full-length anti-EDA antibody, as this would act to increase the avidity of our conjugate's interaction with the ECM. Alternatively, one of the ECM targeting components used here could be substituted with a protein (or peptide) that binds one of the many other ECM components that show differential expression in cancer versus healthy tissue mentioned in Section 1.2.5. Another approach would be to change the target within the tumor, such as to tumor cells themselves. There are many potential targets on the surface of tumor cells, two of which (TRP1 and CD47) have been investigated by our lab previously to target p(Man-TLR7) to the tumor for vaccination [249]. This approach showed very promising results in treating established B16F10 and EMT6 tumors. In this approach, p(Man-TLR7) is directly attached to a source of tumor antigens (tumor cells or tumor debris), which may potentially be a benefit of this targeting approach over ECM-targeting. Interestingly, this approach is effective as a monotherapy and does not synergize with checkpoint blockade [249]. This points to cell-targeted p(Man-TLR7) having a somewhat different mechanism of action than ECM-targeted p(Man-TLR7). In the future, work directly comparing these two strategies could help us to further understand the differences in the mechanisms driving the antitumor immunity observed after vaccination and could allow us to determine if one targeting approach has more clinical translational potential than the other.

One major challenge for the vaccine strategy presented here is the induction of anti-drug antibodies after repeated vaccination (**Fig. 2.22**). This limits the number of doses that can be administered and also poses a safety concern. These antibodies have been observed to bind the protein components of our vaccine. As a result, one possible way to overcome this challenge is to altogether eliminate the protein component of the vaccine and use an entirely new targeting approach. Preliminary work in our lab is being conducting on a version of the p(Man-TLR7) polymer that is thiol reactive. As tumor cells divide under hypoxic conditions, a large number of extracellular thiols are displayed [250]. Previous work has taken advantage of this to target or label tumor cells using thiol-reactive compounds [250]. Thus, the goal of this approach with p(Man-TLR7) is to create a polymeric glyco-adjuvant that will directly bind to tumor cells (without the need of a protein) upon injection. We hypothesize that this approach will reduce the number of adverse events observed upon repeated vaccination with p(Man-TLR7). Further work is necessary to determine the feasibility and efficacy of this approach, especially as compared to our protein targeted approaches described here and previously [249].

Furthermore, the translational potential of our ECM-targeted p(Man-TLR7) could be further improved via optimization for intravenous instead of intratumoral administration. Intratumoral administration is a clinically viable administration route, but it does create limitations on the types of tumors that could be treated. Intravenous administration would allow our vaccine access to virtually any tumor type. While we did see some promising results here (**Fig. 2.17; Fig. 2.20**), they were not as good as the results we observed with intratumoral administration (**Fig. 2.17**). We hypothesize that altering the formulation of our vaccine may improve the results we observe after intravenous administration. Currently, our vaccine contains mannose in order to help target antigen presenting cells and to allow our vaccine to activate

TLR7 within the endosome. However, we have ongoing work in our lab using mannose specifically as a liver-targeting moiety, as mannosylated proteins have been shown to preferentially be taken up by the liver after intravenous injection [251]. This means that upon intravenous administration of our vaccine conjugates, the liver may quickly take up our vaccine due to the inclusion of mannose and therefore reduce the amount of conjugates that are able to localize to the tumor. As a result, we hypothesize that removing the mannose portion of our vaccine could potentially improve the antitumor efficacy after intravenous administration. The major question with this approach, however, is whether our polymeric glyco-adjuvant would still able to activate TLR7 without the mannose to help trigger internalization into the endosome.

Lastly, one of the major advantages of our polymeric glyco-adjuvant platform is its modularity, meaning that the components used here can be easily swapped out for different components with different functionalities. This is particularly relevant for further preclinical testing (particularly in non-human primates) and translation into the clinic, as it would be beneficial to use a version of our polymer that incorporates a dual TLR7/8 agonist in place of the TLR7 agonist used here due to the differences in expression and functionality of the TLR7 and TLR8 receptors in mice and humans [99]. This polymer has been developed in our lab and work is ongoing to assess its efficacy. Furthermore, the incorporation of other adjuvants into this polymer (in place of or in addition to the TLR7 agonist) could act to further maximize the observed therapeutic potential, especially since TLR agonists have been shown to synergize when combined [252]. Work is currently being conducted in our lab to investigate this.

4.2 Discussions and Future Directions in the Use of p(Man-TLR7) for Infectious Disease Vaccination

In the second use of our polymeric glyco-adjuvant vaccine platform described here, we demonstrated that our platform can be used as an effective prophylactic vaccine against a virus for the first time. Previously we had shown promising results using this platform in vaccinating against ovalbumin and malaria antigens [97]. Here, we observed that vaccination with Spike-p(Man-TLR7) elicited high levels of neutralizing antibodies, as well as antigen-specific T cells. These responses were further enhanced when our vaccine was used in combination with the depot-forming adjuvant alum. Overall, this demonstrates that our p(Man-TLR7) vaccine platform is an easily adaptable platform that can be used to generate subunit vaccines against multiple infectious diseases.

In the future, further work may be desirable in order to fully assess the efficacy of this vaccine. In the work presented here, we observed neutralizing antibody responses, but we did not explicitly demonstrate that protective antiviral responses are induced. We hypothesize that the neutralizing antibody responses we see would correlate with protective responses. However, it may be beneficial to fully assess this in the future in order to further understand the translational potential of our vaccine. This could be tested using a viral challenge model in mice [253].

The translational potential of our vaccine could also be improved by using a TLR7/8 dual agonist in place of the TLR7 agonist that is in the COVID-19 vaccine described here. Particularly in human cells, activation of TLR7 and TLR8 has been shown to drive functionally distinct immune responses, so activating both of these receptors may enhance the immune responses observed [109,247]. As mentioned with our cancer vaccines that utilize p(Man-TLR7), this is an active area of investigation with our laboratory.

Another way to improve the therapeutic potential of our COVID-19 vaccine is to further investigate using our vaccine in combination with other adjuvants or even other vaccine technologies. In the results from the present study, combining Spike-p(Man-TLR7) with alum improved the efficacy of our vaccine in multiple ways. In particular, higher titers of neutralizing antibodies, as well as an increased proportion of polyfunctional cytokine$^+$ T cells in the spleen after restimulation, were observed, as compared to responses from vaccination with Spike-p(Man-TLR7) alone (**Fig. 3.7; Fig. 3.12**). Based on this, we hypothesize that combining our antigen-p(Man-TLR7) vaccine with other adjuvants may also result in improved immune responses compared to those observed with our antigen-p(Man-TLR7) vaccine alone. Combining our vaccine technology with other clinically available vaccine technologies (especially those used in clinically available COVID-19 vaccines) could also result in improved immune responses. Preliminary studies have shown than heterologous prime-boost vaccination (commonly with an mRNA vaccine preceded or followed by a viral vector vaccine) may result in an enhanced immune response against SARS-CoV-2 (or at least the same response level) as compared to homologous prime-boost vaccination [254–257]. As further insight into this combinatorial effect is gained, it may be worthwhile to investigate the immune response of our vaccine platform in combination with one of the currently available clinical COVID-19 vaccines in a heterologous prime-boost vaccination schedule. It should be noted, however, that we have not tested our vaccine head-to-head against the other clinically available COVID-19 vaccines. As a result, we do not know how our vaccine directly compares with clinically available vaccines, and further studies are required to answer this question.

Lastly, we observed that RBD-p(Man-TLR7) vaccination failed to elicit neutralizing antibody responses in mice (**Fig. 3.6**). We hypothesized that this was due to the small size of

RBD and the chosen conjugation ratio of RBD to p(Man-TLR7). At the conjugation ratio used in the present study, the p(Man-TLR7) polymer may have sterically masked RBD and prevented the desired B cell responses. Currently, our laboratory is investigating this hypothesis and also trying to elucidate the relationship between conjugation ratio and antibody responses. As this optimization work progresses, we will gain an improved understanding and increase the versatility of our vaccine platform, which will allow us to use our vaccine technology in the development of a wider array of vaccines moving forward.

4.3 Conclusion

In conclusion, here we report the development of an effective therapeutic cancer vaccine and prophylactic COVID-19 vaccine, which both utilize our novel polymeric glyco-adjuvant platform. This platform is modular and easily adaptable, as demonstrated by our use of our polymeric glyco-adjuvant in two distinct contexts. In the work presented here, the protein component of our vaccine conjugates was adapted to the context in which we wished to use our vaccine. In the future, other components of our vaccine can also be adapted. Overall, the vaccines developed here demonstrated the induction of strong humoral and cellular responses. In the case of infectious disease, these responses are both desirable. However, in cancer, a humoral response may not be desired. As a result, consideration must go into the design of any future vaccines using this technology. While further work remains to optimize our platform, the results shown here demonstrate that our easily adaptable and potent p(Man-TLR7) vaccine platform has significant clinical translational potential for use in multiple therapeutic contexts.

REFERENCES

[1] A.J. Pollard, E.M. Bijker, A guide to vaccinology: from basic principles to new developments, Nat Rev Immunol. 21 (2021) 83–100. https://doi.org/10.1038/s41577-020-00479-7.

[2] F.P. Polack, S.J. Thomas, N. Kitchin, J. Absalon, A. Gurtman, S. Lockhart, J.L. Perez, G. Pérez Marc, E.D. Moreira, C. Zerbini, R. Bailey, K.A. Swanson, S. Roychoudhury, K. Koury, P. Li, W.V. Kalina, D. Cooper, R.W. Frenck, L.L. Hammitt, Ö. Türeci, H. Nell, A. Schaefer, S. Ünal, D.B. Tresnan, S. Mather, P.R. Dormitzer, U. Şahin, K.U. Jansen, W.C. Gruber, Safety and Efficacy of the BNT162b2 mRNA Covid-19 Vaccine, N Engl J Med. 383 (2020) 2603–2615. https://doi.org/10.1056/NEJMoa2034577.

[3] L.R. Baden, H.M. El Sahly, B. Essink, K. Kotloff, S. Frey, R. Novak, D. Diemert, S.A. Spector, N. Rouphael, C.B. Creech, J. McGettigan, S. Khetan, N. Segall, J. Solis, A. Brosz, C. Fierro, H. Schwartz, K. Neuzil, L. Corey, P. Gilbert, H. Janes, D. Follmann, M. Marovich, J. Mascola, L. Polakowski, J. Ledgerwood, B.S. Graham, H. Bennett, R. Pajon, C. Knightly, B. Leav, W. Deng, H. Zhou, S. Han, M. Ivarsson, J. Miller, T. Zaks, Efficacy and Safety of the mRNA-1273 SARS-CoV-2 Vaccine, N Engl J Med. 384 (2021) 403–416. https://doi.org/10.1056/NEJMoa2035389.

[4] B. Pulendran, P. S. Arunachalam, D.T. O'Hagan, Emerging concepts in the science of vaccine adjuvants, Nat Rev Drug Discov. 20 (2021) 454–475. https://doi.org/10.1038/s41573-021-00163-y.

[5] American Cancer Society, Cancer Facts & Figures 2021, American Cancer Society, Atlanta, GA, 2021.

[6] J. Duraiswamy, K.M. Kaluza, G.J. Freeman, G. Coukos, Dual blockade of PD-1 and CTLA-4 combined with tumor vaccine effectively restores T-cell rejection function in tumors, Cancer Res. 73 (2013) 3591–3603. https://doi.org/10.1158/0008-5472.CAN-12-4100.

[7] M.A. Curran, W. Montalvo, H. Yagita, J.P. Allison, PD-1 and CTLA-4 combination blockade expands infiltrating T cells and reduces regulatory T and myeloid cells within B16 melanoma tumors, Proc Natl Acad Sci U S A. 107 (2010) 4275–4280. https://doi.org/10.1073/pnas.0915174107.

[8] T. Powles, J.P. Eder, G.D. Fine, F.S. Braiteh, Y. Loriot, C. Cruz, J. Bellmunt, H.A. Burris, D.P. Petrylak, S. Teng, X. Shen, Z. Boyd, P.S. Hegde, D.S. Chen, N.J. Vogelzang, MPDL3280A (anti-PD-L1) treatment leads to clinical activity in metastatic bladder cancer, Nature. 515 (2014) 558–562. https://doi.org/10.1038/nature13904.

[9] F.S. Hodi, S.J. O'Day, D.F. McDermott, R.W. Weber, J.A. Sosman, J.B. Haanen, R. Gonzalez, C. Robert, D. Schadendorf, J.C. Hassel, W. Akerley, A.J.M. van den Eertwegh, J. Lutzky, P. Lorigan, J.M. Vaubel, G.P. Linette, D. Hogg, C.H. Ottensmeier, C. Lebbé, C. Peschel, I. Quirt, J.I. Clark, J.D. Wolchok, J.S. Weber, J. Tian, M.J. Yellin, G.M. Nichol,

A. Hoos, W.J. Urba, Improved Survival with Ipilimumab in Patients with Metastatic Melanoma, New England Journal of Medicine. 363 (2010) 711–723. https://doi.org/10.1056/NEJMoa1003466.

[10] J.M. Pitt, M. Vétizou, R. Daillère, M.P. Roberti, T. Yamazaki, B. Routy, P. Lepage, I.G. Boneca, M. Chamaillard, G. Kroemer, L. Zitvogel, Resistance Mechanisms to Immune-Checkpoint Blockade in Cancer: Tumor-Intrinsic and -Extrinsic Factors, Immunity. 44 (2016) 1255–1269. https://doi.org/10.1016/j.immuni.2016.06.001.

[11] P. Sharma, J.P. Allison, The future of immune checkpoint therapy, Science. 348 (2015) 56–61. https://doi.org/10.1126/SCIENCE.AAA8172.

[12] S. Spranger, T.F. Gajewski, Tumor-intrinsic oncogene pathways mediating immune avoidance, OncoImmunology. 5 (2016) e1086862. https://doi.org/10.1080/2162402X.2015.1086862.

[13] I. Mellman, G. Coukos, G. Dranoff, Cancer immunotherapy comes of age, Nature. 480 (2011) 480–489. https://doi.org/10.1038/nature10673.

[14] D.R. Pattabiraman, R.A. Weinberg, Tackling the cancer stem cells – what challenges do they pose?, Nat Rev Drug Discov. 13 (2014) 497–512. https://doi.org/10.1038/nrd4253.

[15] W. Zou, Regulatory T cells, tumour immunity and immunotherapy, Nat Rev Immunol. 6 (2006) 295–307. https://doi.org/10.1038/nri1806.

[16] N.P. Restifo, M.E. Dudley, S.A. Rosenberg, Adoptive immunotherapy for cancer: harnessing the T cell response, Nat Rev Immunol. 12 (2012) 269–281. https://doi.org/10.1038/nri3191.

[17] J.W. Pollard, Tumour-educated macrophages promote tumour progression and metastasis, Nat Rev Cancer. 4 (2004) 71–78. https://doi.org/10.1038/nrc1256.

[18] D.G. DeNardo, J.B. Barreto, P. Andreu, L. Vasquez, D. Tawfik, N. Kolhatkar, L.M. Coussens, CD4(+) T cells regulate pulmonary metastasis of mammary carcinomas by enhancing protumor properties of macrophages, Cancer Cell. 16 (2009) 91–102. https://doi.org/10.1016/j.ccr.2009.06.018.

[19] M. Quante, S.P. Tu, H. Tomita, T. Gonda, S.S.W. Wang, S. Takashi, G.H. Baik, W. Shibata, B. Diprete, K.S. Betz, R. Friedman, A. Varro, B. Tycko, T.C. Wang, Bone marrow-derived myofibroblasts contribute to the mesenchymal stem cell niche and promote tumor growth, Cancer Cell. 19 (2011) 257–272. https://doi.org/10.1016/j.ccr.2011.01.020.

[20] B. Dirat, L. Bochet, M. Dabek, D. Daviaud, S. Dauvillier, B. Majed, Y.Y. Wang, A. Meulle, B. Salles, S. Le Gonidec, I. Garrido, G. Escourrou, P. Valet, C. Muller, Cancer-associated adipocytes exhibit an activated phenotype and contribute to breast cancer invasion, Cancer Res. 71 (2011) 2455–2465. https://doi.org/10.1158/0008-5472.CAN-10-3323.

[21] J.M. Butler, H. Kobayashi, S. Rafii, Instructive role of the vascular niche in promoting tumour growth and tissue repair by angiocrine factors, Nat Rev Cancer. 10 (2010) 138–146. https://doi.org/10.1038/nrc2791.

[22] P. Lu, V.M. Weaver, Z. Werb, The extracellular matrix: a dynamic niche in cancer progression., The Journal of Cell Biology. 196 (2012) 395–406. https://doi.org/10.1083/jcb.201102147.

[23] L. Zitvogel, L. Apetoh, F. Ghiringhelli, F. André, A. Tesniere, G. Kroemer, The anticancer immune response: indispensable for therapeutic success?, J Clin Invest. 118 (2008) 1991–2001. https://doi.org/10.1172/JCI35180.

[24] O.J. Finn, Immuno-oncology: understanding the function and dysfunction of the immune system in cancer, Ann Oncol. 23 Suppl 8 (2012) viii6-9. https://doi.org/10.1093/annonc/mds256.

[25] S.A. Rosenberg, J.C. Yang, R.M. Sherry, U.S. Kammula, M.S. Hughes, G.Q. Phan, D.E. Citrin, N.P. Restifo, P.F. Robbins, J.R. Wunderlich, K.E. Morton, C.M. Laurencot, S.M. Steinberg, D.E. White, M.E. Dudley, Durable Complete Responses in Heavily Pretreated Patients with Metastatic Melanoma Using T-Cell Transfer Immunotherapy, Clin Cancer Res. 17 (2011) 4550–4557. https://doi.org/10.1158/1078-0432.CCR-11-0116.

[26] T.F. Gajewski, Cancer immunotherapy, Molecular Oncology. 6 (2012) 242–250.

[27] S. Hadrup, M. Donia, P. Thor Straten, Effector CD4 and CD8 T cells and their role in the tumor microenvironment, Cancer Microenviron. 6 (2013) 123–133. https://doi.org/10.1007/s12307-012-0127-6.

[28] J. Galon, A. Costes, F. Sanchez-Cabo, A. Kirilovsky, B. Mlecnik, C. Lagorce-Pagès, M. Tosolini, M. Camus, A. Berger, P. Wind, F. Zinzindohoué, P. Bruneval, P.-H. Cugnenc, Z. Trajanoski, W.-H. Fridman, F. Pagès, Type, density, and location of immune cells within human colorectal tumors predict clinical outcome, Science. 313 (2006) 1960–1964. https://doi.org/10.1126/science.1129139.

[29] K.M. Friedman, P.A. Prieto, L.E. Devillier, C.A. Gross, J.C. Yang, J.R. Wunderlich, S.A. Rosenberg, M.E. Dudley, Tumor-specific CD4+ melanoma tumor-infiltrating lymphocytes, J Immunother. 35 (2012) 400–408. https://doi.org/10.1097/CJI.0b013e31825898c5.

[30] C.J. Melief, Tumor eradication by adoptive transfer of cytotoxic T lymphocytes, Adv Cancer Res. 58 (1992) 143–175. https://doi.org/10.1016/s0065-230x(08)60294-8.

[31] K. Hung, R. Hayashi, A. Lafond-Walker, C. Lowenstein, D. Pardoll, H. Levitsky, The central role of CD4(+) T cells in the antitumor immune response, J Exp Med. 188 (1998) 2357–2368. https://doi.org/10.1084/jem.188.12.2357.

[32] R.E. Toes, F. Ossendorp, R. Offringa, C.J. Melief, CD4 T cells and their role in antitumor immune responses, J Exp Med. 189 (1999) 753–756. https://doi.org/10.1084/jem.189.5.753.

[33] T.J. Curiel, G. Coukos, L. Zou, X. Alvarez, P. Cheng, P. Mottram, M. Evdemon-Hogan, J.R. Conejo-Garcia, L. Zhang, M. Burow, Y. Zhu, S. Wei, I. Kryczek, B. Daniel, A. Gordon, L. Myers, A. Lackner, M.L. Disis, K.L. Knutson, L. Chen, W. Zou, Specific recruitment of regulatory T cells in ovarian carcinoma fosters immune privilege and predicts reduced survival, Nat Med. 10 (2004) 942–949. https://doi.org/10.1038/nm1093.

[34] F.C. Robertson, J.A. Berzofsky, M. Terabe, NKT Cell Networks in the Regulation of Tumor Immunity, Front Immunol. 5 (2014) 543. https://doi.org/10.3389/fimmu.2014.00543.

[35] T. Ding, F. Yan, S. Cao, X. Ren, Regulatory B cell: New member of immunosuppressive cell club, Hum Immunol. 76 (2015) 615–621. https://doi.org/10.1016/j.humimm.2015.09.006.

[36] D.I. Gabrilovich, S. Nagaraj, Myeloid-derived suppressor cells as regulators of the immune system, Nat Rev Immunol. 9 (2009) 162–174. https://doi.org/10.1038/nri2506.

[37] R. Noy, J.W. Pollard, Tumor-associated macrophages: from mechanisms to therapy, Immunity. 41 (2014) 49–61. https://doi.org/10.1016/j.immuni.2014.06.010.

[38] S.I. Grivennikov, F.R. Greten, M. Karin, Immunity, Inflammation, and Cancer, Cell. 140 (2010) 883–899. https://doi.org/10.1016/j.cell.2010.01.025.

[39] J. Bubeník, MHC class I down-regulation: tumour escape from immune surveillance? (review), Int J Oncol. 25 (2004) 487–491. https://doi.org/10.3892/ijo.25.2.487.

[40] S.L. Topalian, C.G. Drake, D.M. Pardoll, Immune checkpoint blockade: a common denominator approach to cancer therapy, Cancer Cell. 27 (2015) 450–461. https://doi.org/10.1016/j.ccell.2015.03.001.

[41] J.F. Grosso, M.N. Jure-Kunkel, CTLA-4 blockade in tumor models: an overview of preclinical and translational research, Cancer Immun. 13 (2013) 5.

[42] D.J. Lenschow, T.L. Walunas, J.A. Bluestone, CD28/B7 system of T cell costimulation, Annu Rev Immunol. 14 (1996) 233–258. https://doi.org/10.1146/annurev.immunol.14.1.233.

[43] G.J. Freeman, A.J. Long, Y. Iwai, K. Bourque, T. Chernova, H. Nishimura, L.J. Fitz, N. Malenkovich, T. Okazaki, M.C. Byrne, H.F. Horton, L. Fouser, L. Carter, V. Ling, M.R. Bowman, B.M. Carreno, M. Collins, C.R. Wood, T. Honjo, Engagement of the Pd-1 Immunoinhibitory Receptor by a Novel B7 Family Member Leads to Negative Regulation of Lymphocyte Activation, J Exp Med. 192 (2000) 1027–1034. https://doi.org/10.1084/jem.192.7.1027.

[44] Y. Iwai, M. Ishida, Y. Tanaka, T. Okazaki, T. Honjo, N. Minato, Involvement of PD-L1 on tumor cells in the escape from host immune system and tumor immunotherapy by PD-L1 blockade, Proc Natl Acad Sci U S A. 99 (2002) 12293–12297. https://doi.org/10.1073/pnas.192461099.

[45] C. Blank, T.F. Gajewski, A. Mackensen, Interaction of PD-L1 on tumor cells with PD-1 on tumor-specific T cells as a mechanism of immune evasion: implications for tumor immunotherapy, Cancer Immunol Immunother. 54 (2005) 307–314. https://doi.org/10.1007/s00262-004-0593-x.

[46] T.R. Simpson, F. Li, W. Montalvo-Ortiz, M.A. Sepulveda, K. Bergerhoff, F. Arce, C. Roddie, J.Y. Henry, H. Yagita, J.D. Wolchok, K.S. Peggs, J.V. Ravetch, J.P. Allison, S.A. Quezada, Fc-dependent depletion of tumor-infiltrating regulatory T cells co-defines the efficacy of anti–CTLA-4 therapy against melanoma, Journal of Experimental Medicine. 210 (2013) 1695–1710. https://doi.org/10.1084/jem.20130579.

[47] S. Spranger, H.K. Koblish, B. Horton, P.A. Scherle, R. Newton, T.F. Gajewski, Mechanism of tumor rejection with doublets of CTLA-4, PD-1/PD-L1, or IDO blockade involves restored IL-2 production and proliferation of CD8(+) T cells directly within the tumor microenvironment, J Immunother Cancer. 2 (2014) 3. https://doi.org/10.1186/2051-1426-2-3.

[48] C.-Y. Chang, H. Park, D.C. Malone, C.-Y. Wang, D.L. Wilson, Y.-M. Yeh, S. Van Boemmel-Wegmann, W.-H. Lo-Ciganic, Immune Checkpoint Inhibitors and Immune-Related Adverse Events in Patients With Advanced Melanoma: A Systematic Review and Network Meta-analysis, JAMA Network Open. 3 (2020) e201611. https://doi.org/10.1001/jamanetworkopen.2020.1611.

[49] J.M. Michot, C. Bigenwald, S. Champiat, M. Collins, F. Carbonnel, S. Postel-Vinay, A. Berdelou, A. Varga, R. Bahleda, A. Hollebecque, C. Massard, A. Fuerea, V. Ribrag, A. Gazzah, J.P. Armand, N. Amellal, E. Angevin, N. Noel, C. Boutros, C. Mateus, C. Robert, J.C. Soria, A. Marabelle, O. Lambotte, Immune-related adverse events with immune checkpoint blockade: a comprehensive review, European Journal of Cancer. 54 (2016) 139–148. https://doi.org/10.1016/j.ejca.2015.11.016.

[50] A. Villa, E. Trachsel, M. Kaspar, C. Schliemann, R. Sommavilla, J.N. Rybak, C. Rösli, L. Borsi, D. Neri, A high-affinity human monoclonal antibody specific to the alternatively spliced EDA domain of fibronectin efficiently targets tumor neo-vasculature in vivo, International Journal of Cancer. 122 (2008) 2405–2413. https://doi.org/10.1002/ijc.23408.

[51] J.N. Rybak, C. Roesli, M. Kaspar, A. Villa, D. Neri, The extra-domain A of fibronectin is a vascular marker of solid tumors and metastases, Cancer Research. 67 (2007) 10948–10957. https://doi.org/10.1158/0008-5472.CAN-07-1436.

[52] A. Pini, F. Viti, A. Santucci, B. Carnemolla, L. Zardi, P. Neri, D. Neri, Design and use of a phage display library. Human antibodies with subnanomolar affinity against a marker of angiogenesis eluted from a two-dimensional gel., The Journal of Biological Chemistry. 273 (1998) 21769–76. https://doi.org/10.1074/jbc.273.34.21769.

[53] M. Kaspar, L. Zardi, D. Neri, Fibronectin as target for tumor therapy, International Journal of Cancer. 118 (2006) 1331–1339. https://doi.org/10.1002/ijc.21677.

[54] C. Hutmacher, D. Neri, Antibody-cytokine fusion proteins: Biopharmaceuticals with immunomodulatory properties for cancer therapy, Advanced Drug Delivery Reviews. 141 (2019) 67–91. https://doi.org/10.1016/j.addr.2018.09.002.

[55] P. Probst, J. Kopp, A. Oxenius, M.P. Colombo, D. Ritz, T. Fugmann, D. Neri, Sarcoma Eradication by Doxorubicin and Targeted TNF Relies upon CD8 $^{+}$ T-cell Recognition of a Retroviral Antigen, Cancer Research. 77 (2017) 3644–3654. https://doi.org/10.1158/0008-5472.CAN-16-2946.

[56] K.L. Gutbrodt, C. Schliemann, L. Giovannoni, K. Frey, T. Pabst, W. Klapper, W.E. Berdel, D. Neri, Antibody-based delivery of interleukin-2 to neovasculature has potent activity against acute myeloid leukemia., Science Translational Medicine. 5 (2013) 201ra118. https://doi.org/10.1126/scitranslmed.3006221.

[57] G. Orend, R. Chiquet-Ehrismann, Tenascin-C induced signaling in cancer, Cancer Letters. (2006). https://doi.org/10.1016/j.canlet.2006.02.017.

[58] A. Dal Corso, R. Gébleux, P. Murer, A. Soltermann, D. Neri, A non-internalizing antibody-drug conjugate based on an anthracycline payload displays potent therapeutic activity in vivo, Journal of Controlled Release. (2017). https://doi.org/10.1016/j.jconrel.2017.08.040.

[59] S.S. Brack, M. Silacci, M. Birchler, D. Neri, Tumor-Targeting Properties of Novel Antibodies Specific to the Large Isoform of Tenascin-C, Clinical Cancer Research. 12 (2006) 3200 LP – 3208. https://doi.org/10.1158/1078-0432.CCR-05-2804.

[60] J. Marlind, M. Kaspar, R. Sommavilla, S. Hindle, C. Bacci, L. Giovannoni, D. Neri, Antibody-Mediated Delivery of Interleukin-2 to the Stroma of Breast Cancer Strongly Enhances the Potency of Chemotherapy, (2008). https://doi.org/10.1158/1078-0432.CCR-07-5041.

[61] B. Chen, W. Dai, D. Mei, T. Liu, S. Li, B. He, B. He, L. Yuan, H. Zhang, X. Wang, Q. Zhang, Comprehensively priming the tumor microenvironment by cancer-associated fibroblast-targeted liposomes for combined therapy with cancer cell-targeted chemotherapeutic drug delivery system, Journal of Controlled Release. 241 (2016) 68–80. https://doi.org/10.1016/J.JCONREL.2016.09.014.

[62] B. Chen, Z. Wang, J. Sun, Q. Song, B. He, H. Zhang, X. Wang, W. Dai, Q. Zhang, A tenascin C targeted nanoliposome with navitoclax for specifically eradicating of cancer-associated fibroblasts, Nanomedicine: Nanotechnology, Biology and Medicine. 12 (2016) 131–141. https://doi.org/10.1016/J.NANO.2015.10.001.

[63] T. Kang, Q. Zhu, D. Jiang, X. Feng, J. Feng, T. Jiang, J. Yao, Y. Jing, Q. Song, X. Jiang, X. Gao, J. Chen, Synergistic targeting tenascin C and neuropilin-1 for specific penetration

of nanoparticles for anti-glioblastoma treatment, Biomaterials. 101 (2016) 60–75. https://doi.org/10.1016/J.BIOMATERIALS.2016.05.037.

[64] J. Lin, S. Shigdar, D.Z. Fang, D. Xiang, M.Q. Wei, A. Danks, L. Kong, L. Li, L. Qiao, W. Duan, Improved Efficacy and Reduced Toxicity of Doxorubicin Encapsulated in Sulfatide-Containing Nanoliposome in a Glioma Model, PLoS ONE. 9 (2014) e103736. https://doi.org/10.1371/journal.pone.0103736.

[65] X. Li, L. Hou, L. Yang, L. Mo, L. Li, F. Qin, Sulfatide-containing lipid perfluorooctylbromide nanoparticles as paclitaxel vehicles targeting breast carcinoma, International Journal of Nanomedicine. (2014) 3971. https://doi.org/10.2147/IJN.S67343.

[66] M.P. Marinkovich, Laminin 332 in squamous-cell carcinoma, Nature Reviews Cancer. 7 (2007) 370–380. https://doi.org/10.1038/nrc2089.

[67] M. Tran, P. Rousselle, P. Nokelainen, S. Tallapragada, N.T. Nguyen, E.F. Fincher, M.P. Marinkovich, Targeting a Tumor-Specific Laminin Domain Critical for Human Carcinogenesis, (2008). https://doi.org/10.1158/0008-5472.CAN-07-6160.

[68] F. Décline, O. Okamoto, F. Mallein-Gerin, B. Helbert, J. Bernaud, D. Rigal, P. Rousselle, Keratinocyte motility induced by TGF-β1 is accompanied by dramatic changes in cellular interactions with laminin 5, Cell Motility and the Cytoskeleton. 54 (2003) 64–80. https://doi.org/10.1002/cm.10086.

[69] Z.-H. Zhou, C.-D. Ji, H.-L. Xiao, H.-B. Zhao, Y.-H. Cui, X.-W. Bian, Reorganized Collagen in the Tumor Microenvironment of Gastric Cancer and Its Association with Prognosis, Journal of Cancer. 8 (2017) 1466–1476. https://doi.org/10.7150/jca.18466.

[70] P.P. Provenzano, D.R. Inman, K.W. Eliceiri, J.G. Knittel, L. Yan, C.T. Rueden, J.G. White, P.J. Keely, Collagen density promotes mammary tumor initiation and progression, BMC Medicine. 6 (2008) 11. https://doi.org/10.1186/1741-7015-6-11.

[71] N. Momin, N.K. Mehta, N.R. Bennett, L. Ma, J.R. Palmeri, M.M. Chinn, E.A. Lutz, B. Kang, D.J. Irvine, S. Spranger, K.D. Wittrup, Anchoring of intratumorally administered cytokines to collagen safely potentiates systemic cancer immunotherapy., Science Translational Medicine. 11 (2019) eaaw2614. https://doi.org/10.1126/scitranslmed.aaw2614.

[72] J.A. Nagy, S.-H. Chang, A.M. Dvorak, H.F. Dvorak, Why are tumour blood vessels abnormal and why is it important to know?, British Journal of Cancer. 100 (2009) 865–869. https://doi.org/10.1038/sj.bjc.6604929.

[73] H. Liang, X. Li, B. Wang, B. Chen, Y. Zhao, J. Sun, Y. Zhuang, J. Shi, H. Shen, Z. Zhang, J. Dai, A collagen-binding EGFR antibody fragment targeting tumors with a collagen-rich extracellular matrix, Scientific Reports. 6 (2016) 18205. https://doi.org/10.1038/srep18205.

[74] J. Ishihara, A. Ishihara, K. Sasaki, S.S.-Y. Lee, J.-M. Williford, M. Yasui, H. Abe, L. Potin, P. Hosseinchi, K. Fukunaga, M.M. Raczy, L.T. Gray, A. Mansurov, K. Katsumata, M. Fukayama, S.J. Kron, M.A. Swartz, J.A. Hubbell, Targeted antibody and cytokine cancer immunotherapies through collagen affinity, Science Translational Medicine. 11 (2019) eaau3259. https://doi.org/10.1126/SCITRANSLMED.AAU3259.

[75] B.P. Toole, Hyaluronan: From extracellular glue to pericellular cue, Nature Reviews Cancer. 4 (2004) 528–539. https://doi.org/10.1038/nrc1391.

[76] S. Misra, P. Heldin, V.C. Hascall, N.K. Karamanos, S.S. Skandalis, R.R. Markwald, S. Ghatak, Hyaluronan-CD44 interactions as potential targets for cancer therapy, FEBS Journal. 278 (2011) 1429–1443. https://doi.org/10.1111/j.1742-4658.2011.08071.x.

[77] H. Ikemoto, P. Lingasamy, A.-M. Anton Willmore, H. Hunt, K. Kurm, O. Tammik, P. Scodeller, L. Simón-Gracia, V.R. Kotamraju, A.M. Lowy, K.N. Sugahara, T. Teesalu, Hyaluronan-binding peptide for targeting peritoneal carcinomatosis, Tumor Biology. 39 (2017) 101042831770162. https://doi.org/10.1177/1010428317701628.

[78] M.J.E. Vallen, S.C.H.A. van der Steen, A.A.G. van Tilborg, L.F.A.G. Massuger, T.H. van Kuppevelt, Sulfated sugars in the extracellular matrix orchestrate ovarian cancer development: 'When sweet turns sour,' Gynecologic Oncology. 135 (2014) 371–381. https://doi.org/10.1016/j.ygyno.2014.08.023.

[79] A. Salanti, T.M. Clausen, M.Ø. Agerbæk, N. Al Nakouzi, M. Dahlbäck, H.Z. Oo, S. Lee, T. Gustavsson, J.R. Rich, B.J. Hedberg, Y. Mao, L. Barington, M.A. Pereira, J. LoBello, M. Endo, L. Fazli, J. Soden, C.K. Wang, A.F. Sander, R. Dagil, S. Thrane, P.J. Holst, L. Meng, F. Favero, G.J. Weiss, M.A. Nielsen, J. Freeth, T.O. Nielsen, J. Zaia, N.L. Tran, J. Trent, J.S. Babcook, T.G. Theander, P.H. Sorensen, M. Daugaard, Targeting Human Cancer by a Glycosaminoglycan Binding Malaria Protein., Cancer Cell. 28 (2015) 500–514. https://doi.org/10.1016/j.ccell.2015.09.003.

[80] B. Zhang, G. Cheng, M. Zheng, J. Han, B. Wang, M. Li, J. Chen, T. Xiao, J. Zhang, L. Cai, S. Li, X. Fan, Targeted delivery of doxorubicin by CSA-binding nanoparticles for choriocarcinoma treatment, Drug Delivery. 25 (2018) 461–471. https://doi.org/10.1080/10717544.2018.1435750.

[81] S.C.H.A. van der Steen, R. Raavé, S. Langerak, L. van Houdt, S.M.J. van Duijnhoven, S.A.M. van Lith, L.F.A.G. Massuger, W.F. Daamen, W.P. Leenders, T.H. van Kuppevelt, Targeting the extracellular matrix of ovarian cancer using functionalized, drug loaded lyophilisomes, European Journal of Pharmaceutics and Biopharmaceutics. 113 (2017) 229–239. https://doi.org/10.1016/J.EJPB.2016.12.010.

[82] C.M. Lee, T. Tanaka, T. Murai, M. Kondo, J. Kimura, W. Su, T. Kitagawa, T. Ito, H. Matsuda, M. Miyasaka, Novel Chondroitin Sulfate-binding Cationic Liposomes Loaded with Cisplatin Efficiently Suppress the Local Growth and Liver Metastasis of Tumor Cells in Vivo 1, 2002.

[83] R. Raavé, T.H. van Kuppevelt, W.F. Daamen, Chemotherapeutic drug delivery by tumoral extracellular matrix targeting, Journal of Controlled Release. (2018). https://doi.org/10.1016/j.jconrel.2018.01.029.

[84] M.M. Martino, P.S. Briquez, E. Güç, F. Tortelli, W.W. Kilarski, S. Metzger, J.J. Rice, G.A. Kuhn, R. Müller, M.A. Swartz, J.A. Hubbell, Growth factors engineered for super-affinity to the extracellular matrix enhance tissue healing., Science (New York, N.Y.). 343 (2014) 885–8. https://doi.org/10.1126/science.1247663.

[85] J. Ishihara, K. Fukunaga, A. Ishihara, H.M. Larsson, L. Potin, P. Hosseinchi, G. Galliverti, M.A. Swartz, J.A. Hubbell, Matrix-binding checkpoint immunotherapies enhance antitumor efficacy and reduce adverse events., Science Translational Medicine. 9 (2017) eaan0401. https://doi.org/10.1126/scitranslmed.aan0401.

[86] P. Lingasamy, A. Tobi, M. Haugas, H. Hunt, P. Paiste, T. Asser, T. Rätsep, V.R. Kotamraju, R. Bjerkvig, T. Teesalu, Bi-specific tenascin-C and fibronectin targeted peptide for solid tumor delivery, Biomaterials. 219 (2019) 119373. https://doi.org/10.1016/J.BIOMATERIALS.2019.119373.

[87] S. Gallucci, M. Lolkema, P. Matzinger, Natural adjuvants: Endogenous activators of dendritic cells, Nat Med. 5 (1999) 1249–1255. https://doi.org/10.1038/15200.

[88] S.N. Mueller, B.T. Rouse, Immune responses to viruses, Clinical Immunology. (2008) 421–431. https://doi.org/10.1016/B978-0-323-04404-2.10027-2.

[89] B.T. Rouse, S. Sehrawat, Immunity and immunopathology to viruses: what decides the outcome?, Nat Rev Immunol. 10 (2010) 514–526. https://doi.org/10.1038/nri2802.

[90] D.G. Brooks, M.J. Trifilo, K.H. Edelmann, L. Teyton, D.B. McGavern, M.B.A. Oldstone, Interleukin-10 determines viral clearance or persistence in vivo, Nat Med. 12 (2006) 1301–1309. https://doi.org/10.1038/nm1492.

[91] C.S. Adamson, K. Chibale, R.J.M. Goss, M. Jaspars, D.J. Newman, R.A. Dorrington, Antiviral drug discovery: preparing for the next pandemic, Chem. Soc. Rev. 50 (2021) 3647–3655. https://doi.org/10.1039/D0CS01118E.

[92] D.J. Newman, G.M. Cragg, Natural Products as Sources of New Drugs over the Nearly Four Decades from 01/1981 to 09/2019, J. Nat. Prod. 83 (2020) 770–803. https://doi.org/10.1021/acs.jnatprod.9b01285.

[93] E. De Clercq, G. Li, Approved Antiviral Drugs over the Past 50 Years, Clinical Microbiology Reviews. 29 (2016) 695–747. https://doi.org/10.1128/CMR.00102-15.

[94] M.A. Strassburg, The global eradication of smallpox, Am J Infect Control. 10 (1982) 53–59. https://doi.org/10.1016/0196-6553(82)90003-7.

[95] T. Ng'uni, C. Chasara, Z.M. Ndhlovu, Major Scientific Hurdles in HIV Vaccine Development: Historical Perspective and Future Directions, Frontiers in Immunology. 11 (2020) 2761. https://doi.org/10.3389/fimmu.2020.590780.

[96] K. Tao, P.L. Tzou, J. Nouhin, R.K. Gupta, T. de Oliveira, S.L. Kosakovsky Pond, D. Fera, R.W. Shafer, The biological and clinical significance of emerging SARS-CoV-2 variants, Nat Rev Genet. (2021) 1–17. https://doi.org/10.1038/s41576-021-00408-x.

[97] D.S. Wilson, S. Hirosue, M.M. Raczy, L. Bonilla-Ramirez, L. Jeanbart, R. Wang, M. Kwissa, J.-F. Franetich, M.A.S. Broggi, G. Diaceri, X. Quaglia-Thermes, D. Mazier, M.A. Swartz, J.A. Hubbell, Antigens reversibly conjugated to a polymeric glyco-adjuvant induce protective humoral and cellular immunity, Nature Materials. 18 (2019) 175–185. https://doi.org/10.1038/s41563-018-0256-5.

[98] J. Kopecek, P. Kopecková, HPMA copolymers: origins, early developments, present, and future, Adv Drug Deliv Rev. 62 (2010) 122–149. https://doi.org/10.1016/j.addr.2009.10.004.

[99] S. Bhagchandani, J.A. Johnson, D.J. Irvine, Evolution of Toll-like receptor 7/8 agonist therapeutics and their delivery approaches: From antiviral formulations to vaccine adjuvants, Advanced Drug Delivery Reviews. 175 (2021) 113803. https://doi.org/10.1016/j.addr.2021.05.013.

[100] Kenneth Murphy, Janeway's Immunobiology, 9th edition, Garland Science, New York, NY, 2016.

[101] M. Dominguez-Villar, A.-S. Gautron, M. de Marcken, M.J. Keller, D.A. Hafler, TLR7 induces anergy in human CD4(+) T cells, Nat Immunol. 16 (2015) 118–128. https://doi.org/10.1038/ni.3036.

[102] G. Peng, Z. Guo, Y. Kiniwa, K.S. Voo, W. Peng, T. Fu, D.Y. Wang, Y. Li, H.Y. Wang, R.-F. Wang, Toll-like receptor 8-mediated reversal of CD4+ regulatory T cell function, Science. 309 (2005) 1380–1384. https://doi.org/10.1126/science.1113401.

[103] F. Heil, H. Hemmi, H. Hochrein, F. Ampenberger, C. Kirschning, S. Akira, G. Lipford, H. Wagner, S. Bauer, Species-specific recognition of single-stranded RNA via toll-like receptor 7 and 8, Science. 303 (2004) 1526–1529. https://doi.org/10.1126/science.1093620.

[104] J.M. Lund, L. Alexopoulou, A. Sato, M. Karow, N.C. Adams, N.W. Gale, A. Iwasaki, R.A. Flavell, Recognition of single-stranded RNA viruses by Toll-like receptor 7, Proc Natl Acad Sci U S A. 101 (2004) 5598–5603. https://doi.org/10.1073/pnas.0400937101.

[105] S. Akira, S. Uematsu, O. Takeuchi, Pathogen recognition and innate immunity, Cell. 124 (2006) 783–801. https://doi.org/10.1016/j.cell.2006.02.015.

[106] F. Ma, J. Zhang, J. Zhang, C. Zhang, The TLR7 agonists imiquimod and gardiquimod improve DC-based immunotherapy for melanoma in mice, Cell Mol Immunol. 7 (2010) 381–388. https://doi.org/10.1038/cmi.2010.30.

[107] T. Kaisho, S. Akira, Regulation of dendritic cell function through Toll-like receptors, Curr Mol Med. 3 (2003) 373–385. https://doi.org/10.2174/1566524033479726.

[108] A. Sato, A. Iwasaki, Induction of antiviral immunity requires Toll-like receptor signaling in both stromal and dendritic cell compartments, Proc Natl Acad Sci U S A. 101 (2004) 16274–16279. https://doi.org/10.1073/pnas.0406268101.

[109] E.L.J.M. Smits, P. Ponsaerts, Z.N. Berneman, V.F.I. Van Tendeloo, The use of TLR7 and TLR8 ligands for the enhancement of cancer immunotherapy, Oncologist. 13 (2008) 859–875. https://doi.org/10.1634/theoncologist.2008-0097.

[110] V. Caisová, A. Vieru, Z. Kumžáková, S. Glaserová, H. Husníková, N. Vácová, G. Krejčová, L. Paďouková, I. Jochmanová, K.I. Wolf, J. Chmelař, J. Kopecký, J. Ženka, Innate immunity based cancer immunotherapy: B16-F10 murine melanoma model, BMC Cancer. 16 (2016) 940. https://doi.org/10.1186/s12885-016-2982-x.

[111] L. Martinez-Pomares, The mannose receptor, Journal of Leukocyte Biology. 92 (2012) 1177–1186. https://doi.org/10.1189/jlb.0512231.

[112] U. Gazi, L. Martinez-Pomares, Influence of the mannose receptor in host immune responses, Immunobiology. 214 (2009) 554–561. https://doi.org/10.1016/j.imbio.2008.11.004.

[113] L.-Z. He, A. Crocker, J. Lee, J. Mendoza-Ramirez, X.-T. Wang, L.A. Vitale, T. O'Neill, C. Petromilli, H.-F. Zhang, J. Lopez, D. Rohrer, T. Keler, R. Clynes, Antigenic targeting of the human mannose receptor induces tumor immunity, J Immunol. 178 (2007) 6259–6267. https://doi.org/10.4049/jimmunol.178.10.6259.

[114] K.-C. Sheng, M. Kalkanidis, D.S. Pouniotis, S. Esparon, C.K. Tang, V. Apostolopoulos, G.A. Pietersz, Delivery of antigen using a novel mannosylated dendrimer potentiates immunogenicity in vitro and in vivo, Eur J Immunol. 38 (2008) 424–436. https://doi.org/10.1002/eji.200737578.

[115] C. Macri, C. Dumont, A.P. Johnston, J.D. Mintern, Targeting dendritic cells: a promising strategy to improve vaccine effectiveness, Clin Transl Immunology. 5 (2016) e66. https://doi.org/10.1038/cti.2016.6.

[116] S. Burgdorf, A. Kautz, V. Böhnert, P.A. Knolle, C. Kurts, Distinct pathways of antigen uptake and intracellular routing in CD4 and CD8 T cell activation, Science. 316 (2007) 612–616. https://doi.org/10.1126/science.1137971.

[117] A.D. Pardee, H. Yano, A.M. Weinstein, A.A.K. Ponce, A.D. Ethridge, D.P. Normolle, L. Vujanovic, G.J. Mizejewski, S.C. Watkins, L.H. Butterfield, Route of antigen delivery impacts the immunostimulatory activity of dendritic cell-based vaccines for hepatocellular

carcinoma, J Immunother Cancer. 3 (2015) 32. https://doi.org/10.1186/s40425-015-0077-x.

[118] T. Tsuji, J. Matsuzaki, M.P. Kelly, V. Ramakrishna, L. Vitale, L.-Z. He, T. Keler, K. Odunsi, L.J. Old, G. Ritter, S. Gnjatic, Antibody-targeted NY-ESO-1 to mannose receptor or DEC-205 in vitro elicits dual human CD8+ and CD4+ T cell responses with broad antigen specificity, J Immunol. 186 (2011) 1218–1227. https://doi.org/10.4049/jimmunol.1000808.

[119] E. Buchbinder, F.S. Hodi, Cytotoxic T lymphocyte antigen-4 and immune checkpoint blockade, The Journal of Clinical Investigation. 125 (2015) 3377–3383. https://doi.org/10.1172/JCI80012.

[120] D.S. Chen, I. Mellman, Elements of cancer immunity and the cancer–immune set point, Nature. 541 (2017) 321–330. https://doi.org/10.1038/nature21349.

[121] T.F. Gajewski, H. Schreiber, Y.-X. Fu, Innate and adaptive immune cells in the tumor microenvironment, Nat Immunol. 14 (2013) 1014–1022. https://doi.org/10.1038/ni.2703.

[122] E. Sato, S.H. Olson, J. Ahn, B. Bundy, H. Nishikawa, F. Qian, A.A. Jungbluth, D. Frosina, S. Gnjatic, C. Ambrosone, J. Kepner, T. Odunsi, G. Ritter, S. Lele, Y.-T. Chen, H. Ohtani, L.J. Old, K. Odunsi, Intraepithelial CD8+ tumor-infiltrating lymphocytes and a high CD8+/regulatory T cell ratio are associated with favorable prognosis in ovarian cancer., Proceedings of the National Academy of Sciences of the United States of America. 102 (2005) 18538–43. https://doi.org/10.1073/pnas.0509182102.

[123] C. Yee, J.A. Thompson, D. Byrd, S.R. Riddell, P. Roche, E. Celis, P.D. Greenberg, Adoptive T cell therapy using antigen-specific CD8+ T cell clones for the treatment of patients with metastatic melanoma: in vivo persistence, migration, and antitumor effect of transferred T cells., Proceedings of the National Academy of Sciences of the United States of America. 99 (2002) 16168–73. https://doi.org/10.1073/pnas.242600099.

[124] S. van Duikeren, M.F. Fransen, A. Redeker, B. Wieles, G. Platenburg, W.-J. Krebber, F. Ossendorp, C.J.M. Melief, R. Arens, Vaccine-induced effector-memory CD8+ T cell responses predict therapeutic efficacy against tumors., Journal of Immunology (Baltimore, Md. : 1950). 189 (2012) 3397–403. https://doi.org/10.4049/jimmunol.1201540.

[125] M. Saxena, S.H. van der Burg, C.J.M. Melief, N. Bhardwaj, Therapeutic cancer vaccines, Nat Rev Cancer. 21 (2021) 360–378. https://doi.org/10.1038/s41568-021-00346-0.

[126] V. Appay, D.C. Douek, D.A. Price, CD8+ T cell efficacy in vaccination and disease, Nature Medicine. 14 (2008) 623–628. https://doi.org/10.1038/nm.f.1774.

[127] R.A. Koup, D.C. Douek, Vaccine design for CD8 T lymphocyte responses., Cold Spring Harbor Perspectives in Medicine. 1 (2011) a007252. https://doi.org/10.1101/cshperspect.a007252.

[128] J. Banchereau, K. Palucka, Immunotherapy: Cancer vaccines on the move, Nature Reviews Clinical Oncology. 15 (2017) 9–10. https://doi.org/10.1038/nrclinonc.2017.149.

[129] A.M. Kerrigan, G.D. Brown, C-type lectins and phagocytosis, Immunobiology. 214 (2009) 562–575. https://doi.org/10.1016/J.IMBIO.2008.11.003.

[130] M.M. Weck, F. Grünebach, D. Werth, C. Sinzger, A. Bringmann, P. Brossart, W. Brugger, TLR ligands differentially affect uptake and presentation of cellular antigens., Blood. 109 (2007) 3890–4. https://doi.org/10.1182/blood-2006-04-015719.

[131] J.Z. Oh, J.S. Kurche, M.A. Burchill, R.M. Kedl, TLR7 enables cross-presentation by multiple dendritic cell subsets through a type I IFN-dependent pathway, Blood. 118 (2011) 3028–3038. https://doi.org/10.1182/BLOOD-2011-04-348839.

[132] L. Borsi, B. Carnemolla, P. Castellani, C. Rosellini, D. Vecchio, G. Allemanni, S.E. Chang, J. Taylor-Papadimitriou, H. Pande, L. Zardi, Monoclonal antibodies in the analysis of fibronectin isoforms generated by alternative splicing of mRNA precursors in normal and transformed human cells., The Journal of Cell Biology. 104 (1987) 595–600. https://doi.org/10.1083/JCB.104.3.595.

[133] F. Oyama, S. Hirohashi, Y. Shimosato, K. Titani, K. Sekiguchi, Deregulation of alternative splicing of fibronectin pre-mRNA in malignant human liver tumors, Journal of Biological Chemistry. 264 (1989) 10331–10334.

[134] Y. Matsumura, H. Maeda, A new concept for macromolecular therapeutics in cancer chemotherapy: mechanism of tumoritropic accumulation of proteins and the antitumor agent smancs., Cancer Research. 46 (1986) 6387–92.

[135] R.A. Romijn, E. Westein, B. Bouma, M.E. Schiphorst, J.J. Sixma, P.J. Lenting, E.G. Huizinga, Mapping the Collagen-binding Site in the von Willebrand Factor-A3 Domain, Journal of Biological Chemistry. 278 (2003) 15035–15039. https://doi.org/10.1074/jbc.M208977200.

[136] A.F. Riddell, K. Gomez, C.M. Millar, G. Mellars, S. Gill, S.A. Brown, M. Sutherland, M.A. Laffan, T.A.J. McKinnon, Characterization of W1745C and S1783A: 2 novel mutations causing defective collagen binding in the A3 domain of von Willebrand factor, Blood. 114 (2009) 3489–3496. https://doi.org/10.1182/blood-2008-10-184317.

[137] E.A. Watkins, J.T. Antane, J.L. Roberts, K.M. Lorentz, S. Zuerndorfer, A.C. Dunaif, L.J. Bailey, A.C. Tremain, M. Nguyen, R.C. De Loera, R.P. Wallace, R.K. Weathered, S. Kontos, J.A. Hubbell, Persistent antigen exposure via the eryptotic pathway drives terminal T cell dysfunction, Science Immunology. 6 (2021) eabe1801. https://doi.org/10.1126/sciimmunol.abe1801.

[138] M.G. Lechner, S.S. Karimi, K. Barry-Holson, T.E. Angell, K.A. Murphy, C.H. Church, J.R. Ohlfest, P. Hu, A.L. Epstein, Immunogenicity of murine solid tumor models as a defining feature of in vivo behavior and response to immunotherapy, J Immunother. 36 (2013) 477–489. https://doi.org/10.1097/01.cji.0000436722.46675.4a.

[139] S. Mariathasan, S.J. Turley, D. Nickles, A. Castiglioni, K. Yuen, Y. Wang, E.E. Kadel III, H. Koeppen, J.L. Astarita, R. Cubas, S. Jhunjhunwala, R. Banchereau, Y. Yang, Y. Guan, C. Chalouni, J. Ziai, Y. Şenbabaoğlu, S. Santoro, D. Sheinson, J. Hung, J.M. Giltnane, A.A. Pierce, K. Mesh, S. Lianoglou, J. Riegler, R.A.D. Carano, P. Eriksson, M. Höglund, L. Somarriba, D.L. Halligan, M.S. van der Heijden, Y. Loriot, J.E. Rosenberg, L. Fong, I. Mellman, D.S. Chen, M. Green, C. Derleth, G.D. Fine, P.S. Hegde, R. Bourgon, T. Powles, TGFβ attenuates tumour response to PD-L1 blockade by contributing to exclusion of T cells, Nature. 554 (2018) 544–548. https://doi.org/10.1038/nature25501.

[140] A.C. Scott, F. Dündar, P. Zumbo, S.S. Chandran, C.A. Klebanoff, M. Shakiba, P. Trivedi, L. Menocal, H. Appleby, S. Camara, D. Zamarin, T. Walther, A. Snyder, M.R. Femia, E.A. Comen, H.Y. Wen, M.D. Hellmann, N. Anandasabapathy, Y. Liu, N.K. Altorki, P. Lauer, O. Levy, M.S. Glickman, J. Kaye, D. Betel, M. Philip, A. Schietinger, TOX is a critical regulator of tumour-specific T cell differentiation, Nature. 571 (2019) 270–274. https://doi.org/10.1038/s41586-019-1324-y.

[141] O. Khan, J.R. Giles, S. McDonald, S. Manne, S.F. Ngiow, K.P. Patel, M.T. Werner, A.C. Huang, K.A. Alexander, J.E. Wu, J. Attanasio, P. Yan, S.M. George, B. Bengsch, R.P. Staupe, G. Donahue, W. Xu, R.K. Amaravadi, X. Xu, G.C. Karakousis, T.C. Mitchell, L.M. Schuchter, J. Kaye, S.L. Berger, E.J. Wherry, TOX transcriptionally and epigenetically programs CD8+ T cell exhaustion, Nature. 571 (2019) 211–218. https://doi.org/10.1038/s41586-019-1325-x.

[142] S. van Duikeren, M.F. Fransen, A. Redeker, B. Wieles, G. Platenburg, W.-J. Krebber, F. Ossendorp, C.J.M. Melief, R. Arens, Vaccine-induced effector-memory CD8+ T cell responses predict therapeutic efficacy against tumors, Journal of Immunology. 189 (2012) 3397–403. https://doi.org/10.4049/jimmunol.1201540.

[143] E.W. Roberts, M.L. Broz, M. Binnewies, M.B. Headley, A.E. Nelson, D.M. Wolf, T. Kaisho, D. Bogunovic, N. Bhardwaj, M.F. Krummel, Critical Role for CD103(+)/CD141(+) Dendritic Cells Bearing CCR7 for Tumor Antigen Trafficking and Priming of T Cell Immunity in Melanoma, Cancer Cell. 30 (2016) 324–336. https://doi.org/10.1016/j.ccell.2016.06.003.

[144] A.J. Radtke, W. Kastenmüller, D.A. Espinosa, M.Y. Gerner, S.-W. Tse, P. Sinnis, R.N. Germain, F.P. Zavala, I.A. Cockburn, Lymph-Node Resident CD8α+ Dendritic Cells Capture Antigens from Migratory Malaria Sporozoites and Induce CD8+ T Cell Responses, PLoS Pathog. 11 (2015) e1004637. https://doi.org/10.1371/journal.ppat.1004637.

[145] S. Spranger, D. Dai, B. Horton, T.F. Gajewski, Tumor-Residing Batf3 Dendritic Cells Are Required for Effector T Cell Trafficking and Adoptive T Cell Therapy, Cancer Cell. 31 (2017) 711-723.e4. https://doi.org/10.1016/j.ccell.2017.04.003.

[146] J.-M. Williford, J. Ishihara, A. Ishihara, A. Mansurov, P. Hosseinchi, T.M. Marchell, L. Potin, M.A. Swartz, J.A. Hubbell, Recruitment of CD103+ dendritic cells via tumor-

targeted chemokine delivery enhances efficacy of checkpoint inhibitor immunotherapy, Sci. Adv. 5 (2019) eaay1357. https://doi.org/10.1126/sciadv.aay1357.

[147] M. Rapp, M.W.M. Wintergerst, W.G. Kunz, V.K. Vetter, M.M.L. Knott, D. Lisowski, S. Haubner, S. Moder, R. Thaler, S. Eiber, B. Meyer, N. Röhrle, I. Piseddu, S. Grassmann, P. Layritz, B. Kühnemuth, S. Stutte, C. Bourquin, U.H. von Andrian, S. Endres, D. Anz, CCL22 controls immunity by promoting regulatory T cell communication with dendritic cells in lymph nodes, Journal of Experimental Medicine. 216 (2019) 1170–1181. https://doi.org/10.1084/jem.20170277.

[148] J.M. Pitt, M. Vétizou, R. Daillère, M.P. Roberti, T. Yamazaki, B. Routy, P. Lepage, I.G. Boneca, M. Chamaillard, G. Kroemer, L. Zitvogel, Resistance Mechanisms to Immune-Checkpoint Blockade in Cancer: Tumor-Intrinsic and -Extrinsic Factors, Immunity. 44 (2016) 1255–1269. https://doi.org/10.1016/J.IMMUNI.2016.06.001.

[149] P. Sharma, J.P. Allison, The future of immune checkpoint therapy, Science. 348 (2015) 56–61. https://doi.org/10.1126/SCIENCE.AAA8172.

[150] K. Frey, C. Schliemann, K. Schwager, R. Giavazzi, M. Johannsen, D. Neri, The Immunocytokine F8-IL2 Improves the Therapeutic Performance of Sunitinib in a Mouse Model of Renal Cell Carcinoma, Journal of Urology. 184 (2010) 2540–2548. https://doi.org/10.1016/j.juro.2010.07.030.

[151] T. List, G. Casi, D. Neri, A Chemically Defined Trifunctional Antibody–Cytokine–Drug Conjugate with Potent Antitumor Activity, Molecular Cancer Therapeutics. 13 (2014) 2641–2652. https://doi.org/10.1158/1535-7163.MCT-14-0599.

[152] S. Wieckowski, T. Hemmerle, S.S. Prince, B.D. Schlienger, S. Hillinger, D. Neri, A. Zippelius, Therapeutic efficacy of the F8-IL2 immunocytokine in a metastatic mouse model of lung adenocarcinoma, Lung Cancer. 88 (2015) 9–15. https://doi.org/10.1016/J.LUNGCAN.2015.01.019.

[153] T. Hemmerle, D. Neri, The Dose-Dependent Tumor Targeting of Antibody-IFN Fusion Proteins Reveals an Unexpected Receptor-Trapping Mechanism In Vivo, Cancer Immunology Research. 2 (2014) 559–567. https://doi.org/10.1158/2326-6066.CIR-13-0182.

[154] G.J.L. Bernardes, G. Casi, S. Trüssel, I. Hartmann, K. Schwager, J. Scheuermann, D. Neri, A Traceless Vascular-Targeting Antibody-Drug Conjugate for Cancer Therapy, Angewandte Chemie International Edition. 51 (2012) 941–944. https://doi.org/10.1002/anie.201106527.

[155] R. Gebleux, S. Wulhfard, G. Casi, D. Neri, Antibody Format and Drug Release Rate Determine the Therapeutic Activity of Noninternalizing Antibody-Drug Conjugates, Molecular Cancer Therapeutics. 14 (2015) 2606–2612. https://doi.org/10.1158/1535-7163.MCT-15-0480.

[156] A. Mansurov, J. Ishihara, P. Hosseinchi, L. Potin, T.M. Marchell, A. Ishihara, J.-M. Williford, A.T. Alpar, M.M. Raczy, L.T. Gray, M.A. Swartz, J.A. Hubbell, Collagen-binding IL-12 enhances tumour inflammation and drives the complete remission of established immunologically cold mouse tumours, Nature Biomedical Engineering. 4 (2020) 531–543. https://doi.org/10.1038/s41551-020-0549-2.

[157] Z.-H. Zhou, C.-D. Ji, H.-L. Xiao, H.-B. Zhao, Y.-H. Cui, X.-W. Bian, Reorganized Collagen in the Tumor Microenvironment of Gastric Cancer and Its Association with Prognosis, Journal of Cancer. 8 (2017) 1466–1476. https://doi.org/10.7150/jca.18466.

[158] P.P. Provenzano, D.R. Inman, K.W. Eliceiri, J.G. Knittel, L. Yan, C.T. Rueden, J.G. White, P.J. Keely, Collagen density promotes mammary tumor initiation and progression, BMC Medicine. 6 (2008) 11. https://doi.org/10.1186/1741-7015-6-11.

[159] S. Ricard-Blum, The Collagen Family, Cold Spring Harb Perspect Biol. 3 (2011) a004978. https://doi.org/10.1101/cshperspect.a004978.

[160] W.R. Jarnagin, D.C. Rockey, V.E. Koteliansky, S.S. Wang, D.M. Bissell, Expression of variant fibronectins in wound healing: cellular source and biological activity of the EIIIA segment in rat hepatic fibrogenesis., Journal of Cell Biology. 127 (1994) 2037–2048. https://doi.org/10.1083/jcb.127.6.2037.

[161] L. Borsi, P. Castellani, G. Allemanni, D. Neri, L. Zardi, Preparation of Phage Antibodies to the ED-A Domain of Human Fibronectin, Experimental Cell Research. 240 (1998) 244–251. https://doi.org/10.1006/EXCR.1998.3946.

[162] J. Patten, K. Wang, Fibronectin in development and wound healing, Advanced Drug Delivery Reviews. 170 (2021) 353–368. https://doi.org/10.1016/j.addr.2020.09.005.

[163] K. Schwager, M. Kaspar, F. Bootz, R. Marcolongo, E. Paresce, D. Neri, E. Trachsel, Preclinical characterization of DEKAVIL (F8-IL10), a novel clinical-stage immunocytokine which inhibits the progression of collagen-induced arthritis, Arthritis Res Ther. 11 (2009) R142. https://doi.org/10.1186/ar2814.

[164] S.T.G. Bruijnen, D.M.S.H. Chandrupatla, L. Giovanonni, D. Neri, D.J. Vugts, M.C. Huisman, O.S. Hoekstra, R.J.P. Musters, A.A. Lammertsma, G.A.M.S. van Dongen, G. Jansen, C.F.M. Molthoff, C.J. van der Laken, F8-IL10: A New Potential Antirheumatic Drug Evaluated by a PET-Guided Translational Approach, Mol Pharm. 16 (2019) 273–281. https://doi.org/10.1021/acs.molpharmaceut.8b00982.

[165] K. Schwager, F. Bootz, P. Imesch, M. Kaspar, E. Trachsel, D. Neri, The antibody-mediated targeted delivery of interleukin-10 inhibits endometriosis in a syngeneic mouse model, Hum Reprod. 26 (2011) 2344–2352. https://doi.org/10.1093/humrep/der195.

[166] T. Hemmerle, S. Zgraggen, M. Matasci, C. Halin, M. Detmar, D. Neri, Antibody-mediated delivery of interleukin 4 to the neo-vasculature reduces chronic skin inflammation, J Dermatol Sci. 76 (2014) 96–103. https://doi.org/10.1016/j.jdermsci.2014.07.012.

[167] M. Fiechter, K. Frey, T. Fugmann, P.A. Kaufmann, D. Neri, Comparative in vivo analysis of the atherosclerotic plaque targeting properties of eight human monoclonal antibodies, Atherosclerosis. 214 (2011) 325–330. https://doi.org/10.1016/j.atherosclerosis.2010.11.027.

[168] F. Bootz, A.S. Schmid, D. Neri, Alternatively Spliced EDA Domain of Fibronectin Is a Target for Pharmacodelivery Applications in Inflammatory Bowel Disease, Inflamm Bowel Dis. 21 (2015) 1908–1917. https://doi.org/10.1097/MIB.0000000000000440.

[169] C. Tacconi, S. Schwager, N. Cousin, D. Bajic, M. Sesartic, J.P. Sundberg, D. Neri, M. Detmar, Antibody-Mediated Delivery of VEGFC Ameliorates Experimental Chronic Colitis, ACS Pharmacol Transl Sci. 2 (2019) 342–352. https://doi.org/10.1021/acsptsci.9b00037.

[170] Z. Julier, M.M. Martino, A. De Titta, L. Jeanbart, J.A. Hubbell, The TLR4 agonist fibronectin extra domain a is cryptic, Exposed by elastase-2; Use in a fibrin matrix cancer vaccine, Scientific Reports. 5 (2015) 1–10. https://doi.org/10.1038/srep08569.

[171] S. Hirosue, I.C. Kourtis, A.J. van der Vlies, J.A. Hubbell, M.A. Swartz, Antigen delivery to dendritic cells by poly(propylene sulfide) nanoparticles with disulfide conjugated peptides: Cross-presentation and T cell activation, Vaccine. 28 (2010) 7897–7906. https://doi.org/10.1016/J.VACCINE.2010.09.077.

[172] J. Berenguer, P. Ryan, J. Rodríguez-Baño, I. Jarrín, J. Carratalà, J. Pachón, M. Yllescas, J.R. Arriba, Characteristics and predictors of death among 4035 consecutively hospitalized patients with COVID-19 in Spain, Clin Microbiol Infect. 26 (2020) 1525–1536. https://doi.org/10.1016/j.cmi.2020.07.024.

[173] S. Chilimuri, H. Sun, A. Alemam, N. Mantri, E. Shehi, J. Tejada, A. Yugay, S.K. Nayudu, Predictors of Mortality in Adults Admitted with COVID-19: Retrospective Cohort Study from New York City, West J Emerg Med. 21 (2020) 779–784. https://doi.org/10.5811/westjem.2020.6.47919.

[174] M. Gottlieb, S. Sansom, C. Frankenberger, E. Ward, B. Hota, Clinical Course and Factors Associated With Hospitalization and Critical Illness Among COVID-19 Patients in Chicago, Illinois, Acad Emerg Med. 27 (2020) 963–973. https://doi.org/10.1111/acem.14104.

[175] WHO Coronavirus Disease (COVID-19) Dashboard, (n.d.). https://covid19.who.int (accessed September 18, 2021).

[176] P. Zhou, X.-L. Yang, X.-G. Wang, B. Hu, L. Zhang, W. Zhang, H.-R. Si, Y. Zhu, B. Li, C.-L. Huang, H.-D. Chen, J. Chen, Y. Luo, H. Guo, R.-D. Jiang, M.-Q. Liu, Y. Chen, X.-R. Shen, X. Wang, X.-S. Zheng, K. Zhao, Q.-J. Chen, F. Deng, L.-L. Liu, B. Yan, F.-X. Zhan, Y.-Y. Wang, G.-F. Xiao, Z.-L. Shi, A pneumonia outbreak associated with a new coronavirus of probable bat origin, Nature. 579 (2020) 270–273. https://doi.org/10.1038/s41586-020-2012-7.

[177] M. Hoffmann, H. Kleine-Weber, S. Schroeder, N. Krüger, T. Herrler, S. Erichsen, T.S. Schiergens, G. Herrler, N.-H. Wu, A. Nitsche, M.A. Müller, C. Drosten, S. Pöhlmann, SARS-CoV-2 Cell Entry Depends on ACE2 and TMPRSS2 and Is Blocked by a Clinically Proven Protease Inhibitor, Cell. 181 (2020) 271-280.e8. https://doi.org/10.1016/j.cell.2020.02.052.

[178] R. Yan, Y. Zhang, Y. Li, L. Xia, Y. Guo, Q. Zhou, Structural basis for the recognition of SARS-CoV-2 by full-length human ACE2, Science. 367 (2020) 1444–1448. https://doi.org/10.1126/science.abb2762.

[179] J. Shang, G. Ye, K. Shi, Y. Wan, C. Luo, H. Aihara, Q. Geng, A. Auerbach, F. Li, Structural basis of receptor recognition by SARS-CoV-2, Nature. 581 (2020) 221–224. https://doi.org/10.1038/s41586-020-2179-y.

[180] J. Lan, J. Ge, J. Yu, S. Shan, H. Zhou, S. Fan, Q. Zhang, X. Shi, Q. Wang, L. Zhang, X. Wang, Structure of the SARS-CoV-2 spike receptor-binding domain bound to the ACE2 receptor, Nature. 581 (2020) 215–220. https://doi.org/10.1038/s41586-020-2180-5.

[181] W. Tai, L. He, X. Zhang, J. Pu, D. Voronin, S. Jiang, Y. Zhou, L. Du, Characterization of the receptor-binding domain (RBD) of 2019 novel coronavirus: implication for development of RBD protein as a viral attachment inhibitor and vaccine, Cellular & Molecular Immunology. 17 (2020) 613–620. https://doi.org/10.1038/s41423-020-0400-4.

[182] D. Wrapp, N. Wang, K.S. Corbett, J.A. Goldsmith, C.-L. Hsieh, O. Abiona, B.S. Graham, J.S. McLellan, Cryo-EM structure of the 2019-nCoV spike in the prefusion conformation, Science. 367 (2020) 1260–1263. https://doi.org/10.1126/science.abb2507.

[183] L. Liu, P. Wang, M.S. Nair, J. Yu, M. Rapp, Q. Wang, Y. Luo, J.F.-W. Chan, V. Sahi, A. Figueroa, X.V. Guo, G. Cerutti, J. Bimela, J. Gorman, T. Zhou, Z. Chen, K.-Y. Yuen, P.D. Kwong, J.G. Sodroski, M.T. Yin, Z. Sheng, Y. Huang, L. Shapiro, D.D. Ho, Potent neutralizing antibodies against multiple epitopes on SARS-CoV-2 spike, Nature. 584 (2020) 450–456. https://doi.org/10.1038/s41586-020-2571-7.

[184] L. Dai, G.F. Gao, Viral targets for vaccines against COVID-19, Nature Reviews Immunology. 21 (2021) 73–82. https://doi.org/10.1038/s41577-020-00480-0.

[185] Y. Dong, T. Dai, Y. Wei, L. Zhang, M. Zheng, F. Zhou, A systematic review of SARS-CoV-2 vaccine candidates, Signal Transduction and Targeted Therapy. 5 (2020) 1–14. https://doi.org/10.1038/s41392-020-00352-y.

[186] B.S. Graham, Rapid COVID-19 vaccine development, Science. 368 (2020) 945–946. https://doi.org/10.1126/science.abb8923.

[187] F. Krammer, SARS-CoV-2 vaccines in development, Nature. 586 (2020) 516–527. https://doi.org/10.1038/s41586-020-2798-3.

[188] London School of Hygiene & Tropical Medicine. COVID-19 Vaccine Development Pipeline, (2020).

[189] P. Tebas, S. Yang, J.D. Boyer, E.L. Reuschel, A. Patel, A. Christensen-Quick, V.M. Andrade, M.P. Morrow, K. Kraynyak, J. Agnes, M. Purwar, A. Sylvester, J. Pawlicki, E. Gillespie, I. Maricic, F.I. Zaidi, K.Y. Kim, Y. Dia, D. Frase, P. Pezzoli, K. Schultheis, T.R.F. Smith, S.J. Ramos, T. McMullan, K. Buttigieg, M.W. Carroll, J. Ervin, M.C. Diehl, E. Blackwood, M.P. Mammen, J. Lee, M.J. Dallas, A.S. Brown, J.E. Shea, J.J. Kim, D.B. Weiner, K.E. Broderick, L.M. Humeau, Safety and immunogenicity of INO-4800 DNA vaccine against SARS-CoV-2: A preliminary report of an open-label, Phase 1 clinical trial, EClinicalMedicine. 31 (2021) 100689. https://doi.org/10.1016/j.eclinm.2020.100689.

[190] M. Voysey, S.A.C. Clemens, S.A. Madhi, L.Y. Weckx, P.M. Folegatti, P.K. Aley, B. Angus, V.L. Baillie, S.L. Barnabas, Q.E. Bhorat, S. Bibi, C. Briner, P. Cicconi, A.M. Collins, R. Colin-Jones, C.L. Cutland, T.C. Darton, K. Dheda, C.J.A. Duncan, K.R.W. Emary, K.J. Ewer, L. Fairlie, S.N. Faust, S. Feng, D.M. Ferreira, A. Finn, A.L. Goodman, C.M. Green, C.A. Green, P.T. Heath, C. Hill, H. Hill, I. Hirsch, S.H.C. Hodgson, A. Izu, S. Jackson, D. Jenkin, C.C.D. Joe, S. Kerridge, A. Koen, G. Kwatra, R. Lazarus, A.M. Lawrie, A. Lelliott, V. Libri, P.J. Lillie, R. Mallory, A.V.A. Mendes, E.P. Milan, A.M. Minassian, A. McGregor, H. Morrison, Y.F. Mujadidi, A. Nana, P.J. O'Reilly, S.D. Padayachee, A. Pittella, E. Plested, K.M. Pollock, M.N. Ramasamy, S. Rhead, A.V. Schwarzbold, N. Singh, A. Smith, R. Song, M.D. Snape, E. Sprinz, R.K. Sutherland, R. Tarrant, E.C. Thomson, M.E. Török, M. Toshner, D.P.J. Turner, J. Vekemans, T.L. Villafana, M.E.E. Watson, C.J. Williams, A.D. Douglas, A.V.S. Hill, T. Lambe, S.C. Gilbert, A.J. Pollard, Oxford COVID Vaccine Trial Group, Safety and efficacy of the ChAdOx1 nCoV-19 vaccine (AZD1222) against SARS-CoV-2: an interim analysis of four randomised controlled trials in Brazil, South Africa, and the UK, Lancet. 397 (2021) 99–111. https://doi.org/10.1016/S0140-6736(20)32661-1.

[191] J. Sadoff, M. Le Gars, G. Shukarev, D. Heerwegh, C. Truyers, A.M. de Groot, J. Stoop, S. Tete, W. Van Damme, I. Leroux-Roels, P.-J. Berghmans, M. Kimmel, P. Van Damme, J. de Hoon, W. Smith, K.E. Stephenson, S.C. De Rosa, K.W. Cohen, M.J. McElrath, E. Cormier, G. Scheper, D.H. Barouch, J. Hendriks, F. Struyf, M. Douoguih, J. Van Hoof, H. Schuitemaker, Interim Results of a Phase 1–2a Trial of Ad26.COV2.S Covid-19 Vaccine, N Engl J Med. (2021) NEJMoa2034201. https://doi.org/10.1056/NEJMoa2034201.

[192] Y. Zhang, G. Zeng, H. Pan, C. Li, Y. Hu, K. Chu, W. Han, Z. Chen, R. Tang, W. Yin, X. Chen, Y. Hu, X. Liu, C. Jiang, J. Li, M. Yang, Y. Song, X. Wang, Q. Gao, F. Zhu, Safety, tolerability, and immunogenicity of an inactivated SARS-CoV-2 vaccine in healthy adults aged 18–59 years: a randomised, double-blind, placebo-controlled, phase 1/2 clinical trial, The Lancet Infectious Diseases. 21 (2021) 181–192. https://doi.org/10.1016/S1473-3099(20)30843-4.

[193] P. Richmond, L. Hatchuel, M. Dong, B. Ma, B. Hu, I. Smolenov, P. Li, P. Liang, H.H. Han, J. Liang, R. Clemens, Safety and immunogenicity of S-Trimer (SCB-2019), a protein subunit vaccine candidate for COVID-19 in healthy adults: a phase 1, randomised, double-blind, placebo-controlled trial, The Lancet. 397 (2021) 682–694. https://doi.org/10.1016/S0140-6736(21)00241-5.

[194] C. Keech, G. Albert, I. Cho, A. Robertson, P. Reed, S. Neal, J.S. Plested, M. Zhu, S. Cloney-Clark, H. Zhou, G. Smith, N. Patel, M.B. Frieman, R.E. Haupt, J. Logue, M. McGrath, S. Weston, P.A. Piedra, C. Desai, K. Callahan, M. Lewis, P. Price-Abbott, N. Formica, V. Shinde, L. Fries, J.D. Lickliter, P. Griffin, B. Wilkinson, G.M. Glenn, Phase 1–2 Trial of a SARS-CoV-2 Recombinant Spike Protein Nanoparticle Vaccine, N Engl J Med. 383 (2020) 2320–2332. https://doi.org/10.1056/NEJMoa2026920.

[195] Johnson & Johnson Initiates Pivotal Global Phase 3 Clinical Trial of Janssen's COVID-19 Vaccine Candidate | Johnson & Johnson, Content Lab U.S. (n.d.). https://www.jnj.com/johnson-johnson-initiates-pivotal-global-phase-3-clinical-trial-of-janssens-covid-19-vaccine-candidate (accessed March 9, 2021).

[196] Office of the Commissioner, FDA Approves First COVID-19 Vaccine, FDA. (2021). https://www.fda.gov/news-events/press-announcements/fda-approves-first-covid-19-vaccine (accessed September 18, 2021).

[197] Sanofi: Press Releases, Friday, December 11, 2020, Https://Www.Sanofi.Com/En/Media-Room/Press-Releases/2020/2020-12-11-07-00-00. (2020). https://www.sanofi.com/media-room/press-releases/2020/2020-12-11 07-00-00 2143517 (accessed March 1, 2021).

[198] Merck out of COVID-19 vaccine race after "disappointing" trial results, (2021). https://www.businessinsider.com/merck-covid-vaccines-drop-out-disappointing-trial-results-2021-1 (accessed March 1, 2021).

[199] G.A. Poland, I.G. Ovsyannikova, R.B. Kennedy, SARS-CoV-2 immunity: review and applications to phase 3 vaccine candidates, The Lancet. 396 (2020) 1595–1606. https://doi.org/10.1016/S0140-6736(20)32137-1.

[200] L. Corey, J.R. Mascola, A.S. Fauci, F.S. Collins, A strategic approach to COVID-19 vaccine R&D, Science. 368 (2020) 948–950. https://doi.org/10.1126/science.abc5312.

[201] H.F. Sewell, R.M. Agius, M. Stewart, D. Kendrick, Cellular immune responses to covid-19, BMJ. 370 (2020) m3018. https://doi.org/10.1136/bmj.m3018.

[202] K. Sauer, T. Harris, An Effective COVID-19 Vaccine Needs to Engage T Cells, Front Immunol. 11 (2020) 581807. https://doi.org/10.3389/fimmu.2020.581807.

[203] A.E. Oja, A. Saris, C.A. Ghandour, N.A.M. Kragten, B.M. Hogema, E.J. Nossent, L.M.A. Heunks, S. Cuvalay, E. Slot, F. Linty, F.H. Swaneveld, H. Vrielink, G. Vidarsson, T. Rispens, E. van der Schoot, R.A.W. van Lier, A.T. Brinke, P. Hombrink, Divergent SARS-CoV-2-specific T- and B-cell responses in severe but not mild COVID-19 patients, European Journal of Immunology. 50 (2020) 1998–2012. https://doi.org/10.1002/eji.202048908.

[204] T. Sekine, A. Perez-Potti, O. Rivera-Ballesteros, K. Strålin, J.-B. Gorin, A. Olsson, S. Llewellyn-Lacey, H. Kamal, G. Bogdanovic, S. Muschiol, D.J. Wullimann, T. Kammann, J. Emgård, T. Parrot, E. Folkesson, M. Akber, L. Berglin, H. Bergsten, S. Brighenti, D. Brownlie, M. Butrym, B. Chambers, P. Chen, M.C. Jeannin, J. Grip, A.C. Gomez, L.

Dillner, I.D. Lozano, M. Dzidic, M.F. Tullberg, A. Färnert, H. Glans, A. Haroun-Izquierdo, E. Henriksson, L. Hertwig, S. Kalsum, E. Kokkinou, E. Kvedaraite, M. Loreti, M. Lourda, K. Maleki, K.-J. Malmberg, N. Marquardt, C. Maucourant, J. Michaelsson, J. Mjösberg, K. Moll, J. Muva, J. Mårtensson, P. Nauclér, A. Norrby-Teglund, L.P. Medina, B. Persson, L. Radler, E. Ringqvist, J.T. Sandberg, E. Sohlberg, T. Soini, M. Svensson, J. Tynell, R. Varnaite, A.V. Kries, C. Unge, O. Rooyackers, L.I. Eriksson, J.-I. Henter, A. Sönnerborg, T. Allander, J. Albert, M. Nielsen, J. Klingström, S. Gredmark-Russ, N.K. Björkström, J.K. Sandberg, D.A. Price, H.-G. Ljunggren, S. Aleman, M. Buggert, Robust T Cell Immunity in Convalescent Individuals with Asymptomatic or Mild COVID-19, Cell. 183 (2020) 158-168.e14. https://doi.org/10.1016/j.cell.2020.08.017.

[205] A. Grifoni, D. Weiskopf, S.I. Ramirez, J. Mateus, J.M. Dan, C.R. Moderbacher, S.A. Rawlings, A. Sutherland, L. Premkumar, R.S. Jadi, D. Marrama, A.M. de Silva, A. Frazier, A.F. Carlin, J.A. Greenbaum, B. Peters, F. Krammer, D.M. Smith, S. Crotty, A. Sette, Targets of T Cell Responses to SARS-CoV-2 Coronavirus in Humans with COVID-19 Disease and Unexposed Individuals, Cell. 181 (2020) 1489-1501.e15. https://doi.org/10.1016/j.cell.2020.05.015.

[206] C.-T. Tseng, E. Sbrana, N. Iwata-Yoshikawa, P.C. Newman, T. Garron, R.L. Atmar, C.J. Peters, R.B. Couch, Immunization with SARS Coronavirus Vaccines Leads to Pulmonary Immunopathology on Challenge with the SARS Virus, PLoS ONE. 7 (2012) e35421. https://doi.org/10.1371/journal.pone.0035421.

[207] P.J. Hotez, D.B. Corry, M.E. Bottazzi, COVID-19 vaccine design: the Janus face of immune enhancement, Nat Rev Immunol. 20 (2020) 347–348. https://doi.org/10.1038/s41577-020-0323-4.

[208] A. Gupta, Is Immuno-modulation the Key to COVID-19 Pandemic?, Indian J Orthop. (2020) 1–4. https://doi.org/10.1007/s43465-020-00121-7.

[209] C. Hörner, C. Schürmann, A. Auste, A. Ebenig, S. Muraleedharan, K.H. Dinnon, T. Scholz, M. Herrmann, B.S. Schnierle, R.S. Baric, M.D. Mühlebach, A highly immunogenic and effective measles virus-based Th1-biased COVID-19 vaccine, PNAS. 117 (2020) 32657–32666. https://doi.org/10.1073/pnas.2014468117.

[210] N. Vabret, G.J. Britton, C. Gruber, S. Hegde, J. Kim, M. Kuksin, R. Levantovsky, L. Malle, A. Moreira, M.D. Park, L. Pia, E. Risson, M. Saffern, B. Salomé, M. Esai Selvan, M.P. Spindler, J. Tan, V. van der Heide, J.K. Gregory, K. Alexandropoulos, N. Bhardwaj, B.D. Brown, B. Greenbaum, Z.H. Gümüş, D. Homann, A. Horowitz, A.O. Kamphorst, M.A. Curotto de Lafaille, S. Mehandru, M. Merad, R.M. Samstein, M. Agrawal, M. Aleynick, M. Belabed, M. Brown, M. Casanova-Acebes, J. Catalan, M. Centa, A. Charap, A. Chan, S.T. Chen, J. Chung, C.C. Bozkus, E. Cody, F. Cossarini, E. Dalla, N. Fernandez, J. Grout, D.F. Ruan, P. Hamon, E. Humblin, D. Jha, J. Kodysh, A. Leader, M. Lin, K. Lindblad, D. Lozano-Ojalvo, G. Lubitz, A. Magen, Z. Mahmood, G. Martinez-Delgado, J. Mateus-Tique, E. Meritt, C. Moon, J. Noel, T. O'Donnell, M. Ota, T. Plitt, V. Pothula, J. Redes, I. Reyes Torres, M. Roberto, A.R. Sanchez-Paulete, J. Shang, A.S. Schanoski, M. Suprun, M. Tran, N. Vaninov, C.M. Wilk, J. Aguirre-Ghiso, D. Bogunovic,

J. Cho, J. Faith, E. Grasset, P. Heeger, E. Kenigsberg, F. Krammer, U. Laserson, Immunology of COVID-19: Current State of the Science, Immunity. 52 (2020) 910–941. https://doi.org/10.1016/j.immuni.2020.05.002.

[211] J. Nikolich-Zugich, K.S. Knox, C.T. Rios, B. Natt, D. Bhattacharya, M.J. Fain, SARS-CoV-2 and COVID-19 in older adults: what we may expect regarding pathogenesis, immune responses, and outcomes, GeroScience. (2020) 1–10. https://doi.org/10.1007/s11357-020-00186-0.

[212] A.C. Walls, Y.-J. Park, M.A. Tortorici, A. Wall, A.T. McGuire, D. Veesler, Structure, Function, and Antigenicity of the SARS-CoV-2 Spike Glycoprotein, Cell. 181 (2020) 281-292.e6. https://doi.org/10.1016/j.cell.2020.02.058.

[213] J. Szebeni, Testing of drug-induced pseudo-allergies in a porcine model, World Allergy Organization Journal. 13 (2020). https://doi.org/10.1016/j.waojou.2020.100250.

[214] J. Szebeni, Complement activation-related pseudoallergy: A stress reaction in blood triggered by nanomedicines and biologicals, Molecular Immunology. 61 (2014) 163–173. https://doi.org/10.1016/j.molimm.2014.06.038.

[215] D. Csukás, R. Urbanics, G. Wéber, L. Rosivall, J. Szebeni, Pulmonary intravascular macrophages: prime suspects as cellular mediators of porcine CARPA, European Journal of Nanomedicine. 7 (2015). https://doi.org/10.1515/ejnm-2015-0008.

[216] M. Gadjeva, ed., The Complement System: Methods and Protocols, Humana Press, 2014. https://doi.org/10.1007/978-1-62703-724-2.

[217] A.M. Didierlaurent, S. Morel, L. Lockman, S.L. Giannini, M. Bisteau, H. Carlsen, A. Kielland, O. Vosters, N. Vanderheyde, F. Schiavetti, D. Larocque, M.V. Mechelen, N. Garçon, AS04, an Aluminum Salt- and TLR4 Agonist-Based Adjuvant System, Induces a Transient Localized Innate Immune Response Leading to Enhanced Adaptive Immunity, The Journal of Immunology. 183 (2009) 6186–6197. https://doi.org/10.4049/jimmunol.0901474.

[218] S.J. Keam, D.M. Harper, Human Papillomavirus Types 16 and 18 Vaccine (Recombinant, AS04 Adjuvanted Adsorbed) [Cervarix™], Drugs. 68 (2008) 359–372. https://doi.org/10.2165/00003495-200868030-00007.

[219] C.M. Wheeler, X. Castellsagué, S.M. Garland, A. Szarewski, J. Paavonen, P. Naud, J. Salmerón, S.-N. Chow, D. Apter, H. Kitchener, J.C. Teixeira, S.R. Skinner, U. Jaisamrarn, G. Limson, B. Romanowski, F.Y. Aoki, T.F. Schwarz, W.A.J. Poppe, F.X. Bosch, D.M. Harper, W. Huh, K. Hardt, T. Zahaf, D. Descamps, F. Struyf, G. Dubin, M. Lehtinen, Cross-protective efficacy of HPV-16/18 AS04-adjuvanted vaccine against cervical infection and precancer caused by non-vaccine oncogenic HPV types: 4-year end-of-study analysis of the randomised, double-blind PATRICIA trial, The Lancet Oncology. 13 (2012) 100–110. https://doi.org/10.1016/S1470-2045(11)70287-X.

[220] R.L. Coffman, D.A. Lebman, P. Rothman, Mechanism and Regulation of Immunoglobulin Isotype Switching, in: F.J. Dixon (Ed.), Advances in Immunology, Academic Press, 1993: pp. 229–270. https://doi.org/10.1016/S0065-2776(08)60536-2.

[221] C.M. Snapper, W.E. Paul, Interferon-gamma and B cell stimulatory factor-1 reciprocally regulate Ig isotype production, Science. 236 (1987) 944–947. https://doi.org/10.1126/science.3107127.

[222] J.P. Coutelier, J.T. van der Logt, F.W. Heessen, G. Warnier, J. Van Snick, IgG2a restriction of murine antibodies elicited by viral infections., Journal of Experimental Medicine. 165 (1987) 64–69. https://doi.org/10.1084/jem.165.1.64.

[223] D. Markine-Goriaynoff, J.-P. Coutelier, Increased Efficacy of the Immunoglobulin G2a Subclass in Antibody-Mediated Protection against Lactate Dehydrogenase-Elevating Virus-Induced Polioencephalomyelitis Revealed with Switch Mutants, JVI. 76 (2002) 432–435. https://doi.org/10.1128/JVI.76.1.432-435.2002.

[224] D. Sterlin, A. Mathian, M. Miyara, A. Mohr, F. Anna, L. Claër, P. Quentric, J. Fadlallah, H. Devilliers, P. Ghillani, C. Gunn, R. Hockett, S. Mudumba, A. Guihot, C.-E. Luyt, J. Mayaux, A. Beurton, S. Fourati, T. Bruel, O. Schwartz, J.-M. Lacorte, H. Yssel, C. Parizot, K. Dorgham, P. Charneau, Z. Amoura, G. Gorochov, IgA dominates the early neutralizing antibody response to SARS-CoV-2, Science Translational Medicine. 13 (2021). https://doi.org/10.1126/scitranslmed.abd2223.

[225] A. Padoan, L. Sciacovelli, D. Basso, D. Negrini, S. Zuin, C. Cosma, D. Faggian, P. Matricardi, M. Plebani, IgA-Ab response to spike glycoprotein of SARS-CoV-2 in patients with COVID-19: A longitudinal study, Clin Chim Acta. 507 (2020) 164–166. https://doi.org/10.1016/j.cca.2020.04.026.

[226] D.M. Hinton, Convalescent Plasma EUA Letter of Authorization, (2021). https://www.fda.gov/media/141477/download.

[227] A.T. Glenny, C.G. Pope, H. Waddington, U. Wallace, Immunological notes. XVII–XXIV, The Journal of Pathology and Bacteriology. 29 (1926) 31–40. https://doi.org/10.1002/path.1700290106.

[228] J.W. Osebold, Mechanisms of action by immunologic adjuvants, J Am Vet Med Assoc. 181 (1982) 983–987.

[229] L.S. Burrell, J.L. White, S.L. Hem, Stability of aluminium-containing adjuvants during aging at room temperature, Vaccine. 18 (2000) 2188–2192. https://doi.org/10.1016/S0264-410X(00)00031-1.

[230] J.W. Mannhalter, H.O. Neychev, G.J. Zlabinger, R. Ahmad, M.M. Eibl, Modulation of the human immune response by the non-toxic and non-pyrogenic adjuvant aluminium hydroxide: effect on antigen uptake and antigen presentation., Clin Exp Immunol. 61 (1985) 143–151.

[231] T.-Y. Kuo, M.-Y. Lin, R.L. Coffman, J.D. Campbell, P. Traquina, Y.-J. Lin, L.T.-C. Liu, J. Cheng, Y.-C. Wu, C.-C. Wu, W.-H. Tang, C.-G. Huang, K.-C. Tsao, C. Chen, Development of CpG-adjuvanted stable prefusion SARS-CoV-2 spike antigen as a subunit vaccine against COVID-19, Scientific Reports. 10 (2020) 20085. https://doi.org/10.1038/s41598-020-77077-z.

[232] P.A. Goepfert, B. Fu, A.-L. Chabanon, M.I. Bonaparte, M.G. Davis, B.J. Essink, I. Frank, O. Haney, H. Janosczyk, M.C. Keefer, M. Koutsoukos, M.A. Kimmel, R. Masotti, S.J. Savarino, L. Schuerman, H. Schwartz, L.D. Sher, J. Smith, F. Tavares-Da-Silva, S. Gurunathan, C.A. DiazGranados, G. De Bruyn, Safety and immunogenicity of SARS-CoV-2 recombinant protein vaccine formulations in healthy adults: a randomised, placebo-controlled, dose-ranging study, Infectious Diseases (except HIV/AIDS), 2021. https://doi.org/10.1101/2021.01.19.20248611.

[233] S.J. Zost, P. Gilchuk, J.B. Case, E. Binshtein, R.E. Chen, J.P. Nkolola, A. Schäfer, J.X. Reidy, A. Trivette, R.S. Nargi, R.E. Sutton, N. Suryadevara, D.R. Martinez, L.E. Williamson, E.C. Chen, T. Jones, S. Day, L. Myers, A.O. Hassan, N.M. Kafai, E.S. Winkler, J.M. Fox, S. Shrihari, B.K. Mueller, J. Meiler, A. Chandrashekar, N.B. Mercado, J.J. Steinhardt, K. Ren, Y.-M. Loo, N.L. Kallewaard, B.T. McCune, S.P. Keeler, M.J. Holtzman, D.H. Barouch, L.E. Gralinski, R.S. Baric, L.B. Thackray, M.S. Diamond, R.H. Carnahan, J.E. Crowe, Potently neutralizing and protective human antibodies against SARS-CoV-2, Nature. 584 (2020) 443–449. https://doi.org/10.1038/s41586-020-2548-6.

[234] E. Shrock, E. Fujimura, T. Kula, R.T. Timms, I.-H. Lee, Y. Leng, M.L. Robinson, B.M. Sie, M.Z. Li, Y. Chen, J. Logue, A. Zuiani, D. McCulloch, F.J.N. Lelis, S. Henson, D.R. Monaco, M. Travers, S. Habibi, W.A. Clarke, P. Caturegli, O. Laeyendecker, A. Piechocka-Trocha, J.Z. Li, A. Khatri, H.Y. Chu, M.C.-19 Collection &amp, P. Team16‡, A.-C. Villani, K. Kays, M.B. Goldberg, N. Hacohen, M.R. Filbin, X.G. Yu, B.D. Walker, D.R. Wesemann, H.B. Larman, J.A. Lederer, S.J. Elledge, Viral epitope profiling of COVID-19 patients reveals cross-reactivity and correlates of severity, Science. 370 (2020). https://doi.org/10.1126/science.abd4250.

[235] C.M. Poh, G. Carissimo, B. Wang, S.N. Amrun, C.Y.-P. Lee, R.S.-L. Chee, S.-W. Fong, N.K.-W. Yeo, W.-H. Lee, A. Torres-Ruesta, Y.-S. Leo, M.I.-C. Chen, S.-Y. Tan, L.Y.A. Chai, S. Kalimuddin, S.S.G. Kheng, S.-Y. Thien, B.E. Young, D.C. Lye, B.J. Hanson, C.-I. Wang, L. Renia, L.F.P. Ng, Two linear epitopes on the SARS-CoV-2 spike protein that elicit neutralising antibodies in COVID-19 patients, Nature Communications. 11 (2020) 2806. https://doi.org/10.1038/s41467-020-16638-2.

[236] L.J. Walker, A.K. Sewell, P. Klenerman, T cell sensitivity and the outcome of viral infection, Clin Exp Immunol. 159 (2010) 245–255. https://doi.org/10.1111/j.1365-2249.2009.04047.x.

[237] J.M. Dan, J. Mateus, Y. Kato, K.M. Hastie, E.D. Yu, C.E. Faliti, A. Grifoni, S.I. Ramirez, S. Haupt, A. Frazier, C. Nakao, V. Rayaprolu, S.A. Rawlings, B. Peters, F. Krammer, V. Simon, E.O. Saphire, D.M. Smith, D. Weiskopf, A. Sette, S. Crotty, Immunological

memory to SARS-CoV-2 assessed for up to 8 months after infection, Science. 371 (2021). https://doi.org/10.1126/science.abf4063.

[238] N.C.T. Kong, J. Beran, S.A. Kee, J.L. Miguel, C. Sánchez, J.-M. Bayas, A. Vilella, F. Calbo-Torrecillas, E. López de Novales, K. Srinivasa, M. Stoffel, B. Hoet, A new adjuvant improves the immune response to hepatitis B vaccine in hemodialysis patients, Kidney International. 73 (2008) 856–862. https://doi.org/10.1038/sj.ki.5002725.

[239] H.H. Tam, M.B. Melo, M. Kang, J.M. Pelet, V.M. Ruda, M.H. Foley, J.K. Hu, S. Kumari, J. Crampton, A.D. Baldeon, R.W. Sanders, J.P. Moore, S. Crotty, R. Langer, D.G. Anderson, A.K. Chakraborty, D.J. Irvine, Sustained antigen availability during germinal center initiation enhances antibody responses to vaccination, Proc Natl Acad Sci USA. 113 (2016) E6639–E6648. https://doi.org/10.1073/pnas.1606050113.

[240] S. Hutchison, R.A. Benson, V.B. Gibson, A.H. Pollock, P. Garside, J.M. Brewer, Antigen depot is not required for alum adjuvanticity, FASEB J. 26 (2012) 1272–1279. https://doi.org/10.1096/fj.11-184556.

[241] M.L. Mbow, E. De Gregorio, N.M. Valiante, R. Rappuoli, New adjuvants for human vaccines, Curr Opin Immunol. 22 (2010) 411–416. https://doi.org/10.1016/j.coi.2010.04.004.

[242] M.J. Newman, J.Y. Wu, B.H. Gardner, K.J. Munroe, D. Leombruno, J. Recchia, C.R. Kensil, R.T. Coughlin, Saponin adjuvant induction of ovalbumin-specific CD8+ cytotoxic T lymphocyte responses, J Immunol. 148 (1992) 2357–2362.

[243] A.S. McKee, M.W. Munks, M.K.L. MacLeod, C.J. Fleenor, N. Van Rooijen, J.W. Kappler, P. Marrack, Alum Induces Innate Immune Responses through Macrophage and Mast Cell Sensors, But These Sensors Are Not Required for Alum to Act As an Adjuvant for Specific Immunity, J Immunol. 183 (2009) 4403–4414. https://doi.org/10.4049/jimmunol.0900164.

[244] J.L. Grun, P.H. Maurer, Different T helper cell subsets elicited in mice utilizing two different adjuvant vehicles: The role of endogenous interleukin 1 in proliferative responses, Cellular Immunology. 121 (1989) 134–145. https://doi.org/10.1016/0008-8749(89)90011-7.

[245] S. Dasgupta, J. Bayry, S. Lacroix-Desmazes, S.V. Kaveri, Human mannose receptor (CD206) in immune response: novel insights into vaccination strategies using a humanized mouse model, Expert Review of Clinical Immunology. 3 (2007) 677–681. https://doi.org/10.1586/1744666X.3.5.677.

[246] M. Bermejo-Jambrina, J. Eder, L.C. Helgers, N. Hertoghs, B.M. Nijmeijer, M. Stunnenberg, T.B.H. Geijtenbeek, C-Type Lectin Receptors in Antiviral Immunity and Viral Escape, Front. Immunol. 9 (2018). https://doi.org/10.3389/fimmu.2018.00590.

[247] K.B. Gorden, K.S. Gorski, S.J. Gibson, R.M. Kedl, W.C. Kieper, X. Qiu, M.A. Tomai, S.S. Alkan, J.P. Vasilakos, Synthetic TLR agonists reveal functional differences between

human TLR7 and TLR8, J Immunol. 174 (2005) 1259–1268. https://doi.org/10.4049/jimmunol.174.3.1259.

[248] M. Puray-Chavez, K.M. LaPak, T.P. Schrank, J.L. Elliott, D.P. Bhatt, M.J. Agajanian, R. Jasuja, D.Q. Lawson, K. Davis, P.W. Rothlauf, Z. Liu, H. Jo, N. Lee, K. Tenneti, J.E. Eschbach, C. Shema Mugisha, E.M. Cousins, E.W. Cloer, H.R. Vuong, L.A. VanBlargan, A.L. Bailey, P. Gilchuk, J.E. Crowe, M.S. Diamond, D.N. Hayes, S.P.J. Whelan, A. Horani, S.L. Brody, D. Goldfarb, M.B. Major, S.B. Kutluay, Systematic analysis of SARS-CoV-2 infection of an ACE2-negative human airway cell, Cell Reports. 36 (2021) 109364. https://doi.org/10.1016/j.celrep.2021.109364.

[249] T.M. Marchell, Engineering Antibody Glyco-adjuvant Conjugates to Treat Established Cold Tumors, The University of Chicago, 2020. https://doi.org/10.6082/uchicago.2809.

[250] V. Menchise, G. Digilio, E. Gianolio, E. Cittadino, V. Catanzaro, C. Carrera, S. Aime, In Vivo Labeling of B16 Melanoma Tumor Xenograft with a Thiol-Reactive Gadolinium Based MRI Contrast Agent, Mol. Pharmaceutics. 8 (2011) 1750–1756. https://doi.org/10.1021/mp2001044.

[251] P. Opanasopit, K. Shirashi, M. Nishikawa, F. Yamashita, Y. Takakura, M. Hashida, In vivo recognition of mannosylated proteins by hepatic mannose receptors and mannan-binding protein, American Journal of Physiology-Gastrointestinal and Liver Physiology. 280 (2001) G879–G889. https://doi.org/10.1152/ajpgi.2001.280.5.G879.

[252] J.K. Tom, E.Y. Dotsey, H.Y. Wong, L. Stutts, T. Moore, D.H. Davies, P.L. Felgner, A.P. Esser-Kahn, Modulation of Innate Immune Responses via Covalently Linked TLR Agonists, ACS Central Science. 1 (2015) 439–448. https://doi.org/10.1021/acscentsci.5b00274.

[253] K.H. Dinnon, S.R. Leist, A. Schäfer, C.E. Edwards, D.R. Martinez, S.A. Montgomery, A. West, B.L. Yount, Y.J. Hou, L.E. Adams, K.L. Gully, A.J. Brown, E. Huang, M.D. Bryant, I.C. Choong, J.S. Glenn, L.E. Gralinski, T.P. Sheahan, R.S. Baric, A mouse-adapted model of SARS-CoV-2 to test COVID-19 countermeasures, Nature. 586 (2020) 560–566. https://doi.org/10.1038/s41586-020-2708-8.

[254] E. Callaway, Mix-and-match COVID vaccines trigger potent immune response, Nature. 593 (2021) 491–491. https://doi.org/10.1038/d41586-021-01359-3.

[255] A.M. Borobia, A.J. Carcas, M.T. Pérez Olmeda, L. Castaño, M. Jesús Bertrán, J. García-Pérez, M. Campins, A. Portolés, M. Gonzalez-Perez, M.T. García Morales, E. Arana, M. Aldea Novo, F. Díez-Fuertes, I. Fuentes-Camps, A. Ascaso, D. Lora, N. Imaz-Ayo, L.E. Baron-Mira, A. Agustí, C. Pérez-Ingidua, A. Gómez de la Cámara, J.R. Arribas, J. Ochando, J. Alcamí Pertejo, C. Belda-Iniesta, J. Frías, C.S. Group, Reactogenicity and Immunogenicity of BNT162b2 in Subjects Having Received a First Dose of ChAdOx1s: Initial Results of a Randomised, Adaptive, Phase 2 Trial (CombiVacS), Social Science Research Network, Rochester, NY, 2021. https://doi.org/10.2139/ssrn.3854768.

[256] R. Groß, M. Zanoni, A. Seidel, C. Conzelmann, A. Gilg, D. Krnavek, S. Erdemci-Evin, B. Mayer, M. Hoffmann, S. Pöhlmann, A. Beil, J. Kroschel, B. Jahrsdörfer, H. Schrezenmeier, F. Kirchhoff, J. Münch, J.A. Müller, Heterologous ChAdOx1 nCoV-19 and BNT162b2 prime-boost vaccination elicits potent neutralizing antibody responses and T cell reactivity, 2021. https://doi.org/10.1101/2021.05.30.21257971.

[257] D. Hillus, T. Schwarz, P. Tober-Lau, H. Hastor, C. Thibeault, S. Kasper, E.T. Helbig, L.J. Lippert, P. Tscheak, M.L. Schmidt, J. Riege, A. Solarek, C. von Kalle, C. Dang-Heine, P. Kopankiewicz, N. Suttorp, C. Drosten, H. Bias, J. Seybold, E.S. Group, C. Conrad, D. Steuer, U. Gläser, A.-S. Sinnigen, C. Rubisch, N. Olk, L. Hasler, A. Sanchez-Rezza, P. Kronenberg, A. Horn, W. Koch, P. Stubbemann, J.-A. Gabelich, F. Münn, J. Tesch, P. Mackeldanz, L. Bergfeld, T. Bleicker, J.I. Beheim-Schwarzbach, A. Hiller, S. Brumhard, L. Bardtke, K. Pohl, D. Wendisch, P. Georg, D. Treue, D. Briesemeister, J. Schlesinger, A. Hetey, L. Kegel, A. Richter, B. Al-Rim, B. Maeß, K. Behn, M. Lysi, S. Zvorc, M. Rönnefarth, S. Schmidt, A. Krannich, I. Schellenberger, G. Schwanitz, V. Schenkel, N. Bethke, C. Hülso, S. Dieckmann, C. Peiser, F. Kurth, V.M. Corman, L.E. Sander, Safety, reactogenicity, and immunogenicity of homologous and heterologous prime-boost immunisation with ChAdOx1-nCoV19 and BNT162b2: a prospective cohort study, 2021. https://doi.org/10.1101/2021.05.19.21257334.

APPENDIX A: FLOW CYTOMETRY GATING STRATEGIES

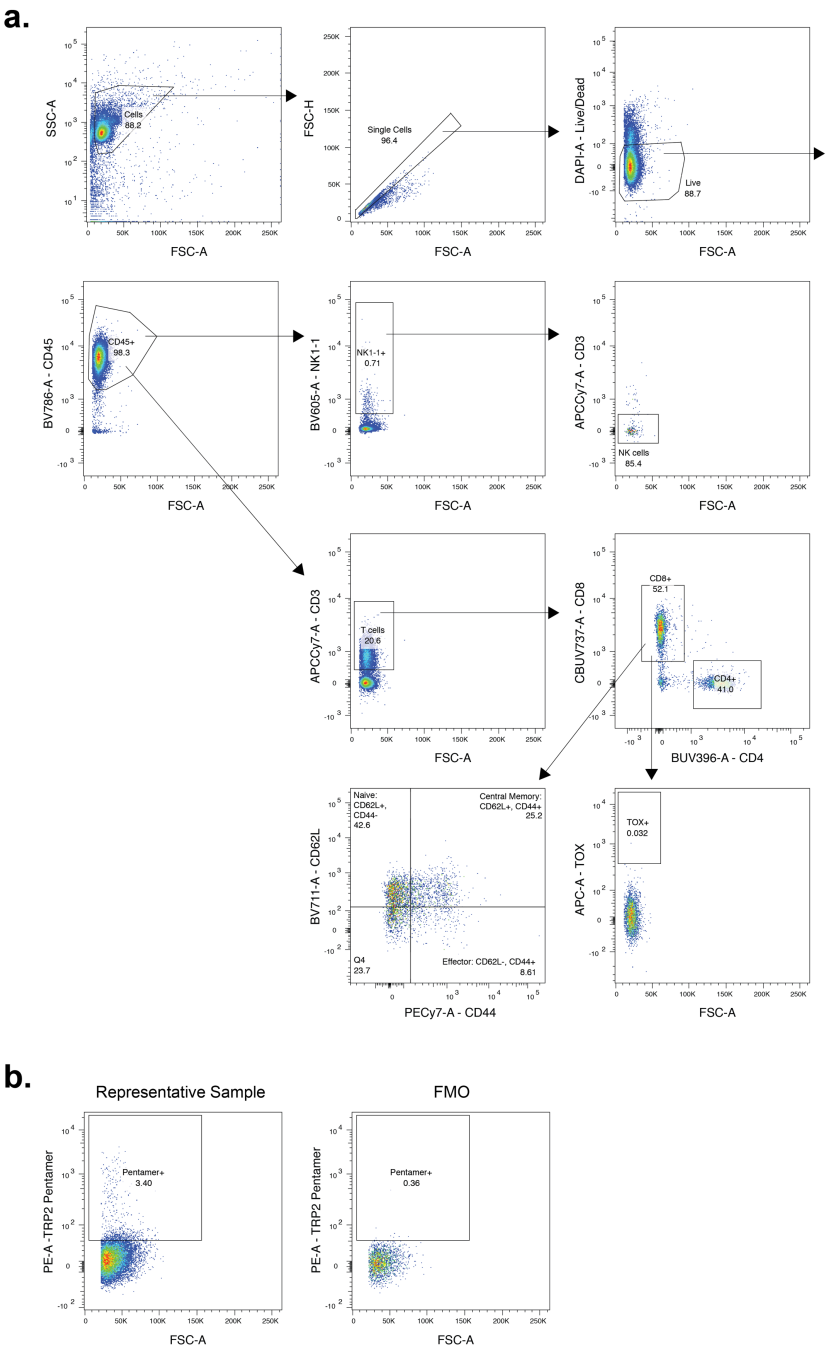

Figure A.1: Representative flow cytometry gating used to characterize immune cells in tumors, tumor-draining lymph nodes, and spleens.

(**a**) Gating strategy used in the analysis of immune cells from Fig. 2.9. (**b**) Representative flow cytometry plots showing TRP2 pentamer$^+$ CD8$^+$ T cells in a representative sample (left) and the fold minus one (FMO) control (right).

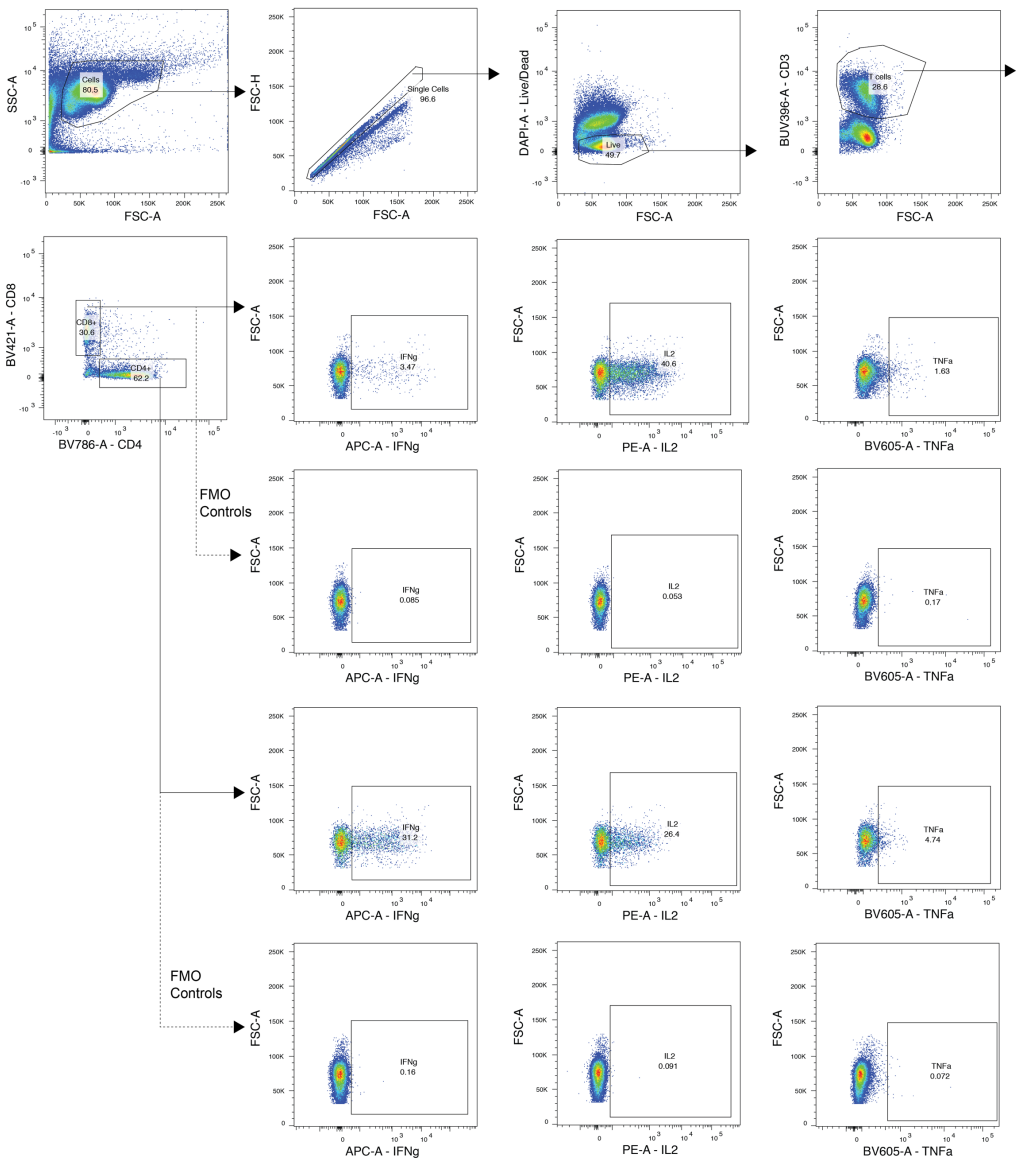

Figure A.2: Representative flow cytometry gating used to characterize cytokine$^+$ T cells from Chapter 2.

Gating strategy used in the analysis of cytokine$^+$ T cells from Fig. 2.10.

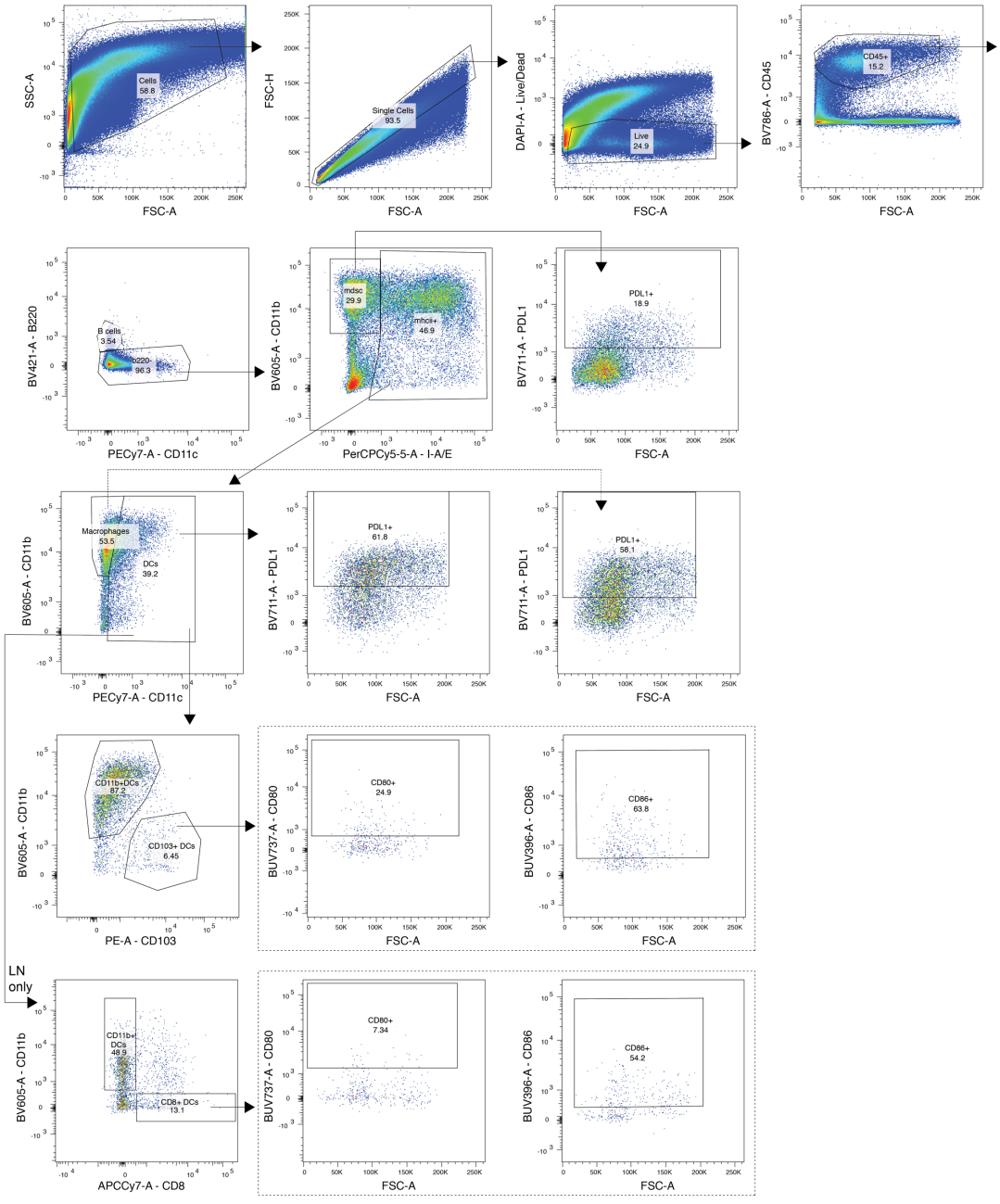

Figure A.3: Representative flow cytometry gating used to characterize myeloid cells in tumors and tumor-draining lymph nodes.

Gating strategy used in the analysis of myeloid cell populations from Fig. 2.11, 2.12, and 2.13.

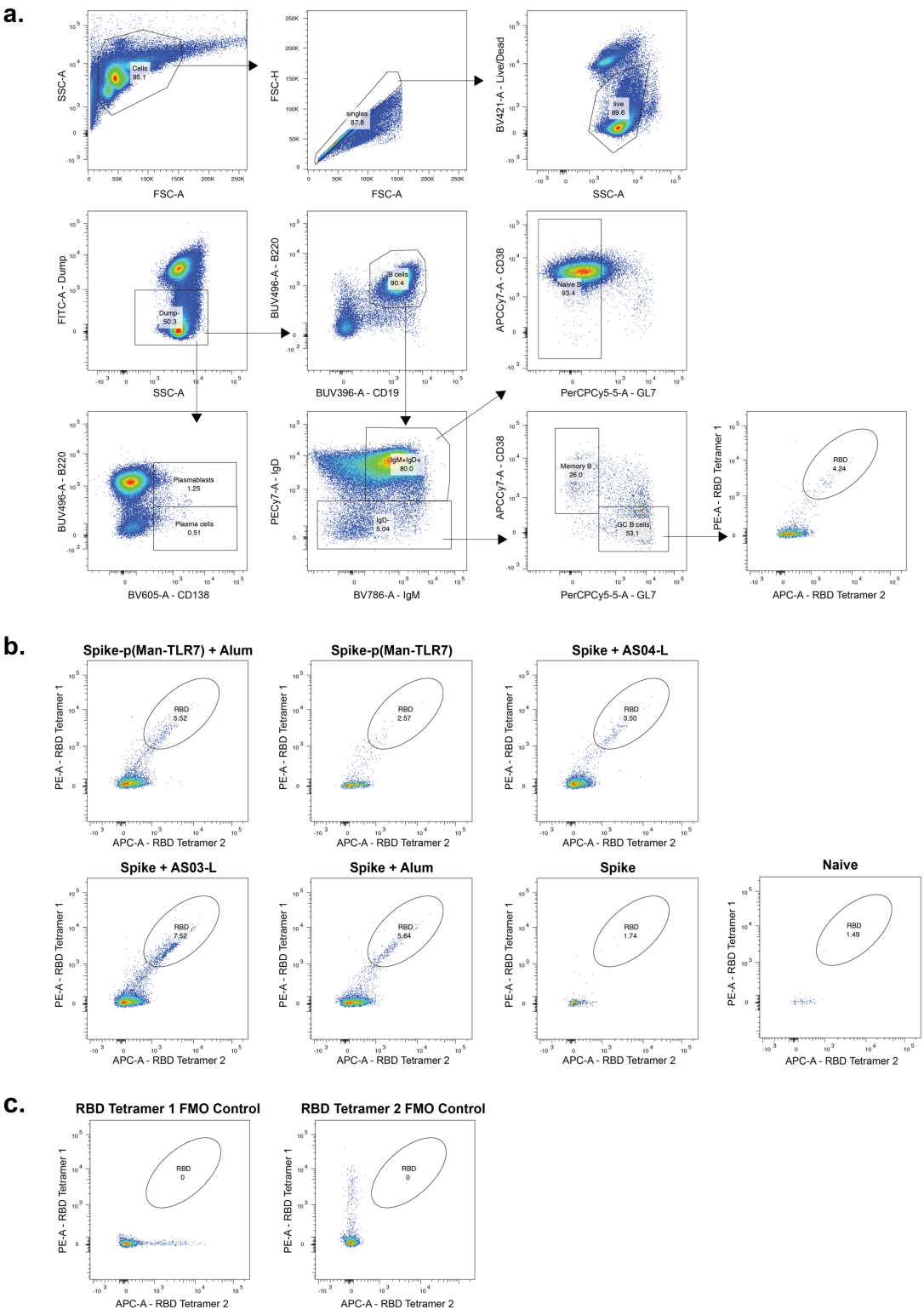

Figure A.4: Representative flow cytometry gating used to characterize B cells.

(**a**) Gating strategy used in the analysis of B cells from Fig. 3.9 and 3.10. (**b**) Representative flow cytometry plots showing RBD-tetramer$^+$ GC B cells from each experimental group. (**c**) Fold minus one (FMO) control flow cytometry plots used for analyzing RBD-tetramer$^+$ GC B cells.

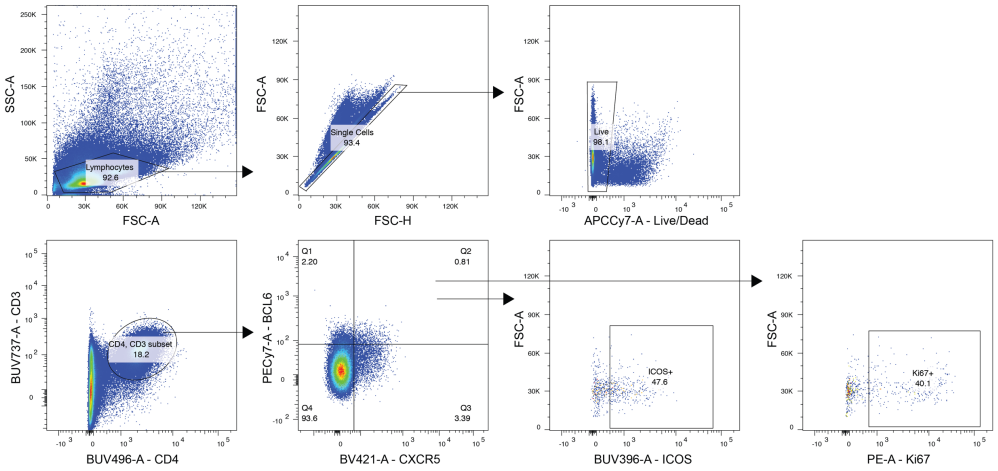

Figure A.5: Representative flow cytometry gating used to characterize T_{fh} cells.

Gating strategy used for the analysis of T_{fh} cells in Fig. 3.11.

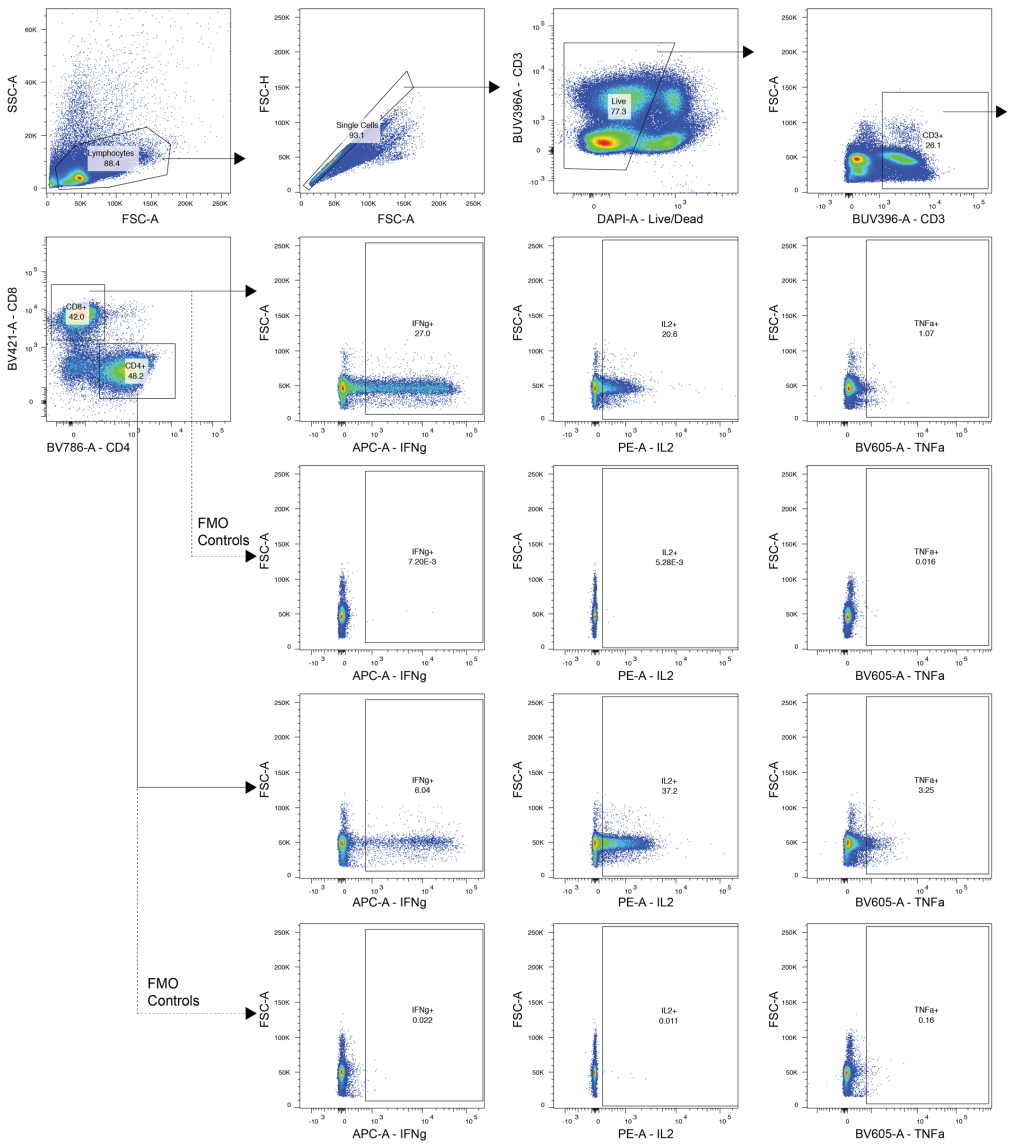

Figure A.6: Representative flow cytometry gating used to characterize cytokine$^+$ T cells from Chapter 3.

Gating strategy used for the analysis of cytokine$^+$ T cells from Fig. 3.12.